Universidad Zaragoza
1542

Tesis Doctoral

BIOMEDICAL APPLICATIONS OF MAGNETIC NANOPARTICLES: MAGNETIC HYPERTHERMIA IN DENDRITIC CELLS AND MAGNETOFECTION IN BRAIN CELLS

Autor

Asín Pardo, Laura

Director/es

Ibarra García, Manuel Ricardo
Goya Rossetti, Gerardo Fabián

FACULTAD DE CIENCIAS
Departamento de Física de la Materia Condensada

2012

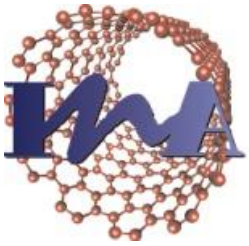

Instituto Universitario de Investigación
en Nanociencia de Aragón
Universidad Zaragoza

BIOMEDICAL APPLICATIONS OF MAGNETIC NANOPARTICLES: MAGNETIC HYPERTHERMIA IN DENDRITIC CELLS AND MAGNETOFECTION IN BRAIN CELLS.

Memoria presentada para optar al grado de Doctor Europeo por la Universidad de Zaragoza

Laura Asín Pardo

Directores:

M. Ricardo Ibarra

Gerardo F. Goya

Departamento de Física de la Materia Condensada

Zaragoza, Marzo 2012.

Index

Abbreviations

AC: alternating current

AMF: alternating magnetic field

APC: antigen presenting cell

BSA: bovine serum albumine

CD40L: CD40 ligando

CPM: counts per minute

CSF: cerebrospinal fluid

DCs: dendritic cells

iDCs: immature dendritic cells

mDCs: mature DCs

ECs: endothelial cells

FBS: fetal bovine serum

FCS: fetal calf serum

FM: ferro or ferromagnetic

FSA: fluorinated surfactant

FSC: Forward Scatter

G. lucidum: Ganoderma lucidum

GFP: green fluorescence protein

GM-CSF: granulocyte-macrophage colony-stimulating factor

H: magnetic field

Hc: coercitivity field

IL: interleukin

Abbreviations

INF-γ: interferon γ

LPS: Lipopolysaccharides

M: magnetization

Ms: saturation magnetization

Mr: remanence magnetization

M-CSF: macrophage colony-stimulating factor

MD: multi-domain

MFH: magnetic fluid hyperthermia

MFI: mean fluorescence intensity

MNPs: magnetic nanoparticles

MOI: multiplicities of infection

MPs: micro particles

NPs: nanoparticles

MRI: magnetic resonance imaging

PBS: Phosphate buffered saline

PCS: photon correlation spectroscopy

PEI: polyethylenimine

PGA: poly-glutamic acid

PGE2: prostaglandina E2

PLGA

RT: room temperature

SD: single-domain

SP: superparamagnetism

SPA: specific power absorption

SPM: superparamagnetic

Abbreviations

SSC: Side or Ortogonal Scatter

TNF-α: tumor necrosis factor α

TU: transformation units

VEGF: vascular endothelial growth factor

VP: virus particle

χ: magnetic susceptibility

Preface

Nanoscience is nowadays one of the most leading research fields and there are many scientific disciplines that benefit of it. Among all these disciplines biomedicine is one of the most promising, since nano-biomedicine developed from to the nanoscience could revolutionize the diagnosis and therapeutic fields. Concerning biomedical applications, magnetic nanoparticles (MNPs) are being intensively studied due to their magnetic and nano sized characteristics, two properties that when combined offer a very promising tool.

Drug delivery, magnetic hyperthermia, magneto-transduction/transfection, cell labelling and Magnetic Resonance Imaging (MRI) are examples of biological application that could be benefit of nanoscience. In this thesis we focus on magnetic hyperthermia and magnetotransduction applications and for that purpose MNPs are key material to be investigated.

In Chapter I an introduction about nanoscience and nanoparticles (NPs), hyperthermia, dendritic cells (DCs) and magnetofection is given in order to know the state of the art of these topics, which are of a great importance in this thesis.

Chapter II deals with materials and methods, explaining in detail all the protocols and materials that have been used to perform the experiments carried out in this thesis. Descriptions of some instruments are given at the end of the work in the annexe.

Magnetic hyperthermia is being investigated in clinics as cancer treatment protocol combined with other therapeutic approaches as chemotherapy or radiotherapy. It has been demonstrated that hyperthermia boosts therapeutic power of the other cancer

treatments [1, 2]. DCs are known to transdifferentiate in endothelial-like-cells in the presence of proangiogenic factors [3, 4], and subsequently take part in new blood vessels formation, called angiogenesis. Thus, our strategy was to upload DCs with MNPs, in order to be able to use them in future *in vivo* experiments to drive the MNPs toward the tumoral area without any risk of immune response against the MNPs. The first part of the Chapter III shows the results obtained from the interaction between the DCs and the MNPs in terms of cytotoxicity, incorporation and maturation effect in DCs after MNPs uptake. The second part of this chapter shows the results concerning the effect of an Alternating Magnetic Field (AMF) exposure on MNPs-loaded DCs which is responsible for the cell death. Variation of some parameters, as exposition time, magnetic field intensity and MNPs concentration has been studied in order to evaluate and control the percentage of cells that suffer from the AMF effects.

The other biological application studied in this thesis is the formation of magnetic viral complexes for transduction of neuronal and glial cells. The relevance of these kinds of cells is the role that they play in neurodegenerative disorders, such as Alzheimer's and Parkinson´s diseases, which are growing in importance in our society due to the increase of the elderly population. The development of new gene therapy strategies in this field is of current major interest. Magnetic complexes were formed with MNPs and adenovirus, in order to perform a magnetic field assisted transduction, known as magnetotransduction. This method improves the efficiency of cell transduction and also allows a magnetic targeting of gene delivery complexes to the desired area. The last part of the Chapter III gathers results related to this approach, where physical and magnetic characterization of complexes is presented. Also transduction results on the efficiency of magnetic complexes in both cell lines in monoculture and co-culture conditions are shown.

In Chapter IV the conclusions can be found that have been reached for both hyperthermia in DCs and magnetofection parts of the work, and finally at the end of this thesis the bibliography used for the elaboration of this work can be found in the order of appearance.

I. Introduction

I.I. Nanoscience and nanoparticles

In the last years there have been a great enthusiasm in the interdisciplinary field of nanotechnology, and it has led to a search for connections between nanostructures, biology and technology. As nanotechnology offers new tools for biology, and biology offers nanotechnology access to new types of functional nanosystems, the scientific interest in the intersection of these different fields has significantly grown. The range of sizes covering by the term nano is 1-100 nm [5]. One way to calibrate the nano size range is to compare it with other small things in our world.

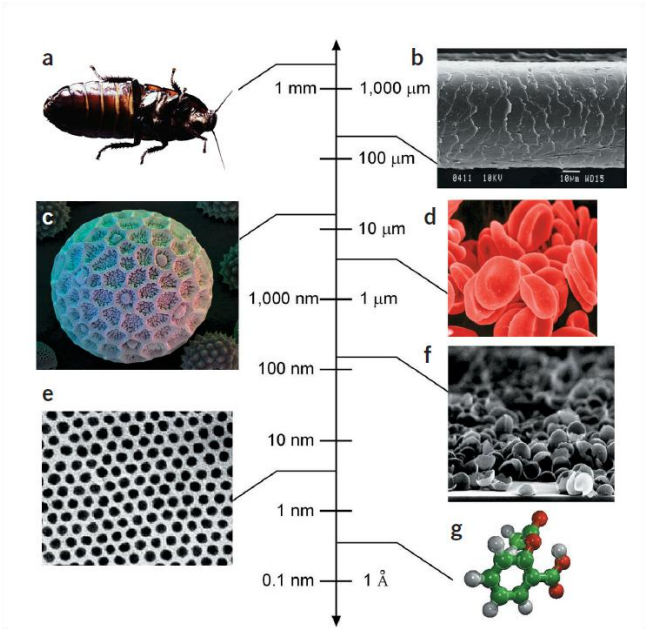

Figure I- 1: Image that shows the size of representative "small" objects: a) A Cockroach, b) a human hair, c) Polygonum pollen grain, d) red blood cells, e) cobalt nanocrystal superlattice, f)aggregate of half-shells of palladium and g) aspirin molecule [5].

Figure I- 1 compares the size of nanocrystals with a human hair, a pollen grain, a red blood cell and an aspirin molecule. Note that a red blood cell is huge in comparison with nanoparticles; it is helpful to realize that the volume of one red cell could hold a million 50 nm nanoparticles.

Nanotechnology is having a major impact on several biological areas. For example pharmacy, where one of the main goals is the design and creation of new biomolecules to be transported and vectorized to target cells; therapeutics drugs production is also being affected by nanotechnology, now many drugs are being produced in nanoparticles form and it improves their incorporation into bloodstream compared to the microparticles or larger particles [6]. Tagging of DNA and DNA based chips is another application of nanotechnology in biology and it has been made possible by coating gold nanoparticles with DNA strands [7]. Other area where biology can benefit from nanoscience is the control and fabrication of new materials and structures. There is a wide variety of surfaces patterned with self-assembled monolayers to guide cell attachment and growth as three dimensional scaffolds for tissue and bone engineering [8]. There are many available nanostructured materials bared in physic-chemist tools for application to biological science. However, apart from biology there are other areas that nanotechnology promises to affect, like information storage, refrigeration, environmental/green chemistry, catalysis, sensors, nanostructured electrodes, improved polymers and better batteries. These improvements that have been just mentioned are some examples but the list is still longer. It is quite apparent that there are innumerable potential benefits for society and the environment. In this thesis, we will focus on some biological applications.

The development in nanotechnology has been carried out in recent years due to the discovering of powerful techniques for characterization and analysis of such materials

down to the atomic scale. Among these techniques we can underline the high-resolution transmission electron microscopy (HRTEM) and the scanning probe microscopy (SPM)

Nanomaterials can be classified depending on the nanosized dimensions. Two dimensional nanostructures are films, coatings and layers with a thickness less than 100nm, one dimensional nanomaterials are tubes, wires and fibers where the dimension that typically is bigger than 100nm is the length and zero dimensional nanostructures are particles, quantum dots and clusters in which quantum effects are observed.

Most current investigated nanomaterials are: carbon and metal based materials, dendrimers and composites. Carbon based materials of interest in nanotechnology are: fullerenes, nanotubes and graphene. Metal based materials as nanogold and nanosilver are relevant for some applications and also magnetic oxides, such as magnetite. Dendrimers are nanosized polymers built from brunch units and the surface of these nanomaterials has numerous chain ends, which can be tailored to perform specific chemical functions. Composites combine nanoparticles within a matrix. In this thesis we are going to focus on nanostructured materials based on MNPs, specifically magnetite (Fe_3O_4)-based NPs.

Nanoparticles are among the most suitable nanoscale materials to be directly useful in biology; magnetic particles labelled with antibodies [9], superparamagnetic iron oxide based particles with dextran coating [10] to enhance contrast in resonance imaging, are nowadays commercially available.

MNPs are promising materials due to their functionality and The possibility to obtain them at controllable sizes from a few nanometres up to tens of nanometres. Thus, we can find MNPs of the size of a virus (20-450nm), a protein (5-50nm) or a gene (2nm wide and 10-100 nm long)[11]. Also, they can be coated with biological molecules to make them interact with biological entities. They can be manipulated by an external

magnetic field gradient and experience magnetic energy losses and relaxation process, under applied alternating magnetic fields. This “action at a distance” adding to the penetrability of magnetic fields into human tissue, opens up many applications. In this way MNPs can be made to deliver a package, such as an anticancer drug, to a targeted region of the body, such as a tumour. The magnetic moment can respond resonantly to a time-varying magnetic field. For example, the particle can be heated, which leads to their use as hyperthermia agents, delivering toxic amounts of thermal energy to targeted part of the human body, such as tumours.

Indeed these multifunctional agents can be used as:

- Cellular labelling [12, 13] as they are much smaller than a living cell.

- Bio-separation [14] and drug targeting [15, 16] when they are expose to a magnetic force.

- Contrast agents for magnetic resonance imaging (MRI) [17, 18] due to the local magnetic field they generate.

- Heat generators [19] [20, 21].

- Enhancers of transduction efficiency when MNPs are bound to virus and cell infection is made in the presence of an external magnetic field, method known as magnetofection [22].

In this thesis, we will focus on two applications, specifically magnetic hyperthermia and magnetofection.

Regarding the choice of magnetic particles for their use in magnetic hyperthermia, the iron oxides magnetite (Fe_3O_4) and maghemite (γ-Fe_2O_3) are the most studied to date because of their generally appropriate magnetic properties and biological compatibility. Candidate materials are divided into two main classes: ferromagnetic or ferrimagnetic (FM) single-domain or multi-domain particles, or superparamagnetic (SPM) particles.

In the next section more information about the different magnetic behaviours of the material is given. The heat generating mechanisms associated with each class are quite different. In general when exposed to an alternating magnetic field magnetic materials generate heat via four possible loss mechanisms: hysteresis, eddy current, Néel paramagnetic switching and friction from Brownian rotation. It is quite possible that all of them contribute to the total heat generated by a particular magnetic sample under application of an AMF, but it is expected that only one or two mechanism dominate. In the case of superparamagnetic Fe_3O_4 nanoparticles which are of a major interest to avoid magnetic aggregation, it is clear that hysteresis loss of energy is not possible and also the eddy current losses is likely negligible. Thus, the two mechanisms that will dominate will be Néel switching and frictional contributions, which are explained in more detail in the section 3, introduction about hyperthermia.

I.II. Magnetism basis

As MNPs are one of the most important tools in this research, some basic concepts of magnetism are needed, and these concepts are also required for several techniques that have been used in this work.

The different types of magnetism are described from the point of view of how materials respond to magnetic fields. The matter is intrinsically magnetic, due to the orbital and spin angular moment, which in turn give rise to an atomic magnetic moment. In some materials there is no collective interaction of atomic magnetic moments (diamagnetism and paramagnetism), whereas in other materials there is a strong long

range exchange interaction between atomic moments (ferromagnetism, antiferromagnetism and ferrimagnetism). Ferromagnetic and ferrimagnetic materials are usually what we consider as being magnetic, the other three, as they are weakly magnetic, are often consider to be "nonmagnetic".

The response of the matter to an applied magnetic field (H) is measured by the density of generated magnetic dipoles (M), i.e. the magnetization. The relation between the two magnitudes is the magnetic susceptibility: $\chi = M/H$. So the magnetic susceptibility indicates the degree of magnetization of a material in response to an applied magnetic field.

Diamagnetism is due to the non-cooperative interaction between electrons when exposed to an applied magnetic field, so that it is usually very weak and it is a fundamentally property of all matter. This behaviour is relevant in all materials in which the atoms have not net magnetic moment. When they are exposed to a magnetic field, a small magnetic moment is induced in opposite direction of the magnetic field, and consequently a negative susceptibility is observed. Schematically in Figure I- 2.a it is shown the Magnetization (M) versus magnetic field (H) of a diamagnet, where we observe a negative slope, which corresponds to the magnetic susceptibility (χ).

Paramagnetic materials are composed by atoms that have a net magnetic moment due to their unpaired electrons, and in the presence of a magnetic field, there is a partial alignment of the magnetic moments along the field direction, resulting in a net positive magnetization. However, when the field is removed the magnetization goes back to zero, like in diamagnetism. When we plot M versus H we observe a positive χ, Figure I- 2.b.

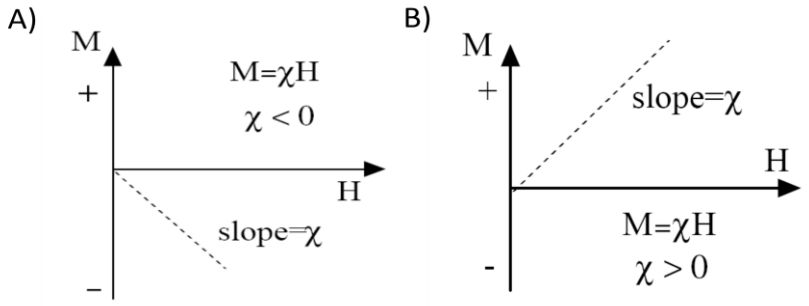

Figure I- 2: Representation of Magnetization versus H in a) diamagnetic materials and b) paramagnetic materials. X is the magnetic susceptibility.

In *ferromagnetic* materials, the atomic moments exhibit very strong interactions produced by long range electronic exchange forces resulting in a parallel or antiparallel alignment of atomic moments, Figure I- 3. The exchange force is a quantum mechanical phenomenon due to the relative orientation of the spin of two electrons. Ferromagnetic materials exhibit parallel alignments of magnetic moments resulting in large net magnetization even in the absence of magnetic field, called spontaneous magnetization.

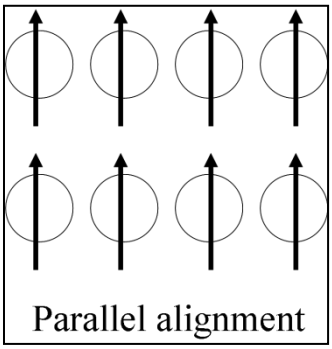

Figure I- 3:Image that show the parallel alignment scheme typical from ferromagnetic materials in the absence of a magnetic field.

When we expose this kind of material to a magnetic field, a maximum induced magnetic moment can be obtained, term know as saturation magnetization (Ms). Ms is an intrinsic property, independent of particle size but dependent on temperature. At a certain temperature, called Curie temperature, thermal energy overcomes the electronic exchange forces and produces a randomizing effect resulting in the fact that the Ms goes to zero. Below the Curie temperature it is said that the ferromagnet is "ordered" and above it, "disordered".

Another very important property of ferromagnetic materials is that they can retain a memory of an applied field once it is removed. This behaviour is called hysteresis, and when we plot the magnetization versus magnetic field we obtain the hysteresis loop, Figure I- 4, where we can distinguish the remanence or remanent magnetization (Mr), which is the magnetization left behind in a material when the magnetic field is removed, and the field that should be applied to remove this remanence, called coercitivity field (Hc).

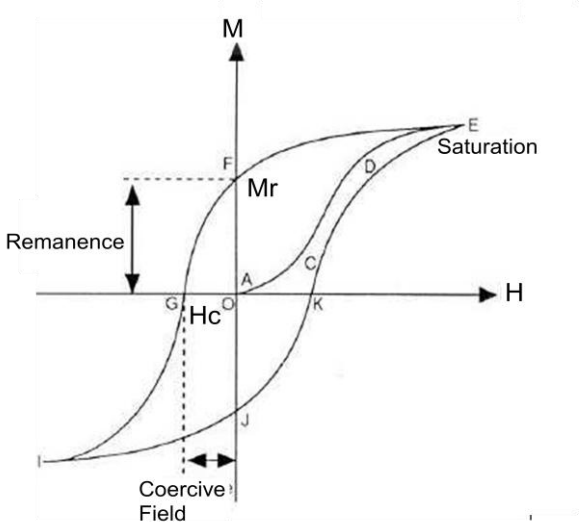

Figure I- 4: Representation of a typical hysteresis loop of a ferromagnet. Mr is the remanent field and Hc is the coercitivity field.

Ferrimagnetic behaviour occurs usually in ionic compounds, as oxides. The magnetic structure is composed of two magnetic sublattices (A and B) separated by oxygen. The magnetic moments of the two sublattices are not equal and oppositely oriented resulting in a net magnetic moment. Ferrimagnetism is similar to ferromagnetism related to spontaneous magnetization, Curie temperature, hysteresis and remanence, what they have different is the magnetic order. Magnetite (Fe_3O_4) is a well known example of a ferrimagnetic material.

If A and B sublattice moments are exactly equal and antiparallel, the net moment is zero in the absence of an external magnetic field. This type of magnetic ordering is called *antiferromagnetism*, Figure I- 5. *Antiferromagnetic* materials have zero remanence and coercitivity.

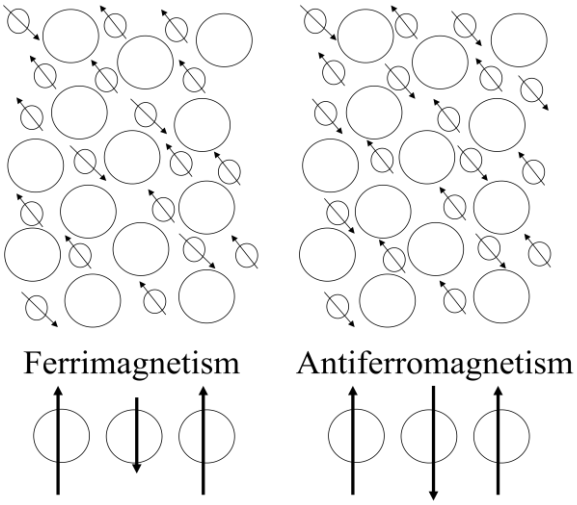

Figure I- 5: Representation of the ferrimagnetism and antiferromagnetism magnetic moments alligment.

As it has been mentioned, ferromagnetic and ferrimagnetic materials exposed to an external magnetic field have a saturation magnetization, which is higher than the spontaneous magnetization reached in the absence of magnetic field. It could be explained considering that these materials are divided into small domains, each of them is spontaneously magnetized to saturation, but the direction of magnetization varies from domain to domain, Figure I- 6.

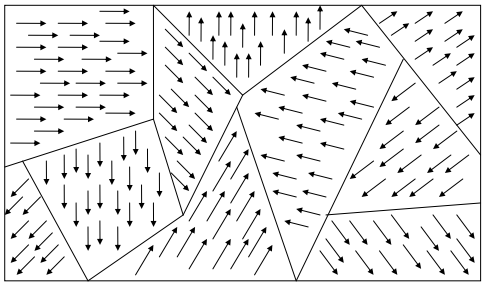

Figure I- 6: Domains scheme of a typical multidomain ferromagnetic material. Domains are magnetized in different directions.

The net vector sum of all the domains is much lower than if the material was exposed to a magnetic field and all the magnetic moments were parallel disposed. The existence of domains also explains other variations of magnetic properties, as coercitivity and remanence variation with the material size.

To change the magnetization of a multidomain particle, displacement of the domain walls is needed. This is a low energy process, which can be accomplished in relatively low magnetic fields. However the only way to change the magnetization within a domain is to rotate the magnetic moment, the energy cost is due to the magnetocrystalline anisotropy or the shape anisotropy. Thus single domain particles are magnetically hard and have high coercitivities and remanence, Figure I- 7.

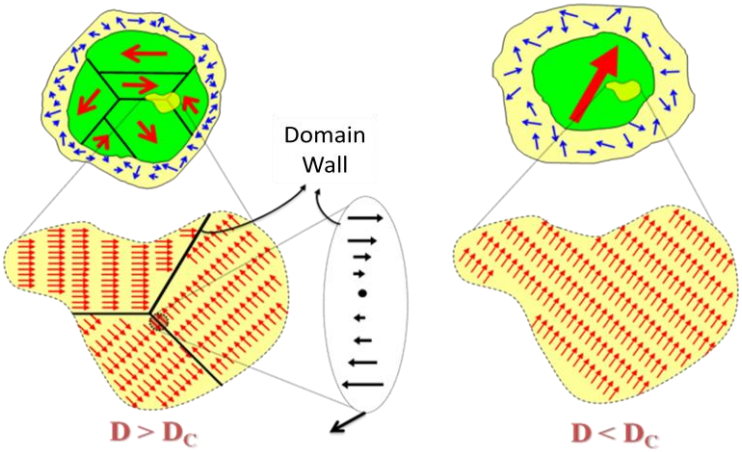

Figure I- 7: Scheme of the magnetic moments comparison between multidomain (left) and monodomain (right) particles. D is the diameter and Dc the critical diameter above which the materials are multidomain.

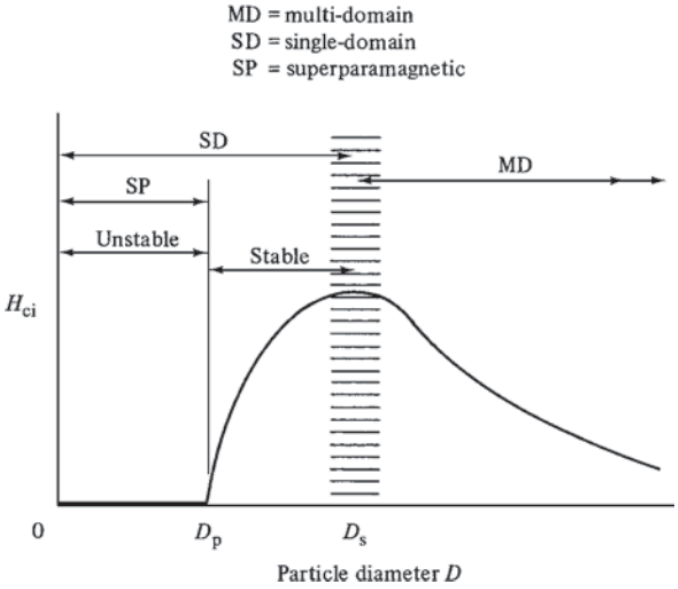

Figure I- 8: Image that shows the coercivity variation in relation with the diameter value [23]. Below a diameter Ds the particles become monodomain and the coercitivity decreases and below a diameter Dp the particles become SP and the coercitivity goes to zero.

As the particle size is reduced (see Figure I- 8), it is typically found that the coercitivity increases, goes to a maximum and tends toward zero. For multidomain particles, magnetization changes by domain wall motion. At a critical diameter, Ds, the particles become single domains, and in this size range the coercitivity reaches a maximum. When the particle size decreases below Ds the coercitivity decreases due to thermal effects and below a critical diameter Dp the coercitivity is zero, again because of thermal effects, which are strong enough to spontaneously demagnetize a previously saturated particles. This magnetic behaviour is called *superparamagnetism* (SP), Figure I- 9.

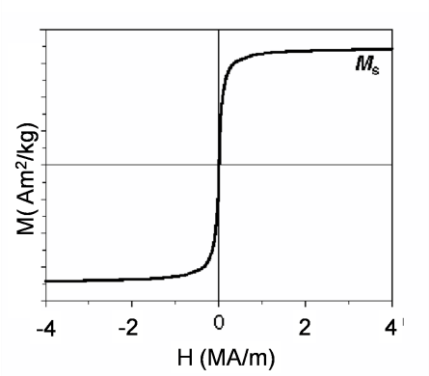

Figure I- 9: Hysteresis loop for a typical superparamagnetic material. Ms is the saturation magnetization. M is the magnetization and H the magnetic field.

When superparamagnetic particles are exposed to an external magnetic field, there will be a net alignment of magnetic moments. This is similar to paramagnetic materials, but the main difference is that in paramagnetic materials the magnetic moment correspods to a single atom, whereas in superparamagnetic material each magnetic moment corresponds to millions of atoms. Like paramagnetics materials, superparamagnets have no net magnetic moment when the magnetic field is removed, their coercitivity is zero, as it has been mentioned before.

If the volume of a SD particle is small enough or the temperature is high enough, termal energy will be sufficient to overcome the anisotropy energy making magnetic moment orientations fluctuate causing a spontaneous reversal of magnetization. This was firt described by Nèel in 1949 who pointed out that if single-domain particles became small enough, Ea (anisotropy energy), would become so small that energy fluctuations could overcome the anisotropy energy forces and spontaneously reverse the magnetization of a particle from one aesy direction to the other, even in the absence of an applied magnetic field.

τ is the relaxation time of the magnetic moment for a superparamagnet and this value can be calculated from equation:

$$\tau = \tau_0 \, e^{K_a V / k_B T}$$

Where τ_0 is the relaxation time pre-factor that determines the possible values for τ in an energy range. K_a is the density of anisotropy energy, V is the volume, K_B is the Boltzmann constant and T is temperature. At a certain temperature τ could have a high value, at this point it is said that the particle is "blocked" as the net magnetic moment is not zero in the absence of an external magnetic field. The blocking temperature, T_B, is related with the following parameters: size and composition of the particle.

The magnetization of non interacting magnetic particles in the superparamagnetism regime is given by this equation:

$$M(H,T) = n\mu L(x)$$

Where *M* is the magnetization, *n* the number of particles, μ the magnetic moment per each single domain particle and *L(x)* is the Langevin function which is (*coth x-1/x*) where $x = \mu H/kT$.

I.III. Magnetic hyperthermia

The term “hyperthermia” refers in general to an increase of internal body temperature, a phenomenon which occurs when a homoeothermic organism is not able to dissipate the heat that is being generated or acquired. Homoeothermic organisms are those who are able to regulate their internal temperature within a range of temperatures regardless environmental temperature. This phenomenon normally occurs when the organism is exposed to an external heat source.

The term “hyperthermia” within the field of clinical medicine, refers to any technique of heat application administered as an adjunct to already established strategies in the treatment of cancer patients, such as radiotherapy and chemotherapy. There are different hyperthermia approaches, but what all of them have in common is that their efficacy is not enough to replace any other of the established therapy modalities when applied alone, but they are suitable enough to enhance the cell-killing effect of cytotoxic drugs and radiation.

The use of hyperthermia treatments as an adjuvant for cancer therapies was discovered in the 80´s and it became a very useful tool due to the fact that cancer cells are more heat-sensitive than normal cells. These studies demonstrated a synergistic response to radiotherapy/chemotherapy and hyperthermia versus radiotherapy/chemotherapy alone [24-27].

Most recent Phase II trials have demonstrated that hyperthermia therapy, combined with chemotherapy or radiotherapy, is beneficial for local tumours treatment and survival in patients with high-risk tumours of several types, as colorectal cancer, ovarian

cancer, malignant pleural mesothelioma and pelvic tumours [28-31]. Maluta et al. evaluated the efects the hyperthermia (HT) combined with chemotherapy (QT) have in patiens (treated between 200 and 2008) with advanced pancreatic cancer showing that the survival rate of the group of patients treated with HT and QT was slightly higher than the group trated only with QT [32].

Concerning the area of the body where it is applied the main hyperthermia approaches are: the local/regional hyperthermia, for example, with current sheet applicators, interstitial hyperthermia that requires the implantation of microwave or RF-antennas or self-regulating thermoseeds, the Whole Body Hyperthermia (WBH) with water-filtered infra-red radiation and other hyperthermic perfusion techniques.

For local and regional hyperthermia there are results from some studies where it is shown the higher response and survival rates for patients treated with hyperthermia plus radiotherapy compared with either radiotherapy or hyperthermia alone [1, 31, 33]. There are also some trials where the efficiency of the hyperthermia combined with chemotherapy is tested, and the results strongly suggest the clinical effectiveness of both treatments [32, 34, 35]. One of the main problems of these techniques is the inhomogeneous temperatures acquired in the target region, due to inhomogeneous temperature distribution and physiological reasons.

Available data on WBH in conjunction with chemotherapy demonstrated feasibility and acceptable toxicity of this approach when radiant heat applicators are employed to induce inhomogeneous temperatures in the whole body up to 42ºC for 1h.This treatment is more invasive than the other approaches and have more toxic effects compared with local and regional hyperthermia. However WBH has the potential to treat metastatic diseases. There is some phase II trials where WBH is apply in conjunct to chemotherapy in order to treat metastatic cancers [29, 30, 36].

Another classification of hyperthermia approaches could be depending on the heat source they use and the way in which these sources release the heat in the target area. Direct heating methods by contact with a heat source, like localized transcutaneous, interstitial and intracavitary, extracorporeal circulation of hot blood in an organ and heating generalized as previously mentioned Whole Body Hyperthermia. Apart from direct methods it also exist indirect ones, heating by transmission of coherent energy relaxing locally to incoherent energy, heat, like mechanical vibration and low or high frequency electromagnetic fields.

In general, hyperthermia cell death has been shown to markedly enhance at temperatures above 43ºC, as well as, in combination with radiation and various cytostatic drugs. The effect of the temperature increase in the survival rate of a growing cell culture it is clearly distinguished a two-step process of cell killing, marked by a growth arrest at the beginning of heat exposure, reflecting a reversible, non-lethal heat damage, followed by exponential cell death [37], Figure I- 10.

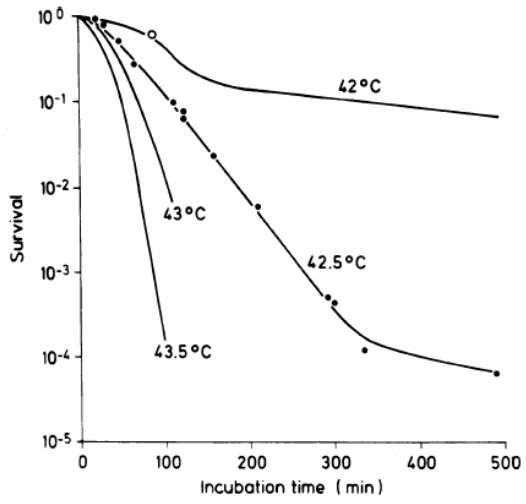

Figure I- 10: Graph that shows the dose-response relationship of thermal cell killing, [37]. At 42ºC it can be distinguished the two steps of the cell killing.

The thermal dose required to induce hyperthermic cell death varies within an order of magnitude for different cell lines [28]. The thermal dose is correlated to the thermal dose required for protein denaturation. The hypothesis has been suggested that the toxicity of the hyperthermia treatments in mainly based on denaturation of cytoplasmatic and membrane proteins in cells [38].

A general disadvantage of hyperthermia is the difficulty to selectively heat up the tumour area without damaging healthy surrounding tissue. Also, this technique cannot attack deeply localized tumours since hyperthermia devices cannot reach them. Two possible solutions for these problems could be having a tumour cell specific heating up agent, and having a hyperthermia approach with an external device that do not need direct physical contact to heat up targeted tissues by applying electromagnetic fields. Magnetic Fluid Hyperthermia (MFH) technique posses these both properties: using low frequencies magnetic fields (100-500 kHz, in radio AM waves range) that do not interact with biological tissues as they are not magnetic, and only heats up in presence of MNPs which act as focusing and heating up agents.

Hyperthermia effects in cells

When we focus on the cellular process that take place when cells are submitted to hyperthermia conditions, many cellular effects have been described.

First, hyperthermia affects fluidity and stability of cellular membranes and impedes the function of transmembrane proteins transport and cell surface receptors. However, none of these phenomena seem to be correlated with the rate of *"in vitro"* cell death [39, 40].

Furthermore, it has been demonstrated that hyperthermia induces various changes in cytoskeleton organization, like cell shape and mitotic apparatus, but as in the

previous case there is no evidence for correlation between these morphological changes and thermosensitivity in some cell lines [41, 42].

"In vitro" hyperthermia experiments between 42- 45ºC showed a dose-dependent decrease of intracellular *"de novo"* synthesis and polymerization of both RNA and DNA molecules during protein synthesis. RNA and protein synthesis recover very rapidly after the treatment, but in contrast DNA synthesis is inhibited for a longer period [43, 44]. Besides, heat shock induces aggregation of denatured proteins at the nuclear matrix due to the insolubility of cellular proteins after heat-induced protein unfolding.

Although protein synthesis is impaired under hyperthermia conditions, the situation is different for the Heat Shock Proteins (HSP), which represent a heterogeneous group of molecular chaperones. They are classified by their molecular weight in five families: small HSP (< 40KDa), HSP60, HSP70, HSP80. HSP90 and HSP100. All these proteins have the same basic functions, i.e. they bind to hydrophobic protein sequences liberated during denaturation, thus preventing them to interact with neighbour proteins and form aggregates. The expression of these proteins is not restricted to the response to elevated temperatures, but they can also be synthesized under other stress conditions as alcohols or heavy metals exposure and oxidative stress [45, 46]. HSP27 and HSP70 are supposed to represent general survival proteins, which defend cells against a variety of potentially lethal stimuli [45, 47]. In hyperthermia HSP are thought to be involved in the protection of cells against heat damage. Intracellular HSP synthesis increases when cultured cells are exposed to a moderate hyperthermia treatment (38-42ºC) [48]. However, at higher temperatures or longer expositions, inhibition of HSP synthesis occurs and an increase of apoptosis can be observed.

Concerning cell death mechanisms, a broad classification can be done in: apoptotic and necrotic cell death. Whereas necrosis is marked by a passive pathological cell

damage followed by an inflammatory response originating from the surrounding tissue, apoptosis represents a genetically controlled and active death program, contributing to maintaining tissue homeostasis. When apoptosis is decreased it can lead to cancer, on the other hand an excess of apoptosis may lead to impaired development and provoke degenerative disease in a given tissue or organism. Interestingly, most of the stimuli activating apoptosis are also able to induce necrosis at prolonged or intensified exposure [49]. It has been described that hyperthermia can induce both necrotic and programmed cell death in vitro in a temperature-depending manner. In murine mastocytoma cells between 42-45 ºC a marked enhancement of the apoptosis takes place, at 45 ºC both apoptosis and necrosis mechanisms are presented and above a 46ºC it is more likely to induce necrosis instead apoptosis [50].

Magnetic hyperthermia

Magnetic hyperthermia (MH) selectively heats up tissues by applying an alternating current (AC) magnetic field to tissues, previously loaded with MNPs. In broad terms, the procedure involves dispersing magnetic particles throughout the target tissue, and then applying an AC magnetic field of sufficient strength and frequency to make the particles heat.

Some regions of the body cannot be heated adequately with currently available hyperthermia systems or are only accessible by traumatic and highly invasive interstitial methods, due to technical and physical limitations. So that, the approach of MFH using MNPs allows to attack deep tissues and could be successful also passing some biological barriers giving the change to reach difficult accessible regions, as the brain.

The first experiments performed with hyperthermia and small magnetic particles were made in the late 50s, but most of the studies were made with inadequate animal

models and poor AC magnetic field parameters [51, 52], so that no clinical applicable results were obtained. In 1993, more than three decades later, it was demonstrated which H-field amplitudes and frequencies are tolerable in humans [53].

Based on the Brown and Neél relaxitivity, it was found, that colloidal dispersions of superparamagnetic iron oxide particles (in the *nano* range size) exhibit an extraordinary specific absorption rate (SAR) with clinical tolerable $H_o f$ (H_o magnetic field, f frequency) combinations in comparison to hysteresis loop of bigger multidomain particles (in the *micro* range size). For this reason it has been a renaissance in the last twenty years in hyperthermia as a cancer treatment method. Systematic in vitro studies were presented [54] which show consistently, that inactivation of cancer cells with AC magnetic field excited nanoparticles is equally eficient as the best homogeneous heating treatment, e.g. water bath heating. Furthermore the huge amount of new biological data on heat response of cells and tissues and the exponential development in the field of nanoscience make the approach of magnetic fluid hyperthermia (MFH) a very promising strategy as a minimal invasive modality for regional selective heat treatment at the microscopic level.

So far a technical problem with hyperthermia is the difficulty of heating the local tumour region volume to the intended temperature without inducing damage of the surrounding healthy tissue. It is the reason why many studies in selectively MNPs uptake have been made, i.e. combining an antibody against a protein overexpressed in a kind of tumour, it has has been shown *in vitro* that uptake of these nanoparticles was antibody-dependent and specific for tumour cells. So that, hyperthermia treatment affects only tumours cells, heating them up to 42,5ºC, and side effects for healthy cells were minimized [55]. Others NPS coating modification with antibodies have been performed and demonstrated selective uptake in mouse models of human breast cancer

[56]. Furthermore, modified amino-silane magnetite NPs are internalized by primary glioblastoma cells but not in normal cells *in vitro* [20].

In vitro studies with bare MNPs and cancer cells have also been performed, and the results show that after 15 minutes of magnetic hyperthermia, cancer cells heat up to 45ºC [57]. *In vivo* experiments using an intra-tumoral injection or intravenous administration of Fe-based surface modified MNPs show that about 200 μg of iron caused a significant anti-tumour affect on murine melanoma [58]. In this study surface of MNPs was modified with porphyrin, assuming that tumours cells due to their elevate sugar metabolism are in constant need of porphyrins as prosthetic groups. More in vivo studies have demonstrated the therapeutic efficacy of this form of treatment in animal models [21]. Most of the laboratory and animal model based studies reported at the beginning were characterized by the use of magnetic field conditions that could not be safely used in human patient. In most instances, reducing the field strength or frequency to safer levels would almost certainly lead to a reduction in the heat output from the magnetic material, making it useless for this application. Enough heat must be generated by the particles to sustain tissue temperatures of at least 42ºC for 30 min or so [11].

Clinical studies were started by Maier-Hauff et al [2], wherein the efficacy and tolerability of hyperthermia induced by amino-silane coated SPIONs combined with radiotherapy was evaluated in 14 patients for the treatment of recurrent glioblastoma multiforme. In 2009, Van Landeghem et al [59] presented the first post-mortem neuropathological study of three patients with glioblastoma undergoing MHT.

The physical mechanism that explains how MNPs absorb energy from the magnetic field and dissipate it to the media in terms of heat is currently under discussion. As already mentioned in the former section, two main mechanisms have been proposed: the relaxation can correspond either to the physical rotation of the particles themselves

within the fluid, or rotation of the atomic magnetic moments within each particle. Mechanical rotation of the particles is referred as "Brownian rotation" while the rotation of the magnetic moment within each particle is known as "Néel relaxation". Each of this process is characterized by a relaxation time: τ_B for the Brownian process depends on the hydrodynamic properties of the fluid; while τ_N for the Néel process is determined by the magnetic anisotropy energy of the SPM particles relative to the thermal energy. The Brownian time value is given by the following relationship:

$$\tau_B = \frac{3\eta V_H}{\kappa T}$$

where η is the viscosity coefficient of the matrix fluid, κ is the Boltzman constant (1.38 x 10^{23} JK^{-1}),T is the temperature (K) and V_H is the hydrodynamic volume of the particles.

The Néel relaxation time is given by the following expression:

$$\tau_N = \frac{\sqrt{\pi}}{2} \tau_0 \frac{\exp \Gamma}{\Gamma^{\frac{1}{2}}}$$

Where $\Gamma = K V / \kappa_a T$, with K_a as the anisotropy constant, V as the magnetic volume and $\tau_0 \sim K^{-1}$.

Both Brownian and Néel process may be present in a ferrofluid. So in a typical ferrofluid the effective relaxation time, τ, is given by:

$$\frac{1}{\tau} = \frac{1}{\tau_B} + \frac{1}{\tau_N}$$

Experimentally distinguish of which of this process predominates in each system is difficult. Theoretical considerations and some experimental results suggest that at frequencies about 250 kHz particles tend to follow Néel relaxation mechanism instead of mechanical respond, Brownian rotation [57].

I.IV. Dendritic cells

Dendritic cells were firstly identified as cells that belong to the immune system by Steinman and his colleagues in 1973 and were named as dendritic cells for their probing, tree-like or dendritic shapes, from the greek term “dendron” meaning tree [60] although skin dendritic cells were discovered previously by Langerhans in 1968, taking the name of Langerhans cells (LC).

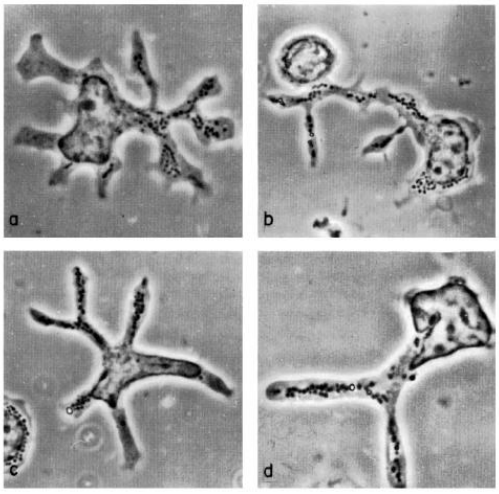

Figure I- 11: First micrographs of dendritic cells, isolated from mouse spleen. [60]

Until recent years, the low amount of DCs in the body, (1-2% of the total leucocytes), and the lack of specific markers caused problems with the purification of DCs, slowing down progress in their further characterization. These obstacles were overcome trough the *in vitro* culture of DCs using cocktails of cytokines and methods to

purify DCs. The recent availability of monoclonal antibodies have provided a reliable source of these cells so that nowadays enough DCs can be prepared from different progenitors, such as bone-marrow progenitors and mouse cell lines cultured with GM-CSF and IL-4 [61, 62].

It has become clear that DCs follow various hematopoietic pathways of differentiation and maturation, and the multiple and heterogeneous subsets of DCs vary in cell surface marker expression, Figure I- 12.

Human cord blood CD34+ hematopoietic progenitors cultured with GM-CSF and TNF-α generate a mixed cell population containing different types of DCs [63, 64]. At day five of culture two subsets of DC precursors can be identified by the mutually specify expression of CD1a and CD14. CD1a generate DCs that contain Birbeck granules, markers that are characteristic of epidermal Langerhans cells. In contrast, CD14+ progenitors mature into CD14-, CD1a+ DCs lacking Birbeck granules. Interestingly CD14+ precursors but not the CD1a+ precursors remain bipotent cells, as they can differentiate into macrophages in presence of M-CSF [64, 65].

DCs can also derive from peripheral blood monocytes cultured with GM-CSF and IL-4. Under this culture condition monocytes generate a homogeneous population of DCs without dividing, and the efficiency of this process is almost 100%. These cells have the characteristics of immature DCs that can be further induced to maturate by inflammatory stimuli such as TNF-α, IL-1 and LPS [66]. Immature DCs still express the M-CSF receptor although they loss it when they become mature DCs [67, 68]. That is to say monocytes represent an abundant source of precursors that can polarize towards DCs or macrophages, depending on the external stimuli. This polarization can be driven in vitro by the addition of appropriate cytokines (GM-CSF plus IL-4 or M-CSF), respectively.

There is also evidence for a lymphoid DC precursor capable of generating both lymphocytes and DCs that has been identified in human thymus [69, 70] and in the human bone marrow [71]. Interestingly, the lymphoid DCs develop in the absence of GM-CSF [72].

DCs derived from human monocytes that have been cultured in GM-CSF and IL-4 supplemented medium are the most commonly used in research.

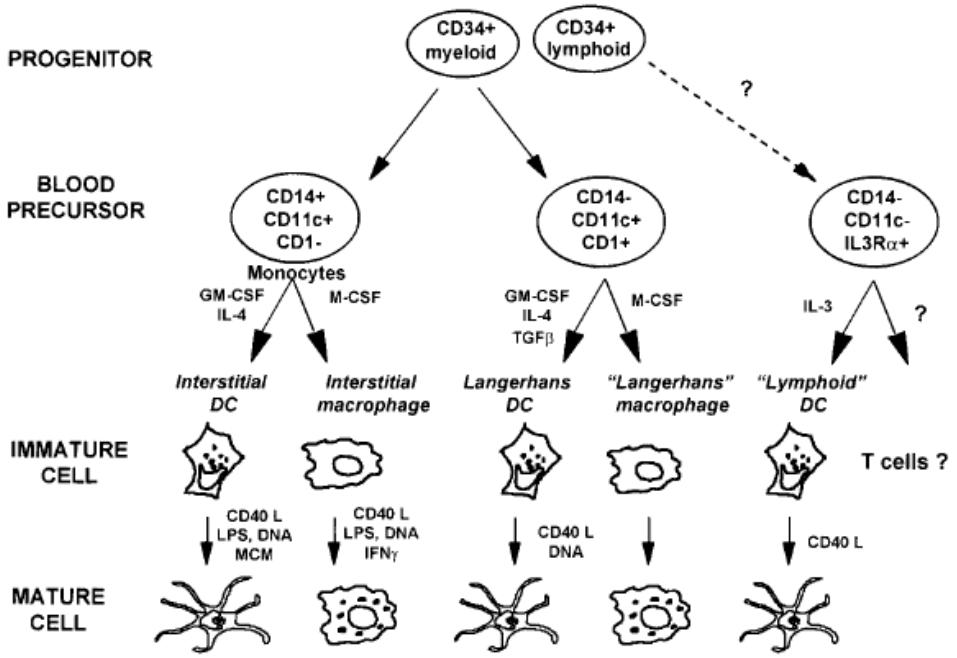

Figure I- 12: Different precursors and subsets of DCs. [73]

DCs function in immune system

DCs control a spectrum of innate and adaptive responses. Innate immunity encompasses many rapid reactions to infections [74]. Adaptive immunity, in contrast, is acquired more slowly and it has two hallmarks; exquisite specificity for antigens, and a durable memory to develop improved function on re-exposure to antigen. Adaptive responses are either immunogenic, providing resistance to infection or cancer, or tolerogenic, leading to silencing when the immune response is undesirable, like in organ transplants or during pregnancy. It has been described that immature DCs might induce regulatory T cells, thus promoting tolerance, whereas mature DCs stimulate effector T cells, supporting immunity [73, 75].

DCs serve as sentinels, recognizing the presence of invading pathogens through various pattern-recognition receptors, and become activated by microbial products to secrete proinflammatory cytokines involved in host defence, thereby linking innate and adaptive immunity [76, 77].

The diverse functions of DCs in immune regulation reflect the heterogeneous subsets with different lineages and maturity, and functional plasticity. The most important hallmark of DCs is that they are specialized to capture and process antigens [78, 79], converting proteins into peptides that are presented on major histocompatibility complex (MHC) molecules and recognized by T cells. Due to this fact DCs are considered the most important antigen presenting cells (APC).

What makes a DC such a good APC? In most periphery tissues DCs are present in the so-called “immature” state, unable to stimulate T cells. Although DCs in this state lack T-cell activation signals, like CD-40 and CD-86, they are extremely well equipped

to capture antigens that are able to induce full maturation and mobilization of DCs from the periphery tissues to the lymphoid organs.

Three different pathways for antigen internalization can be distinguished: first they can take up particles and microbes by phagocytosis, second they can form large pinocytic vesicles in which extracellular fluid and solutes are sampled, this process is called macropinocytosis, and third they express receptors such as C-type lectin receptors like the mannose receptor and DEC-205, as well as Fc receptors, that mediate adsorptive endocytosis. Macropinocytosis and antigen-mediated antigen uptake make antigen presentation so efficient that picomolar and nanomolar concentration of antigen is enough to activate the DCs and to trigger an adaptive immune response, much less than the micromolar levels required by other APCs.

There are two antigen presentation pathways (see Figure I- 13), so-called endogenous and exogenous pathways involving the presence of class I MHC and class II MHC, respectively.

a) Endogenous is the classical pathways that loads peptides from self and intracellular pathogens. Peptides are generated in the proteasome, transferred into the endoplasmatic reticulum and load into the nascent MCH class I molecules. The complex MHC I-peptide presented in the cell membrane will activate the T cells CD8+.

b) In the exogenous pathway the peptides are presented in the cell membrane with MCH class II molecules. The DC is able to produce large amounts of MHC class II-peptide complexes, due to specialized MHC class II rich compartments (MIICs), that are abundant in immature DCs [66]. Upon incorporation, antigens are subsequently degraded in endosomes, and the generated polypeptides are transported into the MIICs for their loading onto the nascent MHC II molecules while DCs mature. These compartments are late endosomal structures which enhance and edit peptide binding to

MHC class molecules. After capturing and processing antigens DCs migrate to secondary lymphoid tissues and give raise to mature DCs. During maturation MIICs convert to non-lysosomal vesicle and discharge their content to the surface. The complexes peptide-MHC II recognize and activates T cells CD4+.

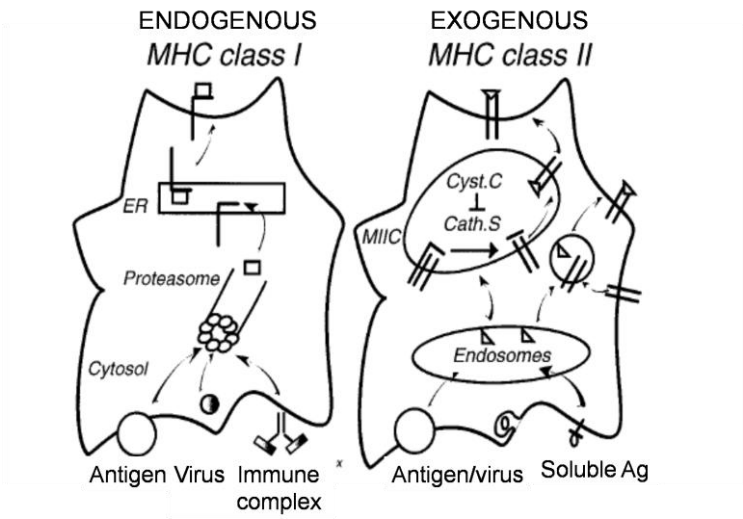

Figure I- 13: Pathways for antigen loading in major histocompatibility complex (MHC) molecules in DCs [73].

Maturation of DCs

Maturation of DCs is crucial for the initiation of immunity. Immature DCs possess high endocytic and phagocytic capacity allowing antigen capture, but express low levels of MHC class II molecules and costimulatory molecules on their surface. Following a maturation signal, immature DCs, localized in peripheral tissues, migrate to the inflammatory regions in response to the production of a large spectrum of inflammatory chemokines. Immature DCs recognize pathogen molecules patterns via pattern-

recognition receptors (PRRs), including the families of Toll-like receptors (TLR) and mannose-like receptors. After recognizing the pathogen DCs release large amounts of cytokines, resulting in the activation of the innate immune cells. Simultaneously, DCs acquire a mature phenotype, which involves (see Figure I- 14):

i. Loss of endocytic and phagocytic receptors
ii. High level expression of MHC II at the surface and increasing production of costimulatory molecules, including CD40, CD80 and CD86. Expression of CD83, which is a specific maturation marker, also increases.
iii. Mature DCs have a distinct cytokine and growth factor prolife.
iv. Changes in morphology
v. High T-cell activation capacity

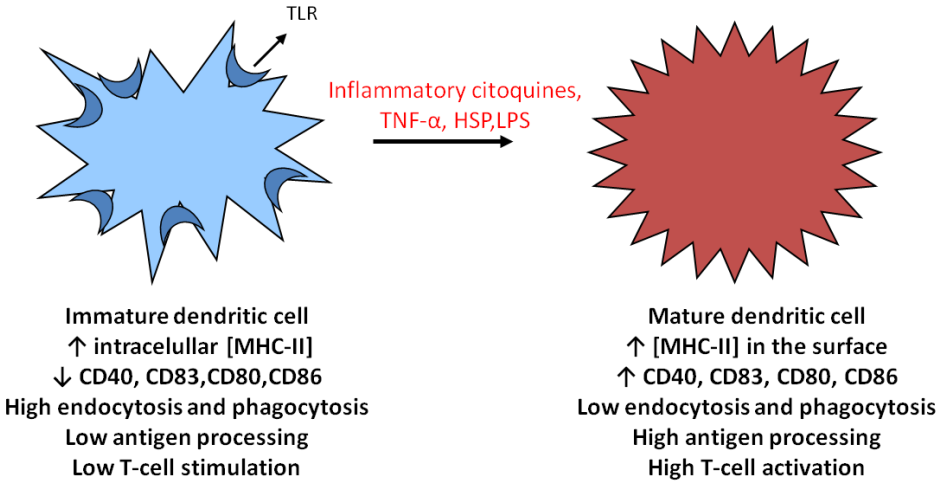

Figure I- 14: Characteristics of immature and mature DCs. TLR are the Toll-like receptors, TNF-α is the tumour necrosis factor, HSP are the heat shock proteins and LPS are the lipopolisacharides.

Consequently, mature DCs move via the afferent lymphatic into the T-cell area, where they induce their activation and differentiation into effector cells, thereby initiating primary immune responses

The ability to prime naive CD4+ T cells constitutes a unique and critical function of DCs both in vitro and in vivo through Ag-MHC class II complex presented in the DCs extracellular membrane. DCs are equalled important in stimulating naive CD8+ T cells, through Ag-MHC class I, see Figure I- 15. In the figure it can be seen that the T Cell Receptor (TCR) of CD4+ and CD8+ T cells recognizes the antigen peptides presented in the DCs membrane through MHC class II and MHC class I molecules, respectively. Also, to sustain a correct T cell activation it is crucial the interaction of the co-stimulatory molecules with their corresponding ligands expressed by T cells, specifically, CD40 binds to CD40L in CD4+ T cells and CD80 and CD86 interact with CD28 molecule expressed in CD8+ T cells.

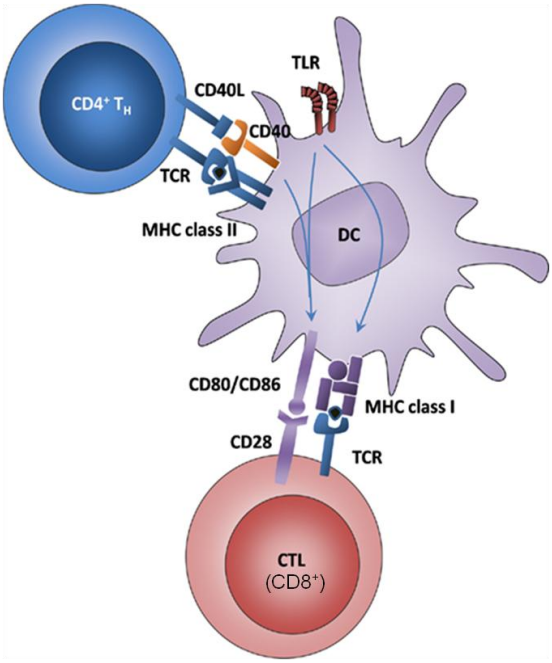

Figure I- 15: CD4+ and CD8+ activation by DCs though MHCII or MHCI molecules, respectively. TCR: T Cell Receptor, TLR: Toll Like Receptor, MHC: Major Histocompatibility Complex, CTL: Cytotoxic T Lymphocytes. CD40 and CD80/CD86 are costimulatory molecules of the DCs and CD40L and CD28 are their ligands molecules presented in CD4+ and CD8+ cells, respectively.

Recognition of MHC-peptide complexes on DCs by Ag-specific TCRs constitutes one signal in DC-T cell interaction. DC-T cell clustering is mediated by several adhesion molecules, like integrins and members of the immunoglobulin superfamily.

Furthermore, when DCs become mature they can produce IL-12, a key cytokine for the generation of Th1 responses [80], and also a wide variety of cytokines and growth factors. DCs subsets may provide T cells with different cytokine/molecule microenvironments that determine the class of immune response. All these signals are essential in order to activate T cell, Figure I- 16. If any of them is absent T cells die and there is no immune response.

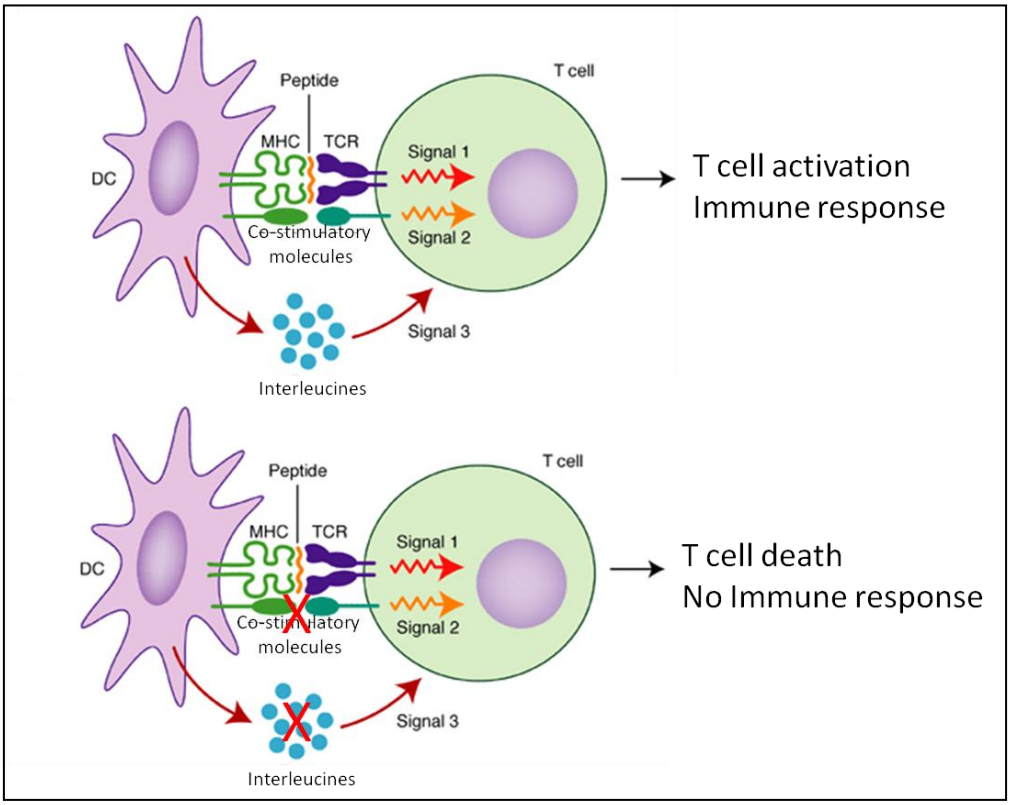

Figure I- 16: Scheme about the signals needed for T cell activation. MHC: Major Histocompatibility Complex and TCR: T Cell Receptor.

Although the primary biological function of DCs is the triggering of specific immune response, DCs can also: regulate inflammatory responses through cytokines and chemokines release and kill bacteria and regulate angiogenesis [4]. DCs express a wide array of pro- and anti-angiogenic mediators that belong to distinct families and can modulate neovascularisation by different mechanisms of action.

It is well known that cytokines such as IL-12 and TNF-α, which are produced by DCs, can stimulate CD4+ T-cells (T helper cells, T_H cells) towards a pro-inflammatory T helper 1 (Th1)-cell fate. Th1 immune response is a pro-inflammatory response responsible for killing intracellular microbes and also related to the autoimmunity diseases. On the contrary, others interleukins such as IL-10 and IL-4 are associated with anti-inflammatory responses, Th2 immune responses, which are responsible for killing extracellular parasites and are related to the promotion of IgE and eosinophilic responses typical from the allergy. It has been shown that some mediators, such us histamine, added with LPS to a monocyte derived DCs culture, reduces IL-12 and enhances IL-10 production, promoting Th2 responses [81].

In physiological conditions in the human body there is a balance between pro-inflammatory and anti-inflammatory responses (Th1 and Th2 responses, respectively). However, in the case of autoimmune diseases or severe allergies, Th1 or Th2 type of response has gained the control of the system. The nature of the cytokines that are produced by the DCs in response to a particular pathogen is a key factor in the nature of the immune response that is triggered.

DCs in tumors

Many tumour components do not elicit an antigen specific T cell response in patients. Nowadays it is known that tumours are neither good inducers of T-cell responses nor good targets for these responses. They often have defects in antigen-processing machinery [82]. It has been shown that DCs that infiltrate colon and basal-cell skin cancers can lack the costimulatory molecules CD80 and CD86 [83], and therefore have reduced T cell stimulatory activity. Likewise, tumours may release factors, such as IL-10, IL-6 and VEGF (vascular endothelial growth factor) creating an immunosuppressive microenvironment in which DC development and function is reduced [84, 85]. Tumours usually contain fewer mature DCs than corresponding healthy tissues [86], and instead have an abundance of immature DCs [87]. This opens new avenues for immunotherapy against tumours-based in DCs antitumor vaccines [88, 89]. The major goal is to induce or up-regulate T cell-mediated tumour-specific immune responses, generating tumour-specific CTLs as well as helper T cells capable of targeting the tumour.

Some approaches for cancer therapy, involving the use of DCs and magnetic hyperthermia, have been proposed. HSP70 expression during and after magnetic hyperthermia application using MNPs induces anti-tumour immunity against the T-9 rat glioma [90], enhances antigen uptake [91] and induces DCs maturation [92, 93]. It has been also reported that intratumoral injection of immature DCs induce anti-tumour effects, relying on antigen loading of DCs *in situ* [94, 95]. Taking into account these two ideas, it has been proposed that injection of DCs directly into tumours can release HSP70 after MNPs assisted hyperthermia and consequently induce an immune response [96].

Not only is the immune response-induction capability important in DCs-based anti-tumours therapy but also their implication in angiogenesis. Tumour angiogenesis refers to the formation of new blood vessels and is a crucial step in tumour development as tumours have to establish a blood supply in order to grow and metastasize. Tumour cells were first thought to control the process that take place at cellular level in tumour angiogenesis. Nevertheless, nowadays it has been shown that bone marrow-derived myeloid cells, such as macrophages, neutrophils, eosinophils, mast cells and dendritic cells have an important role in regulating the formation and maintenance of blood vessels in tumours.

Dendritic cells stimulate angiogenesis by secreting angiogenic factors and cytokines, promoting the proangiogenic activity of T lymphocytes, and trans-differentiating into endothelial cells [97]. Some studies have shown that tumour-derived iDCs exhibit simultaneously expression of both DCs and endothelial markers. These cells are able to assemble into blood vessels in vivo experiments [98]. Moreover incubation of these cells in presence of proangiogenic factors, such as VEGF (vascular endothelial growth factor), make DCs trans-differentiate into endothelial-like-cells [99, 100]. DCs and ECs (endothelial cells) are closely related, there is evidence for a phenotypic overlap between monocyte-derived DCs and microvascular endothelium cells [101]. So, DCs seem to have an important role in angiogenesis not only through their potent ability to secrete cytokines but also through trans-differentiation into ECs.

As it has been previously mentioned, DCs are able to capture antigens, and also whole microbes [102], microparticles [103] and nanoparticles [104]. Combination of the idea that DCs can trans-differentiate into ECs in presence of proangiogenic factors secreted by the tumour and then assemble into blood vessels that irrigate the tumour, with the fact that DCs have been reported to be able to uptake different kind of micro

and nano-particles, make them a potent tool for magnetic hyperthermia-based cancer therapy. The main strategy would be to upload the DCs with MNPs and use them as Trojan Horse to carry the MNPs to the tumour area. DCs, one there, could transdifferentiate into endothelial-like cells and take part of the new blood vessels. Exposing the tumour region to an alternating magnetic field only the cells that contain the MNPs would be suitable to die and subsequently to induce damage in the tumour vasculature triggering tumour regression.

I.V. Magnetofection

Transfection and transduction are classical terms that refer to the process of supplying nucleic acids into cells, by using non-viral or virus-mediated DNA transfer methods, respectively.

After many years of research the introduction of nucleic acid into cells is an extended field of investigation. For this purpose different vehicles for nucleic acid can be used, known as viral and non-viral vectors. This kind of approaches has some limitations, as the multiple barriers that the vector has to overcome to access the target cells and the internalization at the specific location in the intracellular medium.

Virus have naturally evolved and are able to overcome all barriers at cellular level; whereas, non-viral vectors are designed to mimic viral functions to be able to act in a similar way, achieving similar efficiency. Besides, there are some differences between this two means for nucleic acid delivery. Viral vectors typically offer higher transduction efficiency and long-term gene expression, but toxicity, immunogenicity, restricted target cell specificity and high cost constitute a serious drawback for an

extended use. Non viral methods have become widespread because of their relative safety, capacity to transfer large genes, site-specific and their non-inflammatory, non-toxic and non-infectious properties. However, the clinical use of non-viral methods is limited by their low transfection efficiency and their relatively poor transgene expression.

In this thesis we will focus on the transduction, based in the use of viral vectors for gene transfer. There are several distinct types of viral vectors that are commonly used for gene transfer, like retroviruses, adenoviruses and Herpes Simplex virus. Adenoviral vectors are excellent vehicles to transfer genes into a wide variety of cell types due to their ability to transduce dividing and non-dividing cells, their growth efficiency at high titers and their large insertion capacity. These characteristics motivate their use to form magnetic complexes for magnetotransduction.

The first step to initiate a successful transduction-transfection process is the vector contact with the target cell. The probability of this event depends on the vector concentration in the culture medium, and is limited by diffusion under cell culture conditions. Some techniques, as aggregation and precipitation of nucleic acid and also centrifugation, are commonly used in order to increase the vector-target cell contact and thus, increasing the transduction-transfection efficiency. However, some of them are not suitable for being used in *in-vivo* experiments. For this reason, another technique based on using magnetic complexes formed with the DNA transfer vector and MNPs has been developed, it is called magnetofection.

The term magnetofection is defined as nucleic acid delivery under the influence of magnetic field acting on nucleic acid vectors, which are associated with MNPs [105]. The aim of this technique is to achieve therapeutic benefit by improving specificity and avoiding side effects by using magnetic fields to localize magnetic-nucleic acid-vector.

This procedure enhances the interactions between the target cells with the gene transfer vectors [106]. The motivation for using magnetic fields to localize the vectors is the same as in magnetic drug targeting, where active agents are associated with magnetic particles and are accumulated at the target site by a suitable magnetic field. It has been proved that, in animal studies, magnetic drug targeting worked even when the drug application point was far from the target site [107, 108] and that magnetic carriers are well tolerated.

In magnetofection naked nucleic acid or gene vectors are bound to magnetic micro or nano-particles, so size, charge, magnetic responsiveness, biocompatibility and stability of magnetic delivery complexes are relevant parameters to be considered [109]. Figure I- 17 shows the magnetic adenoviral complexes structure and also the schematics of the magnetofection approach, where a magnetic field is used to accumulate nucleic acid vectors at the target cells, improving the transduction efficiency.

The first report about this technique that appears in the literature was in the year 2000 [110] and from then on many groups have been working in order to develop this method and nowadays reagents needed for magnetofection are commercially available. It has been shown that the cell uptake mechanism of the nucleic acid does not change when using magnetofection [111]. The improving rate in transduction-transfection efficiency when using magnetic forces, is just due to the highest contact between gene delivery vector and target cells. Many researchers corroborate that magnetofection is suitable for different kind of nucleic acids, such as plasmid DNA, mRNA and siRNA, and for different kind of vectors, viral and non-viral vectors. It is also known that it works for a wide variety of cell types [112]. Taking all these ideas into consideration magnetofection is considered nowadays a very promising therapy application.

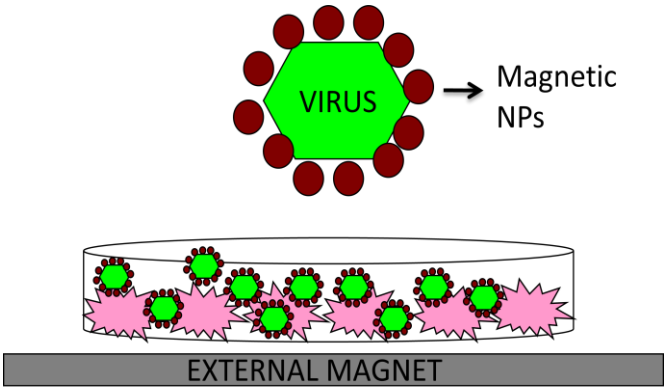

Figure I- 17: Representation of the adenoviral-magnetic complexes and the principle of the magnetofection approach where cells are infected with the adoviral-magnetic complexes in the presence of an external magnetic field to enhance the contact of the virus with the cells and consequently the transduction efficiency.

All the experiments performed in this thesis related to magnetofection constitute a novel approach based on the design of a magnetic adenoviral vector and employ a magnetic field-assisted transduction. This approach will be applied to transduce neurons in order to enhance the levels of neurotrophic factors that prevent their degeneration.

Neurodegenerative disorders such as Alzheimer´s and Parkinson´s diseases are of major concern for public health as the world average population´s age increases. Thus, the development of novel therapeutic strategies for these disorders, like the proposed gene therapy, constitutes an issue of great importance. Neurotrophic factors that prevent the degeneration and enhance recovery of remaining neurons are of clinical interest for neurodegenerative disorders. Among these factors, Glial cell line-Derived Neurotrophic Factor (GDNT) and Insulin-like Growth Factor (IGF-I) are emerging as powerful neuroprotective molecules for the treatment of neurodegenerative pathologies affecting both motor and cognitive functions.

The efficiency of either viral or non-viral vectors for therapeutic gene delivery into the brain still remains as one of the limiting factors to be overcome, due to the presence of biological barriers as the Blood Brain Barrier (BBB). In fact, in spite of the several

protocols for nucleic acid delivery currently in use, both the efficiency and specificity of nucleic acid delivery are far to be achieved [109]. In order to increase the efficiency of this method it should be necessary to increase the concentration of adenovirus at the neighbourhood of the target cells. This will increase the possibilities of the adenovirus to reach the cells and thus, the DNA delivery success.

In this context, the association of MNPs with viral vectors emerges as a promising avenue for the development of highly effective gene delivery tools, since combined MNP-RAd vectors could take advantage from an efficient cell entry and transduction by viral vectors and the use of magnetic forces to increase concentration of the virus around the cells which lead to an increased virus-cell contact at the target site. As mentioned, the vector concentration in the vicinity of the cells is a key parameter in order to accelerate and increase internalization into target cells.

The adenoviruses we have worked with encoded for GFP protein, a very easily detected protein due to its green fluorescence. In this thesis no results about neurotrophic factors expression are shown yet.

II. Materials & Methods

The two approaches that constitute the experiments of this thesis are: DCs interaction with MNPs and their used in magnetic fluid hyperthermia, and magnetotransduction of neuronal and glial cells using magnetic complexes formed between MNPs and adenovirus. As these two parts of the work could be treated as well differentiated and solid blocks we have divided the chapter of material & methods in two sections, one related with the DCs and the other related with the magnetotransduction.

II.I. AMF experiments in dendritic cells

In this part of the chapter II we will describe the protocols and techniques that have been used for the experiments concerning the DCs. Specifically, physical and magnetic characterization of the MNPs were made. MNPs toxicity study was performed using various techniques and DCs maturation state was determined after the incubation with MNPs. Besides, the amount of MNPs incorporated per cell was quantified with a magnetometer SQUID and flow cytometry experiments determined the NPs uptake profile in DCs. Exposure of MNPs-loaded DCs to an AMF is also described in detail. Various electronic and light microscopy techniques were used to determine the morphology of the cells and the localization of the MNPs inside the DCs. Finally, HSP70 protein determination was made by Western Blot in DCs after the AMF exposure.

II.I.I. Magnetic nanoparticles

Nowadays the experience of MNPs synthesis has enormously increased in our group and different kind of them are being synthesized, like cubic Fe_3O_4 NPs and cobalt-ferrite based NPs [113]. However, as the power absorption experiments were the main goal for this part of the work related to DCs, we decided to begin with commercial nanoparticles (Micromod Partikeltechnologie GMBH) and leave the use of house-made ones for further experiments. Actually, some experiments with some types of non commercial NPs were made and the ones that worked better were the ones from Micromod giving results that were in concordance with other authors.

Magnetic hyperthermia experiments were performed on commercial MNPs from 20nm to 250 nm hydrodynamic ratios. Different surface groups/molecules, such as carboxylic groups, amino groups and BSA protein, were chosen. All these MNPs were composed of a magnetite core (Fe_3O_4) coated with a properly functionalized dextran shell. The absorption efficiency of a set of 18 different types of MNPs was tested. As the final goal was to induce cell death by the application of an AMF, we determined the specific power absorption (SPA) in order to identify samples with a maximum heating efficiency.

The SPA of the pure colloids was measured with a house-made ac field applicator (described in page 76) at f = 260 KHz and fields amplitude from 0 to 12.7 kA/m. The applicator was equipped with an adiabatic sample space (~0,5 ml) for measurements in the liquid phase. After SPA measurements two different MNPs (Figure II- 1) were chosen to work with, both with a hydrodynamic ratio of 250nm that consists of a 20nm magnetic core and a dextran coating. One of them was functionalized with amino

groups that resulted in nanoparticles with a positively charged surface, and the others had carboxylic groups providing negative charge in the surface.

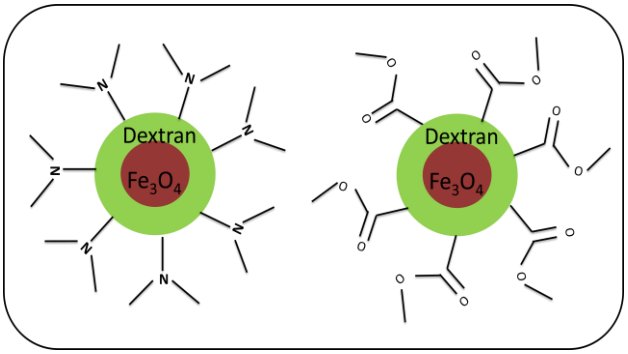

Figure II- 1.Representation of commercial MNPs from Micromod Partikeltechnologie GMBH. (Left) MNPs functionalized with amino groups,NH_2(MNPs)+, and (right) MNPs with carboxylic groups at the surface, COOH(MNPs)-.

Another kind of commercial nanoparticles was chosen (Figure II- 2), consisting of a polystyrene rhodamine derivate core, with a hydrodynamic ratio of 250nm and functionalized with carboxylic groups. These NPs were used for intracellular localization analysis made with confocal microscopy, a technique that requires NPs marked with a fluorescent molecule. Diameter and charge of both carboxylic MNPs and carboxylic fluorescence nanoparticles was the same, so that, cell internalization mechanism and efficiency was supposed to be similar.

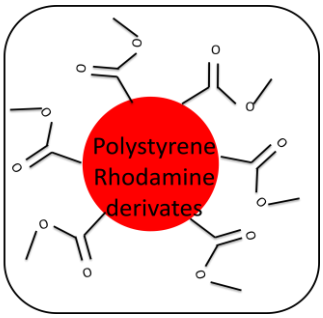

Figure II- 2. Representation of commercial fluorescent nanoparticles from Micromod Partikeltechnologie GMBH functionalized with carboxylic groups.

Some nanoparticles data were provided by the manufacturers (Table II- 1):

Product name	Surface	Size (nm)	PI	Ms (1000 Oe)	Solid content	Excitacion	Emission
Nanomag ®-D	NH2	250	< 0.2	43 emu/g	10 mg/ml	-	-
Nanomag ®-D	COOH	250	< 0.2	43 emu/g	10 mg/ml	-	-
Micromer®-redF	COOH	250	<0.2	-	25 mg/ml	552 nm	580 nm

Table II- 1.Data of the commercial nanoparticles provided by the manufacturers, i.e. surface composition, size, polydispersity index, saturation magnetization, solid content and excitation/emission wavelength. Nanomag®-D (NH_2): NH2(MNPs)+, Nanomag®-D (COOH): COOH(MNPs)- and Micromer®-redF: Rho-NPs.

Particles size distribution profile of all the NPs was measured using dynamic light scattering. Nanoparticles were diluted at the rate 1:200 in distillate water that was just filtered through a 0,2μm filter, in order to remove dust particles. Measurements were made in a N5 Submicron Particle Size Analyzer (Beckman Coulter) and data was represented in terms of intensity. All samples were measured at least three times.

In order to study average size, distribution and morphology of MNPs, transmission electron microscopy was carried out using a FEI Tecnai T20 microscope and operating voltage of 200 KV. A drop of both COOH and NH_2 MNPs solution was placed onto a carbon coated copper grid and the solvent was air-dried. The average particle size and distribution was evaluated by considering 200 particles.

The magnetic characterization of these two colloids was performed in a commercial superconducting quantum interference device (SQUID) magnetometer (Quantum Design MPMS-XL) as a function of a steady magnetic field and temperature. Pure colloids were measured conditioned in sealed sample holders with 200 μl of capacity.

ZFC/FC cycles were measured between 10 and 250K to avoid the melting of the frozen liquid carrier at 8 kA/m. Hysteresis loops M (H) were performed at 250 K and 5K in liquid samples under applied magnetic field up to 4 MA/m.

II.I.II. Dendritic cells culture and MNPs loading

As it has been previously mentioned there are several protocols to obtain DCs. Among all of them we decided to obtain DCs by differentiation of monocytes in a culture medium that contained GM-CSF and IL-4 [66], since the number of DCs that can be obtained though this procedure is higher than with the others methods. The source of monocytes was human buffy coats, which is the fraction of the blood that contains most of the white blood cells and platelets. From each 500mL of blood a fraction of 50mL of buffy coat is obtained. Buffy coats were provided by "Servicio Científico-Técnico de Cultivo Celular" from "Instituto Aragonés de Ciencias de la Salud".

Peripheral blood mononuclear cells (PBMCs) were isolated from buffy coats by Ficoll density gradient (Figure II- 3), with a ratio 2:1 in volume (buffy coat:Ficoll) (*Ficoll Histopaque-1077 Sigma*), by centrifugation at 1400 rpm for 25 minutes. Mononuclear cells, which are localized in the inter-phase ring, were collected trying to avoid erythrocytes and Ficoll contamination. Cells were then washed twice with PBS for 7 minutes at 1200 rpm at room temperature. To remove platelets, cells were centrifuged 10 minutes at 800 rpm.

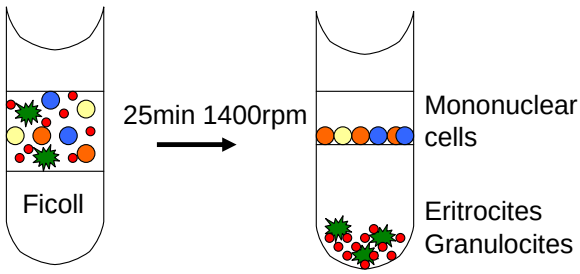

Figure II- 3: Squeme of the gradient centrifugation to separate mononuclear cells from erythrocytes and granulocytes.

Cells were resuspended in 200 µl of binding buffer (PBS pH=7.2 2nM EDTA,) and 40 µl of anti-CD14 magnetic beads (*CD14 Microbeads, Miltenyi*) were added and incubated for 20 minutes at 4ºC. After that time, 1 ml of binding buffer was added and CD14+ cells were isolated by positive immunoselection using a MACS separator (*Miltenyi*) as described by the manufacturer (Figure II- 4). It was very important the binding buffer to be degassed, otherwise the flux could be reduced due to blockage.

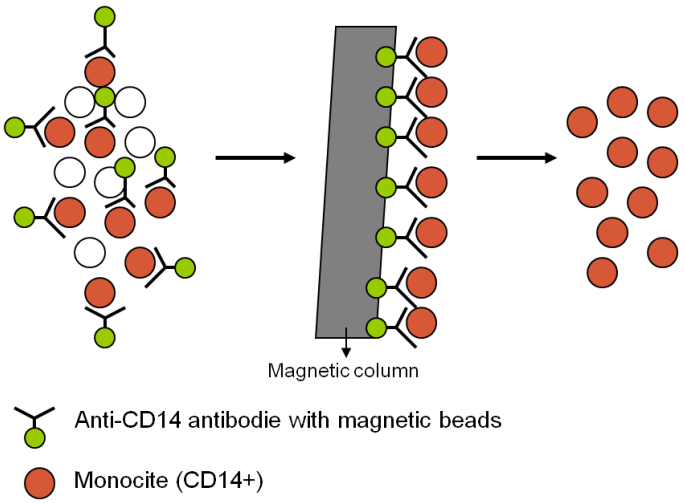

Figure II- 4:Representation of the positive magnetic isolation of monocites from the ononuclear cells using anti CD-14 magnetic beads.

In T75 flask, CD14+ positive cells (10^6/ml) were cultured in RPMI 1640 (*Sigma*) with 10% FBS, 1% glutamine, 1% antibiotics (100 U/ml penicillin and 100 ng/ml streptomycin) and supplemented with IL-4 (25 ng/ml) and GM-CSF (25 ng/ml)(*Sigma*). Cells were cultured at 37ºC with 5% CO2 in a humidified atmosphere for 5 days. Every 2 days, medium was replaced by fresh medium containing the same concentration of interleukins.

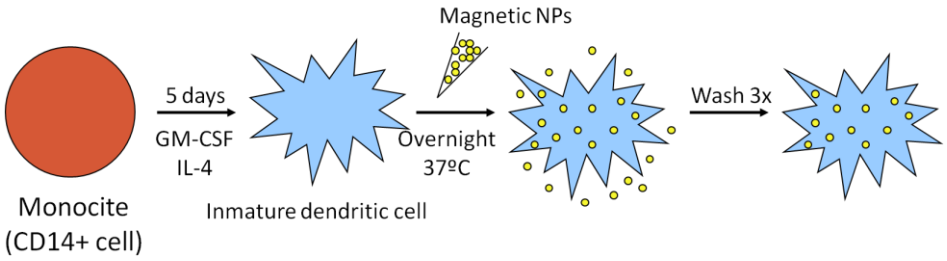

Figure II- 5: Schee of the monocyte differentiation into immature DCs and further MNPs incorporation process. GMCF: granulocyte-macrophage colony-stimulatory factor and IL-4: interleukin 4.

Dendritic cells phenotype was characterized by staining with fluorochrome-labelled antibodies against CD14, CD11c, HLA-DR, CD40, CD80, CD83, CD86 and DC-SIGN. Flow cytometry analysis was performed with the FACScalibur cytometer and FACSDiva software.

On day 5, loosely adherent cells and non-adherent cells were collected from the T75 flask. Cells were washed twice and seeded onto a 12-wells plate at 10^6 cells/ml in complete medium supplemented with IL-4 (25 ng/ml) and GM-CSF (25 ng/ml). Nanoparticles were added to the medium in the desirable concentration and incubated with the DCs at 37ºC overnight (Figure II- 5). The following day, DCs were collected and washed 3 times with culture medium by centrifugation at 800 rpm for 10 minutes

each, in order to remove all the nanoparticles that had not been internalized. After that DCs were ready to use for further experiments.

II.I.III. Viability assay

In this thesis, three different methods were used to determine cell viability after NPs incorporation: MTT, Trypan Blue and annexin-propidium iodide staining. Since each of them is based in different mechanisms related to cell death, resulting data complement each other and give a general idea about the type of cytotoxicity induced by the used MNPs.

The cytotoxicity of both COOH- and NH_2+ colloids (with nominal concentration of 10 mg/ml) was evaluated at the concentration of 50 μg/ml. Cell viability was measured on days 1, 3 and 5 after MNPs addition: MTT, Trypan Blue and Fluorescence Activated Cell Sorting (FACS) using annexin-propidium iodide markers were used. For that purpose DCs at day 5 were collected and counted in a Neubauer chamber. Cells were seeded in 27 wells in 24 well-plates, each well containing 1,5 10^5 cells in 1,5 mL of culture media. 9 wells (3 wells for each day of analysis) were kept as control containing only DCs; in other separate 9 wells, DCs and COOH- particles were added at the same time and finally in other 9 wells DCs and NH_2 particles were mixed. DCs were maintained at 37ºC.

A. MTT

MTT cell viability assay, also called as Mossman test, is a method for cell proliferation and viability measurements based on the reduction of the tetrazolium salt

3,[4,5-dimethylthiazol-2-yl]-2,5-diphenyltetrazolium bromide (MTT). MTT is reduced to insoluble formazan crystals by dehydrogenase (DHO) mitochondrial enzymes from live cells in NADH dependent reactions, Figure II- 6.

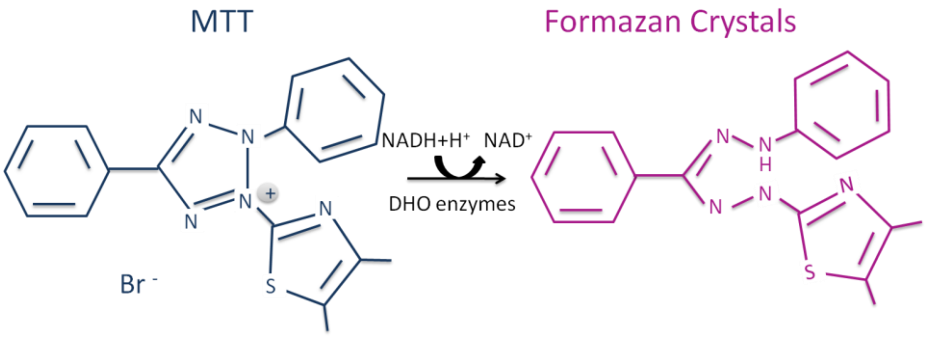

Figure II- 6: Representation of the MTT reduction reaction carried out by dehydrogenase (DHO) mitochondrial enzymes.MTT: 3,[4,5-dimethylthiazol-2-yl]-2,5-diphenyltetrazolium bromide.

For MTT cell viability assay, 10^5 dendritic cells were taken from each sample after washing and placed in a 96 well-plate in 100 µl of culture medium and 20 µl 5mg/mL MTT were added each well. Cells were incubated for about 2 hours at 37 ºC in CO_2 incubator. After this time, purple formazan crystals can be observe and plates were centrifugated at 2500 rcf for 25 minutes in order to sediment the cells and the crystals that could be released to the medium. Supernatants were removed and the resultant formazan crystals were dissolved in 200 µl dimethyl sulfoxide and the absorbance was measured by an ELISA reader at 550 nm. Each assay was repeated three times. The percent viability was calculated as:

$$\%\ Cell\ Viability = \frac{D.O.sample}{D.O.\ control} \times 100$$

B. Trypan Blue

Trypan Blue is a vital stain used to dye selectively dead cells, Figure II- 7. Cells are very sensitive about the cells that pass through their membrane, while they are live cells they have their plasmatic membrane intact and the trypan blue molecule cannot enter. However when membrane damage takes places due to the cell death, the dye enters and cells can be observed dyed in blue. As live cells are not dyed this method is classified as a dye exclusion method.

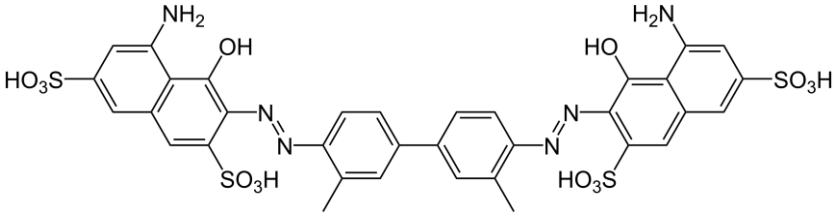

Figure II- 7: Trypan Blue molecule

For cell viability measurement with Trypan Blue 30 µl of cell suspension was diluted with 30 µl of a 0.4% Trypan Blue solution. 10 µl of the resultant solution was placed into a Neubauer chamber an observed under a direct bright field microscope. Blue cells were counted as died cells and cells without dye incorporation were counted as survival cells. Percentage of viable cells was calculated as:

$$\%\ Cell\ viability = \frac{Non\ dyed\ cells}{Total\ cells} \times 100$$

C. Annexin-V and PI measurements by FACS

Annexin-V is a protein very widely used to detect cells undergoing apoptosis. At the beginning of programmed cell death mechanism the translocation of the

phosphatidylserine in the plasmatic membrane takes place. Annexin-V binds to the phosphatidylserine molecule when it is exposed to the extracellular media, Figure II- 8.

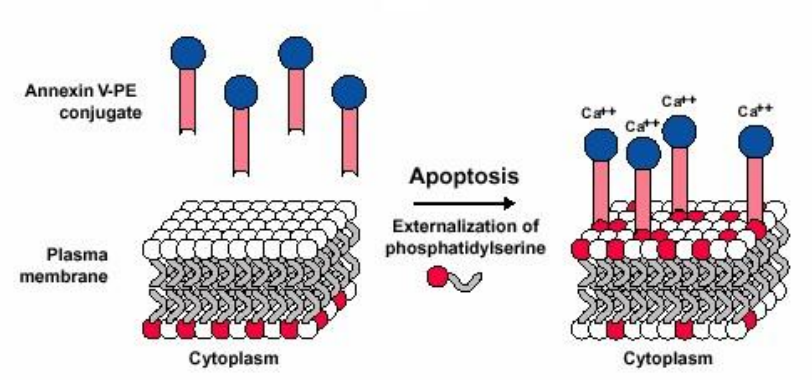

Figure II- 8: Schematic representation of the Annexin V assay.

Furthermore, propidium iodide (PI) molecule is also used to detect any plasmatic membrane damage, due to the fact that this molecule is able to enter into cell only when the membrane is disrupted. This process takes place in necrosis instead apoptosis mechanism.

The use of these two markers is very useful in order to differentiate the cells death mechanism. Apoptotic cells should be positive for Annexin-V, which corresponds to the translocation of the Phosphatidylserine protein, and negative for PI since in the early apoptosis there is no any membrane damage. However, necrotic cells are positive for PI, as the membrane damage is typical for this cell death mechanism, and could be negative or positive for Annexin, depending on the membrane disruption level. Annexin molecule is bigger than the PI and if the membrane is enough destroyed Annexin could enter the cell and bind to the Phosphatidylserine protein even in the cytoplasmatic side.

A commercial kit was used to label the cells with both Annexin-V and PI fluorescence molecules (*Annexin V FITC kit, Immunostep, Spain*). 10^6 cells were

resuspended in 1ml of binding buffer (10 mM Hepes/NaOH pH=7.4 140nM NaCl and 2.5 mM $CaCl_2$). 5 µl of Annexin V-FITC and 5 µl of PI were added to 100 µl of cell suspension and incubated for 15 minutes at 4ºC in darkness.

After incubation time, cells were spun down, supernatants were removed and cells were resuspended in 100 µl of 2% Paraformaldehyde (PFA) containing x mM of $CaCl_2$. Incubation of 15 minutes at room temperature was necessary for cell fixation. After that time cells were again spun down and after removing the fixation solution cells were resuspended in 500 µl of binding buffer.

Once all the samples were prepared, cell viability was checked by flow cytometry using a FACSAria cytometer and FACSDiva software.

The results are represented in dot plot graphs, where the red fluoresnce intensity is represented versus the green fluoresncence intensity having four quadrants. The cells that formed the population in the left-low quadrant were cells negative for both Annexin-V and PI, so corresponded to living cells. The population of the right-low quadrant corresponded to cells that were positive for the Annexin V, so positive for the phosphatidylserine serine translocation, and negative for the PI, i.e. cells in early apoptosis. Population in the left-up quadrant corresponded to cells negative for Annexin V and positive for PI, so they were cells at the beginning of a necrotic death mechanism. Finally, population in the right-up quadrant corresponded to cells positive in both Annexin V and PI markers, thus theses cells were in a late necrosis or in a late apoptosis.

II.I.IV. Maturation markers expression measurement by FACS

The analysis of the maturation status of the DCs before and after the incorporation of MNPs was another point of study in this work. The aim of these experiments was to determine how the MNPs incorporation affects the DCs functionality. Thus, membrane molecules profile of DCs was studied by FACS using fluorochrome-labeled antibodies that recognize the molecules of interest.

Human-monocyte derived DCs at day 5 of culture were counted and 10^6 cells, resuspended in 1ml of culture medium supplemented with IL-4 and GMCSF, were placed each well in a 24-well-plate and co-cultivated with COOH NPs at various concentrations (0.05 mg/ml, 0.15 mg/ml and 0.3mg/ml) for 48h at 37ºC. Lipopolysaccharide (LPS) induced mature dendritic cells were used as positive control. Maturation of DCs was determined by assessing the expression of co-stimulatory and maturation markers.

For FACS analysis, the following monoclonal antibodies were used: CD14, CD45 (BD Bioscience, San Jose, CA), CD11c (eBioscience, San Diego, CA), CD40, CD83 and CD86 (Invitrogen, Carlsbad, CA), DC-SIGN and CD1a.

10^5 cells were suspended in 50ul PBS 2mM EDTA and were stained with 5ul antibodies for 15 min in darkness at room temperature. After incubation time, samples were diluted with 0.5 ml of PBS 2mM EDTA and the fluorescence was measured in a FACSCalibur (Becton, Dickinson and Company, NJ). Fluorescence data were analysed with FACSDiva software and expressed as percentage of positive cells. Also the FSC and SSC data obtained by FACS were collected and taken into account in the results.

II.I.V. Cytokines expression analysis

Maturation state of the DCs was also investigated determining the cytokines expression profile. Multiple analyse was performed by flow citometry (Luminex) to obtain the concentration of the cytokines of interest in the supernatant of the cells culture.

Multiple analysis by flow citometry is based in the binding of different antibodies to latex microspheres (3-4 μm) which are dyed with different amounts of two different dyes generating 96 different colours. Each colour latex microsphere type is bound to one antibody, Figure II- 9 and Figure II- 10.

When the samples are analyzed by the Luminex, first samples pass though a red laser which identifies the colour of the sphere and subsequently the antibody and later the sample is excited by a green laser which determines the amount of analyte bound to the antibodies that is proportional to the amount of analyte presented in the sample.

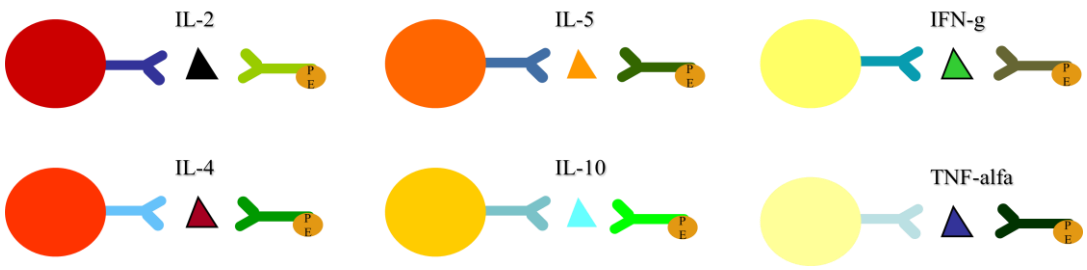

Figure II- 9: Schematic examples for the detection of some molecules. Each cytokine type is recognized by an antibody linked to a microsphere of a particular color, which identifies the cytokine type, and by another antibody linked to a fluorescence molecule that quantifies the cytokine concentration.

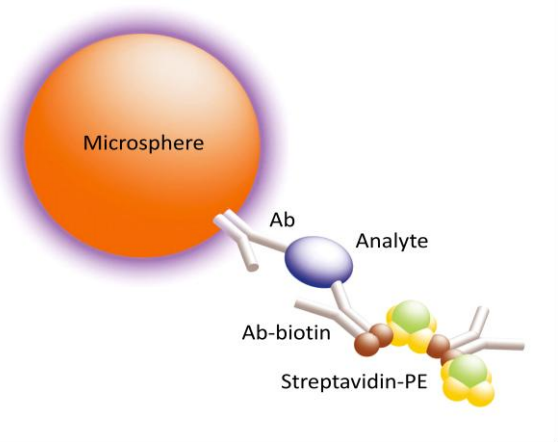

Figure II- 10: Representation of the immune-complex microsphere.

For the quantification of the amount of cytokines released by the DCs incubated with nanoparticles after 48h incubation, supernatants were removed and kept at -20ºC until all the samples were collected. Incubations with different amounts of MNPs were tested, 0.01, 0.02, 0.05, 0.15 and 0.3mg/ml.

To determine the cytokines expression it was used a commercial kit prepared to determine IL-6, IL-10, IL-2, IL-4, IL-15, IL-12, TNF-α, INF-γ and VEGF expression (Ref).

Firstly, standards and controls were reconstituted as described the kit protocol. The standards, controls and samples were incubated with the spheres covered with the antibodies at 4ºC overnight. Plate was centrifugated at 2000 g 5 minutes and the supernatants were discarded. Then two washes with the wash buffer were made and spheres were resuspended with the solution that contained the antibodies incubating the plate 2h at room temperature. Without washing the streptavidin bound to ficoeritrine (PE) was added and incubated 1h at room temperature. Then washings and centrifugation was performed as previously described and finally samples were resuspended into 150 µl of running buffer and measurements were made at the Labcan 200 (Luminex) analyzing the results with the Luminex 100 IS software.

II.I.VI. Quantification of MNPs loaded per cell

In order to quantify the amount of MNPs taken up by a single cell, magnetic measurements were performed using a magnetometer SQUID (Superconducting Quantum Interference Device). It is designed to measure the magnetic moment of a sample, from which the magnetization and magnetic susceptibility can be obtained. Its principle is based on the idea that the measurement of the flux change through a pick up coil system and the signal is proportional to the magnetic moment of the sample which is magnetized by the magnetic field produced by a superconducting magnet.

The main components of a SQUID magnetometer are a superconducting magnet, a superconducting detection coil system and a SQUID connected to the detection coil.

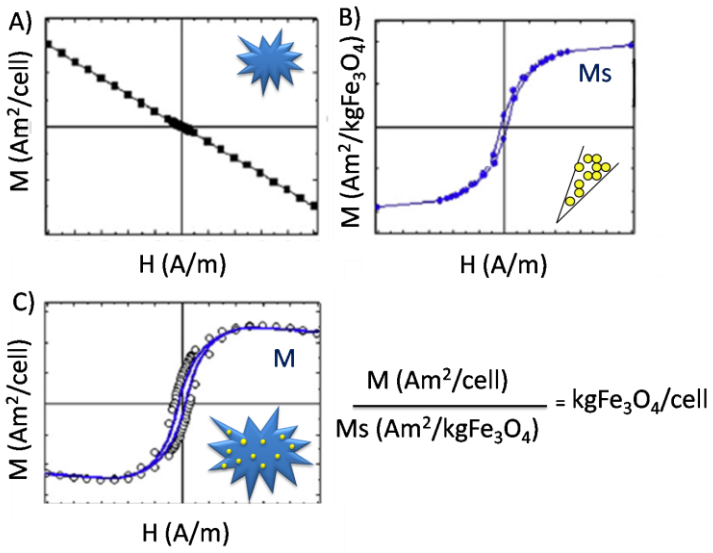

Figure II- 11: Magnetic response from (a) unloaded cells, (b) the magnetic particles in suspension and (c) the response from co-cultured CF with MNPs. With the Ms value from the NPs and the M from the NPs loaded cells it is possible to calculate the amount of NPs that are incorporated by the cells, therefore knowing the number of cells in the sample we obtain the amount of MNPs per cell.

Figure II- 11 represents how the signals of both DCs and MNPs are, and also the signal that is obtained when the MNPs loaded DCs are measured and it can be seen that this signal fits with the addition of the DCs and MNPs signals. Then it is also schematized how the data were treated for calculating the amount of MNPs internalized per cell. Measuring the MNPs alone it can be obtained the saturation magnetization (Ms) of the particles, expressed in emu/g. Thus, when the MNPs loaded DCs are measured it was obtained the magnetization for this sample, so as all the magnetic contribution came from the MNPs it was possible to calculate the amount of MNPs presented in the sample. Since we knew the number of cells that was forming that sample it was calculated the average amount of MNPs internalized per cell in terms of mass.

10^6 DCs on the day 5 of differentiation were placed in each of 6 wells of a 12 well-plate and were incubated overnight at 37ºC with different concentration of magnetic COOH (MNPs)- (0.01, 0.02, 0.05, 0.15 and 0.3mg/ml) and the last one without NPs. After three washings with PBS, to remove the NPs not incorporated, the cells were counted again and resuspended in 100µL of PBS. Also incubation with both COOH(MNPs)- and NH_2(MNPs)+ at a fixed concentration (0.05 mg/ml) was made in order to distinguish any change in incorporation capability due to the charge of the MNPs. A commercial SQUID magnetometer was used to perform static measurements as a function field and temperature. Results were normalized by the number of cells in each sample, as counted by a Neubauer chamber.

II.I.VII. Internalization study by FACS

Magnetic quantification of the MNPs internalized per cell informs about the average amount of MNPs incorporated by cells. Thought this technique is very sensitive it gives an average amount of MNPs internalized per cell. In order to analyze how homogenous the internalization of NPs in DCs was, FACS technique was selected by using Rho derivates fluorescent NPs.

10^6 DCs on the fifth day of culture were seeded into a 24-well plate and incubated overnight with different NPs concentrations; 0, 10, 20, 50, 150, 200, 300, and 500μg/ml. The following day cells were washed three times with fresh medium and analyzed in a FACSCalibur (Becton, Dickinson and Company, NJ). Fluorescence data were analysed with FACSDiva software

II.I.VIII. AMF application experiments

To verify the effects of ac magnetic fields on loaded and unloaded DCs, a '2x2' experiment was designed, as illustrated in Figure II- 12, involving four samples of cultured DCs. The first pair of samples, consisting of *as cultured* blank DCs (i.e., without nanoparticles, Fig. 2a) and NP-loaded DCs (Fig. 2b) were kept without magnetic field exposure and analyzed at the end of the experiment in order to compare the natural viability of the cell culture. For evaluating the effect of the magnetic field, a second pair of samples (blank and NP-loaded DCs, fig. 2 c and d) were exposed to the alternating magnetic field (260 kHz and H = 12.7 kA/m) for 30 minutes, while measuring the medium temperature. Samples b and c were duplicated in some

experiments to test two different kinds of MNPs (COOH and NH_2). After the field exposure, cell viability was measured in the 4 samples, using trypan blue and FACS (annexin-propidium iodide) protocols as described previously.

The hyperthermia experiments were done performing variations in different parameters as: NPs incubation concentration, time of ac magnetic field exposure and magnetic field amplitude. These experiments constituted an excellent platform to elucidate the underlaying cell death mechanism.

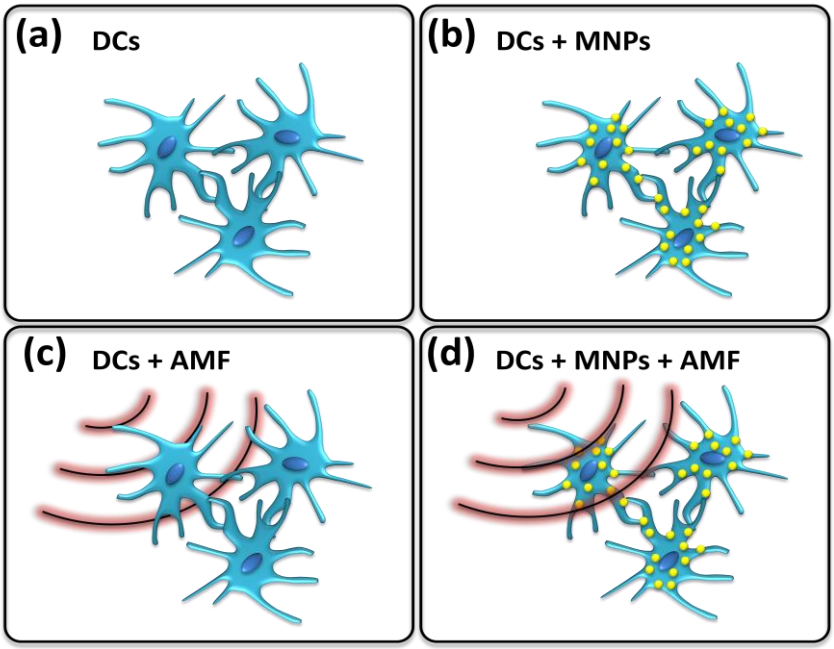

Figure II- 12: Scheme of the '2x2' experiment: (a) DCs without neither MNPs uptake nor magnetic field application (DCs). (b) DCs uploaded with MNPs but without field application (DCs+MNPs), (c) DCs without MNPs for magnetic field application (DCs+AMF), and (d) DCs with MNPs and application of magnetic field.

The device used to apply the AMF to DCs was the house-made device represented in the Figure II- 13 and consist of a coil (1) that generate the magnetic field, (2) a Dewar where the sample holder is located, (3) an optic fibber thermometer to measure the

temperature of the sample when the AMF is being applied and a holder where the sample is placed.

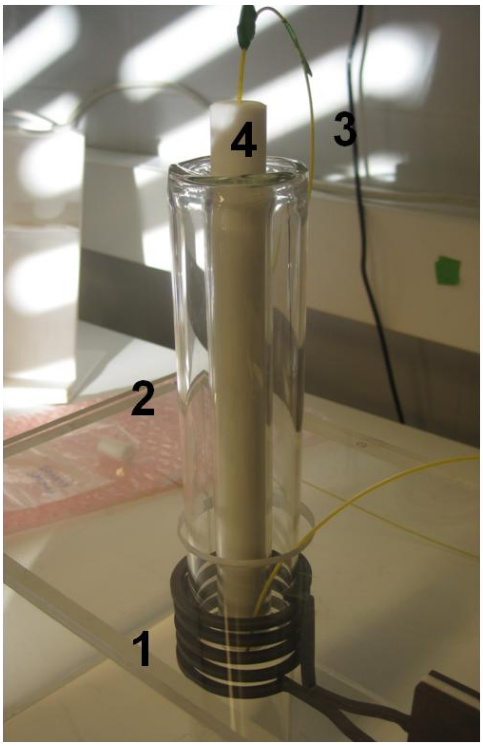

Figure II- 13: Image of the magnetic fluid hyperthermia house-made device. 1) Coil, 2) Dewar, 3) Optic Fiber termometer and 4) Sample holder

For *in vitro* AMF experiments, DCs cultured as described above were collected on day 5 and seeded onto a 12-wells plate at 10^6 cells/ml in complete medium supplemented with IL-4 (25 ng/ml) and GM-CSF (25 ng/ml). COOH and NH_2 NPs suspension were added at a concentration of 0.05 mg/ml in two wells each. Two wells without nanoparticles served us as a control. Cells were cultured overnight at 37ºC. Next day, non adherent cells were collected from each well and washed three times with fresh medium. Cells were resuspended in 500 µl of complete medium.

II.I.IX. Scanning electron microscopy

Scanning electron microscopy (SEM) was used in order to obtain information about the morphology and chemical composition of the cells. Secondary electron (SE) give a well defined three dimension images where morphology of the cells can be observed. Backscattered electrons (BSE) inform about the chemical composition of the sample discerning between heavy and light elements, which is very useful to detect the MNPs inside the cells. The analysis of the X-Ray (EDX) emitted from the sample as a consequence of the electron irradiation allows a chemical mapping at microscopic level. More information about the SEM is described in the Annexe at the end of the thesis.

Coverslips were incubated in a 24-well-plate with 500uL/each well of 0.003% fibronectin in PBS (Sigma) for 2h at 37ºC, washed with RPMI medium twice and then $5x10^5$ DCs on day 5 resuspended in 1mL of complete RPMI supplemented with IL-4 and GM-CSF were added on each coverslip. Different amounts of NPs were added at the same time to the cells (50, 150, 300 and 500 μg/ml) and also in one sample 1 μg/ml of Lipopolysaccharides (LPS, Sigma) was added.

The cells were incubated at 37ºC for 48 h. After that, cells were washed with RPMI medium three times to remove the NPs that were not uptaken and so fixed with 2,5 % Glutaraldheyde in 0,1M sodium cacodylate 3% sucrose solution for an hour and a half at 37ºC. Dehydratation process was carried out by incubating with rising concentrations of methanol: 30, 50, 70, and 100% each of them 5 minutes twice and finally anhydride methanol 10 minutes. Samples were then gold coated in a SC 7620 Mini Sputter Coater (Quorum Technologies) and observed under scanning electron microscopy in an Inspect^{TM} 50 SEM (FEI). Secondary electrons images, electron backscatter diffraction

(EBSD) images and energy-dispersive x-ray spectroscopy (EDX) analysis were performed.

Also DCs after AMF application were observed under SEM, and for that purpose cells were attached to coverslips previously treated with 0.003% fibronectin solution. The rest of the preparation process is the same as the one that has been just described.

II.I.X. Transmission electron microscopy

The intracellular localization of the MNPs was evaluated by transmission electron microscopy (TEM) in DCs cultured with different concentrations of MNPs for 24h. Some information about the TEM is given in the Annexe.

On day 5 of culture, $3x10^6$ cells/well were seed into 12-well-plate in 2mL of medium supplemented with cytokines. Five samples were prepared, first DCs without NPs, three of them with different COOH NPs concentration: 0.05, 0.15 and 0.3 mg/ml, and the last one was incubated at 4ºC with the biggest amount of NPs (0.3 mg/ml). All the samples were incubated overnight at 37ºC but the last one that was incubated at 4ºC. The following day 2mL of Glutaraldheyde 4% in sodium cacodylate 0,2M pH=7,2 were added to each well and the plate was incubated 2h at 4ºC. Next, cells were collected, spun down, resuspended in 1mL of Glutaraldheyde 2% in sodium cacodylate 0,1M and keep at 4ºC.

Then cells were washed three times with sodium cacodylate 0,1M and fixed with 250 µl of potassium ferrocianide 2,5 % in sodium cacodylate 0,1M and 250 µl of osmium tetraoxide 2 % 1h at room temperature keeping from the light. After that, cells were washed twice with cacodylate 0,1M and the dehydratation process was performed

resuspending the cells in increasing concentrations of acetone (50, 70, 90 and 100% 10 minutes each twice).

Cells were infiltrated overnight in a shaker at room temperature with a 1:1

EPON-acetone 100% mixture and the following day this mixture was replaced for 100% EPON resin and incubated for 5 hours in a shaker at room temperature. After that, cells were pelleted in pure EPPON resin and baked at 60ºC for 48h.Ultrathin sections (60-80nm) were cut with a Leica EM UC7 ultramicrotome mounted on 400 mesh nickel grids and allowed to dry at 37ºC. Grids were treated with 2% Uranyl acetate in water for 45 minutes at room temperature, after that, grids were gently washed with distillate water and treated with 2% lead citrate in water for 5 minutes in presence of NaOH in order to maintain a desiccate atmosphere. Samples were observed in a transmission electron microscopy FEI Tecnai T20 microscope with an accelerating voltage of 80 KV.

II.I.XI. Dual Beam

Dual Beam was used as the unique technique that combined the study of the morphology and the internalization of MNPs since the possibility of crossectioning of the ion beam allows us to observe the MNPs in the cytoplasmatic space. How a Dual Beam equipment works is describe in the Annex.

Coverslips were prepared with Fibronectin as it has been mentioned in SEM. Then $5x10^5$ cells were added to each coverslip and in one of them MNPs were added at a concentration of 0.05 mg/ml. GMCSF and IL-4 were added to the medium in order to maintain the DCs differentiation. DCs were incubated overnight at 37ºC and then washed twice to remove the excess of MNPs. Cells were fixed with 2,5 % Glutaraldheyde in 0,1M sodium cacodylate 3% sucrose solution for an hour and a half

at 37ºC. In order to enhance the contrast cells were incubated with 250 µl of potassium ferrocianide 2,5 % in sodium cacodylate 0,1M and 250 µl of osmium tetraoxide 2 % 1h at room temperature keeping from the light. Dehydratation process was carried out as in the sample preparation for SEM. Samples were then gold coated and observed under a Nova 200^{TM} NanoLab Dual Beam, FEI Company. Cells were cut in slices of 10nm of thickness with the ion beam at a voltage of 30 kV and a current of 10 pA and observed with the electrons beam at a voltage of 5 kV and 0.4 nA.

II.I.XII. Confocal microscopy

In order to visualize NPs incorporation by confocal microscopy, Rho-NPs were used, like in the internalization study made by FACS. By confocal microscopy, apart from observing the fluorescent internalized NPs it is possible to observe any cell organelle by using fluorescence labelled antibodies that recognizes some structure typical from each organelle.

As we knew that the NPs were localized in the cytoplasmatic region, it was decided to study the structure of the cytoskeleton to observe whether their configuration is altered by the internalization of the NPs. Actin and Tubulin are proteins that take part of the cytoskeleton structure, so by using antibodies against these proteins it was possible to observe their cellular configuration. Also the nucleus was staining with a fluorescent probe that binds specifically the nuclear DNA.

Confocal microscopy is a technique that allows us to obtain images from a cell selecting the depth. This ability makes this technique very useful to detect the fluorescence in the intracellular medium without any interference signal coming from

the membrane or extracellular space. More details about the functionality of this microscope are given in the Annexe of this thesis.

Coverslips were placed into 24-well-plate and $5x10^5$ cells in day 5 of culture were seeded in each well in 500 µl of complete medium. In every experiment always one coverslip contained DCs without NPs, in order to discard autofluorescence of the cells, and the rest coverslips contained DCs incubated with different concentrations of fluorescent NPs-Rho (0.125, 0.25 and 1.25 mg/ml). All samples were incubated at 37ºC overnight but one sample that was incubated with the higher NPs concentration at 4ºC overnight, and after incubation time the coverslips were washed twice with PBS and fixed with 3% Paraformaldehyde (PFA) for 15 minutes at room temperature. Then, three washings with cooled PBS and NH_4Cl (500 µl PBS and 10 µl NH_4Cl each well) were performed.

Cells were then stained with 1:100 Phalloidin (Sigma) in PBS/HS/Sap (50 µl of Horse serum added to 1 ml 0.1% Sap in PBS) for 20 minutes at room temperature. The coverslips were washed twice with 0.1% Saponin in PBS, twice with PBS and once in distillate water, and further mounted with 4µL of the mounting solution Mowiol containing 1µl of Draq5, which is a nucleus dye.

In other samples, tubulin which is another cytoskeleton protein was dyed. Coverslips were incubated firstly with 1:50 mouse Anti-Tubulin antibody (Sigma) in PBS/HS/Sap for 20 minutes at room temperature. After washing, as previously described, coverslips where then incubated with 1:200 goat secondary antibody against mouse in PBS/HS/Sap (Sigma) for 20 minutes at room temperature. Once incubation time is finished, coverslips were washed Sap/PBS/PBS/H_20 and mounted with 4 µl Mowiol containing Draq5 in a microscope slide. The cells were examined using a SP2 Leica confocal microscopy with identical settings for each sample.

After AMF application also confocal microscopy was performed in order to identify any structural damage inside the cell. So, actin and tubulin proteins were dyed as described before.

It is known that nucleus condensation and fragmentation is an apoptotic signal and these phenomena can be observed if the nucleus is dyed with any nucleus marker, as Draq5. Therefore, after AMF exposure nucleus stained was made to check their structural sate. For the latest samples preparation a compact FV10i Olympus confocal microscopy was used.

II.I.XIII. Western-Blot

Western Blot technique, also called protein immunoblot, allows determining the relative amount of a protein present in a sample and also the estimation of the molecular weight. This technique consists of some steps, first proteins are separated by gel electrophoresis, usually SDS-PAGE, and then proteins should be transferred to a nitrocellulose membrane retaining the same pattern as in the gel. The membrane is further incubated with an antibody that recognizes the protein we want to evaluate. This antibody should be bound to an enzyme, dye or any molecule easy to detect. The last step would be to reveal the location of the antibody with the necessary protocol. Sometimes if the antibody that recognizes the protein of interest is not bound to any detectable molecules a secondary antibody (marked with an observable molecule) that recognizes the first antibody is used. Figure II- 14 shows a schematic illustration of all the steps of a general Western Blot protocol.

For the HSP70 protein detection by Western Blot, global protein extracts were obtained from 10^6 cells each sample. First cells were washed twice with PBS to remove

protein from the culture medium. Cells were spun down and resuspended in 20 µl of Lys x1 solution (1% Triton x-100, 150 nM NaCl, 50 mM Tris/HCl pH=7.6, 10% Glicerol, 1mM EDTA and proteases cocktail stock x100) and incubated for half an hour in ice. Then samples were centrifugated 15 minutes at 14000 rpm 4ºC and the supernatant was mixed with 7 µl of Lys x4 solution (0.5 M Tris/HCl pH=) and kept as the protein soluble fraction at -20ºC. The pellet was resuspended in 20 µl of PBS and mixed with 7 µl of Lys x4 solution and kept at -20ºC as the protein insoluble fraction. Global protein extracts were taken from DCs with and without magnetic hyperthermia and also after having been incubated with different concentration of MNPs. HeLla cells were used as positive control due to their high level expression of HSP70 in basal conditions.

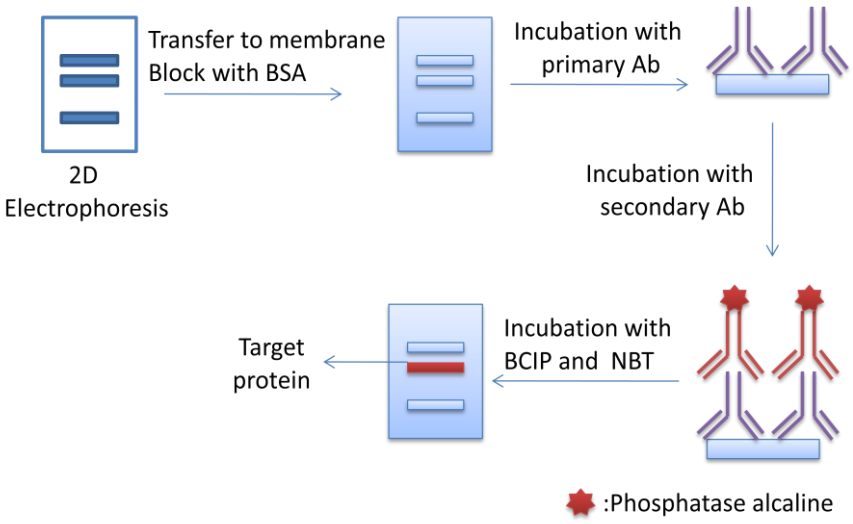

Figure II- 14: Schematic illustration of the Western Blot technique. 2D (two dimensional), BSA (bovine serum albumin), Ab (antibody), BCIP (5-bromo-4-cloro-3-indolil-phospathe) and NBT (nitro-blue tetrazolium).

For Western-Blot performance, samples were unfrozen and boiled in water for 5 minutes. Acrylamide gel was prepared as ¾ 10% resolving gel and ¼ Stacking gel.

20 µl of each sample was placed into the wells and 8 µl molecular weight probes (Full Range Rainbow^{TM}) were placed in a well. Empty wells were always charge with Lys x4 solution. Electrophoresis was performed at 120V for 90 minutes.

After that, Whatman papers (BIO-RAD) got wet by capillarity with 80 ml Transfer buffer mixed with 20 ml of MeOH. Also the nitrocellulose membrane (Hybond^{TM}_C Extra, Amersham Biosciences) and the electrophoresis gel were immersed into this solution for 5 minutes. One Whatman paper was placed on the anode, then the nitrocellulose membrane was placed over the Whatman paper, the gel was placed over the nitrocellulose membrane and finally another Whatman paper was placed on the top. Bubbles were removed carefully. Transference device was assembled and transference was made at 20V 0.4 Amp for 1 hour (Trans-blot-SD Semi-Dry Tranfer cell, BIO-RAD). Once the proteins were transferred, the membrane was placed into a blocking solution (3% Ovalbumin in Buffer B or PBS) previously centrifugated at 3000 rpm for 5-10 minutes. The membrane was incubated with the blocking solution in a shaker for 1 hour at room temperature. After that, 4-5 times vigorously washing with Buffer B (0.01 M Tris pH=8, 0.12 M NaCl, 0.1% Azide, 0.5% Tween-20) was required.

Then, the incubation with the antibodies was performed. Firstly, incubation with the anti-HSP70 monoclonal antibody (Assay Designs) 1:1000 in Buffer A (Buffer B plus 0.1% Ovoalbumin) in a shaker for 1 hour at room temperature was carried out, followed by 4 times washing with Buffer B. After that, incubation with the secondary anti-rabbit antibody IgG (Sigma) bound to phosphatase alkaline was made at a dilution of 1:5000 in Buffer A, for 45 minutes in a shaker at room temperature. 4 washings with Buffer B was again needed and immunocomplexes were detected with a developing solution

freshly prepared, consisting of 11ml of Buffer (TRIS/HCl 0.2 M, $MgCl_2$ 1mM, pH 9.6), 0.185 ml of 4mg/ml 5-bromo-4-cloro-3-indolil-phospathe (BCIP) in dimethylformamide (DMF) and 1.25 ml of 1 mg/ml of nitro-blue tetrazolium (NBT) in DMF. Stock solutions of BCIP and NBT were kept at -20C. Reaction was stop removing the developing solution and washing genteelly the membrane with distillated water.

II.II. Preparation of Adenovirus-MNPs complexes for magnetofection

The second part of the chapter is dedicated to the description of the techniques and protocols used to achieve the formation of magnetic adenoviral complexes and their use in magneto-transduction. Firstly, it was investigated the optimal conditions for the complex formation, specifically, the binding between the virus and the MNPs and the stability of the complex. Then, incorporation of the complexes by the cells and toxicity effects were analyzed. Also a physical characterization of the complexes was performed.

Finally, the transduction efficiency in two cell lines was tested, in order to determine how the use of MNPs associated with the virus in presence of a magnetic field can improve the process.

II.II.I. Cell lines

Three different cell lines were used for all the experiments presented in this part of the thesis:

a) Rat nervous tissue glial cells, referred to as **B92 cells**. For coculture experiments it was necessary to distinguish from other cell lines as N2A cells, so B92 cells were transducted in order to stably express LVSFds-RED protein, referred to as **B92-RED cells**. Both normal B92 and B92-RED cells were cultured in Dulbecco´s modified Eagle´s Medium (DMEM,Sigma) supplemented with 2mM L-Glutamine and 10% Foetal Bovine Serum (FBS). The cells that stably express LVSFds-RED protein were generated by transducing B92 cells with a lentivirus encoding this protein. Two consecutive infection experiments were done in order to achieve a maximum percentage of B92 cells expressing LVSFds-RED protein. Each infection was made as follow: firstly $4.5x10^5$ cells were seeded in 1 ml of culture medium in a well of a 6 well-plate, and were incubated 1 hour at 37ºC to attach the cells. After that, 600 µl of lentivirus ($6.95\ 10^8$ VP/ml, ~$4x10^6$ TU/ml) were added to the cells and after 30 minutes of incubation at 37ºC, 3 ml of fresh culture medium was added. Cells were maintained at 37ºC and further cells passages were made.

b) Mouse Albino neuroblastoma cells, named as **N2A cells**, were maintained in DMEM medium (Biochrom AG) with 2mM L-Glutamine and 10% FBS.

Both B92 and N2a are brain cell lines and were selected as the target cells to be transduced.

c) Human Embryonic Kidney cells, **HEK 293 cells**, were cultured in DMEM (Biochrom AG) supplemented with 2mM L-Glutamine and 10% SFB. All cell lines were grown at 37ºC in a humidified atmosphere of 5% CO_2. This cell line was used for

virus titration. HEK 293 cells are very easy to transduce, that is why, virus titter is usually determined in this cell line.

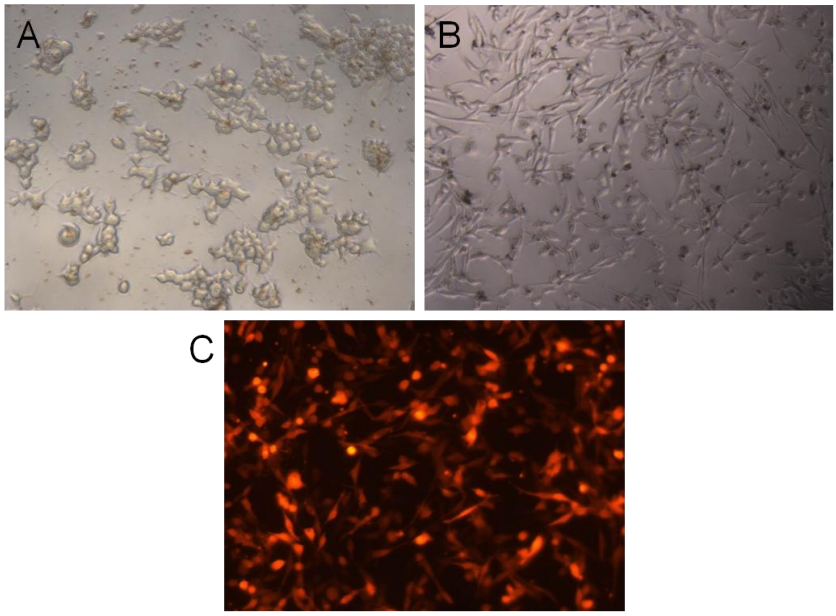

Figure II- 15: Images of A) N2A neuronal cells, B) B92 glial cells and C) B92-RED cells.

II.II.II. Magnetic nanoparticles

Three different kinds of magnetite core-shell MNPs were used for the MNPs-virus complex formation. Since the final application was to vectorize them with an external magnetic field, their magnetic properties are of a great importance.

a) **PEI-Mag** nanoparticles are a core/shell type iron oxide MNPs consisting of a fluorinated surfactant (ZONYL FSA or lithium 3-[2-(perfluoroalkyl)ethylthio] propionate) combined with 25 kDa branched polyethylenimine (PEI-25_{Br}). The size of the magnetic core was 9 nm.

b) **SO-Mag**, consisted of a shell formed by the condensation product of TEOS and THPMP also combined with PEI-$25_{Br.}$ The core size of this kind of MNPs was 11 nm.

c) **G1** MNPs are 80 nm cubic shape magnetite particles. These naked nanoparticles were functionalized in order to confer a positive charged surface, needed for the virus binding. The coating protocol was performed adding PEI-25_{Br} in a ratio 1:1 (weight Fe: PEI) and leaving the mixture in the ultrasound for about 2h.

Physical characterization of all the samples was performed by measuring the hydrodynamic ratio, polydispersity index and Z-potential by photon correlation spectroscopy (PCS) in water using a Malvern 3000 HS Zetasizer (UK). Furthermore, TEM analysis was made in order to determine the size following the same protocol that was described for the MNPs used IN DCs experiments, page 72.

Besides, magnetic characterization was performed in a magnetometer SQUID (Quantum Design MPMS-XL), where the saturation magnetization was obtained.

Iron content of all the MNPs was determined with a colorimetric method. Firstly, 20 µl of the suspension of the MNPs was taken and 200 µl of concentrated HCl were added. After complete dissolution of the material the volume was adjusted to 5 ml with ddH_2O and 20 µl of the resulting solution were sampled. 20 µl of concentrated HCl, 20 µl of 10% hydroxylamine-hydrochloride solution, 200 µl of ammonium acetate buffer, 80 µl of 0.1% of 1,10-phenanthroline solution and 730 µl of ddH_2O were added. The mixture was mixed well and allowed to stand for 20 min. Then absorbance was measured at 510 nm.

PEI-Mag and **SO-Mag** particles were synthesized at the Intitut für Experimentelle Onkologie, Klinikum rechts der Isar, München and **G1** particles were synthesized in our laboratory.

These three types of MNPs were chosen because with the ones synthesized in the lab in Munich previous results in magnetofection with other virus and other cell line were promising [114]. G1 particles were chosen to compare how the complexes behave when they are formed with bigger MNPs, which are more suitable for magnetic-transduction due to the larger magnetic moment.

II.II.III. Adenovirus titration

The construction of the viral adenovector used in this thesis was performed "Instituto de Investigaciones Bioquímicas, University of La Plata" (INIBIOLP). This adenovector, termed RAd-GFP, harbors the gene for green fluorescence protein (GFP) under the control of cytomegalovirus promoter (CMV). Successfully transduced cells express GFP and can therefore be readily detected by fluorescence microscopy which makes GFP a suitable reporter gene

Physical viral titration was determined by UV optical absorbance (OD) at 260nm. This method is based on the use of an extinction coefficient for the virion which could be determined empirically by several methods [115, 116] . The extinction coefficient is the measurement of how strongly a specimen absorbs light at a given wavelength, it is normally represented by ε, from the Beer-Lambert law: $A = \varepsilon\ l\ c$. Where A is the absorbance (no units), ε is the extinction coefficient (L/mol cm), l is the length path of the sample (cm) and c is the concentration of the compound in the solution (mol/L). The extinction coefficient for wild type adenovirus is $9.09\ 10^{-13}$ OD ml/cm virion, calculated from the data of Maizel et al [115].

A volume of 20 µl from stock virus was mixed with 380 µl SDS 0.1%, vortex for 2 minutes and centrifuged at 8000 rpm for 5 minutes. Supernatant absorbance was measured at 260 nm in a UV spectrophotometer.

Biological virus titer was determined by infecting **HEK 293** cells at different concentrations. To determine virus titer it is necessary to infect easy-to-transduce cells, thus, HEK 293 cells, which meet this requirement, are used commonly for that purpose. The starting concentration was 10^{-6} of the virus stock and 8 successive dilutions 1:2 (in PBS) were tested. The number of cells per well was 300 and the volume of the dilutions of the virus added per well was 50 µl. After two days, percentage of positive cells was determined by FACS and once the data are fitted to a Boltzmann sigmoid function, virus dilution needed to infect 50% of the cells can be obtained. Considering that one positive cell has been infected by one infectious unit we can calculate the virus titration, transformation units per millilitre (TU/ml).

A partially-deactivated virus was used for TEM and AFM experiments; the titter of this virus was performed in the same conditions as described above. Deactivation was carried out by a photochemical reaction with psoralen under exposure to long-wavelength UV light (320-380 nm) [117].

II.II.IV. Adenovirus-MNPs complexes association and stability study

The first step was to achieve the optimum conditions for the formation of the magnetic complex between the adenovirus and MNPs. The association of the components was studied and also the stability of the complex in different biological media, important for biological applications.

The assessment of adenovirus association to the MNPs, and its stability in physiological media were done by radioiodination of the virus.

The radioiodination method was the reaction described by Fraker and Speck {Fraker, 1978 #232}. Briefly, 100 µl of a 0.1% solution of 1,3,4,6-tetrachloro-3α,6α-diphenilglycouril (Iodo-Gen™ reagent, Sigma Aldrich) in chloroform were transferred into an Eppendorf tube. The solvent was removed firtly in air and then under high vacuum. 120 µl of the adenovirus stock were mixed with 4 µl of $Na^{125}I$ (14.8 MBq, Amershan Bioscience) and placed into the Eppendorf tube that contained the Iodo-Gen™ reagen. The mixture was incubated 25 min at room temperature. In order to separarate the ^{125}I-labelled virus from the unbound ^{125}I a gel filtration was performed. The mixture was diluted to 500 µl with PBS+10% Glycerol buffer and then passed though a PD-10 columm preequilibrated with PBS+10% Glycerol buffer. The final ^{125}I-labelled virus fraction contained $2.11x10^{11}$ VP/ml and a radioactivity of 2.6 kBq/µl.

Magnetic complexes were prepared in PBS with decreasing virus-to-particle ratios of: 40, 20, 10, 5, 2.5, 1.25, 0.625, 0.312, 0.156 and 0.078 fgFe/VP. The protocol consisted of mixing virus and MNPs in the minimum possible volume in U-bottom 96 well plates, and 30 min incubation at RT for assembling the complex, addition of PBS at the resulting complexes in order to achieve a volume of 150 µl. 50 µl of each sample were transferred into wells from 3 plates, containing already 50 µl of PBS, FBS and CSF (cerebrospinal fluid) respectively, and were incubated for 15 minutes at RT. To sediment the magnetic complexes, the plate was placed on a 96-well magnet plate (OZ Bioscience, Marseille, France) for 30 min. 50 µl of each supernatant were carefully collected for gamma counting using an automatic gamma counter (Wallac 1480 Wizard 3, Finland). The percentages of virus particles associated and magnetically sedimented with MNPs in PBS were calculated with the expression:

$$\%\, Virus\ bound = (1 - \frac{CPM\ sample}{CPM\ ref}) \times 100$$

Where CPM_{sample} and CPM_{ref} is the measured radioactivity, in terms of count per minute, in the sample and in a virus probe before adding the MNPs respectively. Each determination of viral/MNP binding was done in triplicate.

II.II.V. Size, Z-potential and magnetic responsiveness measurements for complexes

The virus-MNP complexes were prepared using the three kinds of above mentioned MNPs, at different virus-to-particle ratios (40, 20, 10, 5, 2.5, 1.25, 0.625 and 0.3125 fgFe/VP), by mixing the adenovirus and the MNPs and incubating for 20 min at room temperature. Volume binding was adjusted with PBS to 100 µl and virus concentration was 1.5 10^{10} VP/ml. After the 20 minutes the complexes were diluted in PBS to final volumes 2mL for concentrations of 40, 20, 10, and 5 fgFe/VP, and 1mL final volume for the rest of the concentrations.

Hydrated particle diameters and Z-potentials were determined by PCS, in a Malvern 3000 HS Zetasizer (UK). Hydrodynamic diameters values were taken as size distribution report by intensity.

The magnetic responsiveness of virus-MNPs complexes was determined using a turbidity method under applied magnetic field. In addition, to determine whether or not the sedimentation was driven by the applied magnetic field, 40 fgFe/VP Adenovirus-PEI-Mag complex was also measured in absence of the magnetic field. This method has

been used and described previously by others researchers [112, 118]. For this purpose 500 µl of the complexes once they were formed were placed in an optical cuvette placed in a spectrophotometer (Beckman DU 640) and exposed to a defined magnetic field gradient, and the time course of optical density at 360nm was recorded. The gradient field was generated by positioning two mutually attracting packs of four quadrangular neodymium-iron-boron (Nd-Fe-B) permanent magnets symmetrically on each side of the cuvette holder and parallel to the light beam.

The magnetic mobility was calculated taking into account the time at which the 90% of the complexes were magnetically sedimented (t 0.1) and the medium path that the complexes had covered, which was in all cases 1mm.

II.II.VI. AFM

Virus, MNPs and their complexes were prepared for AFM experiments. Virus samples were prepared in a dilution 1:10 from the stock, final concentration was 1.6 10^{11} VP/ml in PBS. NPs concentration was 0.25 µgFe/µl for PEI particles, 0.98 µgFe/µl for SO particles and 0.067 µgFe/µl for G1 particles. Complexes were formed at a MNPs-to-VP ratio of 2.5 for G1 NPs and 1 for both PEI and SO MNPs, 1.6 10^{10} VP/ml in a final volume of 30 µl in PBS. 2 µl of each sample was place onto smooth and clear mica surfaces and air dried. Next, the samples were carefully rinsed with double-distilled water in order to remove buffer salts, and then dried again.

Imaging was performed in air using a NanoWizard®I atomic force microscope (JPK Instrumenst AG, Berlin, Germany) coupled with an inverted Axiovert S100 microscope (Carl Zeiss AG, Oberkochen, Germany). Silicon cantilevers NSC36/AlBS with a force

constant of 2 N/m and a resonance frequency of 150 kHz were used for imaging in tapping mode. Images were acquired using the WSxM software.

II.II.VII. TEM

TEM was performed in order to investigate the morphology of the magnetic complexes. Negative stain sample preparations was performed following the method of Stilwell [119]. Formvar/carbon-filmed 400 mesh cooper grids were used to deposit the samples. MNPs alone, deactivated virus alone and magnetic complexes were observed. 0.0208 μgFe/μl of MNPs and 3.30 10^{10} VP/ml were the concentrations chosen to observe the samples with a final volume of 12 μl in PBS resulting in a MNPs-to-VP ratio of 0.63 for the magnetic complexes.

A 5 μl drop of the sample was placed onto the grid and incubated for 10 minutes. Then, samples were rinsed carefully with drops of double-distillate water in order to remove the salts of the PBS. After that, all samples but the MNPs alone were stained with 10 μl of 1% phosphotungstic acid solution for 3 minutes. Next, sample were air dried and subsequently observed under the electron microscope at an accelerating voltage of 80 kV (TITAN™ 80-300 S/TEM, FEI Company).

II.II.VIII. Complexes internalization

The aim of this kind of experiments was to compare the amount of the virus that was internalized per cell when the transduction was performed with the virus alone and in the absence of the magnetic field and when it was performed with the magnetic

complexes and in the presence of the magnetic field. This data was important to test the efficacy of the magnetotransduction.

For evaluation of virus internalization into cells 15000 cell were seeded in 96-well plates. The following day cells were infected with a mixture of ^{125}I-labelled and unlabelled virus at a ratio 1:1. Complexes were formed as described above with the three different kinds of MNPs, and virus alone was used as a reference point. MOI used for this experiment was between 400 and 0.

24 hours post infection the cells were washed with PBS and treated with 100 units/ml heparin solution for 20 minutes at 37'C, to remove the virus that had not been internalized. Next, the cells were washed again with PBS and then lysed with 50 µl of lysis buffer. The cell lysate in each well was carefully collected using a pipette, transferred into a scintillation vial, and counted using the gamma counter. All of the samples were done in triplicate. The applied virus doses were counted as reference data ($CPM_{applied}$). Internalized virus particles were calculated as:

$$Internalized\ VP/cell = \frac{CPM\ sample}{CPM\ applied} \times Applied\ VP/cell$$

For Dual Beam analysis cells 24 post-infection were split out and washed by centrifugation 3 times with fresh medium. Cells were then prepared and observed as the DCs samples preparation for Dual Beam described in page 87.

II.II.IX. Viability assay

Cytotoxicity test using MTT assay (page 75) was performed in order to compare the toxicity of the virus alone with the toxicity of the magnetic complexes.

10000 cells were seeded in 96-well plates and the following day virus and complexes were added to the cell culture. MOI selected were between 400 and 0 and complexes were formed at a virus-to-nanoparticles ratio of 2.5 fgFe/VP. This experiment was done in quadruplicate.

Incubation was performed as described previously and after two days cells were very carefully washed with PBS and 100 µl of 1mg/ml MTT solution, prepared in PBS with 5mg /ml glucose, was added. Cells were incubated with MTT 1h at 37ºC. Afterwards, 100 µl of solubilisation solution, consisting of 10% Triton X-100 in 0.1 N HCl in anhydrous isopropanol, was added to dissolve formazan crystals. Plates were left in a shaker at 37ºC 2 h, in order to dissolve all the crystals. The optical density was measured at 590 nm and cell viability was expressed as respiration activity normalized to the reference data for untreated cells.

II.II.X. Infection experiments

Infection experiments were performed in N2A and B92 brain cells, which are our target cells to genetic modification. All the infection experiments were made in 96 well plates. Different MOI and different particle-to-virus ratios were tested in order to identify the best conditions to obtain the highest transduction efficiency.

The magnetic virus complexes were prepared by mixing a dilution series of MNPs suspension in water with virus particles in PBS. The virus concentration for the

assembling always reminded constant at 1.5 10^{10} VP/ml, and the binding final volume, the net VP and the amount of MNPs added depended on the virus-to-particle ratio and the number of cell wells that are needed to infect in each experiment. An incubation time of 20 min at RT was required for forming the complexes, followed by dilutions with PBS. The volume that was added per well was 50 µl and the range of multiplicities of infection (MOI=TU/cell) tested in infection experiments were between 0 and 200.

For infection experiments 15000 cells were seed in a volume of 150 µl in each well of 96-well plates. After 24 h the medium was replaced with 150 µl of fresh complete medium that contained 50 µl of the virus alone, the magnetic complexes form as described above or 50 µl of PBS as negative control. Cells were infected with the virus or complexes positioning the plate on a 96-well magnet for 30 minutes at 37ºC. After that time, the magnetic plate was removed, no medium change was performed and the cells were further incubated at 37ºC for 48 h

For the sample preparation for FACS analysis, cells were washed with 100 µl of PBS, then 20 µl of Trypsin (Biochom) were added and cells were incubated at 37ºC until cells were detached. Next, Trypsin is neutralized with 150 µl of culture medium without dye (DMEM/F-12, Gibco, Invitrogen) and cells are collected and added to the FACS tubes, filled with PBS and centrifugated at 1300 rpm for 5 min. Then, supernatants were removed and pellets were resuspended in 250 µl of Cytofix (BD) and incubated 10 min at RT. Tubes were filled again with PBS and centrifugation was performed in the same conditions as it is described above. Supernatants were removed and cells were resuspended in 250 µl of PBS. Cells were then ready to be analyzed in FACS. For FACS analysis a BD FACSVantage^{TM} cytometer was used and data was treated with BD Cell Quest^{TM} Pro sorfatware. 20000 cells were measured for each

sample. Efficiency of the transfection was measured as percentage of cells positive by GFP protein.

Apart from infection of both N2A and B92 cell lines in monoculture, coculture infection experiments were done in order to mimic biological conditions. In the human being glial cells and neuronal cells are in relation 9:1. Thus, with coculture experiments it was tested whether the transduction efficiency in each cell line was influenced by the interaction with other cell line.

N2A and B92 cells coculture was done by seeding 10^4 B92 cells and 5 10^3 N2A cells in each well of 96 well-plates, that corresponds with a 70% of B92 cells and 30% of N2A cells, approximately. B92 cells expressing LVSFds-RED protein were used in order to be able to distinguish them from N2A cells by FACS. Infection, at MOI of 200, 100, 50 and 25, was carried out with the adenovirus alone, and with the magnetic complex formed with PEI-Mag nanoparticles at a ratio of 2,5 fgFe/VP. Infection of both cells lines in monoculture was done in parallel at the same conditions. Infection conditions are the same as the ones mentioned above. Two days after the infection cells were removed and prepared for FACS analysis as it has been described previously. Data of transduction efficiency in cells in coculture was compared with the cells in monoculture.

III. Results & Discussion

III-I: DCs and MNPs interaction

As it has been mentioned in the general introduction, we aim to use the MNPs loaded DCs as Trojan horse to vectorize the MNPs to the tumour area in order to expose this region under AMF and subsequently trigger damage in the tumoral vasculature. The ability of dendritic cells to capture different kind of extracellular antigens and molecules is well known [120, 121]. Furthermore, it has been described that DCs are capable of up-taking different kind of nanoparticles [122, 123]. The high antigen/ particle capture capability make the DCs a good cell type to internalize MNP and to carry them to the target area.

For the Trojan horse strategy to work properly, the MNPs selection was an important step in our work. As magnetic hyperthermia was the main goal, the criterion followed to choose the MNPs was to search for a maximum specific power absorption value, in other words, the best capability of the nanoparticles in heating when they are exposed to a magnetic field. As the heating of the cells was expected to be proportional to the amount of incorporated MNPs into the cells, we further searched for those MNPs with the highest affinity to these cells.

In adition to the data on the magnetic colloids provided by the manufacturers, an meticulous characterization concerning size, size distribution, physicochemical and magnetic properties was performed in those samples previously selected based on the highest heating capacity (i.e., largest SPA values).

In the present chapter we present the study on the interaction between MNPs and dendritic cells. Specifically, we studied the incorporation of MNPs by the cells under

different conditions of concentration. To analyze the quantities caught up during upload we have used several and complementary experimental techniques such as: FACS and SQUID. For a direct observation of the final distribution of the MNPs within the intracellular space at the single-cell level, we used different imaging techniques including transmission electron microscopy, scanning electron microscopy, dual beam microscopy and confocal microscopy.

As for many other biomedical applications of MNPs, a crucial requirement for the Trojan horse strategy to work was that the cytotoxicity produced by MNPs should not affect the DCs cell viability. Therefore, as a further step in our analisys we determined whether DCs could incorporate this type of MNPs without affecting their viability.

The influence of MNPs in the immune system cells is poorly understood. Specifically, it has been reported that the incorporation of NPs in DCs trigger a maturation stimulus which affects the cell biology [124, 125]. On the other hand, it has been also reported that some kinds of NPs do not affect the maturation stage of the DCs [126]. So there exists controversia in the effect the nanomaterials have in the DCs biology. As mentioned in the introduction chapter, in order to use the MNPs-loaded DCs as Trojan Horse, DCs should retain their capability for transdiferenciating into endothelial-like-cells and this process is known to occur in the immature state of the cells. Therefore, we performed a sytematic study on the expression of cell membrane molecules to see whether the MNPs were able to induce maturation. With the term ‘maturation’ we refer to a phenotypic rather than a functional description. The expression of some cytokines was also studied due to the fact that it is strongly linked with the maturation process.

III.I.I. Characterization of the magnetic nanoparticles

A. Specific power absorption

A set of 18 different types of colloids having MNPs with different hydrodynamic sizes and surface functional groups was tested. The core composition of all these MNPs was magnetite, Fe_3O_4. The criterion to select the two kind of MNPs for hyperthermia experiments, among a wide variety of particles, was the specific power absorption value (SPA), due to the fact that the better ability to generate heat when submitted to alternate magnetic fields the highest effect in cell viability is supposed to be observed. Since the highest internalization of MNPs was desirable, the cell affinity for MNPs with different charges was also tested.

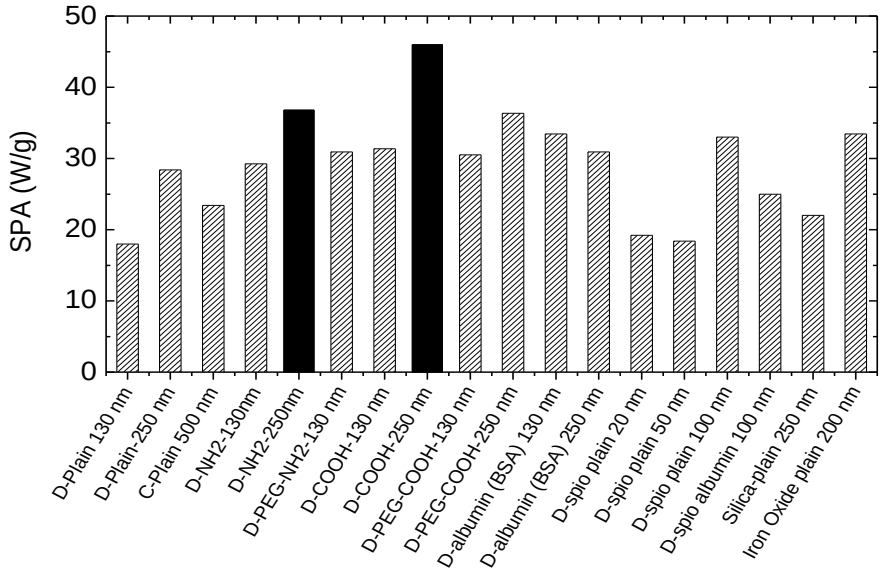

Figure III-I- 1.SPA values obtained from the different kinds of commercial MNPs tested. Black bars correspond to the MNPs selected for further experiments, NH_2(MNPs)+ (left) and COOH(MNPs)- (right).

The different types of nanoparticles represented in (Figure III-I- 1) displayed some variation of their Specific Power Absorption values. This is consistent with the different sizes of their magnetic cores from 5 to 16 nm since the power absorption is known to depend strongly on particle size, size dispersion, particle interactions (through magnetic dipolar interactions) and the hydrodynamic diameter [127, 128]. It is well known that, for a given magnetic material of the MNPs, there is a narrow size window at which the SPA is maximum, and this size value depends on the saturation magnetization and magnetic anisotropy of the core material. From the samples analyzed, the two finally selected for this thesis were chosen because they had the largest SPA and very similar physical and magnetic properties but opposite surface charge. The MNPs were: NH_2(MNP)+ and COOH(MNP)- with SAR values of: **36,8 W/g** and **46 W/g** respectively. The two MNPs selected allow us to check the effect the surface charge has on the MNPs internalization and the capability of these MNPs to induce cell death when submitted to an AMF. From here on we will refer only to these two selected types of MNPs because they were the ones all the experiments with DCs were made with.

B. Hydrodinamic diameter

The hydrodynamic diameters of the MNPs were measured by Dynamic Light Scattering (DLS) on the magnetic colloids *as provided* (i.e., suspended in water) at room temperature. Both NH_2(MNP)+ and COOH(MNP)- samples displayed a log-normal profile (Figure III-I- 2) with a broad peak at ca. 220 nm, and a ‘tail’ from the contribution of larger particle sizes. The large value of d_H (~18 times the size of the magnetic core) exemplifies the importance of the organic coating for biomedical applications, since particle aggregates close to the micrometer range should be difficult

to incorporate by usual endocytosis mechanisms. As the original colloids were diluted for DLS measurements, the observed dispersion of the particles sizes (σ_H = 0.40-0.50 values of the log-normal function) reflected the existence of cluster units within the colloid, in agreement with the agglomeration observed in the TEM images discussed below.

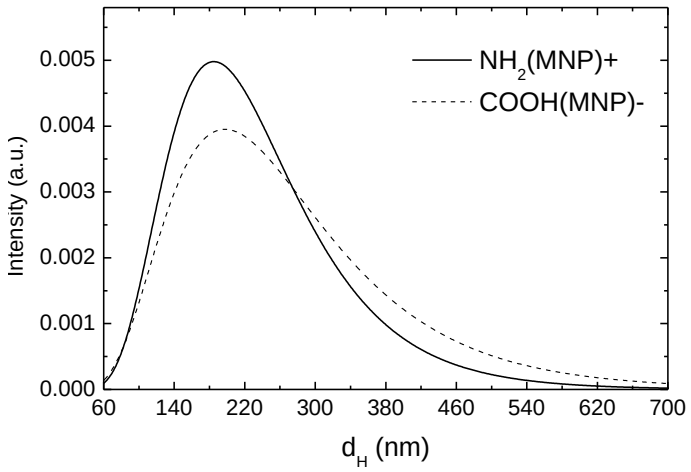

Figure III-I- 2. Graph that shows the DLS results for the NH_2(MNP)+ (solid line) and COOH(MNP)- (dashed line) nanoparticles.

Size of the fluorescent nanoparticles was also measured by DLS in order to check that the hydrodynamic radius was similar to the COOH(MNP)- and to be able to confirm that despite the core size and composition, the hydrodynamic diameter and external composition is the same in both magnetic and fluorescent nanoparticles, and therefore it is expected that DCs could interpret COOH(MNP)- and Rho-NPs as a single kind of NPs. MNPs were needed to perform experiments with the AMF, SQUID quantification and electron microscopy. However, fluorescence NPs were needed to perform experiments with FACS and confocal microscopy.

As it can be seen, hydrodynamic diameter of fluorescent nanoparticles was about 300 nm, so slightly bigger than MNPs, which were around 220 nm. However it seems not to be a problem for incorporation process, because as it will be shown, DCs incorporate both magnetic and fluorescence NPs types efficiently.

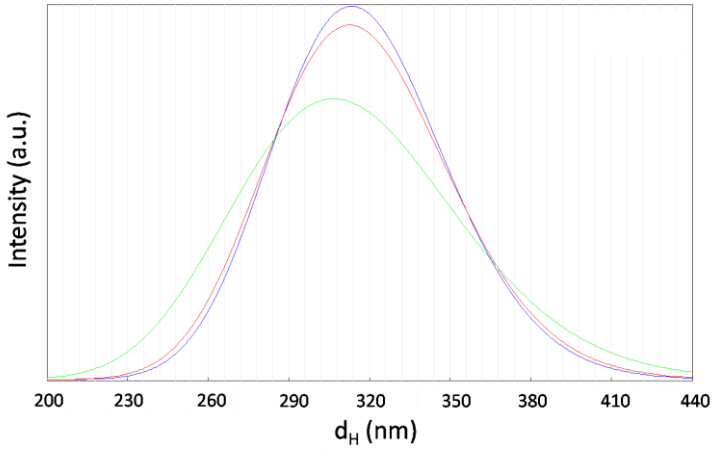

Figure III-I- 3.Graph that shows the DLS results for the fluorescent nanoparticles; each line corresponds to one repetition.

C. TEM

Figure III-I- 4 shows a typical TEM image of the samples chosen for this work, specifically the sample that is observed in this image is COOH(MNP)-. As a general feature, we observed cubic-rounded shapes of the magnetic cores, with some degree of agglomeration even after strong ultrasonic process and high dilutions. Therefore the presence of agglomerates in the colloidal suspension cannot be discarded, which is in concordance with the observed hydrodynamic diameter. The average size of the

magnetic cores was obtained after counting > 100 nuclei from different images, and fitting the resulting histogram with a log-normal function. This shape was chosen after finding in both samples a significant fraction of large, cubic-shaped particles. The resulting diameters and dispersion were <d> = 13 and 15 nm, σ = 0.5 and 0.6 for samples NH_2(MNP)+ and COOH(MNP)- respectively.

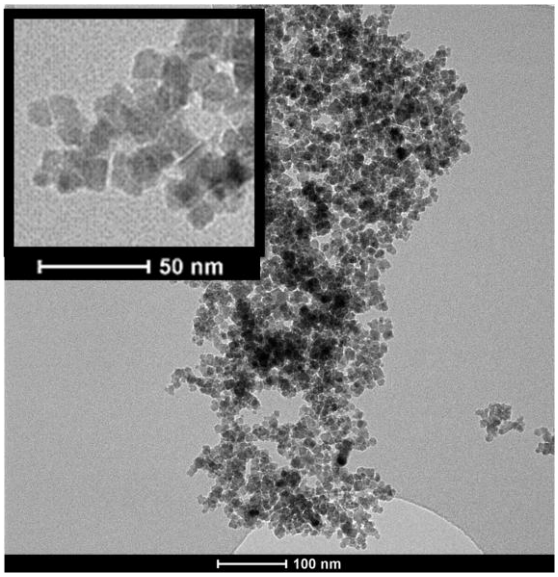

Figure III-I- 4. TEM images for the MNPs functionalized with carboxili groups, COOH(MNP)-, prepared by dilution in water.

D. Magnetization

The M(T) curves taken in Zero Field Cool (ZFC) and Field Cool (FC) at 8 kA/m, for both NH_2(MNP)+ and COOH(MNP)- samples, showed similar behavior, reflecting the similar size and polidispersity of the magnetic cores of both samples. The continuous increase of the M(T) data taken in ZFC mode and the absence of a maximum detected

up to 250 K in M(H) measurements (Figure III-I- 5) suggested that the blocking temperature (T_B) was near above 250K. The single-domain nature of the particles was inferred from the absence of the jump in M(T) curves in ZFC mode, expected for the Verwey transition in multidomain particles[129-131]. As it has been observed by TEM, the core size was about 13-15 nm, thus, blocking temperature was expected to be lower than the value obtained if magnetic interactions between MNPs were not taken into account. However, as it could be seen in TEM images, MNPs were forming aggregates, so this could be the reason that made the blocking temperature be above 250K.

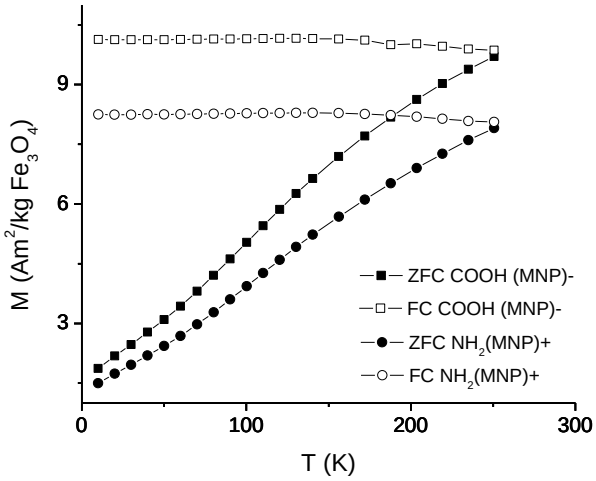

Figure III-I- 5: Zero Field Coold and Field Cool (ZFC-FC) measurements for both, COOH(MNP)- and NH_2(MNP)+ colloids, showing a blocking temperatures around 250 K. Measurements were made at 8 kA/m.

In agreement with the proximity of the T_B inferred from M(T) data, hysteresis loops M(H) performed at 250 K in both colloids showed nearly zero coercive field H_C (see Figure III-I- 6, upper hysteresis loop), supporting the picture of single domain nanoparticles in the superparamagnetic regime. From these hysteresis loops saturation

magnetization values were extracted, resulted in **53 Am^2/kg Fe_3O_4** for NH_2(MNP)+ and **56 Am^2/kg Fe_3O_4** for COOH(MNP)- .The magnetization obtained from the M(H) curves at low temperatures, 10K (see Figure III-I- 6, low hysteresis loop), were **62 Am^2/kg Fe_3O_4** for NH_2(MNP)+ and **66 Am^2/kg Fe_3O_4** for COOH(MNP)- ,a slightly reduced value when compared to bulk Fe_3O_4 and a increased value when compared with the Ms at 250K, that is frequently found in d~10 nm Fe_3O_4 particles and attributed to surface spin disorder [129]. At T=10K $T<T_B$ for both samples and therefore the MNPs are in the blocked state, in agreement with the observed values of coercitivity Hc extracted from the hysteresis. H_C = **32.33±0.6 kA/m** and **32.43±0.5 kA/m** for NH_2(MNP)+ and COOH(MNP)-, respectively. These values are similar to those reported for bulk magnetite REF.

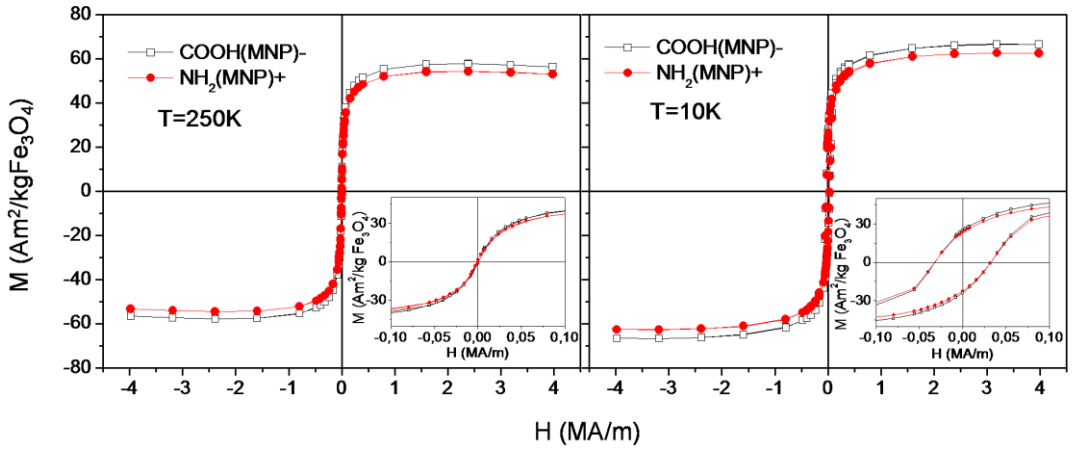

Figure III-I- 6: Hysteresis loops M(H) for both COOH(MNPs)- and NH_2(MNPs)+ colloids. Left panel: M(H) at T= 250K. Right panel: M(H) at T=10K. The insets show the magnification of the low field region in both cases. Measurements were made in frozen colloids.

It is known that below a critical size, any domain structure of a magnetic nanoparticle will collapse into a single domain [23]. For magnetite, it has been proposed that the critical size is about 30 nm [131]. The observed magnetic behaviour is consistent with a single-domain structure of the NPs core, in agreement with previous results on similar Fe_3O_4 NPs within this size window [129, 131]. This is a requisite for effective energy absorption through Néel relaxation mechanisms.

The relevant chemical and physical parameters are summarized in Table III-I- 1.

Sample	**Core material**	**Surface charge**	$\mathbf{d_{CORE}}$ (nm)	$\mathbf{d_H}$ (nm)	$\boldsymbol{\sigma_H}$	$\mathbf{M_S}$* (Am^2/kg)	$\mathbf{H_C}$* (A/m)	**SPA** (W/g)
NH_2(MNP)+	Fe_3O_4	NH_2^+	13(2)	244(2)	0.48	53	96	36(6)
COOH(MNP)-	Fe_3O_4	$COOH^-$	15(2)	217(2)	0.43	56	96	46(6)

*Table III-I- 1: Chemical and physical parameters of the nanoparticles used in this work, surface functional groups, core size d_{CORE}, hydrodynamic size (d_H) and distribution (σ_H), saturation magnetization (M_S), coercive fields H_C and specific power absorption (SPA) values. *: data at T = 250 K.*

In summary, Table III-I- 1 shows that both MNPs have similar physical and magnetic parameters. The only difference between them is their surface charge.

III.I.II. DCs differentiation from PBMCs

Concerning the DCs culture, the first required step is the isolation of the monocytes and their further differentiation into DCs. Monocytes (CD14+) cultured over 5 days in the presence of GM-CSF and IL-4 showed the characteristic phenotype of immature DCs. The phenotype characterization performed by FACS and the corresponding histograms are represented in Figure III-I- 7, as the number of analyzed cells versus the observed fluorescence intensity. The black vertical reference line indicates the maximum fluorescence signal obtained from non stained cells. In this way, any fluorescence signal obtained with higher intensity than the reference value is considered as positive, and those with lower intensity than the reference value are plotted as negative. With this convention, those peaks obtained on the left and right sides of the reference line are graphically interpreted as negative and positive staining, respectively.

After 5 days of differentation, the DCs were characterized by measuring the expression of main membrane markers in order to know whteher the differentiation from monocytes to DCs worked properly and know the maturation stage of the CDs obtained. The markers selected to be analyzed were: CD45 (a leukocyte common antigen); CD40 (a common feature of TNF receptor family members which play an important role in DCs maturation) and CD11c (a transmembrane protein present at high levels on most human DCs), CD14 (which is expressed by monocytes) and also CD83 and CD86 (typically absent for immature DCs but present after maturation).

CD45, CD40 and CD11c are reported to be expressed in DCs [66]. CD14 is known to be expressed in monocytes but absent in DCs so its expression informs about the efficiency of the differentiation process from monocytes to DCs [132]. CD83 and CD86

are known to be expressed in mature DCs but almost unexpressed in immature DCs [132], so their expression level informs about the maturation stage of the DCs obtained.

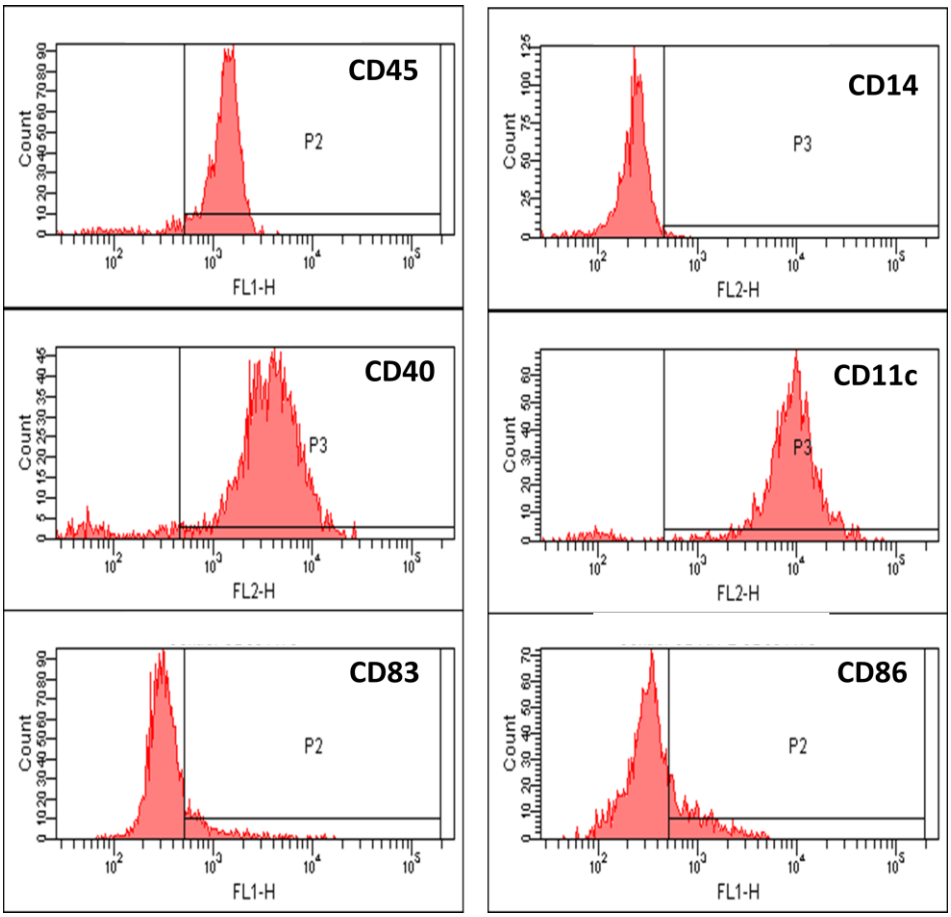

Figure III-I- 7: Histograms that show the surface antigen expression measured by FACS for 5 day-cultured cells. The labels ,CD, in each figure denote the fluorescence molecule bound to each antibody: FITC (fluorescein isothiocyanate) or PE (phycoerythrin). The vertical axis corresponds to the number of analyzed cell (count) and the horizontal axis corresponds to the fluorescence intensity.

The expression of all the markers is represented in Figure III-I- 7 and it could be seen that the cells obtained after 5 days of differentiation are positive for the expression of CD45, CD40 and CD11c and negative for the expression of CD14, CD83 and CD86.

All the above results (both positive and negative) combined confirm that the phenotype of the cultured cells correspond to immature DCs. This result is a requisite for MNPs vectorization to neoplastic tissue, since the overall strategy relies on the ability of immature DCs to transdifferentiate into endothelial cells when cultured under angiogenic growth factors [3] or tumor conditioned media [133]. It is known that when DCs are stimulated by antigens and consequently reach the mature state, they lost their capacity to differentiate into any other type of cell [134, 135]. Therefore, keeping the immature phenotype of DCs until they reach the desired organ is essential for the therapeutic application proposed in this thesis.

III.I.III. Viability assay

Polystyrene particles have been widely used for incorporation studies in DCs because they are easily available from different commercial providers, with different fluorescent markers, surface charge and well defined sizes from hundreds of nanometers to few microns [136]. With the use of this kind of particles, it has been demonstrated that cytotoxic effects depend on both size and surface charge [136, 137]. Cytotoxicity of other kinds of nanoparticles has been also already tested showing that there was not any toxic effect on DCs due to the nanoparticles incorporation [104, 138]. However it has also been described that many cytotoxic effects can be triggered by incorporation of NPs. Among the effects most commonly reported are the *direct toxicity* effects as changes in the cellular metabolism [139], alterations in plasmatic membrane integrity

[140, 141] and modifications of mitochondrial metabolism [142]. In addition to these direct effects on cell viability, NPs have been described to generate long-term side effects, i.e., *indirect toxicity* [143], involving changes in cytoskeleton architecture that lead to morphological cell changes, proliferative rate diminution or migration and differentiation defects [144, 145].

As already described in the Materials & Methods, it was mentioned in the previous chapter, three different methods of cell viability measurement were used. The simplest and quickest method, the Trypan Blue assay, consisted of using a vital dye which entered only in the cells that had any plasmatic membrane damage, so blue dyed cells were counted as dead cells. That is why with this method we were not able to determine the death mechanism. Though some early apoptotic stages can be identified because of the "blebs" presence, Trypan Blue gives only information to identify death cells from alive ones whatever the death mechanism involved. The Trypan Blue results shown in Figure III-I- 8, showed that the viability of DCs after 1, 3 and 5 days of co-culturing with both NH_2(MNP)+ and COOH(MNP)- decreased in a similar trend than the control sample (without MNPs), remaining above 65-70% at the fifth day of culture. It is noteworthy that the DCs used in this work were primary cells that did not duplicate and therefore they had typically a finite life span in culture, as opposite to immortalized cell lines. Therefore the use of this primary line implied a small but noticeable continuous decrease of cell viability from the first day even for control cells. Figure III-I- 8 shows this behavior for all samples analized. However, when compared within the same day, magnetically charged cells showed the same viability percentage than control cells within experimental error.

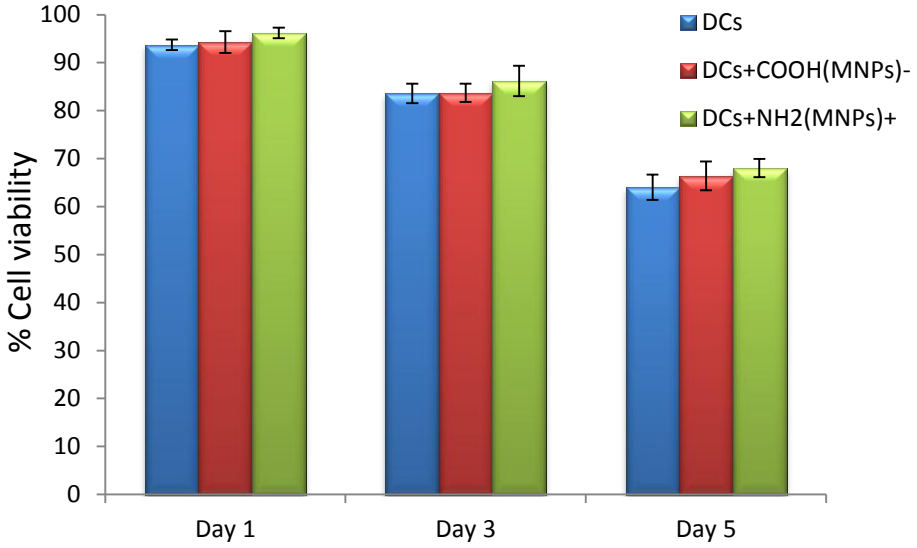

Figure III-I- 8: Trypan blue results of cell viability along five days for DCs loaded with positively (NH_2(MNP)+) and negatively (COOH(MNP)-) charged nanoparticles. The primary DC culture without MNPs showed a natural decrease of viability from ca. 95% to 64 % at the fifth day. The same trend, within experimental error, was displayed by the DCs loaded with both types of MNPs. Experiments was done in triplicate, Number of experiments=3.

In order to verify these results we performed a second cell viability test using MTT, which determined the mitochondrial activity of the cells. The MTT results represented in Figure III-I- 9 confirmed the results from Trypan Blue data regarding the cell viability up to five days was not affected by the incorporation of MNPs irrespective of the surface charge. The bigger error bars obtained from this protocol, as compared to the previous TB experiments are related to this technique. The larger variability usually observed in MTT essays may come from the seeding step for the cells in a 96 well-plate, where potential errors during counting and pipetting processes are likely to accumulate. Also the step where the supernatant was removed after the sedimentation of the formazan crystals might introduce any error if any crystal was accidentally removed.

The cell viability data obtained by MTT test is often normalized to a blank sample, i.e., DCs without MNPs, and this is the reason why viability of blank sample was always 100% and values for the rest of the samples were higher when compared with values obtained in Trypan Blue. Trypan Blue data represented the real percentage of cell death, whereas MTT data represented the percentage of cell death of the sample of interest in relation with the reference sample.

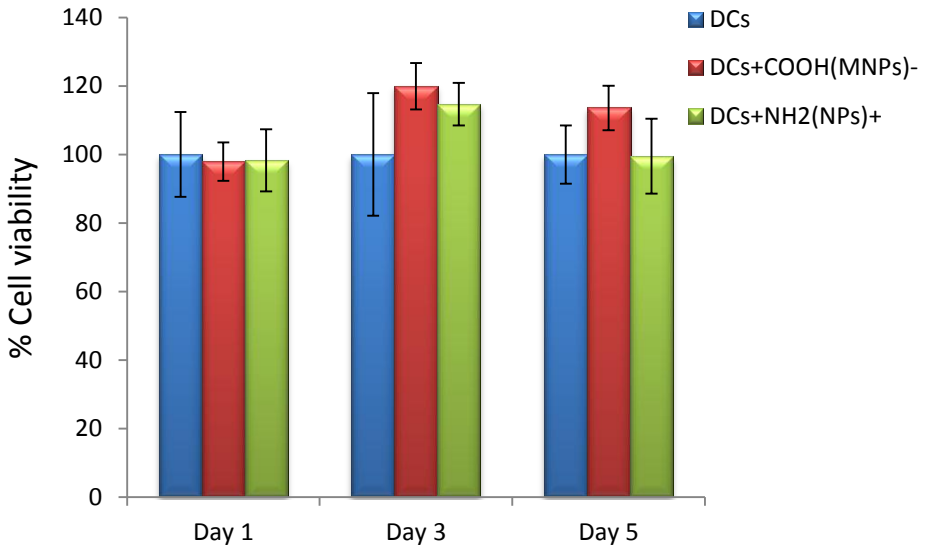

Figure III-I- 9. MTT results along five days for DCs loaded with positively (NH_2(MNP)+) and negatively (COOH(MNP)-) charged nanoparticles. The same trend, within experimental error, was displayed by the DCs loaded with both types of MNPs. Number of experiments=3.

Finally, as a further confirmation of the cell viability trends, annexin-V/ propidium iodide staining protocol was used. As explained in the Materials and Methods section the Annexin-V binds to phosphatidylserine, a protein that translocate to the extracellular side of the plasmatic membrane at the early stage of apoptosis, whereas propidium iodide (PI) can only enter the cell only when some damage in the cellular membrane

exists. Cell permeability to PI is a typical manifestation of a necrotic process related to cell death. So with this assay we were able to distinguish between early apoptosis and necrosis, or late-stage- apoptosis that ends with a disruption in the cellular membrane.

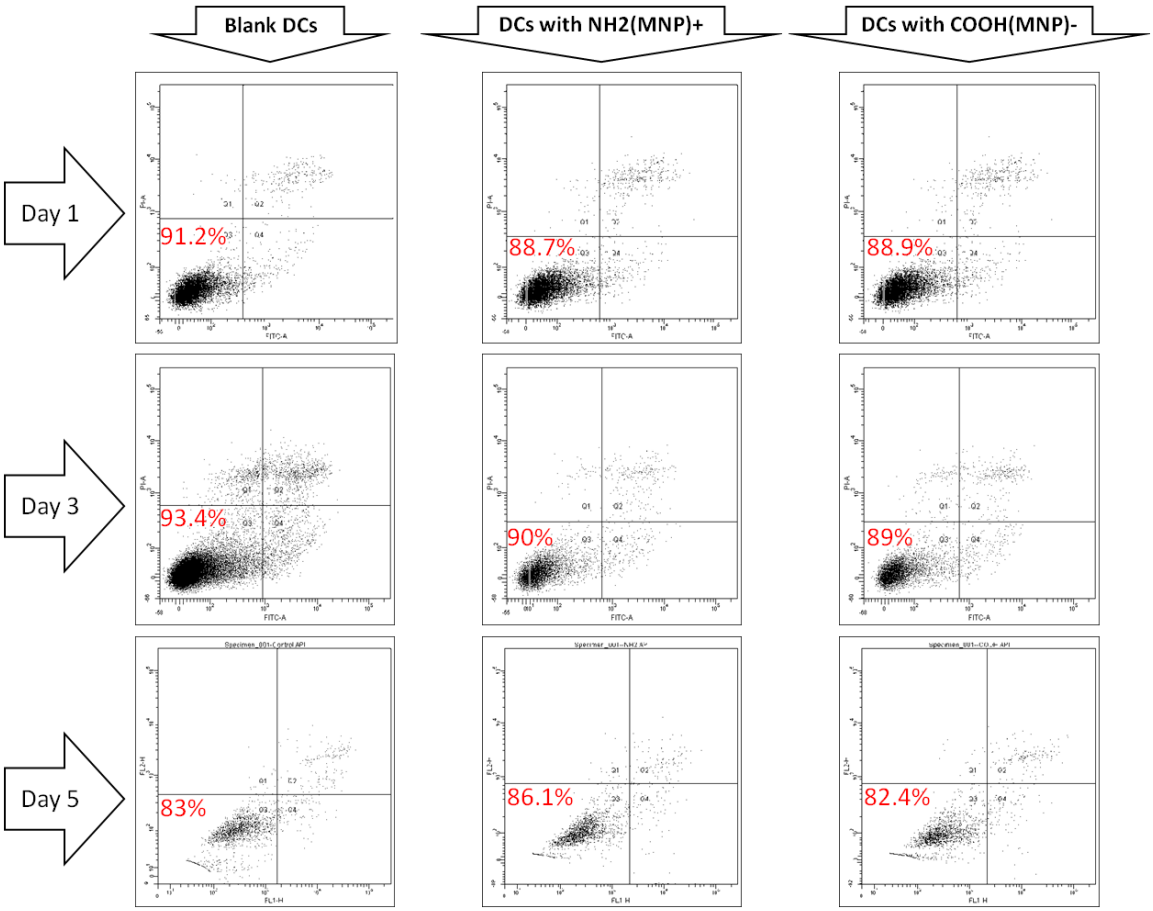

Figure III-I- 10: Dot plot representations from flow cytometry data on the DC viability along five days of co-culture with positively (NH2(MNP)+) and negatively (COOH(MNP)-) charged MNPs. The numbers in each representation corresponds to the percentage of viable cells.

Cells incubated with the MNPs for 1, 3 and 5 days, as in Trypan Blue and MTT method, were stained with Annexin V and IP markers. Cells were then analyzed by FACS and dot plot representations are collected in Figure III-I- 10 where X axis represented the green fluorescence intensity (for FITC-Annexin V) and the Y axis represented the red fluorescence intensity (for PI, that emitted a strong red fluorescence). For each sample 5000 counting events were collected, i.e., the analyzed population consisted of at least 5000 cells for each experiment. Each dot corresponded to one cell. It can be clearly seen that for all the samples the cell population was negative for both markers, and the cell viability value remains above 80%. These results are in agreement with the results obtained from Trypan Blye and MTT tests. No cytotoxicity effect was observed neither for the NH_2(MNP)+ nor COOH(MNP)- samples. In the next sections we will show that the cells internalized both types of MNPs efficienly resulting in hundreds of MNPs per cell.

It is important to highlight that no differences in cell viability between positively and negatively charged nanoparticles were observed. Furthermore, as it will be shown, the amount of material incorporated per cell for COOH(MNP)- was higher than for NH_2(MNP)+ (almost the double).

We can conclude that despite the efficient internalization of MNPs in DCs and the higher affinity for internalizing COOH(MNP)- due to the negative charge of the particles, there was no observed any cytotoxic effects for neither MNPs types.

Concerning the cytotoxicity effects the nanomaterials have in DCs, in the literature are reported both positive and negative effects depending the nanomaterials characteristics. Kunzmann et al. compared the toxicity effects in DCs of silica-coated NPs (30 and 50nm) with dextran-coated rion oxide NPs (20 and 50 nm) observing that the former showed a dose-dependent toxicity (at 50-100 μg/mL after 24 and 48h of

incubation) and a higher degree of internalization whereas the latter presented no cytotoxicity effects [138]. Migdal et al. studied the effects hybrid titanium dioxide/para-amino benzoic acid NPs have in DCs, showing that the NPs were captured by the DCs but no toxic effects were observed at 100 μg/mL after 48h of incubation [104]. These are two examples that confirm that the cytotoxicity of MNPs depends on several parameters as the cell type and the characteristics (as size, shape and surface molecules) of the nanomaterials.

III.I.IV. TEM

As we have just mentioned, the MNPs did not have any cytotoxic effect in the DCs, therefore, the next step was to study wheter the MNPs were incorporated by the cells or were just adhered to the membrane and consequently were no toxic. For that purpose, direct observation methods as TEM , SEM and confocal microscopy were used. The information obtained from these techniques combined with the quantification of the captured MNPs performed by SQUID measurements, will inform us about the feasibility of using the DCs as vehicles for the MNPs in the Trojan horse strategy.

Observing the cells by TEM we studied the final intracellular localization of the MNPs in cells incubated with differerent amount of MNPs during 24h. This technique allow us to qualitatively compare the amount of MNPs internalized at different concentrations, but for quantitative comparation we performed magnetic measurements by magnetomer SQUID, as will be shown latter.

Figure III-I- 11 shows that in the DCs incubated with MNPs (B,C and D), the MNPs were found located in membrane-enclosed vesicles, indicating the involvement

of an active uptake mechanism such as endocytosis or phagocytosis. The reference sample (A) that consisted of just DCs shows the absence of these vesicles. We can confirm that MNPs uptake was concentration-dependent, as higher uptake was observed after incubations with higher concentrations, as it can be very clearly seen in Figure III-I- 11. The MNPs concentrations investigated were: 50,150 and 300 μgFe_3O_4/ml. It can be observed that DCs incubated with 150 and 300 μgFe_3O_4/ml incorporated much higher amount of MNPs than the DCs incubated with 50 μgFe_3O_4/ml. However between the concentrations of 150 and 300 μgFe_3O_4/ml the difference in the amount of MNPs uploaded is less perceptible. So, we can suggest that there exists a limit concentration, at which the DCs uptake saturates.

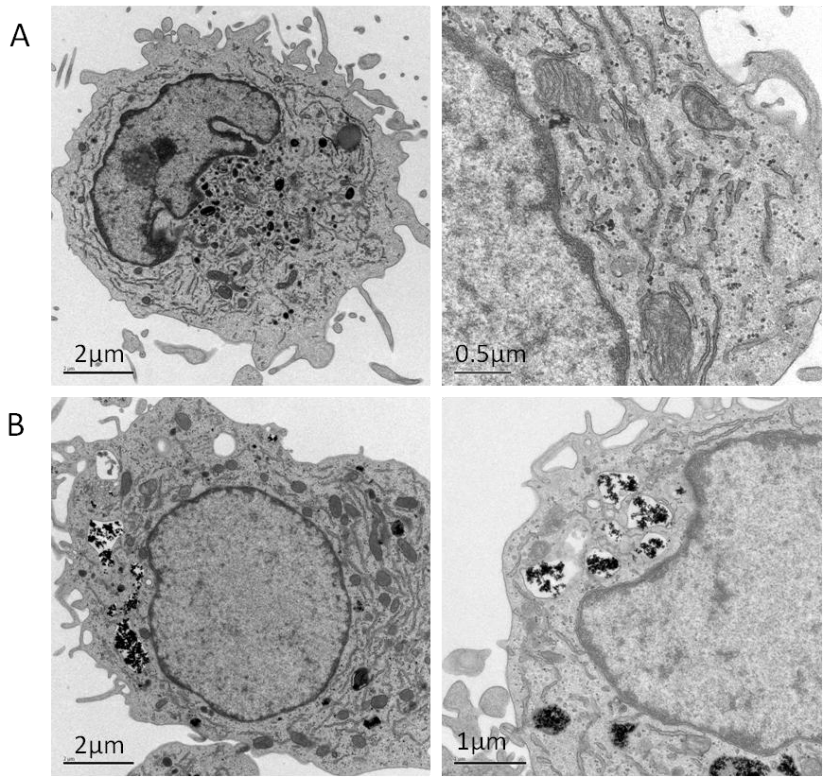

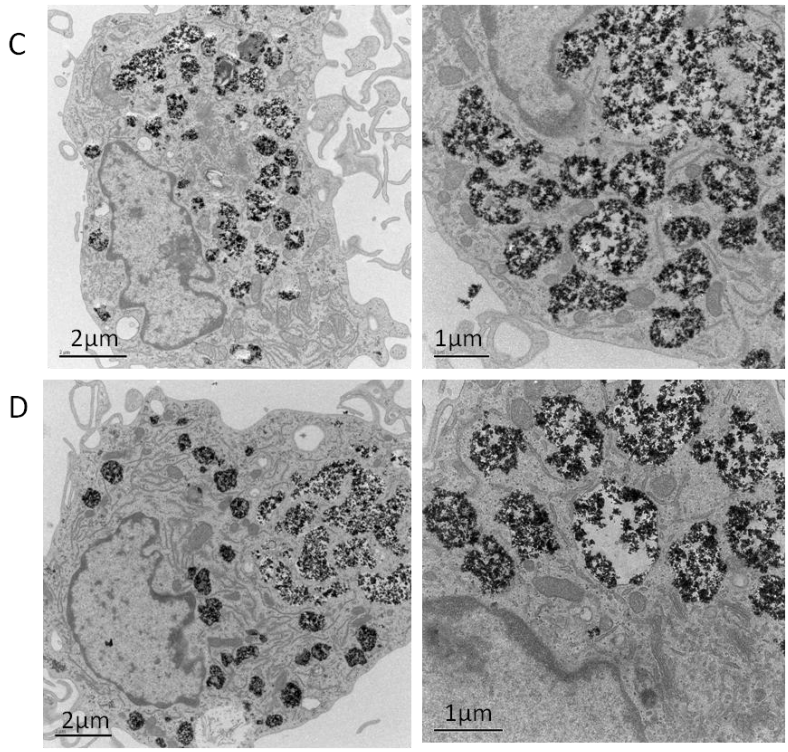

Figure III-I- 11: Transmission Electron Microscopy images of DCs uploaded with COOH(MNP)- nanoparticles (right and left are two different magnifications). A) DCs without MNPs, as reference sample, B) DCs incubated with 50 µgFe_3O_4/ml, C) DCs incubated with 150µgFe_3O_4//ml MNPs and D) DCs incubated with 300 µgFe_3O_4//ml MNPs.

For hyperthermia experiments the MNPs incubation concentration was up-to 50µgFe_3O_4/ml, and this low concentration was, as will be discussed later, enough to trigger cell death mechanism. Taking these micrographs into account, in hyperthermia conditions we had not took advantage of the highest incorporation capability of DCs, as higher amount of MNPs could be incorporated at higher incubation concentrations.

Concerning the localization of the DCs we could observe that the MNPs were confined inside endocityc vesicles in the cytoplasm region. The MNPs were aggregated inside the vesicles, as it can be observed in the images at higher magnification. The

MNPs were never localized inside the nucleous, as they are quite big and the lack the signal for passing the nuclear pores. It has been reported that particles up to 30nm functionalized with peptides that acts as nuclear import signal are able to reach the nucleous [146]. Our particles have a hydrodynamic diameter of 220 nm, much bigger than 30nm, so it was expected to be localized in the cytoplasm of the cells.

It should be highlighted that there were no MNPs attached to the plasmatic membrane in the extracellular side even at the highest concentration, thus, we can assume that the washing protocol we followed it is enough to remove the non incorporated MNPs.

The above results are consistent with previously reported data [19] showing that monocyte-derived DCs are able to incorporate Fe@C MNPs, and that the intracellular distribution of these MNPs is mostly located in cytoplasmatic compartments. Also, several studies have reported the uptake of different complexes by the DCs; the inclusion of latex-type nanospheres from sizes between 220nm and 500nm that reveal that the final lozalization of the NPs was the cytoplasm, never the nucleus [122, 123], and their capacity to incorporate a wide range of antigens and molecules [120, 121]. In many cell lines the uptake of MNPs occurs in a concentration and time dependent manner [147] that depends on some specific features of the MNPs involved.

III.I.V. SEM

There is a tight link between morphology of the DCs and their maturation stage. As mentioned in the Introduction when DCs mature several changes takes place; their main function is to activate T cells and trigger the immune response, their phenotype changes, as it will be shown in next sections and also their morphology changes. Mature DCs

show an activated phenotype consisting of elongated cell morphology compared with DCs in the immature stage. Maturation of DCs can be stimulated by incubating the immature DCs with Lipopolysacharides (LPS), which is a common component of the bacteria membrane, so we used this induced mature DCs as the positive control for comparing the effects the MNPs have in the immature DCs.

In order to study the morphology of the DCs and subsequently their maturation satge and also the MNPs uptake we performed scanning electron microscopy (SEM) experiments. Secondary electrons give a well-defined, three-dimension appearance images and the analysis of the images reveal important changes of morphology between the immature and the mature DCs.

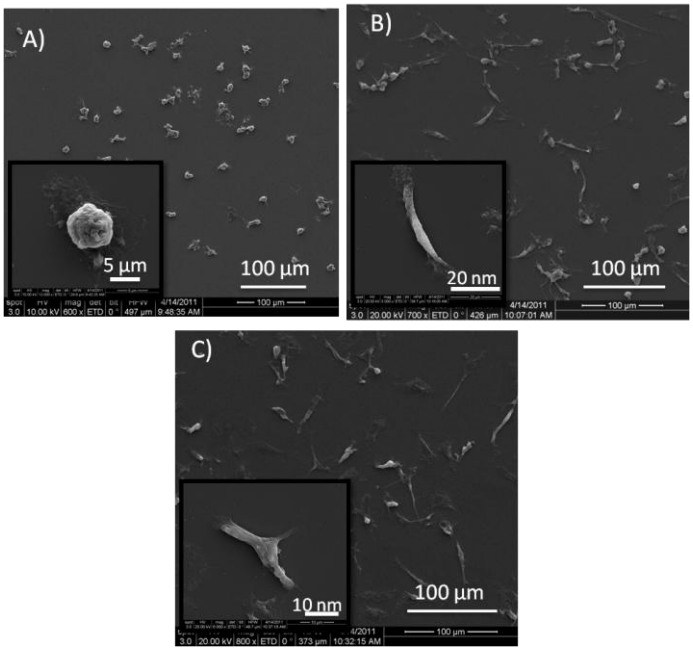

Figure III-I- 12: SEM micrographs of (a) DCs control , (b) DCs after 48h of incubation with MNPs and (c) DCs after 48h of incubation with LPS. Inset images were obtained at higher magnification.

Figure III-I- ***12*** show images of DCs incubated with MNPs and LPS that showed an elongated morphology (mature stage) when compared with the reference immature DCs

that presented a round morphology. These results are in concordance with previous morphology studies [148, 149]. These results indicate that DCs suffer a maturation stimulus due to the incubation with the MNPs. This is in agreement with the results concerning the maturation status of the DCs that will be next shown.

Since heavy elements backscatter electrons more strongly than light elements, in EBSD images the heavy elements areas appear brighter, so that the contrast between areas corresponds to different chemical composition. Based on the EBSD images information we selected different areas where EDX analysis was performed.

We observed that in the DCs without NPs heavy elements were not presented, so in the EBSD images the cells appeared in darkness, Figure III-I- 13. Analysing the EDX results we did not observed any presence of Fe.

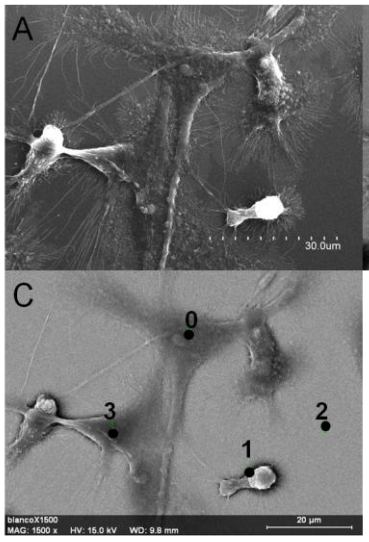

D

Atomic %

	C	O	Na	Mg	Si	Ca
0	44.5	37.4	3.3	1.2	12.5	1.1
1	18.2	56	5.5	1.5	16.7	2
2	6.8	56	7.4	2.5	25.6	1.7
3	48.8	36.8	3	1	9.8	0.7

Figure III-I- 13. SEM images of control DCs sample. A) Secondary electron image, B) EBSD image, C) the numbers indicate the spotos selection for EDX analysis and D) results of EDX analysis at each selected spot expressed in atomic percentage.

On the other hand, when we observed the samples of cells incubated with MNPs, the EBSD images of all of them revealed the presence of MNPs inside of the cell, and EDX analysis in different areas of the cells showed a high Fe content, Figure III-I-14,due to the NPs uptake. The amount of MNPs incorporated by the cells in this micrograph looks like higher as in the Figure III-I- 11-C, which corresponds to the same MNPs incubation concentration. This is because in TEM images we observe a cut of the cell with a depth of about 70nm and in SEM images we are observing the whole cell. We can confirm that the MNPs are inside the cells because we can distinguish the nucleo of the cells without MNPs. If the MNPs were in the extracellular area attached to the cell membrane we would see the whole cell surface covered with MNPs and not only the area that corresponds to the cytoplasmatic region.

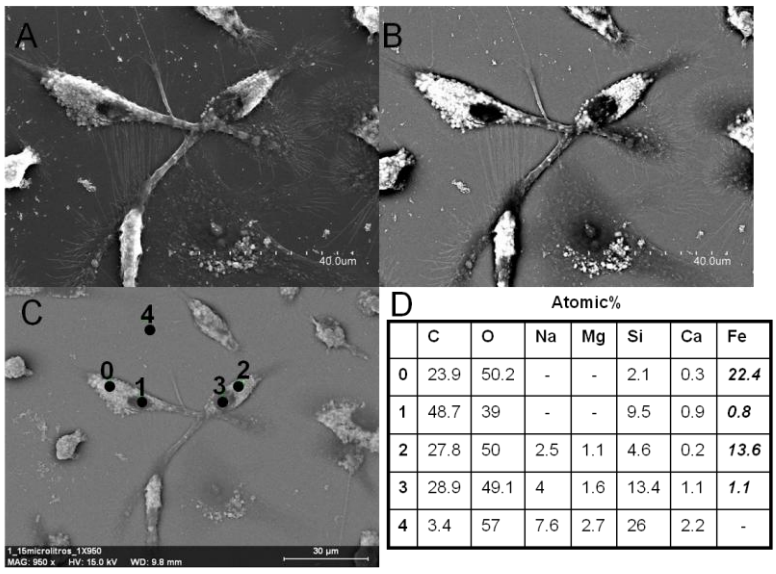

D

Atomic%

	C	O	Na	Mg	Si	Ca	Fe
0	23.9	50.2	-	-	2.1	0.3	***22.4***
1	48.7	39	-	-	9.5	0.9	***0.8***
2	27.8	50	2.5	1.1	4.6	0.2	***13.6***
3	28.9	49.1	4	1.6	13.4	1.1	***1.1***
4	3.4	57	7.6	2.7	26	2.2	-

Figure III-I- 14. SEM images for DCs incubated with 150 µgFe_3O_4/ml of MNPs. A) Secondary electron image, B) EBSD image, C) the number indicate the spots selection for EDX analysis and D) results of EDX analysis at each selected spot expressed in atomic percentage.

III.I.VI. Dual Beam

In adittion to the Scanning and Transmission electron microscopy, it was performed Dual Beam in order to observe at in the same cell the morphology and a corss-section. It is possible because Dual Beam has an electron beam to observe the morphology of the sample, as in a SEM, and an ion beam, to cut the sample allowing to observe a corss-section of the sample.

The samples that we observed by Dual Beam were: DCs as reference sample and DCs incubated with 50 μgFe_3O_4/ml of COOH(MNPs)-. Cross-sections of both samples are presented in the Figure III-I- 15. In the sample of DCs incubated with the MNPs (left image) MNPs aggregares can be observed in the cytoplasmatic space. These samples are just fixed and dehydrated, they are not contrasted as for TEM microscopy, thus, it was difficult to identify the different organelas and the nucleous in the cross-sections images due to the poor contrast given by the non contrasted cells.

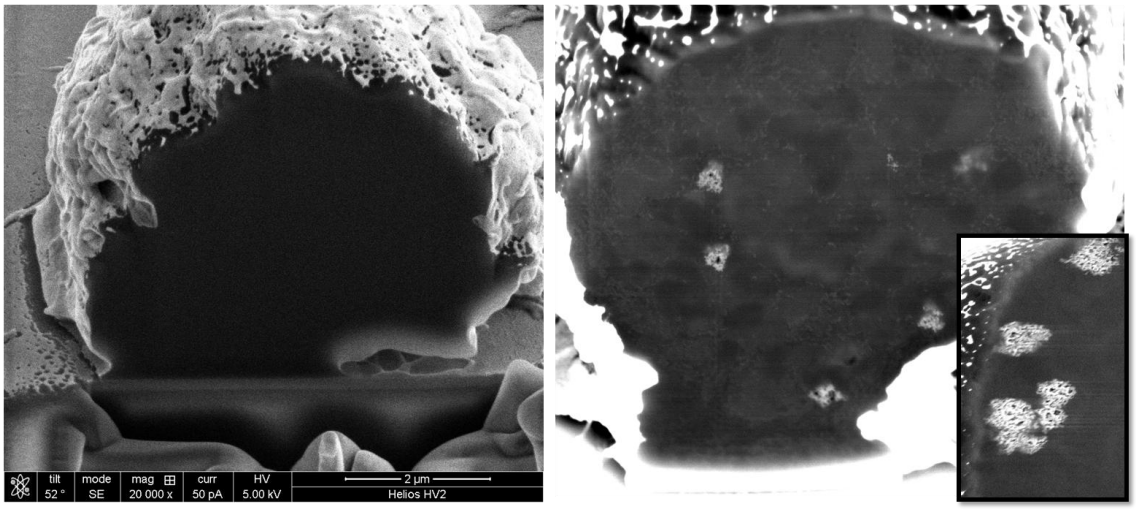

Figure III-I- 15: Dual Beam images for DCs (left) and DCs incubated with 50 μgFe_3O_4/ml (right).

Though the bright particles were identified as the MNPs becase they appeared only in the DCs cultivated with MNPs, EDX was performe to anayze this aggregates and to ensure that they corresponded to the MNPs. Figure III-I- 16 shows images at different magnifications of DCs incubated with the MNPs and the pink square demarcates the area of EDX analysis. The map obtained from the EDX analysis shows the presence of Fe that came from the MNPs. Thus we can confirm that the bright particles were the aggregates of the MNPs and that Dual Beam is a suitable technique to study the internalization of magnetic material in cells.

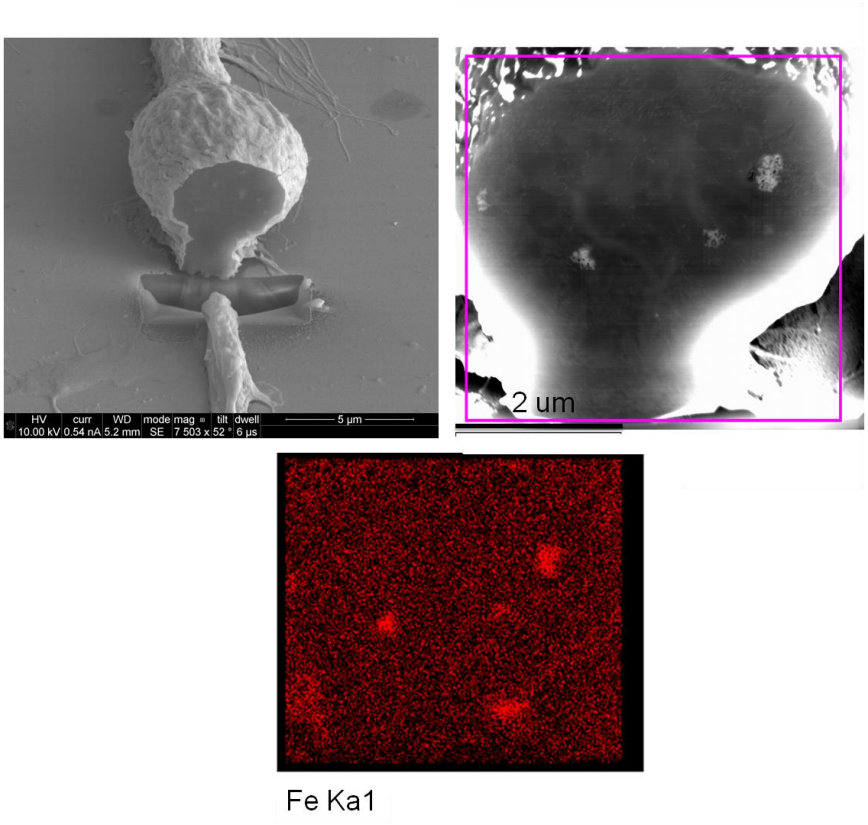

Figure III-I- 16: Dual Beam images for DCs incubated with 50 µgFe_3O_4/ml (Up images, at two different magnifications). Pink square selects the area where the EDX was performed. EDXmapping results for the selected area (Fe detection)(Down).

III.I.VII. Confocal microscopy

Confocal microscopy was performed in order to observe the cell internalization of the nanoparticles and to study the mechanism to incorporate NPs into the cytoplasm. This information is important because these mechanisms determine the upload kinetics and intracellular fate of the nanoparticles. Endocytosis is recognized as the most common among active mechanisms for MNPs uptake by different cellular types including HeLa, fibroblasts and DCs.

There is some controversy regarding the mechanisms governing the internalization of nanoparticles in DCs. While some authors have shown that NPs are internalized via phagocytosis [122, 123, 150], using the inhibitory effect of cytochalasin B (a well-known phagocytosis inhibitor) on the NPs internalization process of DCs, other studies reported endocytic-like internalization process [138, 151], showing that the internalization activity is significantly reduced when DCs are treated with cytochalasin D (which prevents the actin of the cytoskeleton reorganization during an active endocytosis). There is also evidence of macropinocytosis process [104] where several inhibitors of receptor mediated endocytosis were used. Since these inhibitors did not affect NPs internalization authors concluded that the uptake mechanism is macropynocitosis. In the absence of MNPs surface functionalization with specific biologic ligands, like the present MNPs, the most probable mechanism involved in the uptake of these MNPs is a non-specific endocytosis mechanism.

Images for DCs incubated with NPs-Rho and cytoskeleton proteins staining are shown in Figure III-I- 17. One of the samples containing DCs was stained with DRAQ-5 to label the nucleus (Figure III-I- 17-A) and was analyzed to verify whether there was cell auto-fluorescence that could be detected in our working conditions. The results

showed that there was no auto-fluorescence signal captured in any channel. To demonstrate a good channel separation with no interference at all, the images are shown in each channel separately and then the overlay of all the three. Besides, two samples consisted of DCs incubated with NPs-Rho (125 μg/ml) at 37ºC were prepared, one of them was further stained with Phalloidin-FITC (Figure III-I- 17-B), and in the other one Tubulin staining was performed (Figure III-I- 17-C). The last sample was DCs incubated with the NPs-Rho at 4ºC, in order to see whether NPs were able to be incorporated through a passive mechanism that did not need for energy (Figure III-I-17-D). All samples were also stained with DRAQ-5 dye, to show the nucleus.

Both Phalloidin and Tubulin staining allow visualizing the morphology of the DCs. Fluorescent nanoparticles are clearly observed inside the cell and allowed to confirm that the final location was at the cytoplasm. However due to the absence of colocalization studies we were not able to clearly determine whether the NPs were inside organelles or at the cytoplasmatic space. Furthermore, it can be observed that with the incubation at 4ºC, performed in order to verify whether the NPs uptake was inhibited at low temperature, the NPs uptake became inhibited, and thus we could confirm that the uptake was an active process, i.e. that requires energy to proceed. This result is in agreement with previous studies in human and murine DCs showing that, for these cells, NPs are captured via phagocytosis, an internalization mechanism that requires an active cellular role [122] [123]. Based on the general outstanding that particles captured by phagocytosis remain in the endo-lysosomes, and knowing that lysosomes contain cellular waste materials, if the MNPs inside these organelles vibrate during the AMF application, it may cause the disruption of the lysosomes membrane and the release of the lysosomal content to the cytoplasmatic media, being toxic to the DCs and causing cell death.

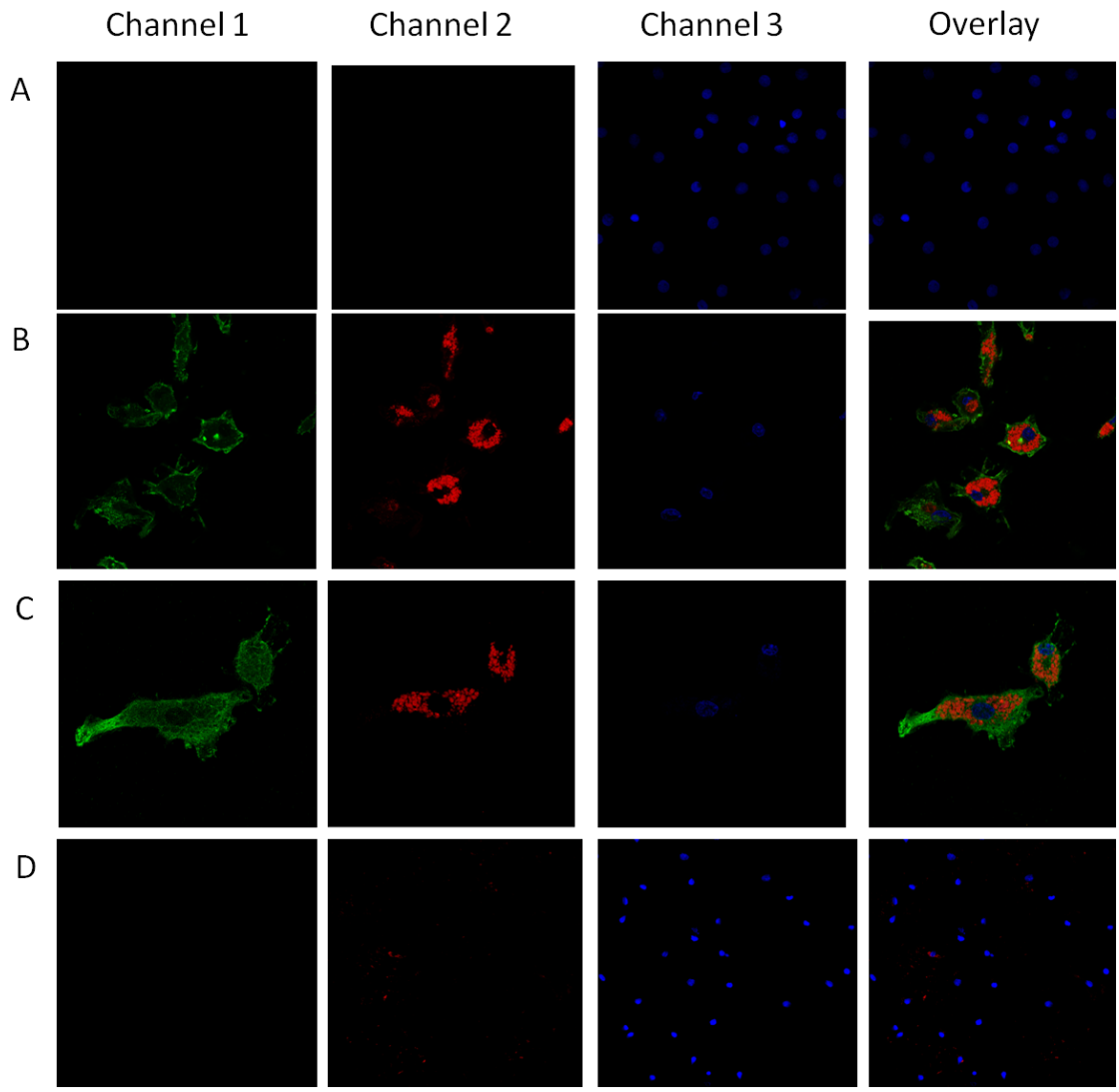

Figure III-I- 17: Confocal images obtained in each fluorescence channel (channels 1, 2 and 3 captured green, red and blue fluorescence, respetively). The last column shows the overlay of the three channels. A) DCs , B) DCs incubated with NPs-Rho, stained with Phalloidin, C) DCs incubated with NPs-Rho after Tubulin stain and D) DCs incubated with NPs-Rho at 4ºC overnight. All the samples were stained with DRAQ-5.

The previous results on NPs-Rho upload were obtained using a particle concentration of 125 µg/ml. To further determine whether the amount of uptaken NPs was dependent on the concentration during incubation, further experiments were performed by incubating the DCs with increasing concentration of NPs-Rho from 0.25 to 1.25 mg/ml.

It is worth to mention here that, in these experiments using confocal microscopy, the concentration values of fluorescent NPs-Rho used were much higher than the corresponding incubation concentrations of MNPs used for TEM and SEM imaging (50-300 µg/ml and 150, respectively). Therefore images from fluorescence and electronic microscopy cannot be directly compared, since at the high concentrations for confocal microscopy images the corresponding TEM images should appear as fully 'saturated' with MNPs.

Confocal microscopy images confirmed this result, Figure III-I- 18 shows that the increasing amount of MNPs incorporated was hardly to detect. DCs were full of NPs, so we could confirm that incubation of DCs at these NPs concentrations made DCs saturate their incorporation capability. Also incubation with the highest NPs concentration was performed at 4ºC to make sure that the incorporation process was inhibited even at very high NPs dose. Image presented in Figure III-I- 18-C show that the DCs did not incorporate any NPs at 4ºC even at this high NPs concentration, which is in agreement with the results of the Figure III-I- 17.

These results confirmed the inhibition of the uptake process at 4ºC and established that the mechanism was energy-dependent. This idea linked to the fact that these NPs had no any specific biological molecule at their surface (different from the positively charged NH_2^+) suggested that the process of internalization was a non-specific endocytic pathway.

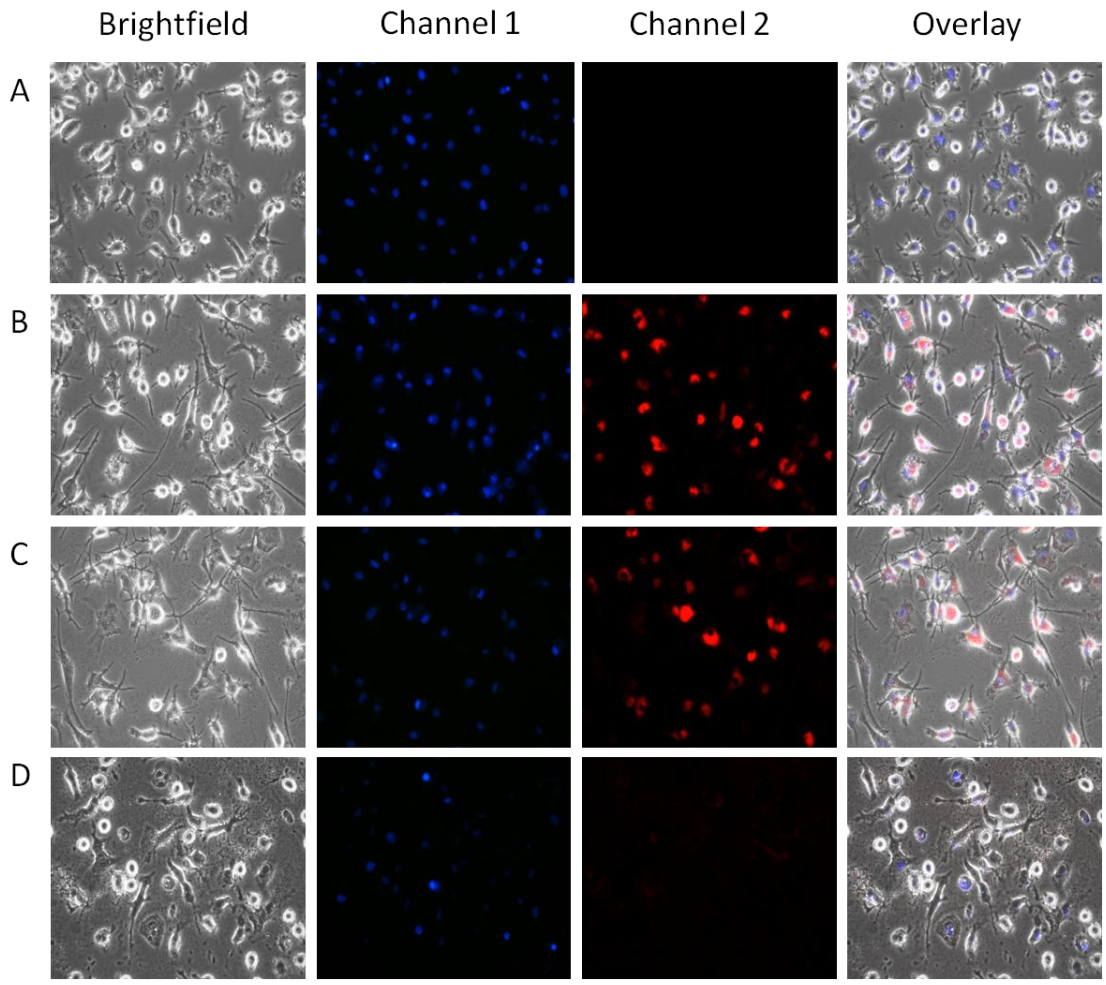

Figure III-I- 18. Confocal images of DCs incubated with different amounts of NPs-Rho: A)Control DCs, B) DCs incubated with 50 µg/ml of NPs-Rho, C) DCs incubated with 300 µg/ML of NPs-Rho and D) DCs incubated with 300 µg/ml of NPs-Rho at 4ºC. It is shown separately the brightfield image, channel 1 that shows nucleusstaining, channel 2 that shows red fluorescence emitted by the NPs-Rho and finally the overlay.

It is known that immature DCs express receptors related to surface pattern recognition, for specific types of pathogens. Previous works have shown that morphological changes during internalization can be understood in terms of

phagocytosis as the main pathway for the uptake of non-functionalized NPs [122, 123] [150]. These morphological changes include (but are not restricted to) gerenalized membrena ruffling and the formation of large (micrometer-sized) vesicles as the incorporation proceeds. Other pathways, like clathrin-mediated endocytosis and caveolae, are less distortive for the cell membrane, and form much smaller vesicles of, about 50 to 100 nm size. Our results showed that the vesicles developed during early stages of internalization were around 1μm, as seen from TEM images, supporting the phagocytosis as the main mechanism.

III.I.VIII. Quantification

In the previous sections it has been shown and discussed the application of several techniques, as confocal microscopy and electronic microscopy to assess the uptake and final intracellular distribution of the MNPs. Although these techniques allow a precise determination of the MNPs location, they are not suitable to quantify the amount of material incorporated.

In toxicity experiments, for example, the viability of cells is measured against the concentration of *added* MNPs to the culture, but not the fraction internalized. The quantification of the amount of MNPs effectively incorporated by DCs at different conditions is required, for example, to estimate the heat the MNPs will release during AMF application. It will help to understand the mechanisms of cell death induced by the MNPs during AMF experiments.

Few options in terms of techniques for such quantification are described in literature as a tool for measuring the amount of incorporated iron-based nanoparticles. Because of the similar nanometric size of the nanoparticles as compared to the

wavelength visible light, light microscopy is not a viable option. Other techniques as inductively coupled plasma-mass spectrometry (ICP-MS) [138], ferrozine-based colorimetric iron assay [152], thiocyanate-based colorimetric iron determination [153] and magnetophoresis [57] are used for nanoparticles quantification.

Alternatively, the magnetic response, as magnetic susceptibility or magnetization of a bulk sample can be used to quantify the amount of magnetic particles inside a cell. Ström et al. have developed novel devices based in magnetic measurements [154] through the construction of a desktop magnetic susceptometer specially adapted for liquid samples or particles in suspension that required a few seconds for a measurement. Magnetization-based measurements of internalized nanoparticles if of course restricted to applications involving only ferro- or ferri-magnetic materials, more likely those with large saturation magnetization values. However, SQUID magnetometers have evolved along the last decades to provide trustable systems with the capacity of measuring extremely small magnetic fields of about 10 fTesla (theoretically, a single quantum of flux).

Therefore the quantification method we selected was the currently "traditional magnetometry" (using a SQUID magnetometer) due its high sensitivity and the experience in our group. Furthermore, to the best of our knowledge, this is the first attempt reported in the literature that uses SQUID measurements to quantify the magnetic material incorporated by cells. Thus, magnetic measurements on the MNP-loaded DCs were performed as a novel and quite straightforward way to determine the amount of magnetic material effectively incorporated. We consider this method suitable to perform quantitative measurements because as far as we have observed through Transmission Electron Microscopy, there are no MNPs attached to the cell membrane (as it can be seen in Figure III-I- 11). Thus, we consider that washing by centrifugation

is enough to remove the MNPs that have not been internalized which are in the supernatant medium.

All measurements were done using the same amount (of the order of 10^6) cells. The measurement of a control sample (i.e., 1x106 DCs without NPs) at the same temperature was important in order to subtract the strong diamagnetic signal from the DCs as compared to the magnetic signal coming from the internalized MNPs, specially at low temperatures where diamagnetic signal dominates. In this way, once the diamagnetic signal intrinsic of the DCs from the control sample was subtracted, the resulting signal was attributed to the incorporated MNPs.

In order to know the specific magnetization of the MNPs used in our experiments, the magnetization curves of the pure colloids of both COOH(MNPs)- and NH_2(MNPs)+ were also measured. As describe at the beginning of this chapter, for T= 10Kthe saturation magnetization M_S found was 66 and 62 Am^2/kg Fe_3O_4 for COOH(MNPs)- and NH_2(MNPs)+ samples, respectively. By referring to these values of the pure colloids, and knowing the number of cells per sample, we calculated the amount of magnetic material, and the number of MNPs per cell. The use of the saturation magnetization as the reference parameter to estimate the amount of magnetic material was based on the assumption that the saturation magnetization of the MNPs does not change when NPs are internalized. This seems a trustable hypothesis, since M_S depends on the magnetic phase of the MNPs, and is independent on the aggregation state of the NPs inside the cells.

The results for both COOH(MNPs)- and NH_2(MNPs)+ incorporated when cells were incubated at 50 μgFe_3O_4//ml are **1.5±0.8 pgFe_3O_4/cell (1.1±0.6 pgFe/cell, 253±144 MNPs/cell)** and **0.8±0.2 pgFe_3O_4/cell (0.6±0.2 pgFe/cell, 130±37 MNPs/cell)** respectively. The cells incubated with COOH(MNPs)- particles may incorporate almost

the double amount of MNPs compared to the NH_2(MNPs)+ ($p<0.25$). As for further experiments we decided to work with just one type of MNPs, and no big differences in cytotoxicity were detected between positively and negatively charge nanoparticles, we choose the COOH(MNPs)-, as they were internalized more efficienly and they have a slightly higher saturation magnetization and SPA value. The data from magnetic measurements revealed that incorporation of MNPs in DCs was higher for negatively charged MNPs, Figure III-I- 19. Contraty to our results, Zupke et al. studied the incorporation of positively (NH_2) and negatively (COOH) charged NPs (100-150 nm) in human DCs showing that DCs internalized more efficiently the negatively charged NPs by a factor of 3-4 [155].

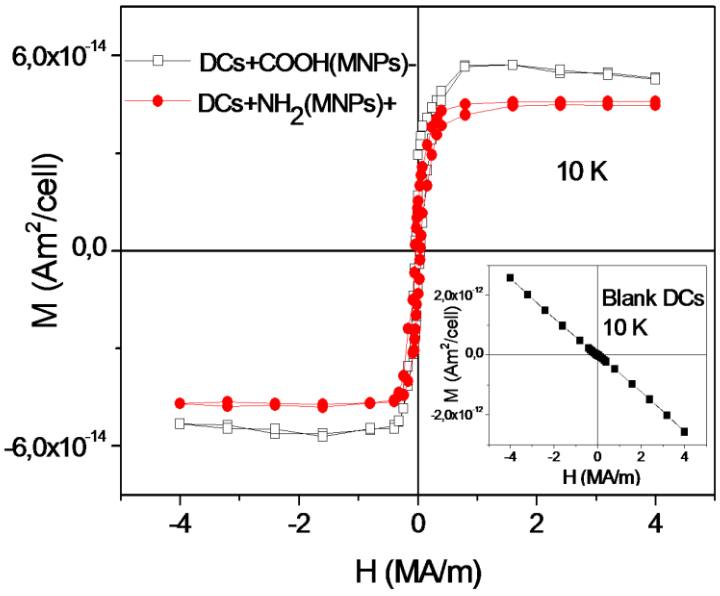

Figure III-I- 19: Hysteresis loops of magnetically-loaded DCs taken at T = 10 K. Main panel: low-temperature magnetic signal from $1x10^6$ DCs cultured with 50 µgFe_3O_4/ml COOH(MNP)- (open squares) and NH2(MNP)+ (circles). The diamagnetic signal of $1x10^6$ blank DCs (lower inset) has been subtracted in all cases.

As it can be seen, since the blocking temperature of these MNPs is about 250K, hysteresis loops measured at 10K revealed that the MNPs inside the DCs were unblocked and presented a coercivity of 32 kA/m, Figure III-I- 20 , the same value as the one obtained from the measurements of the particles alone, Figure III-I- 6.

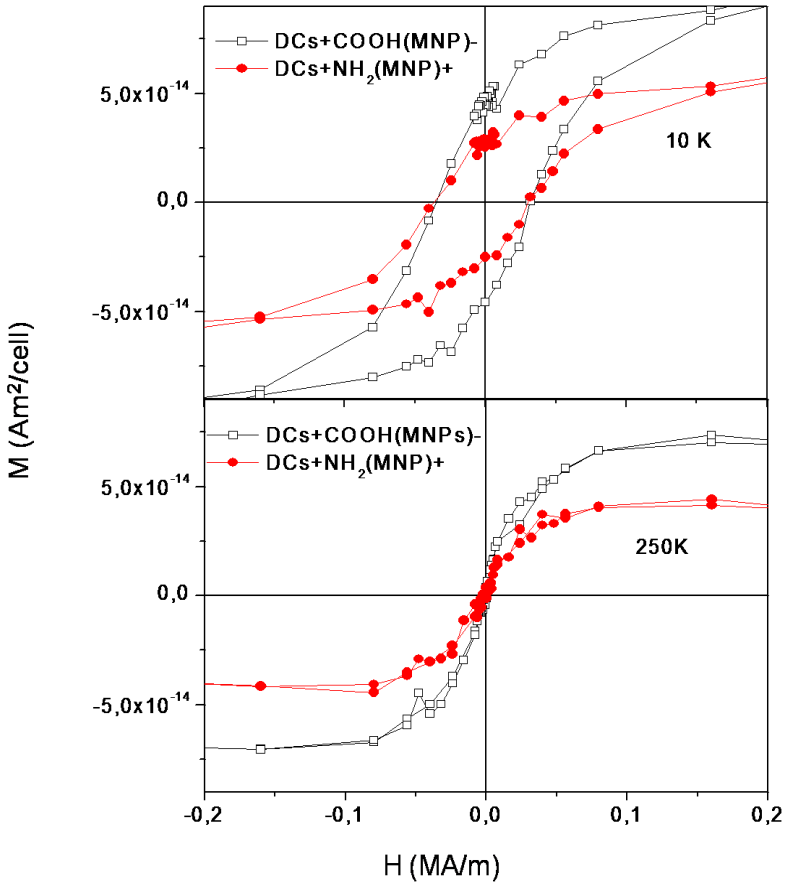

Figure III-I- 20: Hysteresis loops of DCs loaded with COOH(MNP)- (squares) and NH2(MNP)+ (circles) at 10K and 250K.

In order to study the physical state of aggregation of the NPs at the intracellular space, we have analyzed the magnetic state of the NPs at 250K in samples of DCs+MNPs. Similarly to the pure colloids at room temperature, Figure III-I- 5, the particles uploaded by the cells also displayed SPM behaviour reflected in the M(H) curves with null coercivity at 250 K, Figure III-I- 20.

This result indicates that the Fe_3O_4 phase is not reduced/oxidized in the intracellular medium and that the particle size distribution remains essentially unaltered after the incorporation into DCs (i.e., no selective sizes are incorporated). As discussed previously, TEM images showed that MNPs are agglomerated inside endosomal spaces [19], and therefore we conclude that the dextran/functionalized shell is thick enough to prevent strong interparticle interactions. This is an important issue regarding heating experiments *in vitro*, since strong interacting NPs could result in a decrease of the power absorption [156].

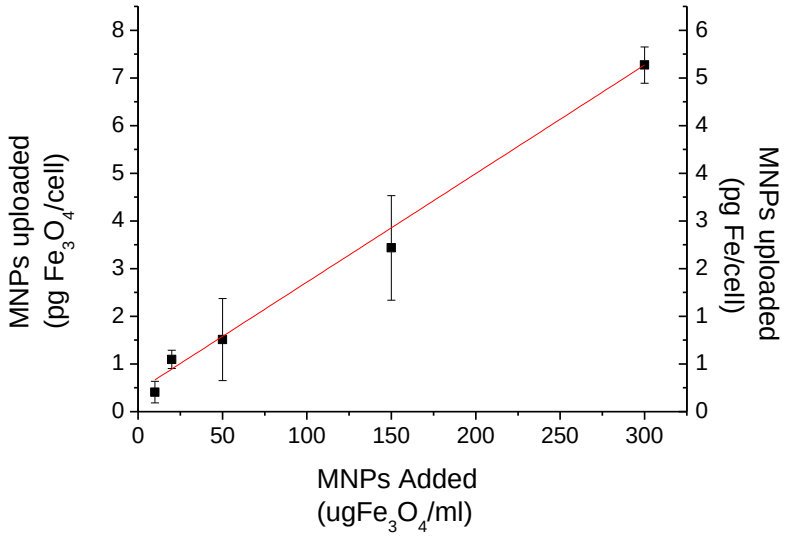

Figure III-I- 21: Graph showing the relation between the amount of COOH(MNPs)-incorporated per cell at increasing incubation concentrations.

The M(H) data at low temperature obtained from DCs cultured with increasing concentrations of COOH(MNP)- demonstrated that MNPs are incorporated into DCs in a dose-dependent way, as it has been seen in TEM images. The gradual increase for increasing amount of MNPs added (10, 20, 50, 150 and 300 μgFe_3O_4/ml) indicated larger amounts of magnetic material incorporated by the cells. It is noteworthy that the increase in the amount of magnetic material incorporated at the increasing incubation concentrations (from 10 to 300 μgFe_3O_4//ml) remained almost proportional from $0.4\pm0.2 pgFe_3O_4$/cell at the lowest concentration ($10\mu gFe_3O_4$/ml) up to $7.2\pm0.3 pgFe_3O_4$/cell, Figure III-I- 21.

Using the M_S values of the pure ferrofluid and the average volume of the magnetic cores extracted from TEM images, we were able to determine the average number of NPs per cell (Table III-I- 2), obtaining from $0.7x10^2$ to $1.2x10^3$ NPs/cell. This relatively small number of particles was able to induce cellular death when submitted to alternate magnetic fields, as will be discussed in the next sections.

$\mu g\ Fe_3O_4$/ml Added	pg Fe_3O_4/cell Uploaded	pg Fe/cell Uploaded	MNPs/cell Uploaded
10	0.4±0.2	0.3±0.1	68±38
20	1.1±0.2	0.8±0.1	183±32
50	1.5±0.8	1.1±0.6	253±144
150	3.4±1.1	2.5±0.8	574±183
300	7.3±0.4	5.3±0.3	1216±64

Table III-I- 2: Amount of MNPs per cell when incubating cells in increasing MNPs concentrations.

III.I.IX. Internalization study by FACS

Nanoparticles internalization study was performed in DCs with fluorescent NPs in order to know whether all the cells incorporate a similar amount of NPs or the uptake is inhomogeneous.

Figure III-I- 22 represents the data obtained by FACS of the percentage of cells that internalized fluorescent NPs when the DCs were incubated with increasing amount of NPs. As it can be seen the percentage of cells that uploaded the NPs seems to be almost constant, being around the 50-60% of the cells at all the NPs concentrations. At 10µg/ml the 43(±8)% of cells internalized the particles and at the highest concentration, 500µg/ml, 63(±7)% of the cells were positive for the uptake. Though the NPs concentration during incubation was 50-fold higher, the percentage of cells that captured them was just 0.2 times higher.

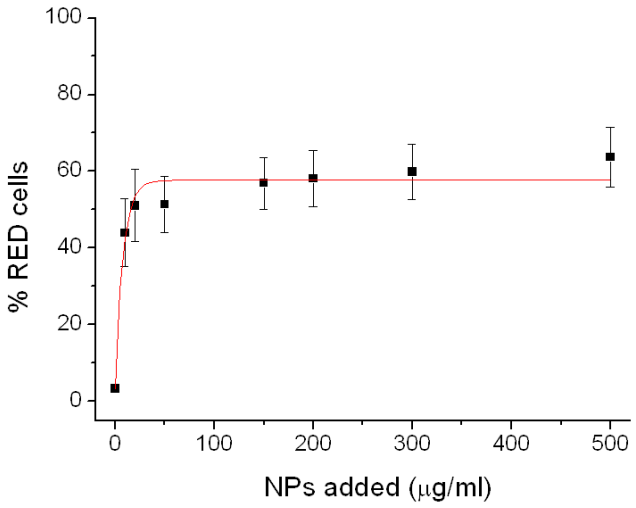

Figure III-I- 22: Representation of the percentage of cells that have internalized Rho-NPs vs the NPs incubation concentration. Measurements were made by FACS. Number of experiments=3.

Figure III-I- 23 represents the data obtained by FACS concerning the mean fluorescence intensity (MFI) of the population that positively internalized the fluorescence NPs.

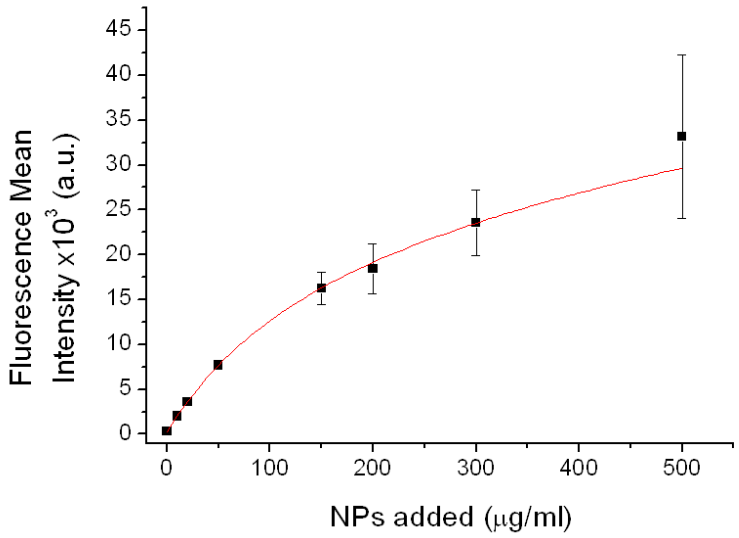

Figure III-I- 23: Representation of the fluorescence mean intensity of the population of DCs that have internalized Rho-NPs versus the NPs incubation concentration. Measurements were made by FACS. Nunmber of experiments=3.

When the results about the MFI were analyzed we saw that there was a tendency of increase this value when the NPs concentration of incubation also increased. The MFI value for the cells incubated with 10μg/ml of NPs was 2000(±280) and when the NP concentration was 50 times higher, 500μg/ml the mean fluorescence intensity was 33113 (±9140), so the MFI increased 16 times. This result indicates that the more NPs are in the medium during the incubation with the DCs, the higher amount of them is internalized by the cells. This value of the MFI referred only of the population of DCs that captured the NPs, and this was possible due to the fact that FACS analyzed cells

one by one and with this technique we were able to distinguish the cells population that had uptaken NPs from the population that had not.

These results clearly indicated that the internalization process was not homogenous in all the cells, as about 40-50% of the cells did not internalized NPs at any NP concentration. However, the cells that internalized the NPs did it in a dose-dependent way. SQUID results should be considered as the average of NPs that were incorporated per cell in the case that internalization was a homogenous process.

III.I.X. Membrane molecules expression profile

As it has been previously mentioned, one of the possible applications for the magnetically-loaded DCs, that it is still needed to be studied, is to inject these cells in the tumour area. These cells are expected to transdifferentiate into endothelia-like-cells and to take part of the formation of the new blood vessels. The transdifferentiation process from DCs into endothelia-like cells is known to occur in the immature state of the DCs [3]. So it was crucial to know whether the MNPs had any effect in the maturation of the DCs.

In order to determine the maturation state of the DCs, the analyzed molecules were:

a) CD40, CD83 and CD86, which are co-stimulatory molecules known to be up-regulated when the DCs mature.
b) DC-SIGN with a high expression in immature DCs that decreases in mature DCs.
c) CD11c, which is a type I transmembrane protein found at high levels on most human dendritic cells.

d) CD14 a monocyte marker that is absent in DCs.

e) CD45 a common leukocyte membrane molecule.

f) CD1a that is a protein structurally related with the mayor histocompatibility complex (MHC) and mediates the presentation of lipid and glicolipid antigens.

The results are represented in Figure III-I- 24. The expression of CD14 in all the samples was almost cero so we could confirm that after five days of differentiation in presence of GM-CSF and IL-4 there was no monocyte presence that is in concordance with literature [66]. As DCs are leukocytes we observed a positive expression of CD45.

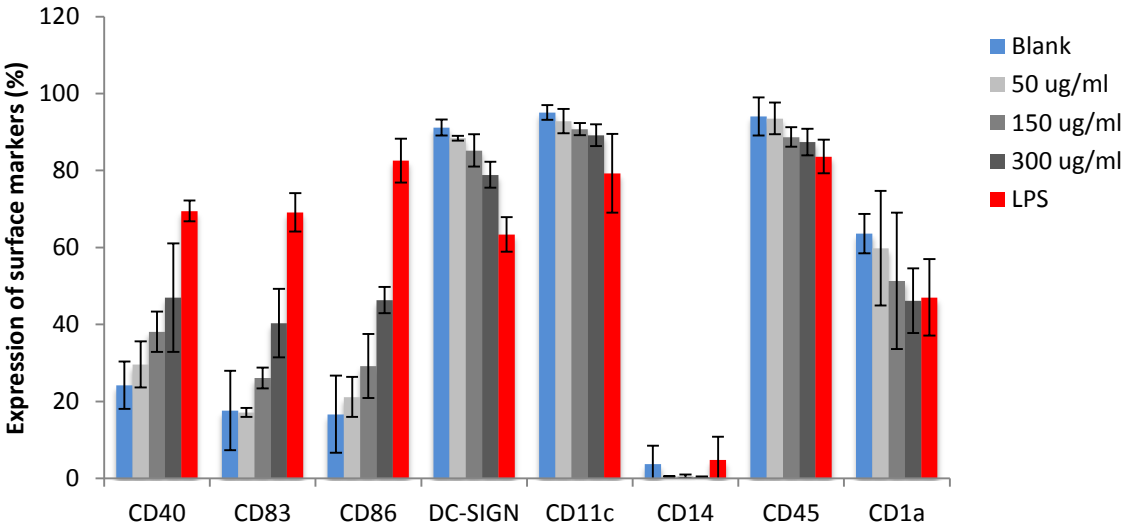

Figure III-I- 24: Molecule expression measured by FACS, expressed as percentage of positive cells. Blank samples are immature DCs, DCs incubated with 50, 150 and 300 μg Fe_3O_4/ml of MNPs for 2 days and LPS (mature DCs stimulated with 0.1 μg/ml LPS for 48 h).

When we compared the percentage of cells that expressed co-stimulatory molecules such as CD40 and CD86 in the blank sample, in the LPS induced positive control and

when the cells were incubated with an increasing amount of MNPs, we observed that the higher amount of MNPs the most percentage of cells expressed these markers.

CD83 is one of the best-known maturation markers for DCs. The effect on this molecule was the same as the co-stimulatory molecules one, the percentage of CD83+ cells increased when increasing the amount of MNPs and it was maximum for the LPS induced mature DCs.

Related with these three up-regulated molecules, in any case did we observe the percentage of positive cells achieved in the LPS-induced positive control but it was significantly higher than the blank sample that corresponds with immature DCs.

Differentiation of human monocytes into immature DCs is characterized by increased expression of DC-SIGN, CD11c and CD1a [66, 157], however when we observed the expression for these molecules after incubating immature DCs with both MNPs and LPS it was down-regulated compared with blank cells. DCSIGN is a DC-specific C-type lectin and mediates antigen uptake, so as maturation of DCs implies a decrease of antigen capture, we observed a down regulation of this molecule, being in concordant with other authors [157] [158]. According to the antigen presenting molecule CD1a we observed a decrease in the percentage of CD1a+ cells when DCs were stimulated with LPS and with MNPs previously showed by others authors [158, 159].

Regarding CD11c molecule expression, it could be seen that with MNPs and LPS there was a slightly decrease. There is no evidence in the literature about the effect of cell maturation on the expression of this marker. So we can say that when DCs mature the level of expression of CD11c decreases.

With these results we can confirm that a dose-dependence effect on the expression of maturation markers takes place when we incubate the immature DCs whit MNPs and

that the molecular expression pattern corresponds with an increase of CD40, CD83 and CD86 and with a decreased of DC-SIGN, CD11c and CD1a.

As FSC (Forward Scatter) correlates with the cells volume and SSC (Side or Ortogonal Scatter) depends on the inner complexity of the particle, when we analyzed the results of these two parameters we were able to see the effect of the incorporation of the MNPs. Regarding the complexity of the cell we observed that the presence of the MNPs inside the cells affected to the morphology of the cells. The higher amount of MNPs the more complex the cells were, Figure III-I- 25. However, when we analyzed the results of the FCS we observed that the cells size did not change after MNPs uptake, Figure III-I- 26.

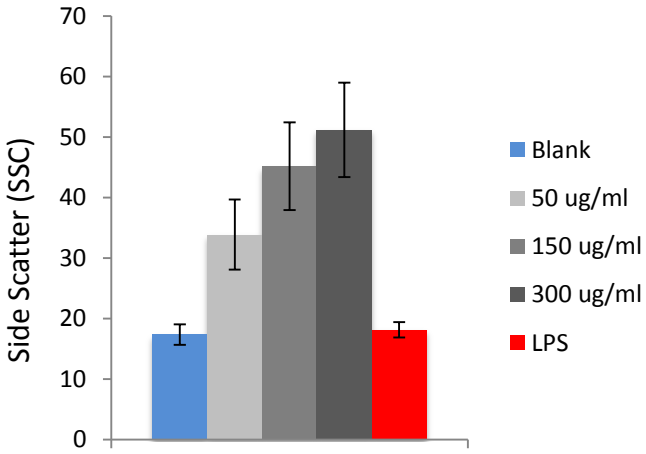

Figure III-I- 25: Side Scatter (SSC) results measured by FACS to immature DCs, DCs incubated with 50, 150 and 300 μgFe_3O_4/ml and mature DCs stimulated with LPS. It could be seen that the higher the amount of MNPs is the more complex morphology have the cells.

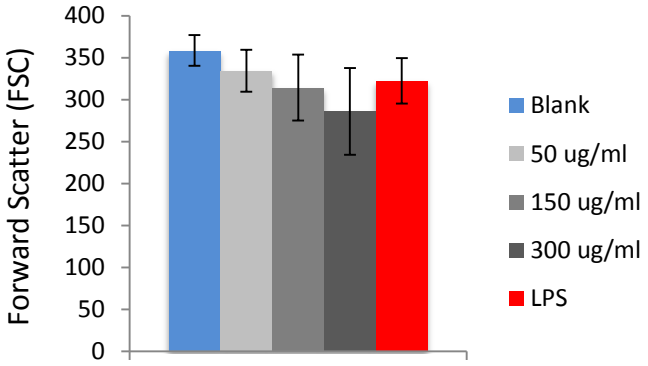

Figure III-I- 26: Forward Scatter (FSC) results measured by FACS to immature DCs, DCs incubated with 50, 150 and 300 µgFe_3O_4/ml and mature DCs stimulated with LPS. It could be observed that the presence of MNPs inside the DCs does not affect the volume and the size of the cells.

As main conclusion of this study, we can confirm that incubation with this kind of MNPs triggered a dose-dependent maturation effect in immature DCs, resulting in an increase of the typical maturation markers (CD40, CD83 and CD86) which is in concordance with the literature as it can be seen in the Table III-I- 3, and a decrease in DC-SIGN, CD1a and CD11c as correspond to the observed maturation process. The observed DC-SIG decrease expression correlated well with a maturation of the DCs being a consensus in literature. However, the maturation effect in the expression of CD1a and CD11c is not yet clear. Concerning the CD1a expression, there exists a controversy in the literature; some authors observed either an increased expression [160] or a decrease [158, 159, 161], but the more often observed effect is the decrease in the CD1a expression, which is in agreement of our results. There is no evidence in the literature of the CD11c expression change when the maturation process takes place. The high expression of this molecule in immature DCs is reported in literature, but no studies about the expression modulation due to maturation have been performed so far.

Our results provide the first evidence that confirm that the expression of CD11c decreases when DCs mature.

The same effect of maturation in DCs due to nanoparticles could be found in literature. Carbon NPs showed to have the capability of increase the expression of CD86 [162] and PGA NPs trigger the up-regulation of CD40 and CD86 [124].

On the other hand, in a previous work [126], it was studied that the uptake of multiwalled carbon nanotubes (CNT) by immature dendritic cells (iDCs) did not induce phenotypical changes in iDCs, neither affects the normal activation by LPS. Also studies using titanium dioxide/para-amino benzoic acid NPs incorporation demonstrated that this kind of NPs maturation process was not induced [104].

Summarizing, our results provide one of the most extensive and careful phenotype characterization of uploaded DCs with MNPs. From these results we undoubtedly asses that MNPs acts as stimulus in the maturation process of DCs.

		CD40		CD86		CD83		DC-SIGN		CD1a		CD11c		CD14		CD45	
	stimulus	iDCs	mDCs	iDCs	mDCs	iDCs	mDCs	iDCs	mDCs	iDCs	mDCs	iDCs	mDCs	iDCs	mDCs	iDCs	mDCs
Our results		+	++	+	++	+	++	++	+	++	+	++	+	-	-	++	+
[155]		+	++	+	++	+	++										
[139]	LPS	+	++	+	++	+	++										
[150]	LPS			+	++	+	++	++	+	+	++						
[149]	LPS							++	+	++	+	++		-			
[147]	LPS							++	+					-			
[148]	G. lucidum PS	+	++	+	++	+	++	++	+	++	+						
[152]	carbon NPs			+	++												
[156]	PGE2+TNF-α			+	++	-	++	++	+								
[157]				+		+											
[151]	LPS, INF-γ	+		+		-	++			++	+	++		-			
[158]	TNF-α, LPS	+	++							++				-	-		
[60]	TNF-α, CD40L	+	++							++		++		-			
[159]	Nanodiamons			+	++	+	++										
[160]	TNF-α			+	++	+	++			++	-						
[100]	LPS			+	++												
[153]	PGA NPs	+	++	+	++												
[161]	LPS			+	++	+	++			+	++						
[99]	PLL MPs					+	++										

Table III-I- 3: Results in literature about the membrane molecule expression profile when DCs are stimulated with different external factors. [163], [148], [160], [159], [157], [158], [162], [164], [165], [161], [166], [66], [125], [167], [104], [124], [168], [103]. +: normal expression, ++: high expression, -: no expression.

III.I.XI. Cytokine expression

Immature and mature DCs differ with regard to their phagocytic activity, surface expression of co-stimulatory molecules, like CD-83 and CD-86, and cytokine production. In this section we will concentrate in the study of the cytokine production profile before and after the incubation of the DCs with the MNPs.

The different types and levels of cytokines produced by DCs generate the microenvironment which regulates the quality and the quantity of the immune response [75, 169]. Important cytokines produced by DCs are IL-12 family, IL-10, IL-6 and TNF-α [170, 171].

a) IL-12 drives naïve Th cell differentiation towards a T helper 1 (Th1) phenotype.
b) IL-10 is a regulatory cytokine with pleiotropic functions that is a strong inhibitor of IL-12 mediated immunoregulation and trigger the activation of T regulatory cells.
c) IL-6 suppresses the function of T cells with a regulatory phenotype, which make all these cytokines important regulators of adaptative immune responses.
d) TNF- α is an angiogenic growth factor, which is also produced by DCs, and can bias CD4+ T-cell priming towards a pro-inflammatory T helper 1 (Th1)-cell fate which is based in the cellular immunoresponse.

As it was mentioned, quantification of a set of 9 different cytokines in the cellular medium was performed in a Luminex device. Among these cytokines there were IL-12, IL-10, IL-6 and TNF- α. Results of the levels of expression of these cytokines in the supernatant of DCs incubated with different amount of MNPs are represented in Figure III-I- 27. It can be seen that DCs cultured with COOH(MNPs)- secreted increasing amounts of IL-6 and TNF- α in a MNPs-dose dependent manner. DCs stimulated with

LPS were our positive mature DCs sample, and the level of expression for IL-6 and TNF- α was the highest in this cells. Besides, exposure of DCs to these MNPs did not induce appreciable levels of IL-12 and IL-10. However when DCs were stimulated with LPS an increased amount of IL-12 and IL-10 was detected. From these results we could extract the idea that DCs suffer a maturation stimulus when they are incubated with MNPs. Being in concordance with the previous results about the membrane markers expression profile. Regarding the mechanism by which DCs are stimulated by the MNPs, we can propose two hypotheses. The first one is that the MNPs dispersed in the culture media may activate the DCs via cell surface interactions with pattern recognitions receptors. The second is based in the fact that the MNPs are internalized by the DCs and it is possible that their incorporation trigger the maturation of the DCs. The maturation stimulus it is also possible to be a combination of the two above mentioned hypotheses.

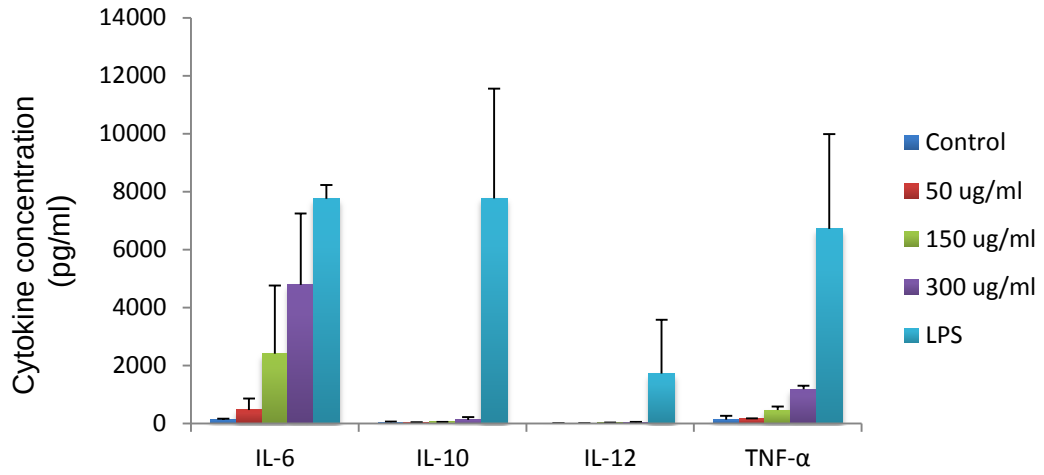

Figure III-I- 27: Histogram showing the effect of COOH(MNPs)- on the cytokines secreted by immature DCs (control), by DCs after an 48h incubation with 50, 150 and 300 μgFe_3O_4/ml and by mature DCs stimulated with LPS. Interleukines 6, 10 and 12 were analyzed and Tumour necrosis factor α (TNF-α).

We compare our results with some studies reported in the literature and collected in Table III-I- 4. We observed that other experiments with different kind of NPs showed an increase in the expression of cytokines (IL-6 and TNF-α [125, 148]) triggered by the NPs. Regarding other cytokines, they reported also the lack of IL-12 expression and an increase in the expression of IL-10, unlike our observation. Although we observed an increment in the expression of IL-12 and IL-10 in DCs maturated with LPS, we did not observe the same effect in DCs cultivated only with MNPs.

In summary, this results indicated that COOH(MNPs)- could induce the maturation of the human monocyte derived DCs provoking the increase of the expression of IL-6 and TNF-α and having no effect in the levels of IL-12 and IL-10 expressed by the DCs. Other studies reported an increase in just the expression of IL-6 and TNF-α without mentioning other cytokines, which fits perfectly with our results [124].

	maduration stimuli	IL-12 p-70	IL-6	IL-10	TNF-α	IL-8
Our results	NPs	-	↑	-	↑	
Our results	LPS	↑	↑	↑	↑	
Ghoneum M. et al, 2010	Nanodiamons		↑	↑	↑	
Reis ES et al, 2008	LPS	↑	↑	↑	↑	
Babensee, 2008	PLGA MPs	-	↑	↑	↑	↑
Jahns J. et al, 2011	LPS			↑	↑	
Migdal C. et al, 2010	LPS				↑	↑
Uto T. et al, 2009	PGA NPs		↑		↑	

Table III-I- 4: Table that summarizes the results reported in the literature about the changes in the cytokine expression profile (IL-12. IL-6, IL-10, IL-8 and TNF-α) of DCs after the maturation process. ↑ means expression and – means no expression. The empty places correspond to cytokines that were not measured.

III.I.XII. Conclusions

Taking into account the most relevant results obtained in this part of the thesis we can conclude that human monocyte-derived DCs are able to internalize MNPs of 220nm functionalized both with amino and carboxylic groups. The intracellular localization of the MNPs is in endocytic vesicles in the cytoplasm, the MNPs never enter into the nucleus. The internalization process is inhomogeneous in this kind of cells, as a half of the cells always do not internalize NPs. However, the uptake of MNPs is made in a dose dependent way, the higher NPs concentration during incubation the more NPs are internalized. With a magnetometer SQUID it is possible to determine the average number of MNPs internalized per cell. The results for both COOH(MNPs)- and NH_2(MNPs)+ incorporated when cells were incubated at 50 μgFe_3O_4//ml are **1.51±0.86 pgFe_3O_4/cell (1.09±0.62 pgFe/cell, 250±140 MNPs/cell)** and **0.88±0.25 pgFe_3O_4/cell (0.64±0.18 pgFe/cell, 130±37 MNPs/cell)** respectively. We have observed at slightly increase in the internalization of negatively charged MNPs compared with the positively charged ones.

It has been also studied the effect of the MNPs internalization in the DCs. We have observed that there is no any toxic effect up to 5 days after the incubation with positively or negatively charged MNPs at a concentration of 50 μgFe_3O_4/ml. However during the incubation time the DCs become mature in a dose-dependent way in terms of membrane molecule expression profile and cytokine expression. The maturation stimulus triggered by the NPs is in concordance with the effect caused in DCs by other kind of nanomaterials [124, 162].

III-II: Magnetic Fluid Hyperthermia in DCs

Within the strategy, described in the Introduction, of using DCs to vectorize MNPs for magnetic hyperthermia, the last step was to investigate whether cell death of magnetically-loaded DCs could be induced by an external alternate magnetic field (AMF). So, the aim of this section of the work was to perform an in depth study of the effect of an external magnetic field on DCs uploaded with MNPs.

Many studies performed on the 80´s have demonstrated a synergistic response to radiotherapy/chemotherapy and hyperthermia versus radiotherapy/chemotherapy alone [24-27]. Most recen clinical trials have demonstrated that hyperthermia therapy, as an adjuvant of chemotherapy or radiotherapy, is beneficial for treating patients with tumours of several types [28-32]. In magnetic hyperthermia approach the heat is obtained by coupling an alternating current to MNP-loaded tissues. The first clinical trials have been reported in the last decade and they have shown that using superparamagnetic nanoparticles it is feasible to achieve hyperthermic temperatures [2, 59, 172].

DCs are described to take part in the generation of the new vessels which give support to tumour, called angiogenesis [173]. That is why DCs may be a suitable carrier to take MNPs to the tumoral area. A relevant feature of DCs as carriers for MNPs is to mimic biological units and to elude the immune response of the body. The cargo of the DCs could be designed to be either “nude” MNPs for hyperthermia therapy or functionalized MNPs with specific drugs to be released by the application of alternating magnetic fields.

Previous in-vitro studies on MFH using MNPs in prostatic adenocarcinoma (PC3) cells, performed by Fortin et al [57], showed that maghemite and cobalt ferrite MNPs internalized in PC3 cells under MFH (300kHz and 31mT) were heated up to 45º after 15 minutes.

Clinical studies of hyperthermia therapy induced by heating implanted MNPs at the tumour place, have shown that thermotherapy using MNPs could be safely applied to the treatment of brain tumours and that the hyperthermic temperatures, medium of 44.2ºC (42.4-49.5ºC) could be achieved, [2]. Recently, magnetic hyperthermia strategies passed preclinical trial stages and received regulatory approval as a clinical protocol for thermotherapy [174].

Aside the MFH, other approaches are being developed in order to induce cell damage with metallic gold NPs, using for example laser-induced techniques. In this approach the reason of the damage caused in cells is thermal ablation effects [175]. Other approach is based in inducing mechanical cell death by application of low frequency magnetic fields on Nikel Nanowires [176] or lithographically defined microdiscs [177].

We have performed a screening regarding many factors, as MNPs concentration, application time and magnetic field in order to optimize the process and also to be able to modulate the percentage of dead cells. Concerning the death mechanism, preliminary experiments have been carried out.

III.II.I. AMF effect

The hyperthermia experiments were performed at fixed conditions of MNPs incubation concentration (50 μgFe_3O_4/ml), magnetic field parameters (260 kHz and 12.7kA/m) and time (30 min). Only MNPs-loaded DCs submitted to AMF died, this drastic effect was modulated by the change of those parameters. Tuning the amplitude and frequency of the applied magnetic field and also the duration of the AMF experiment we aim to obtain information on the mechanism of cell damage.

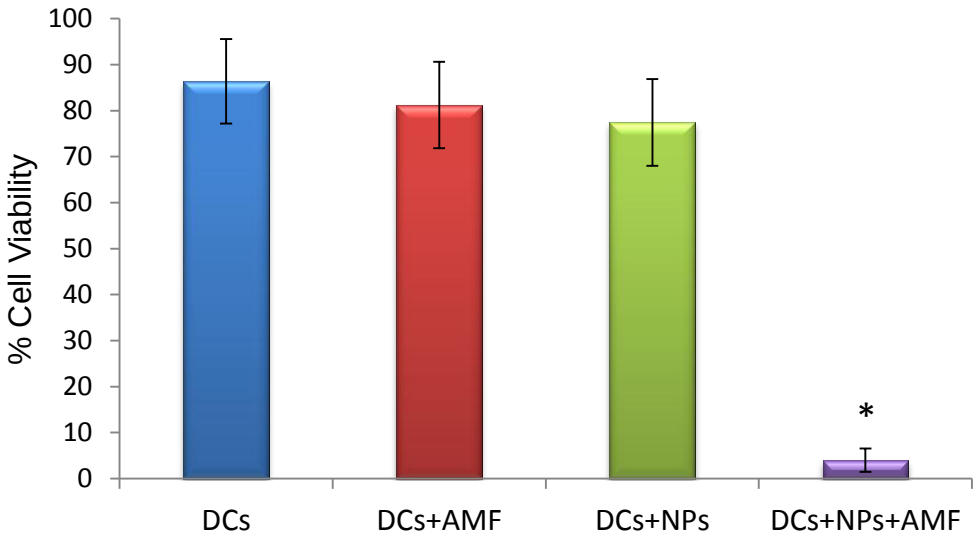

Figure III-II- 1: DCs viability results for the 2x2 experiment illustrated in materials and methods. DCs: control DCs samples; DCs+AMF: DCs without MNPs after 30 min of AMF application (H_0 = 12.7 kA/m, f = 260 kHz, t = 30 min); DCs+MNPs: DCs with 50 μgFe_3O_4/ml MNPs and without AMF, and DCs+MNPs+AMF: DCs incubated with MNPs after applying AMF (H_0 = 16 mT, f = 260 kHz, t = 30 min). Number of experiments=6. * *Significant difference (p<0.0005) from the control sample (DCs).*

The effects of AMF on magnetically-loaded DCs and the corresponding control samples in the 2x2 experiment are shown in Figure III-II- 1. These results were obtained by applying an AMF (f = 250 kHz, H_0 = 12.7 kA/m) on DCs incubated with a concentration C_{NP} = 50 μgFe_3O_4/ml of COOH(MNPs)- during a time t_{app}=30 min. It is clear that a major percentage (95±4%) of death is only achieved for the magnetically-loaded DCs, whereas the unloaded cells were not affected by the AMF. Moreover, from cytotoxicity experiments we showed that NPs alone did not have any toxic effect in the cells. Only the combination of the incorporation of the MNPs and the AMF application originated a drastically reduction in cell viability.

As already mentioned in page 38, apoptosis or cellular programmed death is recognized by an early event that is considered as a fingerprint of this process: the exposition of phosphatidylserine in the external surface of the plasma membrane. Annexin-V and IP dyes were used in order to know whether the death mechanism was apoptosis or necrosis. It is important to stress that the experimental protocols were designed to perform the viability analysis immediately after exposure to the magnetic field. Trypan Blue measurements were performed just after the AMF application, however, the time elapsed between AMF exposure and FACS measurement was approximately 3 hours.

Figure III-II- 2 shows the FACS dot-blots representations after hyperthermia experiments performed in the same conditions as described above and using both kinds of MNPs. Sample (a) consisted of DCs without MNPs and without AMF and gave us the reference viability data of the culture, always remaining above 90%. Sample (b) was DCs without MNPs but submitted to the AMF, and it can be seen that the magnetic field alone did not induce any cell damage. Samples (c and e) were constituted by DCs that had internalized COOH(MNP)- and NH_2(MNP)+ respectively.

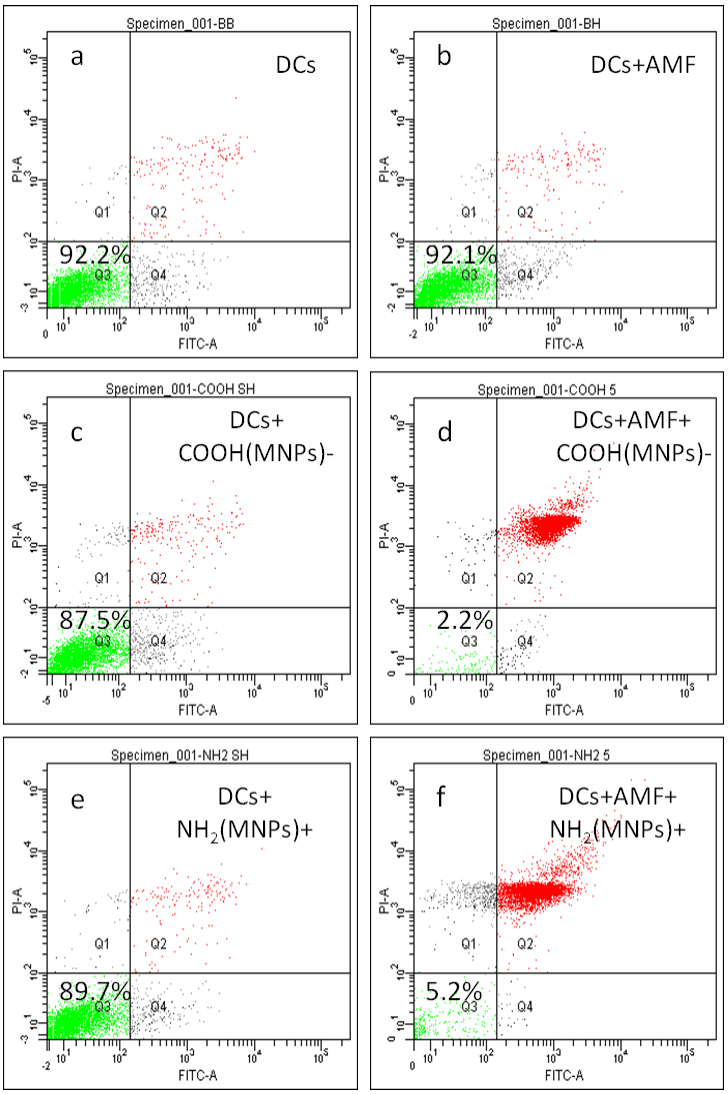

Figure III-II- 2: Experimental results of the '2x2' experiment with two kind of MNPs. Dot-blots representations from FACS data for: (a) control DCs, (b) DCs after applying 30 min of AMF, (c) DCs with COOH(MNP)- particles, (d) DCs loaded with COOH(MNP)- particles after applying 30 min of AMF, (e) DCs with NH_2(MNP)+ particles and (f) DCs loaded with NH_2(MNP)+ particles after applying 30 min of AMF . The green dots at quadrant Q3 indicate the viable cells in each experiment. Annexin-V and IP were used as markers. The red dots indicate the cells positive for both markers, so the death cells. The percentage that is represented is the viability percentage.

These samples corroborated the information extracted by the cytotoxicity experiments that is the MNPs had no toxic effect on the DCs. Finally, samples (e and f) consisted of MNPs-loaded DCs, with COOH(MNP)- and NH_2(MNP)+ respectively, after the exposure to AMF. These cells were positive for the Annexin staining (which reveals the translocation of phosphatidylserine) and positive for the propidium iodide staining (which reveals damages in the plasma membrane). There are two options that explain this result:

i) The cells presented such membrane damage that Annexin entered the cells and dyed the intracellular phosphatidylserine, which fits with the necrotic cell death.

ii) The cell died by apoptosis triggering the translocation of phosphatidylserine and the late apoptosis events caused membrane damage.

After the analysis of the results we were not able to deduce whether the cells died by "pure" necrotic death mechanism or by apoptosis. For a detailed investigation on the mechanisms of cell death we decided to vary some parameters as: MNPs incubation concentration, field application time and the magnetic field amplitude.

Interestingly, besides the drastic effect on the cell viability due to AMF, the temperature of the cell medium measured by the macroscopic optic sensor remained within the 29-31 ºC,

Figure III-II- ***3***, i.e., few degrees above the starting temperature of 26 ºC, but well below the values of 42-45 ºC needed to trigger temperature-induced apoptosis by hyperthermia. The absence of macroscopic temperature increase together with the level of cell death observed in samples d) and f) in Figure III-II- 2 raised the question about a possible intracellular mechanism, different from the temperature increase of the extracellular medium (i.e., magnetic hyperthermia).

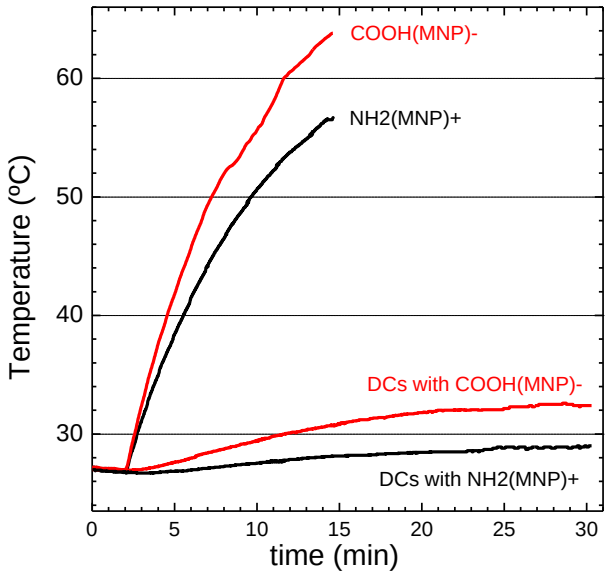

Figure III-II- 3: Heating curves for pure colloids NH2(MNP)+ and COOH(MNP)-, during application of alternating magnetic fields (H = 12.7 kA/m, f = 260 kHz). The same experiment for DCs loaded with NH2(MNP)+ and COOH(MNP)- (bottom curves) yielded much smaller temperature increasing up to 29-32 ºC after 30 min of AMF.

In a series of comprehensive experiments using $CoFe_2O_4$ and γ-Fe_2O_3 MNPs, Fortin *et al.* [57] have shown that a concentration of about 15 pg of Fe at the intracellular level is enough to raise the temperature up to 45ºC after 15 min of AMF application (700 kHz, 31mT). In our experiments, we observed a lower amount of NPs uptake (maximum of 7 pgFe_3O_4/cell, 5 pgFe/cell, when DCs were co-cultured in the presence of 300µgFe_3O_4/ml for 12 h). The MNPs concentration for hyperthermia experiments was 50µgFe_3O_4/ml, which gives a result of about 1.5 pgFe_3O_4/cell, which corresponds to 1 pgFe/cell, so this low amount of magnetic material is not enough for increasing the extracellular medium temperature.

Furthermore, we found that reducing the application time down to 15 minutes very similar values of cell death was found (see below). Thus, these experimental parameters were considered as the upper limit for the energy needed to be delivered during experiments and, in order to find the conditions for a controlled cell death, we further explored different combinations of field amplitudes H_0, nanoparticles concentrations C_{NP}, and application period (t_{app}).

A. Effect of the AMF amplitudes in cell viability

Figure III-II- 4 shows the results of a series of six AMF application experiments using different field amplitudes H_0 (6.4, 9.5 and 12.7 kA/m with f= 260 kHz, t_{app} = 15 min), together with the three controls (**DCs**: CDs without MNPs and no AMF; **DCs+AMF**: CDs without MNPs with H_0=12.7 kA/m; and **DCs+NPs**: DCs incubated with 50 μgFe_3O_4/ml of COOH(MNPs)- but without AMF). It can be seen that the effect of increasing the field amplitude from 9.5 to 12.7 kA/m resulted in a decrease of cell viability from 55% to 25%, to be compared with the ~80-85% of the three control samples. However, even at the lowest field amplitude (6.4 kA/m) the cell viability value was lower compared to the control samples. The error bars are obtained after experiments performed in 6 samples. This is in good agreement with the proposed mechanism of cell death by AMF.

Differences in TB and FACS results for some samples could be seen, especially for those cells incubated with MNPs and submitted under AMF exposure. The viability value measured by TB was always higher than that value obtained by FACS, except for those samples that did not suffer any damage, i.e. cells that remain alive. Our

explanation for this phenomenon is the time gap between both measurements, as TB is performed just after hyperthermia treatment and for FACS measurements we had to wait until the last sample was ready and then take all the samples to the place where this analysis was made.

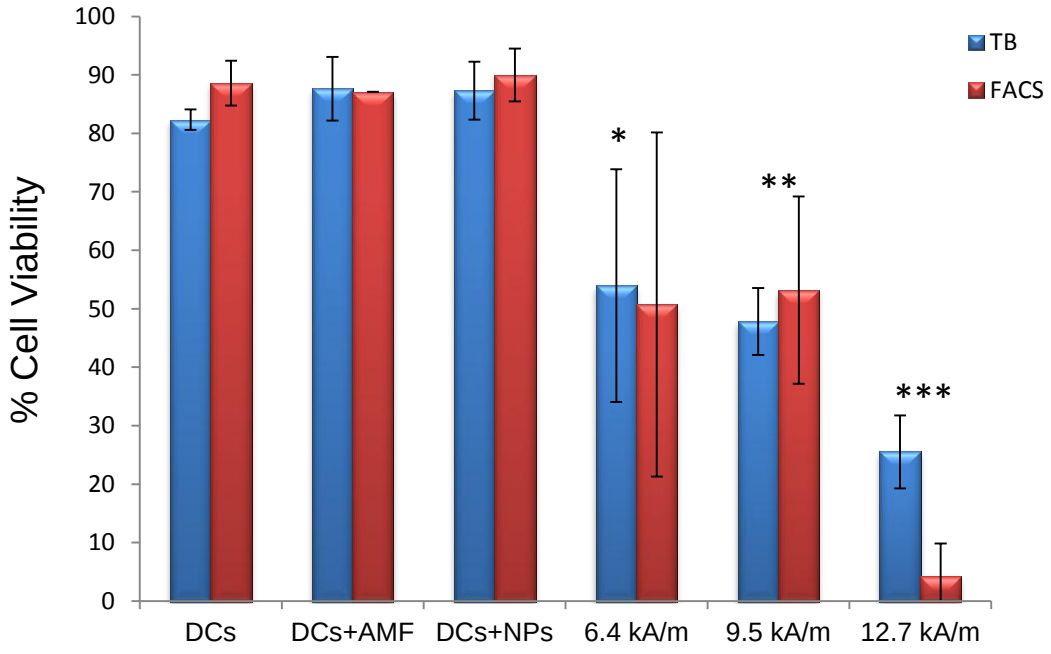

*Figure III-II- 4: Effect of the AMF amplitude H_0 (at f = 260 kHz, t = 15 min) on the cell viability of DCs incubated with 50 $\mu g Fe_3O_4$/ml, as measured by Trypan Blue and Fluorescence-activated cell sorting (FACS). Number of experiments=6. The AMF amplitude for the sample (DCs+AMF) was 12.7kA/m. * Significant difference (p<0.1) from the control sample (DCs).** Significant difference (p<0.05) from the control sample. *** Significant difference (p<0.0025) from the reference sample.*

B. *Effect of the application time of the AMF and MNP concentration in cell viability*

Figure III-II- 5 shows the effect of increasing application time on cell viability at fixed magnetic field amplitude of 12.7 kA/m, after overnight incubation with a concentration of MNPs C_{NP} = 20 and 50 μgFe_3O_4/ml. It can be seen that in DCs incubated with 20 μgFe_3O_4/ml after 5 minutes of AMF application the cell viability does not significantly decrease. Moreover, both TB and FACS methods give coincident values within experimental error. However, increasing the application time to 10 minutes resulted in a smaller viability of 65% of the total cells as measured by TB technique, whereas FACS analysis showed about 50% of cell viability. After 15 minutes of AMF application the viability further decreased, again showing appreciable differences between TB and FACS analysis.

The experiments performed using a higher concentration of MNPs during incubation (C_{NP} = 50 μgFe_3O_4/ml) resulted in the same gradual increase of cell death with AMF application times. Furthermore, the final percentage of cell death was somewhat higher as compared to those DCs cultured with C_{NP} = 20 μgFe_3O_4/ml for the corresponding AMF application time. Although the systematic effects of application period t_{app} and MNPs concentration on cell viability are clear from Figure III-II- 5, it must be noticed that there is a rather large dispersion of values for t_{app} = 5 and 10 min, and C_{NP} = 20 μgFe_3O_4/ml, i.e., the *range of parameters at which cell death is triggered*. This dispersion can be understood in terms of:

a) The intrinsic nature of a DC primary cell culture as the used in the present work.
b) The nature of the triggering mechanisms involved in cell death.

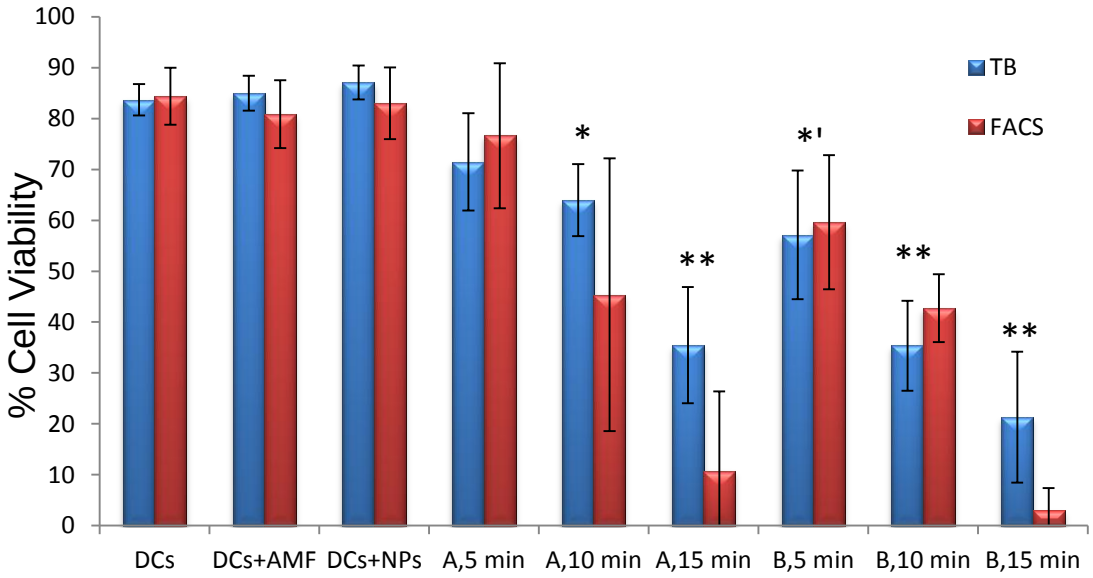

*Figure III-II- 5: Effect of different AMF application times t= 5, 10 and 15 min (at f = 260 kHz, H_0 = 1276 kA/m) on the cell viability of DCs incubated with 20 (A) and 50 (B) μgFe_3O_4/ml, as measured by Trypan Blue and Fluorescence-activated cell sorting (FACS). Number of experiments=3. The exposure time for the sample (DCs+AMF) was 15 min. * Significant difference ($p<0.025$) from the control sample (DCs). ** Significant difference ($p<0.0005$) from the control sample. *' Significant difference ($p<0.01$) from the reference sample.*

The variability in cell response regarding MNPs uptake and final distribution inside the cells will result in different distributions of MNPs at different endosomes, and thus a broad range of energies needed for triggering death mechanisms at each single cell. This physical situation could explain the high sensitivity in the critical range of parameters at which cell death is triggered.

The observed differences in cell viability obtained using TB and FACS protocols at the beginning seemed to be related to the different intervals elapsed between the

experiments and the analysis of the samples, as it was previously mentioned. Furthermore, we performed further specific experiment applying AMF (H_0 = 12.7 kA/m; *f* = 260 kHz; C_{NP} = 50 μgFe_3O_4/ml and t_{app} = 15 min) to analyze the evolution of the DCs viability at different times after the experiment. The results (Figure III-II- 6) showed that, immediately after the experiment, the amount of viable cells was about 60%, showing a small but noticeable decrease (to 52 %) when analyzed after 15 minutes with the same protocol. However, after 4 h the TB analysis revealed a major decrease (to less than 2 %) of viable cells in the same sample. These results are consistent with the differences observed between FACS and TB protocols in all the hyperthermia experiments performed.

It is noteworthy that this differences between TB and FACS results were only observed in the samples of cells that have suffer "medium" damage, because for those cells that have no suffer damage the viability value remain the same after the gap between both test (Figure III-II- 5, references samples and cells after 5 min of AMF) and those cells that have suffer a serious damage died so quickly that even with TB measurements, just after AMF application, almost 100% of cell death is observed (Figure III-II- 7, cells after 30 min of AMF).

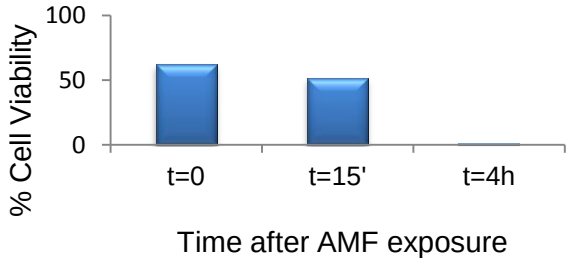

Figure III-II- 6: Viability of magnetically loaded DCs measured by Trypan Blue immediately after AMF application (t=0), after 15 min (t = 15') and after 4 h. The experiment was performed at H_0 = 12.7 kA/m, f = 260 kHz and t_{app}=15 min.

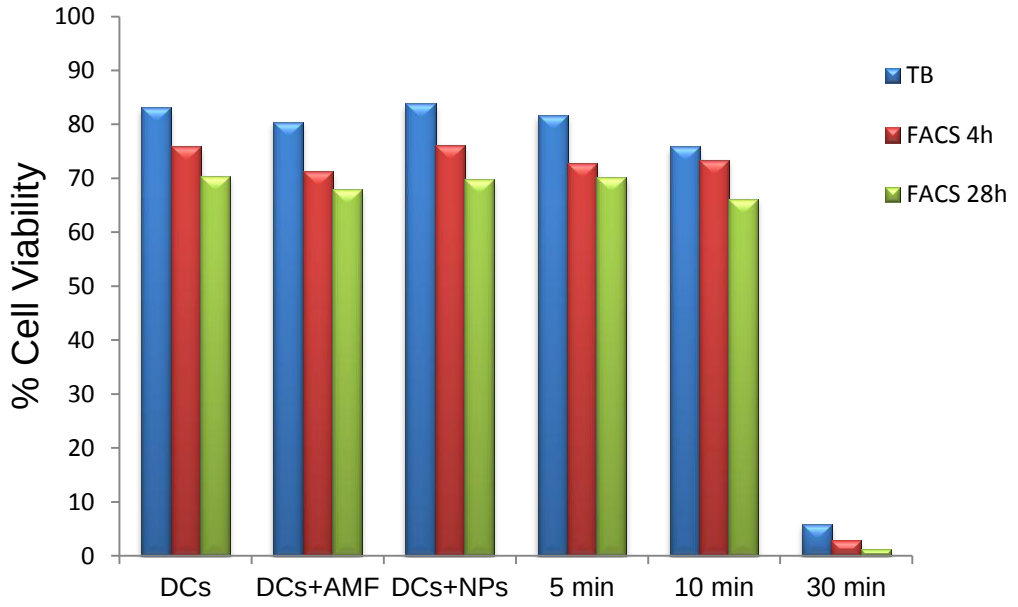

Figure III-II- 7: Viability of magnetically loaded DCs measured by TB just after the 5, 10 and 15 min AMF application and by FACS, 4 and 28 hs after the 5, 10 and 15 min AMF application (H_0= 12.7 kA/m,C_{NPs}=50 $\mu g Fe_3O_4$/ml).

As a result of these experiments we established that we needed to wait 4 hours after hyperthermia treatment in order to analyze the real cell viability value. We followed the evolution of the viability after 4 and 28 h after the experiments, to see whether the cells that were supposed to have no suffer any damage could suffer any side effect at longer times. The results, represented in Figure III-II- 7, indicated that those cells not affected during the experiments were able to remain alive, suggesting that no long-term side effects took place after magnetic field exposure.

As a result of the observed difference in cell viability values between TB and FACS analysis and also the evaluation of the internalization with fluorescent NPs, revealed that only 50-60% of the DCs uptake NPs. Nevertheless, we observed a 100% of cell

death after 4 h at the optimized conditions. A set of AMF experiments was performed to investigate the capacity of cell death induced by supernatants of the DCs with MNPs after AMF exposure. If 100% of the cells died after AMF application, even though ~40-50% of the cells had not incorporate MNPs, it was neither possible that the death mechanism was exclusively a localized temperature increase inside the cells nor a necrotic cell death caused by mechanical effect of the MNPs inside the cells. An explanation could be associated with the disruption of the organelles of the cells loaded with MNPs which results in the release of some toxic agent in the culture medium. This in turn will produce the death of the rest of the cells. Furthermore, the combination of this two death mechanism could explain the differences observed in the cell viability values measured by FACS and TB, since the death of the DCs that contained MNPs was very fast and the death of the cells that did not contain MNPs was slower and only observed after 4h, when the FACS analysis was performed.

Figure III-II- 8 represent the results obtained by FACS for the three references samples, as in all AMF experiments, DCs 100% incubated with MNPs (50 μgFe_3O_4/ml) and a mixture of 1:1 (50%) DCs incubated with MNPs and blank DCs. After AMF application in some samples the supernatant was replaced with fresh culture medium. Another sample was prepared by adding the supernatant of DCs with MNPs after AMF exposure to reference DCs (without MNPs and without AMF). As it can be seen, no matter the percentage of the DCs that contains MNPs 100% of the cells died after 4h (when the FACS analysis was made). When the supernatants of these samples were removed just after AMF exposure, the observed cell viability increased supported the idea that the supernatant contained some toxic agent that kill the DCs that did not die during the AMF exposure. Moreover, the DCs that received the supernatant of death cells after AMF treatment died 100%, in agreement with the previous results.

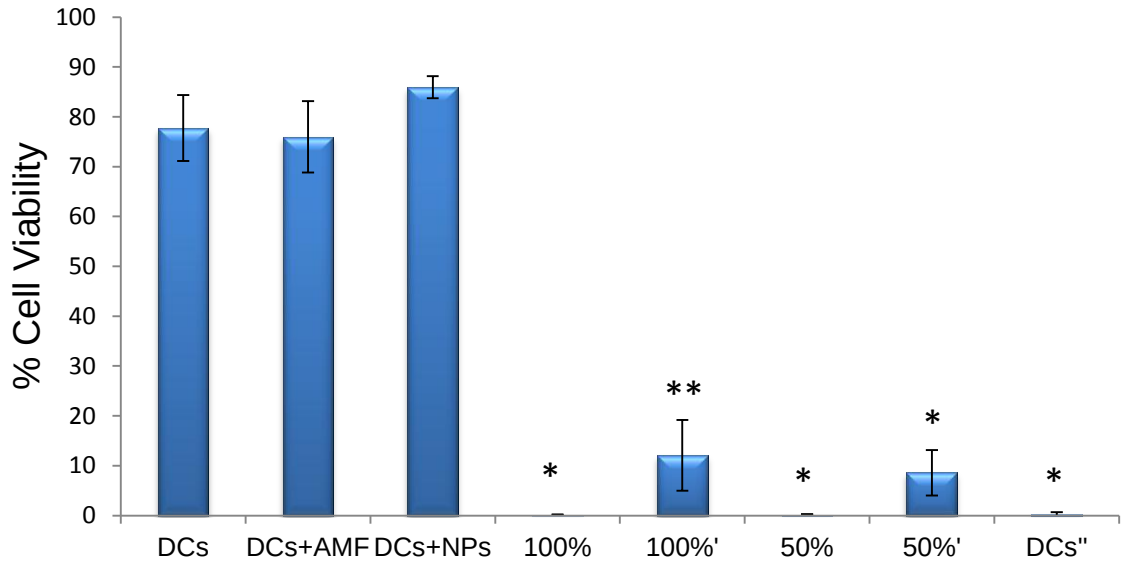

*Figure III-II- 8: Cell viability measured by FACS after AMF application for 15min at a Hf= 260 kHz and a H= 12.7 kA/m. 100% refers to the fact that all the DCs were incubated with 50 μgFe_3O_4/ml of MNPs. 50% refers to a mixture 1:1 between DCs incubated with the MNPs and DCs without MNPs. (') in these samples just after AMF exposure the cell medium was replaced with fresh culture medium. ('') DCs without MNPs and without AMF exposure that receive the supernatant of DCs with MNPs after AFM application. Number of experiments=3. Significant difference ($p<0.0025$) from the control sample (DCs). ** Significant difference ($p<0.005$) from the control sample.*

The effects of AMF on the viability of magnetically-loaded cells from a wide variety of cell lines have been in most cases related to the temperature increase registered during the experiments [178-182]. However, it is not clear how the small amount of incorporated magnetic material (of the order of few pg/cell) was able to increase the temperature of the complete cell medium to the required 42-46 ºC for hyperthermia-triggered apoptosis mechanisms [182]. Theoretical calculations from a model of MNPs-membrane interactions suggested that the effects of the power released by MNPs under AMF is to destroy the membrane integrity [183]. It has been recently

observed that cell death by application of AMF takes place even without temperature increase of the cell medium [184], [185], this relevant issue has been associated with a local MNP-intracellular medium interaction [184].

The amount of incorporated MNPs into the DCs is well below the minimum required to increase the intracellular temperature during AMF exposure [184]. Based on the knowledge that, during vesicle trafficking, endocytic and phagocytic vesicles fuse with lysosomes, we can assume that the final localization of the internalized MNPs are secondary lysosomes. Lysosomes contain more than forthy different hydrolytic enzymes as: proteases, lipases and nucleases. Thus, when MNPs-loaded cells are submitted to AMF the vibration of the agglomerates of the MNPs confined inside the lysosomes provoke the disruption of the organelle membrane, and subsequently the relase of all the lysosomal content to the cytoplasmatic space. The fast and massive release of all these material may be toxic for the cell and trigger the cell death.

It has been reported that agglomeration of MNPs inside vesicles results in noticeable effects on their heating properties, i.e. to decrease their SPA due to increased magnetic dipolar-dipolar interactions [186]. It is worth to mention that these results refer to the *average* temperature rise of the magnetic colloids as measured by a macroscopic temperature probe, which could differ from the local temperature inside the vesicles. The latter will depend on several factors like the heat generation rate at the given experimental conditions and the thermal properties of the membranes and surrounding medium.

We have demonstrated that is possible to control the induced cell death of MNPs loaded dendritic cells, by adequate tuning of the physical AMF parameters and/or the final amount of MNPs in the intracellular medium. DCs cultures containing around 1 pg of MNPs per cell showed a clear decrease of viable cells after AMF application period

larger than 10 minutes. Irrespective of the amount of viable cells after AMF application in different conditions, FACS analysis showed clear indication of a necrotic-like process on the cell population affected by the AMF. These data indicate that power release by the MNPs can locally alter relevant cell structures and/or metabolic processes yielding irreversible cell damage due to the release of some toxic substance to the extracellular medium.

III.II.II. HSP-70 expression

As it has been mentioned, no macroscopic temperature increase was detected during AMF exposure. However, thought the amount of MNPs incorporated by the DCs was not enough to raise the temperature of the culture medium, could be that the temperature increased locally inside the cells, where the MNPs were located. For this reason we decided to analyze the expression of HSP70, one of the most common heat shock proteins, known to be up-regulated when the cells face some stimulus, as the temperature increase.

Soluble protein fractions were collected after hyperthermia experiments as described in materials and methods, and were further separated in a 2D electrophoresis followed by Western Blot in order to detect HSP70 expression.

Samples analyzed were:

- Three controls of hyperthermia experiments (DCs, DCs+AFM, DCs+MNPs)
- Cells cultivated with 20 μgFe_3O_4/ml submitted to 5 min, 10 min and 15 min of 12.7 kA/m AMF.
- DCs incubated with 50μg/ml of MNPs after 5 min and 10 min of 12.7 kA/m AMF were analyzed.

In Figure III-II- 9 the image of one Western Blot can be seen.

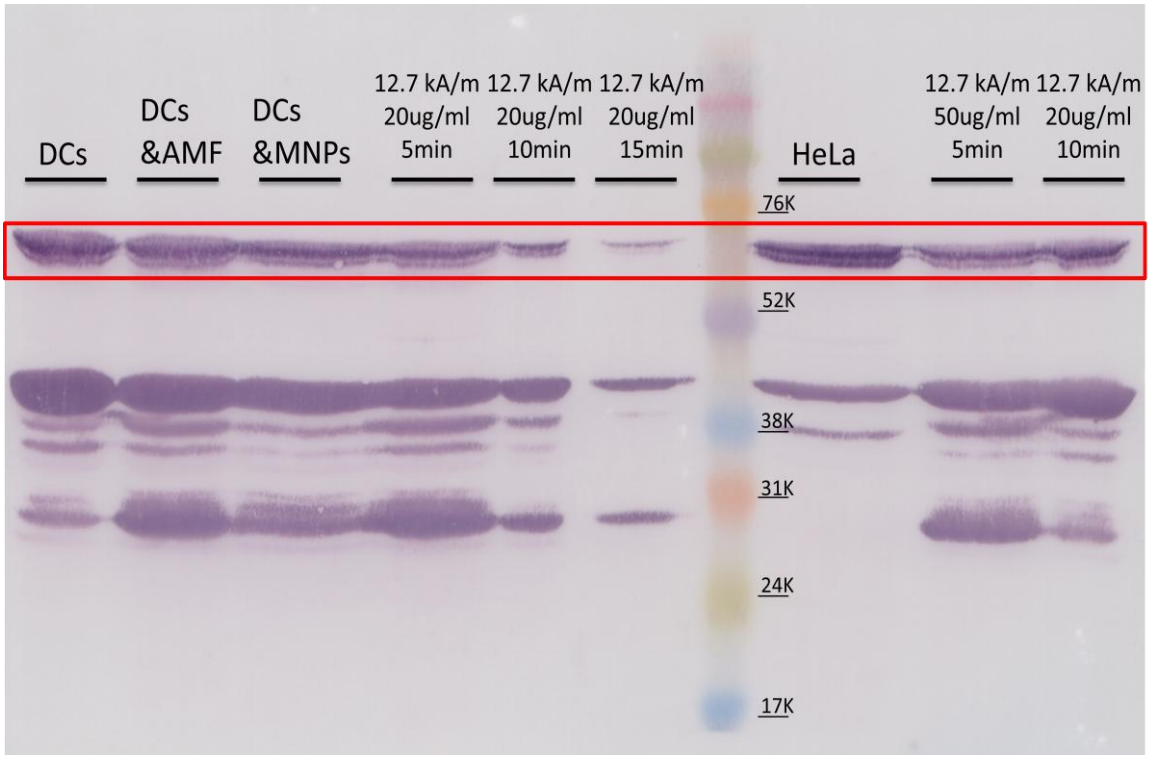

Figure III-II- 9: Western Blot from 2D gels loaded with extracts of 10^6 cells each sample. HeLa cells were used as positive control. Red cuadrant correspond with the HSP70 protein. Rest of bands correlates with Actin protein.

Molecular weight of the HSP70 is 70kDa, and as a weight control sample was used we could identify the bands that corresponds to the HSP70 protein, which are the ones selected by the red rectangle. HeLa cells were used as positive control because it is known that these cells highly express the HSP70 protein. When it was compared the expression of HSP70 in DCs reference samples and HeLa cells it could be seen that the basal expression of HSP70 in DCs was high. Actually, the bands for both cell lines were comparable. That is why we were not able to observe any increase in the expression of

this protein in cells under hyperthermia conditions. In the sample that corresponds to DCs incubated with 20μgFe_3O_4/ml of MNPs after 15 min of 12.7 kA/m AMF the band of both HSP70 and Actin was less intensive and this is due to the fact that cells died and we lost part of the sample.

III.II.III. SEM

In order to observe the morphology of the cells after hyperthermia treatments, scanning electron microscopy was performed. As the main objective was to observe the morphology, secondary electrons images were collected (Figure III-II- 10).

The SEM images revealed that the observed cell death after AMF application on magnetically-loaded DCs is accompanied by the concurrent loss of the structure of the cell membrane that is typical of this kind of cells. DCs alone Figure III-II- 10-A showed their typical membrane structure with plenty of ramifications, DCs without MNPs after AMF application had the same structure as reference DCs, so no morphology changes were induced just by the AMF exposure. It is worth noticing that DCs uploaded with MNPs did not present aggregates of MNPs in the cell surface, this is an indication of the cleaning protocol efficiency and also the lack of morphological effects. However DCs loaded with MNPs after AMF application presented a complete disrupted cytoplasmatic membrane structure. It can also be noticed in this cells the appearance of membrane channels as a consequence of AMF application, which is likely the responsible mechanism to turn the membrane permeable and the death cause.

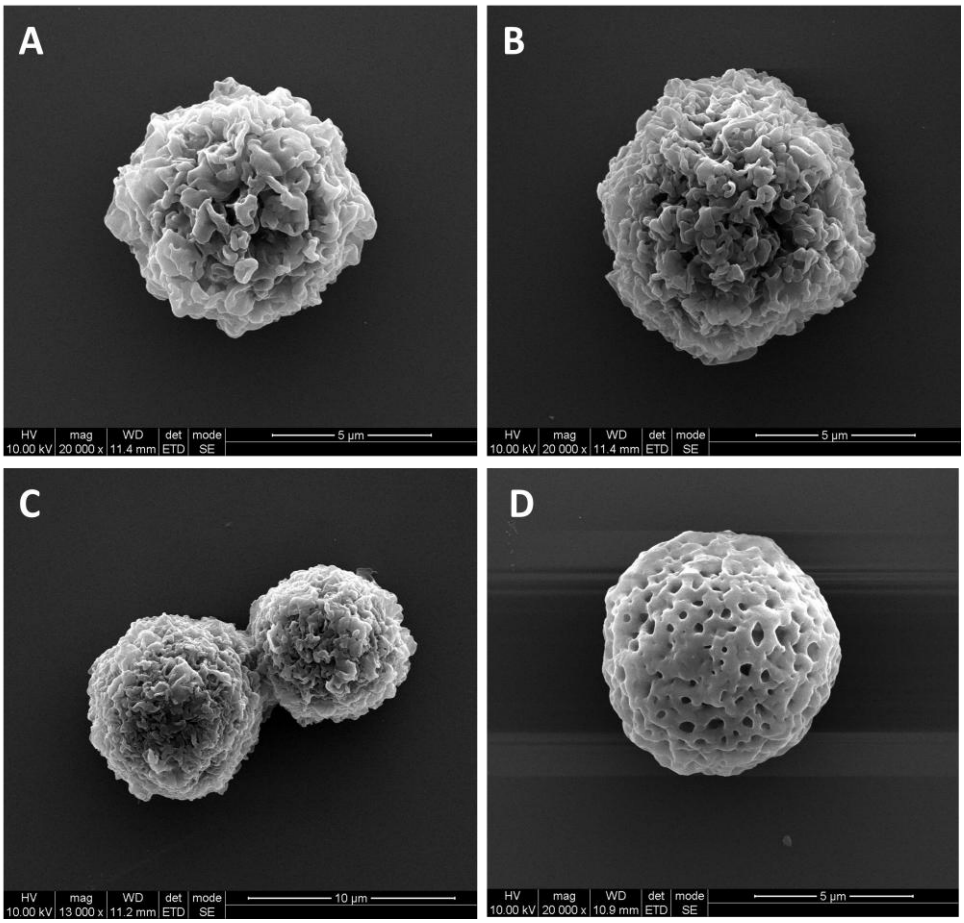

Figure III-II- 10: SEM images a) DCs, b) DCs without MNPs after the application of the AMF, c) DCs with MNPs without AMF and d) DCs loaded with MNPs after the application of the AMF (20 µg/ml MNPs, 16mT, f=260 kHz and 15 min).

III.II.IV. Conclusions

From this part of the thesis we can conclude that the incorporation of MNPs combined with the application of an AMF is a suitable tool to trigger cell death. The MNPs incorporation and the AMF *per se* do not cause any cell damage, but the combination of both make the cells to die.

It is noteworthy that the temperature of the cell medium during the AMF application did not increase. So the cell death can not be attributed to a high temperature increase as reported by other authors in the literature [187]. Our explanation for the fast cell death observed is that the cell death is related to the confinement of the MNPs aggregated inside lysosomal structures that makes these MNPs-agglomerates able to disrupt the lysosomal membrane by the energy release during AMF application. Due to this membrane disruption, the release of the lysosomal content into the cytoplasm could trigger the fast cell death observed. There is evidence of cell death in MNP loaded cells (MCF-7 and MDA-MB-468) after AMF application without observing temperature increase [185].

Concerning the cell death mechanism we have observed a fast necrotic-like cell death. The percentage of cells that die after the AMF application depends on the amount of captured MNPs, on the magnetic field amplitude and on the exposure time. The morphology of the cells after the AMF application reveals the appearance of channels in the cell membrane that could contribute to their death.

III-III: Preparation of Adenovirus-MNPs complexes for magnetofection

Magnetofection is one of the possible biological applications of MNPs in the field of gene therapy. It can be defined as a method for nucleic acid delivery under the influence of magnetic fields. The magnetic force exerted acts on nucleic acid vectors (viral or nonviral) that are associated with MNPs. The first reports about this technique are from the year 2002, [188], but after a fast growth and establishment of the basic principles, the term magnetofection is nowadays widely used in the scientific literature.

In this thesis we will concentrate in viral vectors, which have been associated through electrostatic interactions with different types of MNPs, with the aim to improve the transduction efficiency on neuronal target cells.

The target for nucleic acid transduction was neuronal cells: mouse neuronal line N2A and rat glial cell line B92, cells that belong to the Central Nerve System (CNS). The reason for choosing these cell lines is based on the impact that gene therapy could have on the improvement of treatments of neurological disorders. Viral vectors utilized for clinical CNS gene transfer studies include recombinant Adeno-Associated virus (rAAV), Lentivirus (LV), Adenovirus (Ad), and Herpes-Simplex virus (HSV). Adenoviral vectors are excellent vehicles to transfer genes into nervous system due to their ability to transduce dividing and non-dividing cells, their ability to be grown to very high titers and their large insert capacity.

Taking all this concepts into account we decided to perform the magnetofection approach using magnetic-adenoviral vectors in order to try to enhance transduction efficiency in both N2A and B92 cell lines. Though the final objective of this part of the thesis work was to boost the transduction efficiency in the target cell lines a previous extensive characterization of the complexes formed between adenovirus and MNPs had to be performed. Optimization of the complexes formation was carried out studying the binding, stability, internalization in the cells and physical and magnetic characterization at different particle-to-virus ratio.

III.III.I. Magnetic nanoparticles

Magnetotransfection experiments were performed by using three types of MNPs already described in section (II.II.II, page 95): PEI-Mag, SO-Mag and G1 particles. The characterization of the three types of MNPs used in this part of the work was made by TEM, DLS and SQUID. Also the iron content of the ferrofluid was calculated by a colorimetric assay as described in page 95.

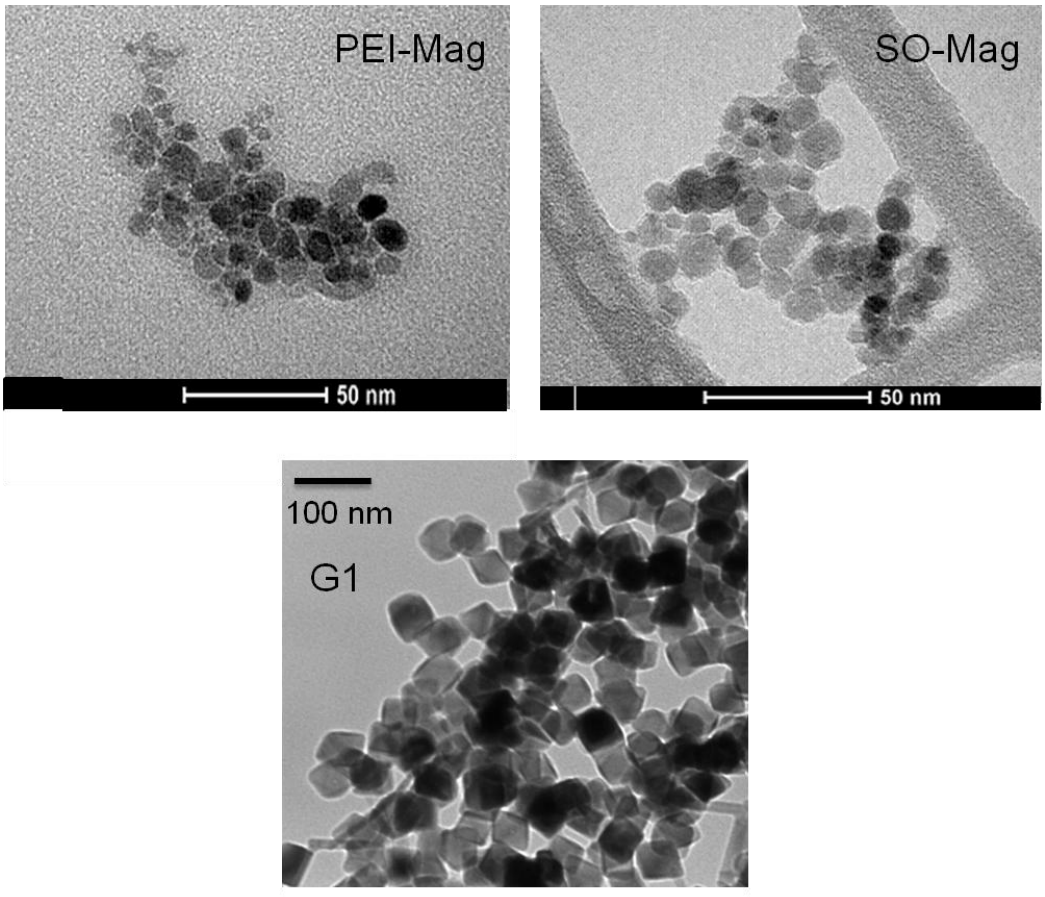

Figure III-III- 1: Micrographs of PEI-Mag, SO-Mag and G1 particles obtained by TEM at 200 kV.

Figure III-III- 1 shows the images obtained by TEM for the **PEI-Mag**, **SO-Mag** and **G1** particles. These particles were previously characterized and described in the literature so we knew that the average crystalline size of their cores was **9** and **11nm** for **PEI-Mag** and **SO-Mag** particles, respectively, calculated from X-ray diffraction (XRD) [189]. For **G1** particles we were able to extract the size distribution from the TEM micrographs, resulting in an average core size of **60nm**.

DLS measurements were performed to obtain the hydrodynamic diameters of the particles in suspension. The results are collected in the Table III-III- 1 and we can see that the **PEI-Mag** particles had a hydrodynamic diameter of about **150nm** and **SO-Mag** particles of about **400nm**. Though the core size was very similar for these two different particles we can see that the SO-Mag particles had a much bigger hydrodynamic diameter, given by the shell or by aggregation of several nanoparticles. G1 particles aggregated forming big clusters of nanoparticles and consequently precipitated, so it was not possible to measure them by DLS.

The zeta potential obtained was positive for the three different MNPs. Positive charges were indeed needed for ionic binding to the virus particles, which are negatively charged. **G1** particles were the more positive ones, with a value of zeta potential of **+32 mV**. **PEI-Mag** particles showed a value of **+40 mV** and **SO-Mag** particles resulted in **+40 mV**.

The iron content in the ferrofluid was determined by a colorimetric assay. For the formation of the complexes between the virus and the MNPs the magnitude that was always used was the amount of iron (given by the MNPs) per virus particle, here on referred to as particle-to-virus ratio (fgFe/VP). The results were **2.5, 9.8 and 0.67 mgFe/mL** ferrofluid for **PEI-Mag, SO-Mag and G1** particles respectively.

The magnetic behavior was determined by a magnetometer SQUID. The M(T) curves taken in ZFC and FC modes showed very different behaviour for all the particles, Figure III-III- 2. **PEI-Mag** particles showed a blocking temperature of about **100K,** however ZFC and FC did not meet because at about 230 K the sample seem to be defreezed and the magnetic signal that was measured from then on was higher than the expected to be. **SO-Mag** particles showed a blocking temperature of about **90K**. The blocking temperature obtained from PEI-Mag and SO-Mag particles corresponded to the single-domain nature of the magnetite particles of around 10nm [129].

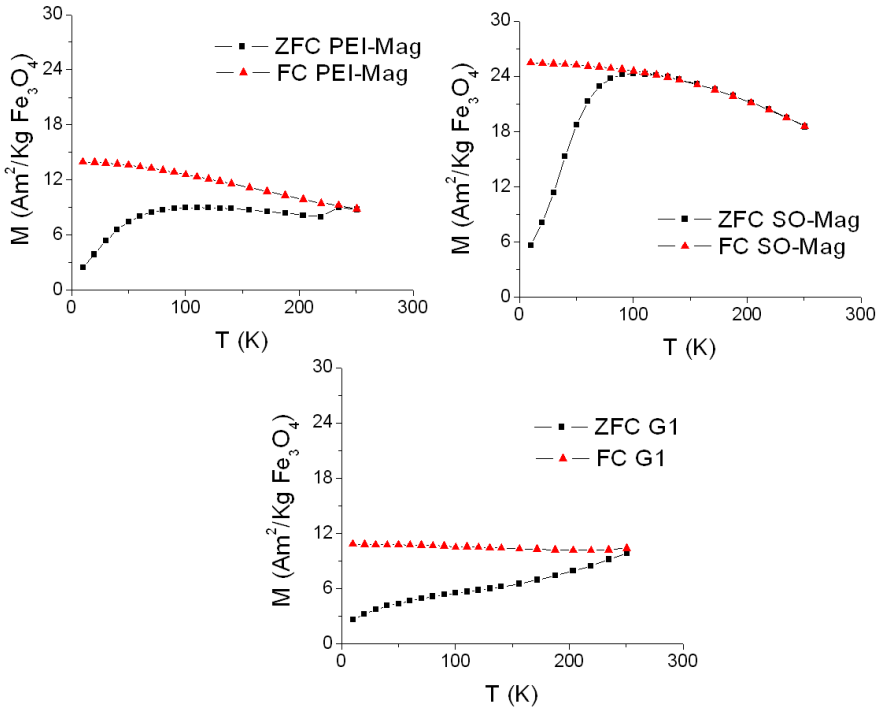

Figure III-III- 2: Zero Field Cool and Field Cool (ZFC-FC) data for all the colloids, PEI-Mag, SO-Mag and G1. H_{FC}= 8 kA/m.

On the other hand in the graph of **G1** particles there was no maximum up to 250K, as in the commercial particles used in the previous experiments. As it will be shown latter at 250K there was a small coercitivity, thus, temperature blocking for G1 particles was supposed to be near above 250K. The blocking temperature obtained from G1 particles is also in agreement with results shown in the literature that show that T_B for magnetite nanoparticles of 50nm was 300K [129].From the measurements we can extract the single domain behaviour of the three types of MNPs due to the absence of the Verwey transition that is observed in multi-domain magnetite particles.

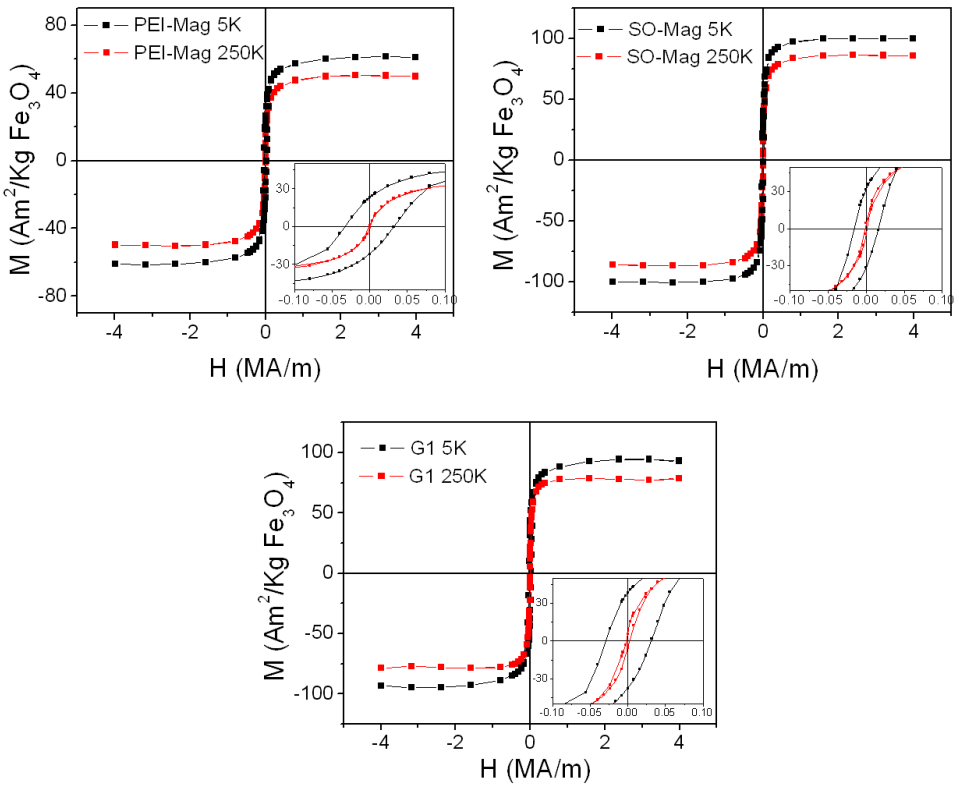

Figure III-III- 3: Hysteresis loops M(H) at 5K and 250K of PEI-Mag, SO-Mag and G1 particles. Inset show the magnification of the low field region.

Figure III-III- 3 shows the hysteresis loops obtained from all the MNPs at 5K and 250K. **PEI-Mag** particles showed saturation of magnetization of **49.7 $Am^2/kgFe_3O_4$** at 250K and due to the fact that at 250K the particles were above the blocking temperature and subsequently unblocked, they showed a null coercitivity. At 5K the saturation magnetization increases up to **61.2 $Am^2/kgFe_3O_4$** and the coercivity at this temperature, where the nanoparticles are blocked, was **32 kA/m**.

SO-Mag particles had a saturation magnetization value of **85.7$Am^2/kgFe_3O_4$** at 250K and for the same razon of PEI-Mag particles they shoed a null coercitivity. The values obtained at 5K were **99.7 $Am^2/kgFe_3O_4$** for the saturation magnetization and **16kA/m** for the coercivity field.

At 250K the Ms obtained from G1 particles was **78.6 $Am^2/kgFe_3O_4$** and since the blocking temperature was near above 250K the particles at this temperature were blocked and subsequently presented a coercivity field of **2.03kA/m**. At 5K the Ms value was **92.7 $Am^2/kgFe_3O_4$** and the coercitivity increases up to **32 kA/m**.

Thus, with these results we can confirm that not only the MNPs were single-domain but they had also a superparamagnetic behaviour because at room temperature they were unblocked and had no coercivity.

Table III-III- 1 collect all the data obtained from the characterization of PEI-Mag, SO-Mag and G1 particles, including the iron content that was measured though a colorimetric assay.

	PEI-Mag	SO-Mag	G1
Core size (nm)	9	11	60
Saturation magnetization (A m^2/ Kg Fe_3O_4)	61.2	99.7	92.7
Shell composition	FSA and PEI-25_{Br}	TEOS, THPMP and PEI-25_{Br}	PEI-25_{Br}
Hydrodynamic diameter (nm)*	152.5 ± 0.6	396.5 ± 6	-
Polidispersity index*	0.12 ± 0.006	0.18 ± 0.011	-
Zeta potential (mV)*	+39.09 ± 1.13	+ 40.45 ± 0.42	+32.04±3.98
Fe content (mg/ml)	2.5	9.8	0.67

*Table III-III- 1: Relevant parameters of the PEI-Mag, SO-Mag and G1 particles. Core size, saturation of magnetization, shell composition, hydrodynamic ratio, polydispersity index and zeta potential values are given. * Measured in dH_2O.*

III.III.II. Virus titration

Before infection experiments, the quantification of both total number of adenovirus particles and infection units was needed. There are different parameters that are connected with these two magnitudes: the VP:I ratio which represents the total viral particle (VP) number relative to infectious units and the bioactivity defined as the inverse of the P:I ratio, in other words, the percentage of the infection units respect to the total number of virus particles.

Among those physically based methods to assess the total number of adenovirus the most used are: electron microscopy [190], optical absorbance [115], Pico Green

fluorescent staining [191] and anion-exchange HPLC [192]. Because of previous expertise in our laboratory we chose the optical absorbance protocol, which had demonstrated very good reliability to asses other viral physical titrations. This method has been demonstrated to be more accurate than other methods as electron microscopy for total virion concentration determination [193].

The resulting optical absorbance at 260nm was 0.1939, so taking into account that the virus dilution was 1:20 the total number of virus particle resulted in **$4.26\ 10^{12}$ VP/ml**.

Besides, biologically based methods are required for the determination of the titre of infectious particles. For this purpose many protocols are described in the literature, as the "plaque assay", end "point assay" and "flow cytometry". Among of all these methods we decided to use the flow cytometry one, because with this method a large number of experiments can be screened in the shortest period of time.

"Plaque assay" is considered to be a standard method due to its inherent accuracy and reproducibility. This method consist of a monolayer of permissive cells that are infected with serial dilutions of virus stock and incubated until visible and quantifiable plaques are formed due to the viral propagation and multiple rounds of lysis. However, plaque assays are time-consuming, as they last up to 14 days.

The "endpoint assay" is an alternative technique in which a large number of wells or plates are scored as infected or non-infected rather than enumerated, [194]. The endpoint assay for virus titration is much less tedious and cheaper alternative to the plaque assay. Despite these advantages, many researchers hesitate to use this assay because of perceived lower accuracy and overestimation of titers.

Finally, "flow cytometry" has been extensively used for the detection and quantification of green fluorescent protein (GFP), consequently we decided to use this

method to calculate the number of GFP expression positive cells after infection with the adenovirus. There are more studies that show that this method for adenoviral vectors carrying the GFP reporter gene titration is a useful tool for the rapid determination of the biological titers [195].

Biological virus titration was performed in easy-to-transfect cells like HEK 293 as described in material and methods section. Two days after the infection, cells were collected and analyzed by FACS. The percentage of positive cells was represented versus log dilution in each point, Figure III-III- 4.

At low multiplicity of infection (< 0.3 TU/ml) a linear relationship between the proportion of infected cells, assessed by flow citometry, and the dilution factor can be drawn. In this linear zone of infection one infected cell corresponds to a single infectious event as described previously [196].

In these conditions, the titre can be calculated as:

$$Titre \quad \frac{TU}{ml} = \frac{\%infected\ cells\ x\ Total\ Number\ cells}{100\ x\ volume\ x\ dilution}$$

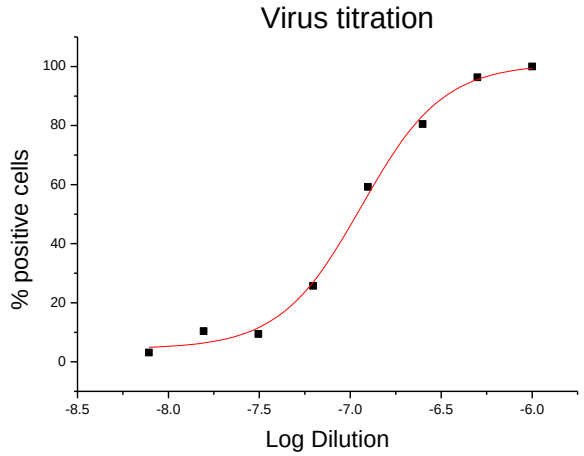

Figure III-III- 4: Virus titration data obtained by FACS. % positive cells are represented versus log Dilution used in each point.

The experimental data was adjusted using a sigmoidal Boltzman function:

$$y = A_2 + \frac{A_1 - A_2}{1 + \exp(\frac{(x - x_0)}{dx})}$$

A_1= 4.4, A_2= 100, x_0= -6.94 and dx= 0.2243. These values were obtained when the curve was fitted, and we calculated the dilution value necessary to obtain 50% of transfected cells, resulted in 1.5 10^{-7} dilution. From the initial number cells seeded in each well (3000 cells) we obtained the number of cells transfected that correspond with the amount of transfected units as 1500 cells. Therefore, the virus titration resulted in **2.61 10^{11} TU/ml**.

Comparison of titer determined by both physical and biological methods suggested that not every virion of a preparation of adenovirus vector is functional with regard to transfer and expression of the transgene. Hence, adenovirus vector bioactivity, as it has been above mentioned, is a very useful concept, defined as:

$$Bioactivity = \frac{number\ of functional\ virions}{total\ number\ of\ virions} \times 100$$

where the value goes from 0 to 100% representing the fraction of virions able to achieve detectable transfer and expression of the transgene in the target cell under defined conditions. With our data the bioactivity of the adenoviral vector resulted in **6.13%**.

III.III.III. Adenovirus-MNPs complexes association and stability

The level of association between the virus and the MNPs was measured, with adenovirus marked with radiation as described in the page 103, at different particle-to-virus ratio, in order to know the optimal amount of MNPs that should be used to form the magnetic complexes with the adenovirus, avoiding the virus to be partially unbound and also trying not to add excess of MNPs that do not contribute to form the magnetic complexes. Adenovirus particles have a negative Z-potential value while magnetic particle used have a positive Z-potential value, so self-assembly of the virus with MNPs is probably governed by electrostatic interactions.

Figure III-III- 5 shows the percentage of the magnetically sedimented virus particles as a function of the particle-to-virus ratio in terms of iron weight per virus particle (fgFe/VP) in PBS, the same medium where complexes were formed. Magnetically sedimented virus corresponded to the virus bound to MNPs that was formed the complexes.

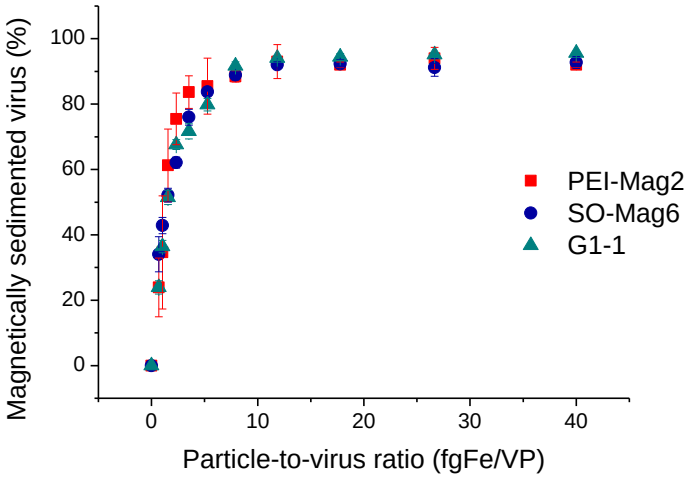

Figure III-III- 5: Adenovirus association with MNPs versus MNPs-to-virus ratio, in PBS. Results for PEI-Mag, SO-Mag and G1 particles are represented together.

Maximum binding and sedimentation of almost 100% is achieved with all PEI-Mag, SO-Mag and G1-1 MNPs in the range of 5-40 fgFe/VP. Taking these results into account we decided to form the magnetic complexes at a ratio around 5 fgFe/VP, because at this ratio the maximum binding was already achieved and we minimize the amount of possible unbound MNPs.

The stability of the magnetic complexes was measured in presence of biological fluids as cerebospinal fluid (CSF) and fetal calf serum (FCS) by mixing 1:1 the complexes already formed in PBS with each of these biological fluids. Magnetically sedimented virus percentages for each of the MNPs kind in the three media: PBS, CSF and FCS at different particle-to-virus ratios, are represented in Figure III-III- 6.

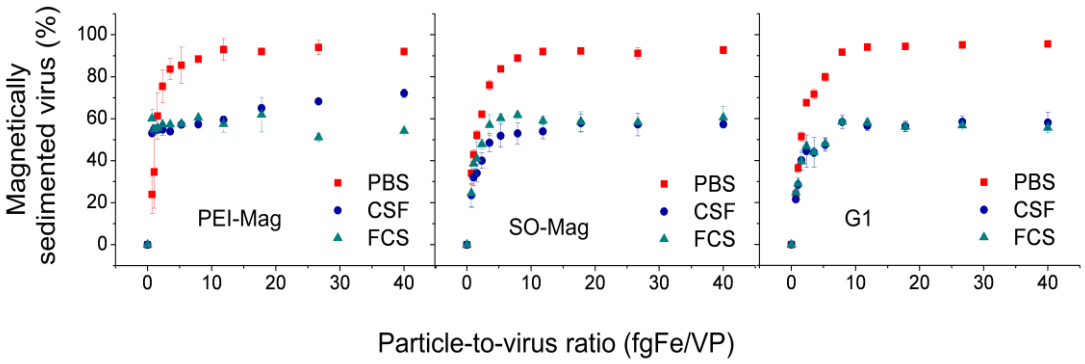

Figure III-III- 6: PEI-Mag, SO-Mag and G1 complexes stability after the dilution in 1:1 of CSF or FCS.

As it can be seen in the graphs, stability of the complexes decreases after the dilution in biological media. For all the types of MNPs the maximum virus binding value was between 50-60 %. As it could be observed in PBS, at 5 fgFe/VP the percentage of the virus that was bound to the particles forming the complexes was maximum, and from this point up this value remains the same. In PBS almost 100% of

the virus was bound to the MNPs but in both biological mediums, CSF and FCS, the maximum binding rate decreases until 50-60%. The particle-to-virus ratio where the maximum binding is achieved in FCS and CSF was again 5 fgFe/VP, as in PBS medium. So the lower magnetically sedimentation of the virus when the complexes were diluted in 50% of FCS and CSF was due to partial dissociation of the virus and MNPs complexes.

Despite that the magnetic-adenoviral complex partially split when they are diluted in CSF and FCS, the transduction efficiency for in vitro experiments is really good, as it will be shown later.

III.III.IV. Size, Z-potential and magnetophoretic measurements

Table III-III- 2, Table III-III- 3 and Table III-III- 4 show the values of the mean hydrodynamic diameters (Dh), polydispersity index (PI) and Zeta potential (ξ) for the complexes formed with the three kinds of MNPs at different particle-to-virus ratios in PBS.

Fg Fe/VP	Dh (nm)	*PI*	ξ (mV)
0	125.8	0.155	-9.68
0.3125	785	0.553	13.4
0.625	400	0.406	14.2
1.25	296	0.368	14.4
2.5	252	0.253	15.4
5	227	0.235	15.4
10	238	0.249	15.5
20	224	0.18	15.1
40	230	0.22	15.4

Table III-III- 2: Table that collect the results for complexes formed with PEI-Mag NPs at different ratios. Dh: hydrodynamic diameter, PI: polydispersity index and ξ: Zeta potential.

fgFe/VP	Dh (nm)	*PI*	ξ (mV)
0	125.8	0.155	-9.68
0.3125	680	0.928	-8.54
0.625	655	0.982	-5.27
1.25	1513	0.356	-3.18
2.5	2080	0.286	-2.71
5	1424	0.513	-0.0573
10	1676	0.476	0.853
20	3667	0.232	3.08
40	> 10000	0.034	5.5

Table III-III- 3: Table that collect the results for complexes formed with SO-Mag NPs at different ratios. Dh: hydrodynamic diameter, PI: polydispersity index and ξ: Zeta potential.

fgFe/VP	Dh (nm)	*PI*	ξ (mV)
0	125.8	0.155	-9.68
0.3125	659 (89%), 85 (11%)	1	12.7
0.625	1104 (88%), 153 (12%)	0.902	13.7
1.25	1114 (92%), 86 (8%)	0.878	16.6
2.5	1120	0.686	16.9
5	798.2	0.894	15.6
10	1001	0.592	17
20	1132	0.714	17.7
40	1599 (80%), 5246 (20%)	0.426	16.5

Table III-III- 4: Table that collect the results for complexes formed with G1-1 NPs at different ratios. Dh: hydrodynamic diameter, PI: polydispersity index and ξ: Zeta potential.

The hydrodynamic diameter of the virus alone was around 120nm. Furthermore, hydrodynamic diameters of complexes formed with PEI-Mag particles were the smallest

ones. From particle-to-virus ratios values of 5 fgFe/VP the Dh was around 230 nm. The ratio of 5 fgFe/VP was the value at which the virus formed complexes with the MNPs. So at lower particle-to-virus ratios there were not enough amount of MNPs to form the complexes with all the virus. It can be seen that at these ratios the Dh values were bigger than 230nm, and that the smaller the amount of MNPs was the bigger the Dh was. It could be that at lower particle-to-virus ratios the MNPs interacted with more than one virus and formed larger complexes and for that reason we observed higher Dh. Similar effects in the Dh were observed with the same kind of MNPs and other virus by other authors [114, 189]. Concerning the zeta potential values in these complexes it can be seen that from 2.5-5 fgFe/VP the value remained around 15.4 mV and for lower ratios the zeta potential was quite smalle due to the lack of MNPs to form complexes. With these results we could conclude that complexes based in PEI-Mag particles are formed by insulated virus particles surrounded by several MNPs.

Complexes formed with SO-Mag particles at all ratios led to big aggregates, probably comprising several virus and MNPs. Besides, the zeta potential increases from -9.68 mV (the zeta potential values for the virus) to +5.5 mV, so at these zeta potential values, which were near the neutral range, there was not enough stability to avoid aggregation. For that reason, the more MNPs added the bigger the aggregates were. It is noteworthy that the magnetic moment of SO-Mag particles was higher than the magnetic moment of PEI-Mag particles, and the high magnetic moment might also contribute to the complexes aggregation. From these results we could extract the idea that for the same amount of iron of PEI-Mag and SO-Mag particles the amount of positive charges supplied by the PEI molecules was much bigger for PEI-Mag particles. Both particles had similar magnetite core diameter so the amount of iron per particle should not be very different. Thus, attributing the difference in PEI amount to a

difference in the number of particles and subsequently to a differences in the surface area functionalized with PEI is not possible. The only difference could be the amount of PEI molecules linked to the particle surface, so we can confirm that SO-Mag particles had less PEI molecules attached to their particle surface and that causes the complexes to aggregate. Similar results were obtained with this kind of MNPs in other experiments [189].

Finally, complexes based in G1-1 particles also formed aggregates consisted of several virus and MNPs. The Dh was about 1 μm and the zeta potential value about 17 mV. In this case there were enough PEI molecules in the surface of the MNPs that led a high positive zeta potential value, however, there was still complexes aggregation that could came from the magnetic interactions originated in the big magnetic moment of the G1 particles.

In the following we describe the results related to the magnetophoretic mobility of the complexes, in which the magnetic sedimentation was measured as described in page 104. The results are shown in the Figure III-III- 7 and confirmed that the mobility of the complexes was strongly influenced by the application o a magnetic field and mainly driven by the magnetic forces. This experiment discards the possibility of sedimentation due to the size of the complexes. Based in these results there is no doubt about the fact that sedimentation of the complexes is just because magnetic interactions. After half an hour of measuring the absorbance of the magnetic complex solution, when the measurement was made without the magnetic field, the absorbance had no change showing that the stability of the complexes after one hour and a half was really good.

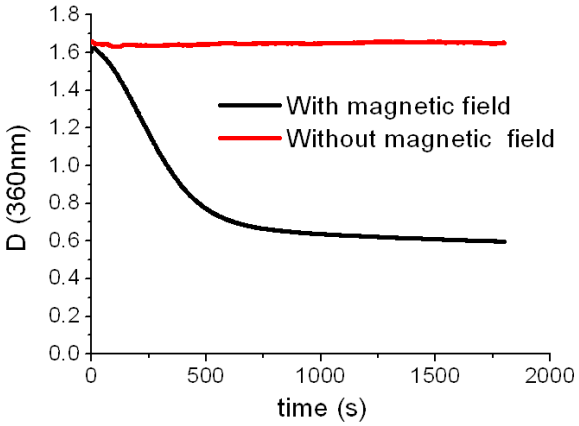

Figure III-III- 7: Kinetic curves for complexes formed with PEI-Mag particles at a particle-to-virus ratio of 40 fgFe/VP. Black curve was obtained in the presence of the magnetic field and red curve without applied magnetic field. D: optical density.

Figure III-III- 8 shows the magnetophoresis results obtained on complexes formed with the three kinds of MNPs at different particle-to-virus ratios. As expected, higher particle-to-virus ratio resulted in an enhanced magnetic response. Comparing the data from the three MNPs used, it was inferred that the complexes formed with PEI-Mag particles had the lowest magnetic influence, being in concordance with the results showed previously in relation to the size of the complexes. Complexes formed with PEI-Mag were the smaller ones, so the magnetic moment of these complexes was the smaller one and that is why they had the lowest magnetic interaction.

G1-1 and SO-Mag complexes had a much higher magnetic effect when compared them with PEI-Mag complexes, and between them SO-Mag complexes were the ones with the highest magnetic moment, again in concordance with the rest of results. The bigger the complexes were the faster they magnetically sediment due to the fact that its total magnetic moment increases.

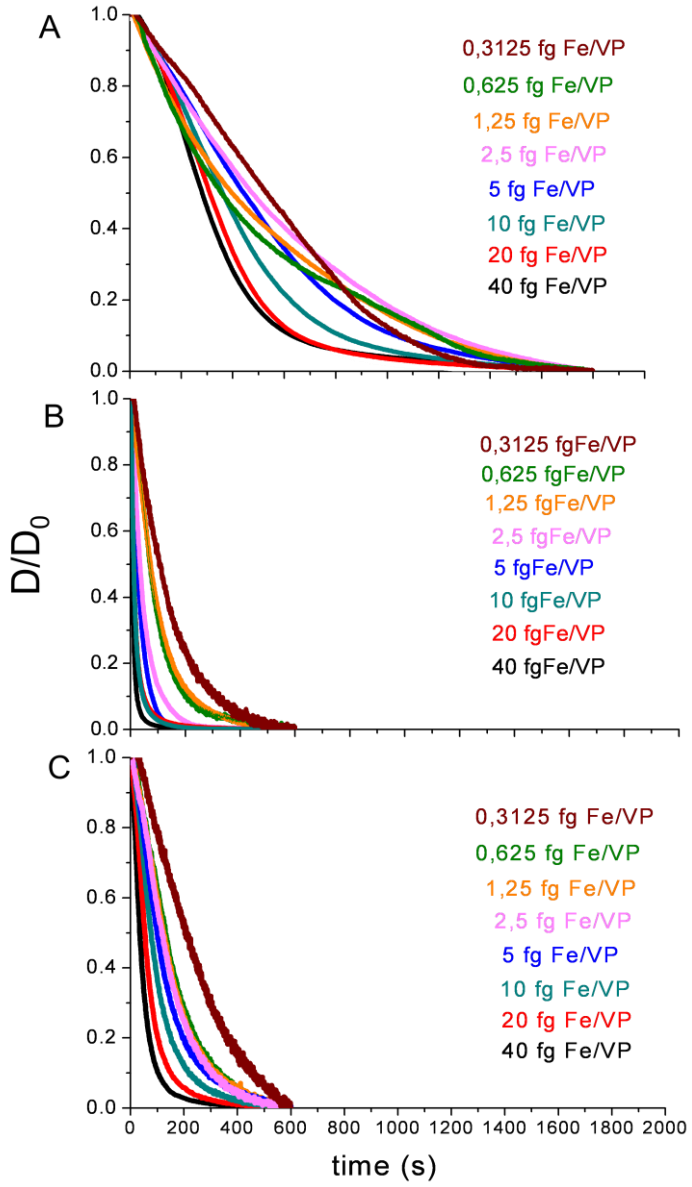

Figure III-III- 8: Relative optical density D/D_0 as a function of time, showing the magnetophoretic sedimentation for complexes formed with PEI-Mag NPs (A), SO-Mag NPs (B) and G-1 NPs (C) at different particle-to-virus ratio.

From the analysis of these results it was obtained the average velocity of each magnetic complex at the different particle-to-virus ratios. For that purpose $t_{90\%}$ was extracted from the curve data, $t_{90\%}$ is the time required for magnetically sedimenting the 90% of the complexes in the magnetophoresis experiments made in the spectrophotometer, this is the time when the D/D_0 value decreases down to 0.1. As the average path the complexes moved through was 1mm it was possible to calculate the average velocity, Table III-III- 5. Average velocity data is extracted from the magnetic mobility curves so the tendency we observed in the results was the same. Complexes formed with PEI-Mag particles were the slower ones, as they were the smaller ones, and complexes formed with SO-Mag and G1 particles had a higher average velocity due to its bigger size and consequently they have a larger magnetic moment.

	$t_{90\%}$ (s)			Average velocity, u_z, (m/s)		
fgFe/VP	PEI-Mag	SO-Mag	G1	PEI-Mag	SO-Mag	G1
0	-	-	-	-	-	-
0.3125	1050	134.5	451	9.524E-07	7.435E-06	2.217E-06
0.625	1188	202	308	8.417E-07	4.950E-06	3.247E-06
1.25	1178	228.5	287.5	8.489E-07	4.376E-06	3.478E-06
2.5	1236	118	325	8.091E-07	8.475E-06	3.077E-06
5	1032	79	334.5	9.690E-07	1.266E-05	2.989E-06
10	820	45.5	218	1.219E-06	2.198E-05	4.587E-06
20	652	49.5	151	1.534E-06	2.020E-05	6.622E-06
40	628	23.5	103.5	1.592E-06	4.255E-05	9.662E-06

Table III-III- 5. Results of the time needed to magnetically sediment 90% of the complexes (t0.1) and the average velocity of the complexes formed between the adenovirus and the three different kinds of MNPs.

III.III.V. Morphological characterization of the complexes

To visualize and analyze the structure of magnetic complexes formed between the virus and the different kind of MNPs, Atomic Force Microscopy (AFM) and Transmission electron microscopy (TEM) was performed. The virus alone was also analyzed.

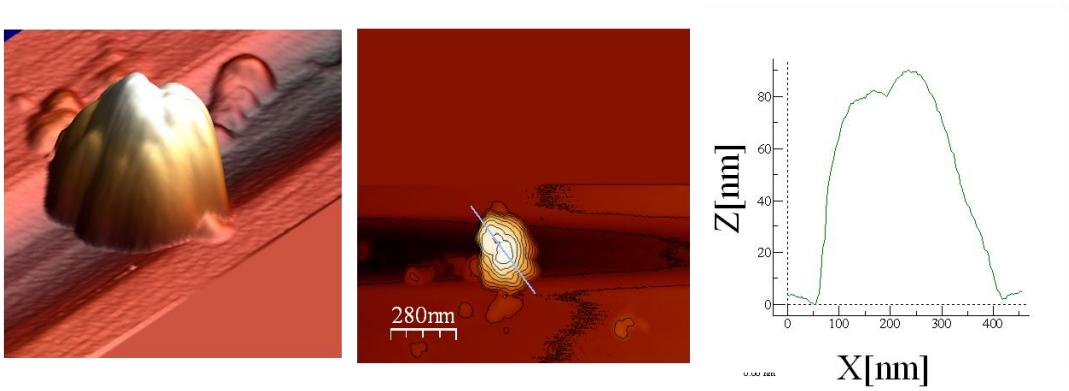

Figure III-III- 9: Atomic force microscopy images. From left to right: AFM 3D image, contour plots and height profile histogram for the virus alone.

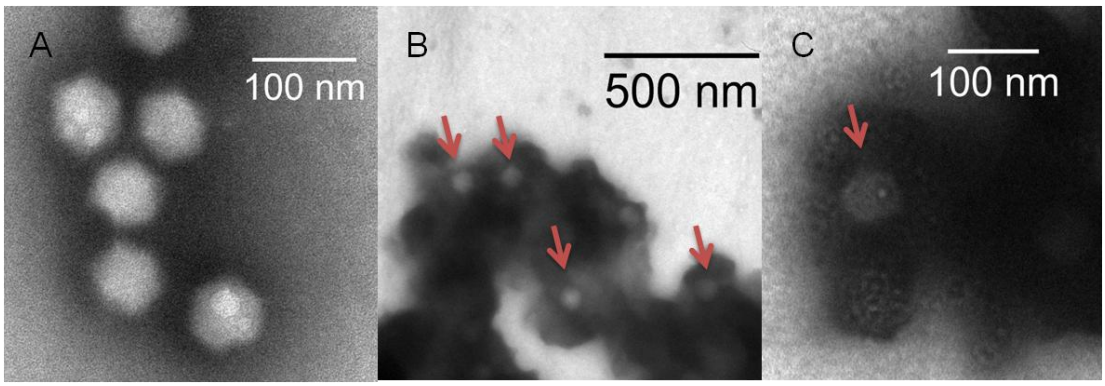

Figure III-III- 10: Microgrpahs of the virus (A) and complexes formed with PEI-Mag particles at a particles-to-virus ratio of 0.6fgFe/VP (B,C). Red arrows point to the virus indide the MNPs aggregates.

Figure III-III- 9 shows the AFM images obtained from the virus alone. From the height profile it could be seen that the virus size was around 80nm. Figure III-III- 10-A shows the virus size and morphology observed by TEM. It can be seen the hexagonal virus morphology and the size of 80 nm, as observed by AFM. It can be observed that the virus usually are aggregated, thus, by AFM we observed a cluster of about 200nm of with and 80nm of height, that corresponded to a cluster of virus.

The TEM images obtained from the magnetic-adenoviral complexes were not very good because the MNPs formed aggregates and it was vey difficult to identify the virus particles inside the aggregates. In Figure III-III- 10-B and C it can be seen some virus particles surrounded by MNPs aggregates (dark particles). The virus particles corresponded to the particles marked with the arrows. In Figure III-III- 10-C the hexagonal virus morphology can be distinguished.

Figure III-III- 11 shows the images taken for the complexes formed with PEI-Mag particles. In the 3D image we could observe a particle that because of their size of 80nm was identified as a viral particle, surrounded by PEI-Mag particles, which were smaller. The idea that complexes with PEI-Mag were formed by single viral particles linked to several MNPs is in concordance with hydrodynamic diameter results that showed that from 2.5-5 fgFe/VP complexes were formed by insulated viral particles. PEI-Mag nanoparticles were detected in AFM as particles of about 20nm, as it can be seen in the height profile, or as bigger particles if there were more than one nanoparticle together, as the 40-50 nm peak detected in the image that is shown. The size of almost all complexes observed by AFM was around 300nm, which was in accordance with the size determined by DLS.

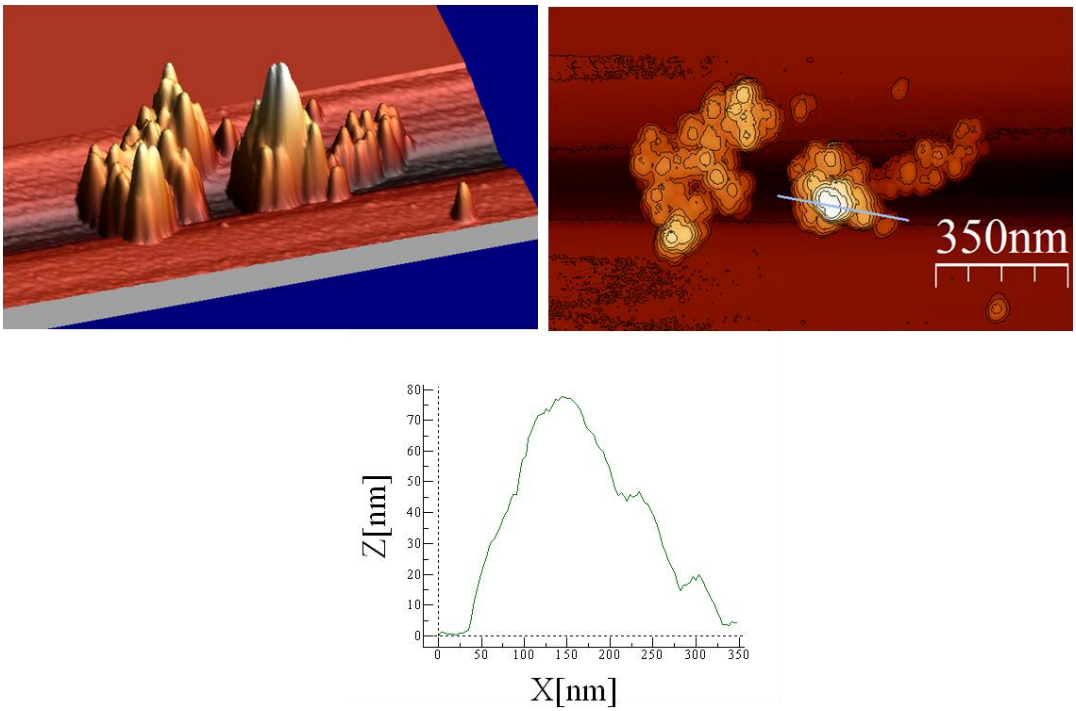

Figure III-III- 11: Atomic force microscopy images. From left to right: AFM 3D image and contour plots (Up) and profile histogram (Down) for complexes formed with PEI-Mag nanoparticles. Complexes were formed at 5 fgFe/VP.

In Figure III-III- 12 the images taken of the complexes formed with SO-Mag nanoparticles are presented. The size of the upper complex that is shown was about 700nm and the lower one about 300 nm. The size of the complexes was not homogeneous, from 300nm to several microns, but we selected these two because it was possible to observe a viral particle. It could be observed in the height profile a particle of about 80nm, which was supposed to be a viral particle. In these complexes we could not confirm that they were formed by an insulated viral particle surrounded by several MNPs due to the fact that the complexes were bigger and we couldn't identify the component of the bigger peaks, as the one observed in the complex of the image of 160nm. It could be several MNPs or a mixture of viral and magnetic particles. So our

theory for the complexes formed with SO-Mag particles is that they are formed by several viral particles and several MNPs. However we could observe some smaller complexes, as the lower one in the Figure III-III- 12 where the complex seemed to be formed by one virus and several MNPs.

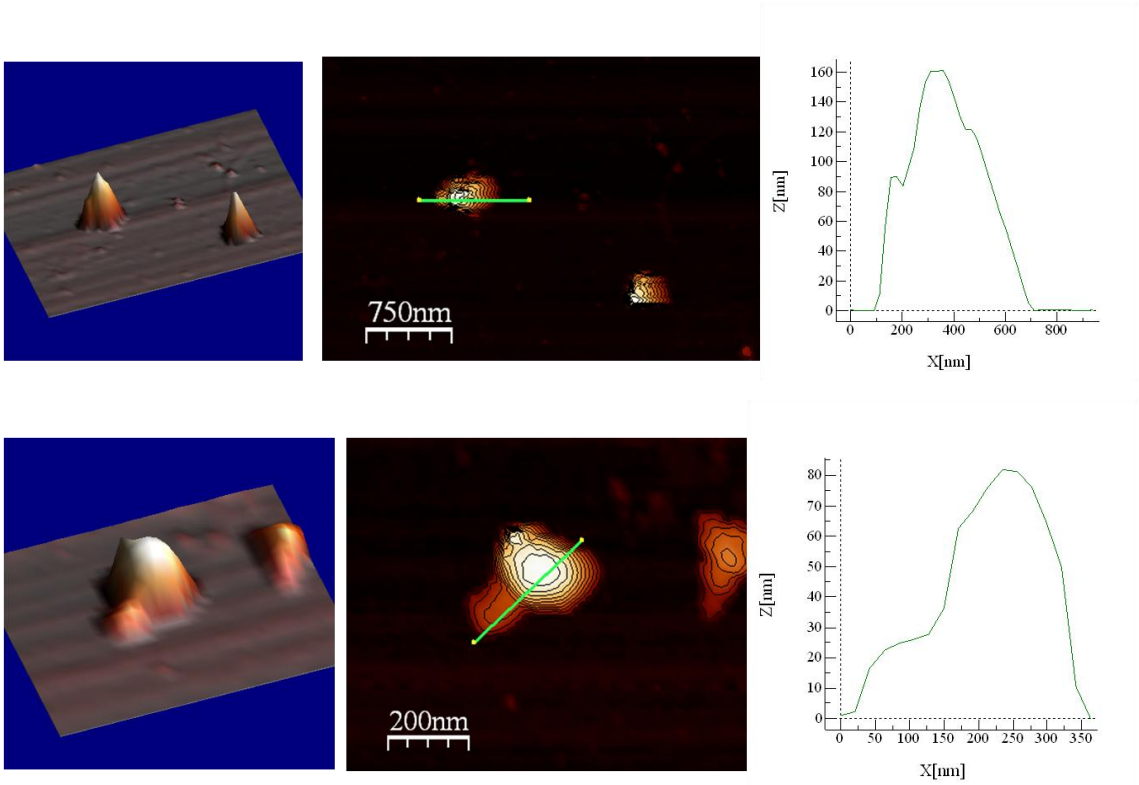

Figure III-III- 12: Atomic force microscopy images. From left to right: AFM 3D image and contour plots (Up) and profile histogram (Down) for complexes formed with SO-Mag nanoparticles. Complexes were formed at 5 fgFe/VP.

Figure III-III- 13 shows the images of the complexes formed with G1 nanoparticles. Sizes of the complexes were from half micron to one micron, and the two presented here were about one 500nm and one micron. Here there is evidence of the fact that

complexes were formed by several virus, as the peak of about 80nm height, which corresponds to the viral particle, had a width of about 300nm in both images that corresponds to 3 viral particles. So, as for SO-Mag nanoparticles, complexes formed with G1 nanoparticles were compounded by several viral particles and several MNPs.

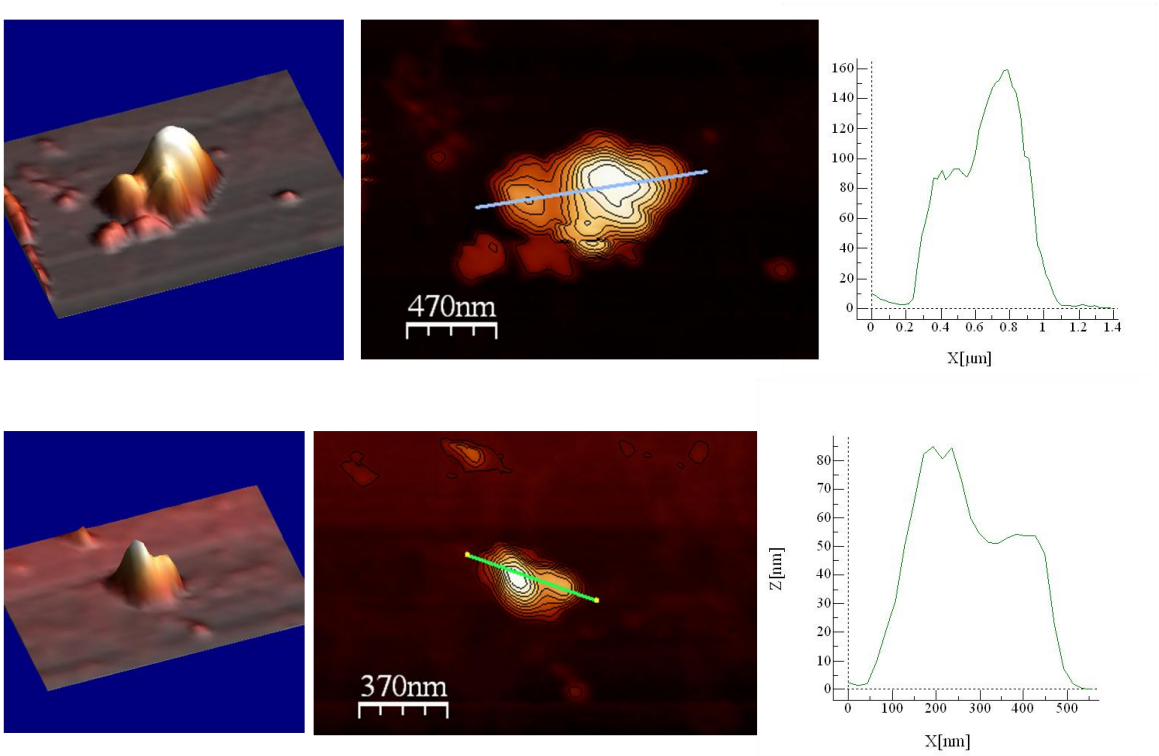

Figure III-III- 13: Atomic force microscopy images. From left to right: AFM 3D image, contour plots and profile histogram for complexes formed with G1 nanoparticles. Complexes were formed at 5 fgFe/VP.

All these results are in agreement with the results obtained for the complexes by DLS. PEI-Mag and SO-Mag particles had been used by other authors to form complexes with other kind of virus, specifically oncolytic virus, and the results obtained are in agreements with the results presented here [114, 189].

III.III.VI. Complex internalization

In order to check whether the magnetic field had any influence in the amount of virus internalized per cell, internalization experiments were made. The final objective of this experiment was to be able to relate the increase in the amount of internalized virus per cell with the parallel improvement of the transduction efficiency.

Two types of cells were used, N2A neuronal cells and B92 glial cells, which were the ones selected to further transduction experiments.

In Figure III-III- 14 percentages of virus internalized per cell are represented in both N2A and B92 cells versus multiplicity of infections (MOI=Transformation Unit per cell) applied, 24 hours post infection. The slope obtained from fitting a straight line to the experimental data corresponds to the percentage of the applied amount of virus that was internalized. In Table III-III- 6 the percentage, in terms of slope, of internalized virus are represented.

It can be seen in both cell lines that the amount of virus internalized per cell when the infection is performed with PEI-Mag and SO-Mag complexes is much higher than when it is carried out with the virus alone or with the complexes formed with G1 particles. Furthermore complexes with G1 particles lead to an increase in the virus internalization when it is compared with the virus alone. However it is not as high as the other two kinds of complexes.

These results demonstrate that the internalization of virus particles per cell with the magnetic complexes in the presence of an external magnetic field was 5- to 7-fold higher when using complexes formed by PEI-Mag and SO-Mag particles and 2-3-fold higher for complexes made with G1-1 MNPs as compared to virus alone in both cell lines.

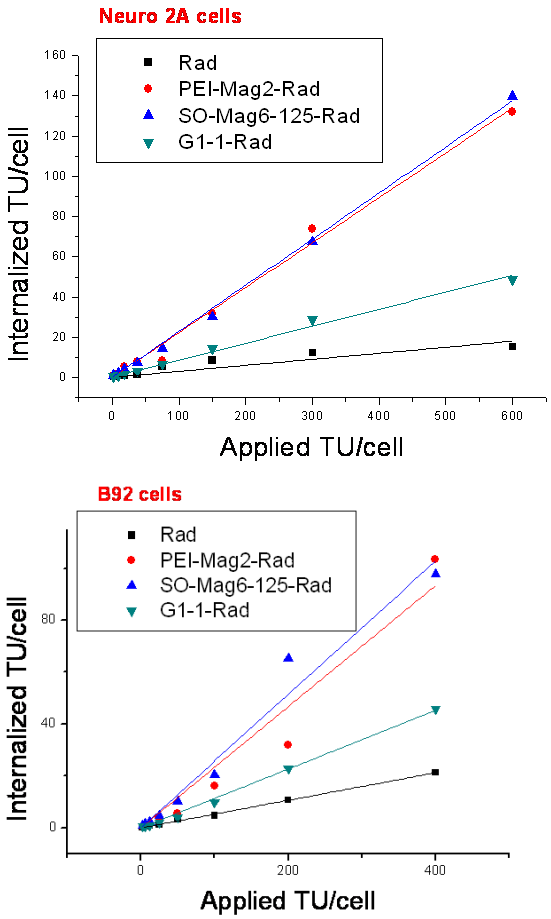

Figure III-III- 14: Representation of the transforming units (TU) internalized per cell versus TU applied per cell in N2A cells (up) and B92 cells (down).

The increase in the virus internalization in magnetotransduction has also been shown in the literature for other cell lines and magnetic complexes consisting of other kind of virus and magnetic particles [114].

Particles	Neuro 2A	Glial B92
RAd-A	0,03 -> 3%	0,053 -> 5.3%
RAd-A_PEI-Mag2	0,22 -> 22%	0,23 -> 23%
RAd-A_SO-Mag6	0,23 -> 23%	0,26 -> 26%
RAd-A_G1-1	0,085 -> 8.5%	0,11 -> 11%

Table III-III- 6: Table that contains the slope values that correspond to the percentage of virus internalized per cell for the virus alone and PEI-Mag, SO-Mag and G1 based complexes in N2A and B92 cell lines.

Dual-Beam allowed observing the internalization of the MNPs inside the cells during the infection process. Figure III-III- 15 shows an image of N2A control sample (left) and images of N2A cells two days after the infection with magnetic complexes formed with the adenovirus and G1 particles (middle and right).

Bright particles can be detected in the cytoplasmatic area of the cells that were previous infected with magnetic adenoviral complexes. The absence of these particles in the control sample allows us to discard these particles as artifact. So, bright particles must correspond to the MNPs that formed the complexes. Red arrows in Figure III-III-15 show the aggregates of G1 particles that are in the cytoplasm area of the cells. Furthermore, the obtained images were very similar to the images obtained for magnetically uploaded DCs.

As far as we know this is the first time that it is reported the internalization of the MNPs during the magnetofection. It was not possible to identify the virus inside the cells, so we do not know wehether the virus was still bound to the MNPs. But what we

can confirm is that the entire complexes were uptaken by the cells, the virus and the MNPs.

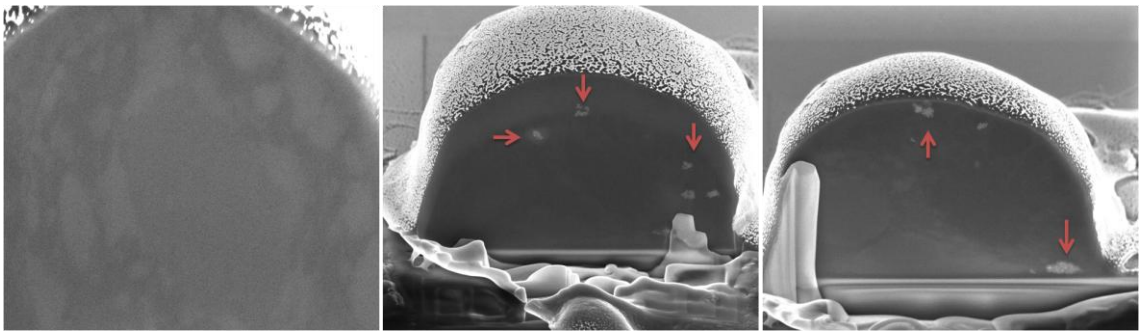

Figure III-III- 15: Images taken durinf slicing in Dual Beam of control N2A cells (left) and N2A cells two days after the infection with magnetic complexes formed with G1 particles (medium and right). Red arrows show the aggregates of G1 particles.

III.III.VII. Viability assay

In order to check whether the virus alone or any of the magnetic complexes used had any toxic effect in both cell lines, viability measurements were carried out. For that purpose MTT test was performed 24 hours post infection at different MOI and a fix particle-to-virus ratio of 2.5 fgFe/VP.

Figure III-III- 16 shows the results, given as percentage of viable cells, for N2A and B92 cells, after 24 hours of incubation with the virus and the magnetic complexes. In both cell lines the maximum toxic effect was observed at the highest MOI value of 400, but toxicity was never higher than 50%. Comparing the results in both cell lines there were no detectable big differences in toxicity between N2A cells and B92 cells. However, looking at the results for the different adenoviral magnetic complexes and

comparing them with the toxicity due to the infection with the virus alone, we could see that G1-1 based complexes presented the highest toxic effect.

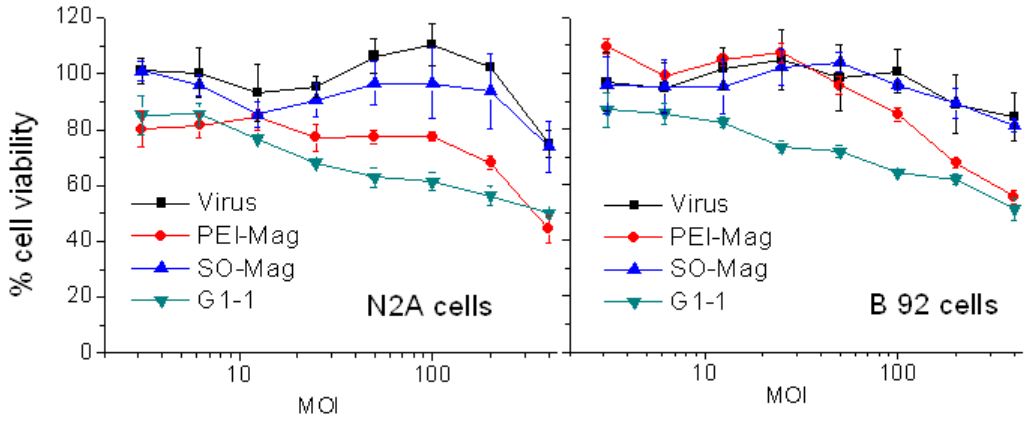

Figure III-III- 16: Graphs that contain the MTT results for N2A cells (Left) and B92 cells (Right) 24 hours post infection with the virus alone and complexes formed with PEI-Mag, SO-Mag and G1-1 particles. MOI: multicitplycity of infection.

For in vivo experiments MOI values that would be desirable are much lower than 200, so toxic effects are not a problem at these conditions.

The analysis of physical characteristics of the magnetic complexes, as well as their level of internalization by the cells and their toxicity studies were the necessary steps for optimizing the complexes formation and for knowing how the magnetic complexes affect the cells. So from here on, we are going to focus in the transduction process using these magnetic complexes in the presence of an external magnetic field.

III.III.VIII. Infection experiments

Infection experiments in both N2A and B92 cell lines were performed, at a fixed NPs-to-virus ratio (2.5 fgFe/VP) and various MOI (up to 200 TU/cell). Transduction efficiency was measured 2 days post-infection with FACS, since the reporter gene encoded a fluorescent protein (GFP) transgene expression was readily detected with this technique. The results were expressed as percentage of cells that were GFP positive.

Figure III-III- 17 shows the results for N2A and B92 cell lines. Each figure compares the transduction efficiency between the virus alone and the magnetic complexes formed with PEI-Mag, SO-Mag and G1 particles at various MOI (from 12.5 to 200 TU/cell).

Analyzing the results it can be seen that the trend in N2A and B92 cells is completely different. The former cell line was much easier to transduce than the latter, as shown by the transduction efficiency results recorded with the naked virus. N2A cells reached high values of about 65% percentage of cells positively transducted at MOI value of 200. However, B92 cells showed no transduction success even at MOI of 200 TU/cell.

Comparing transduction between the different kind of magnetic adenoviral vectors and the virus alone, it can be observed that in N2A cells improvement of the efficiency of the process was obtained at every MOI tested. At low MOI, up to 100, the complex that worked the best in N2A cells was the one made with PEI_mag particles. SO-Mag based complex also boosted the transduction efficiency of the virus alone. Besides, the complexes made with G1 particles at low MOI values did not increase the efficiency of the process. However at the highest MOI, 200, the percentage of the cells positively

transduced was the same for the three complexes and the increase respect to the virus alone was 20%.

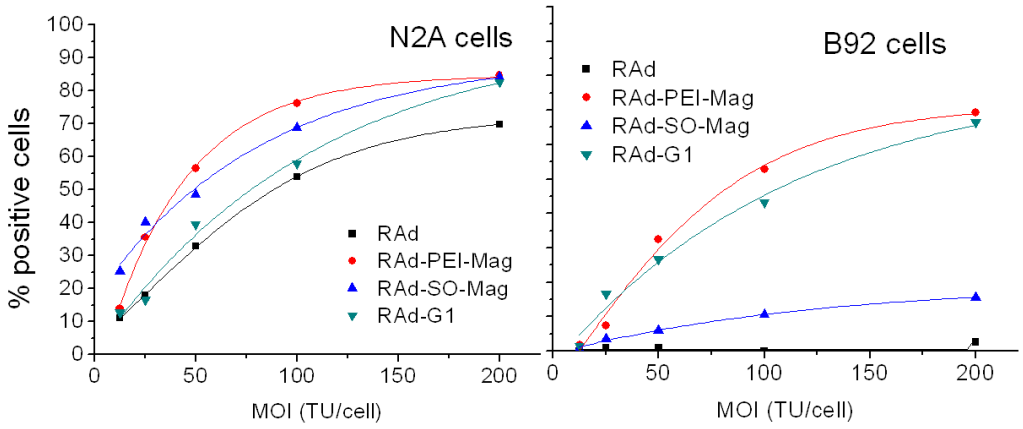

Figure III-III- 17: Graphs that contains the transduction efficiency results for virus alone and magnetic adenoviral complexes formed with PEI-Mag, So-Mag and PEI-Mag and G1-1 particles), in N2A cells (Left) and B92 cells (Right). Anlaysis was made 48h post-infection.

On the other hand, in the case of B92 cells the improvement in the transduction efficiency is much bigger, due to the fact that just with the virus alone no transduction was observed and with magnetic adenoviral complexes up to 80% of cells were positive in GFP expression. Nevertheless, no all the magnetic adenoviral complexes boosted the transduction in the same way. PEI-Mag and G1-1 based complexes were the ones that gave better results, up to 80% of transduction efficiency at the highest MOI and SO-Mag based complexes showed a much slighter transduction improvement in B92 cells, reaching 15% of GFP positive cells at MOI of 200. From these results we can conclude that the transduction efficiency of this adenovirus is improved when it is bound to MNPs and the transduction is made in the presence of a magnetic field. The improvement is observed even in cells that are hard to be transduced, as the B92.

Apart from analyzing the percentage of cells that were positive for GFP expression 48h post-infection, fluorescence microscopy was used 24h post-infection to study the kinetics of the transduction for each type of magnetic complexes.

Figure III-III- 18 shows images obtained for N2A cells (left) and B92 cells (right) which were infected with the virus alone (A), complexes formed with PEI-Mag (B), SO-Mag (C) and G-1 particles (D).

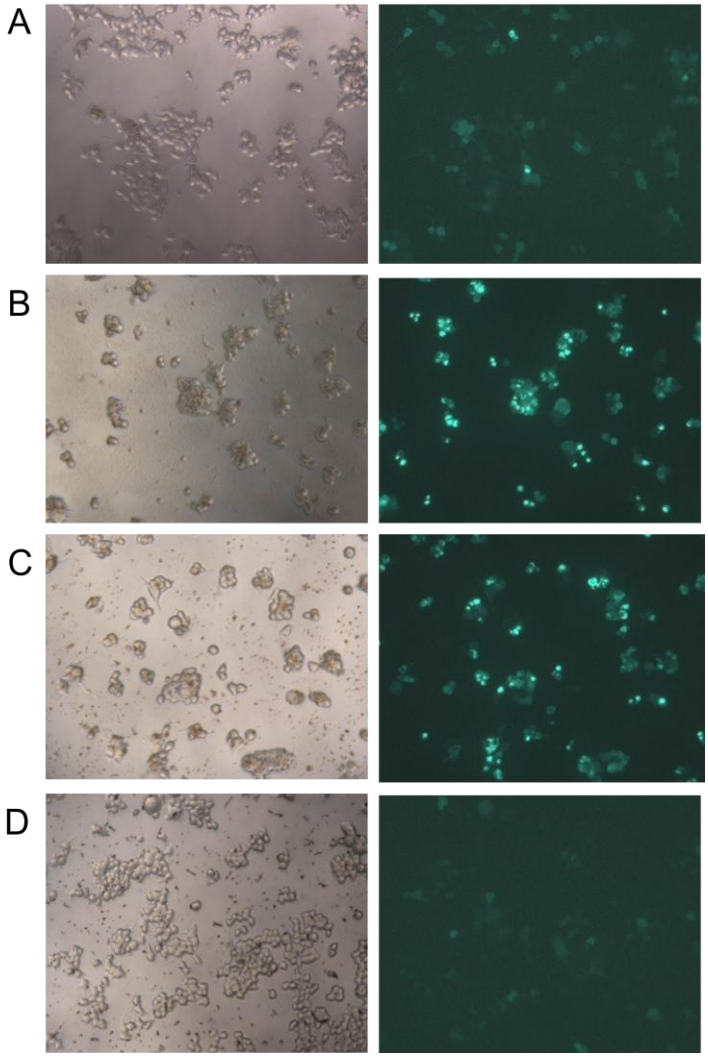

Figure III-III- 18: Images of N2A cells infected with A) the virus alone, B) complexes formed with PEI-Mag NPs, C) complexes formed with SO-Mag NPS and D) complexes formed with G1 NPs. Images were obtained 24h post-infection. Infection was performed at a MOI of 200 and the particle-to-virus ratio for the complexes formation was 2.5 fgFe/VP.

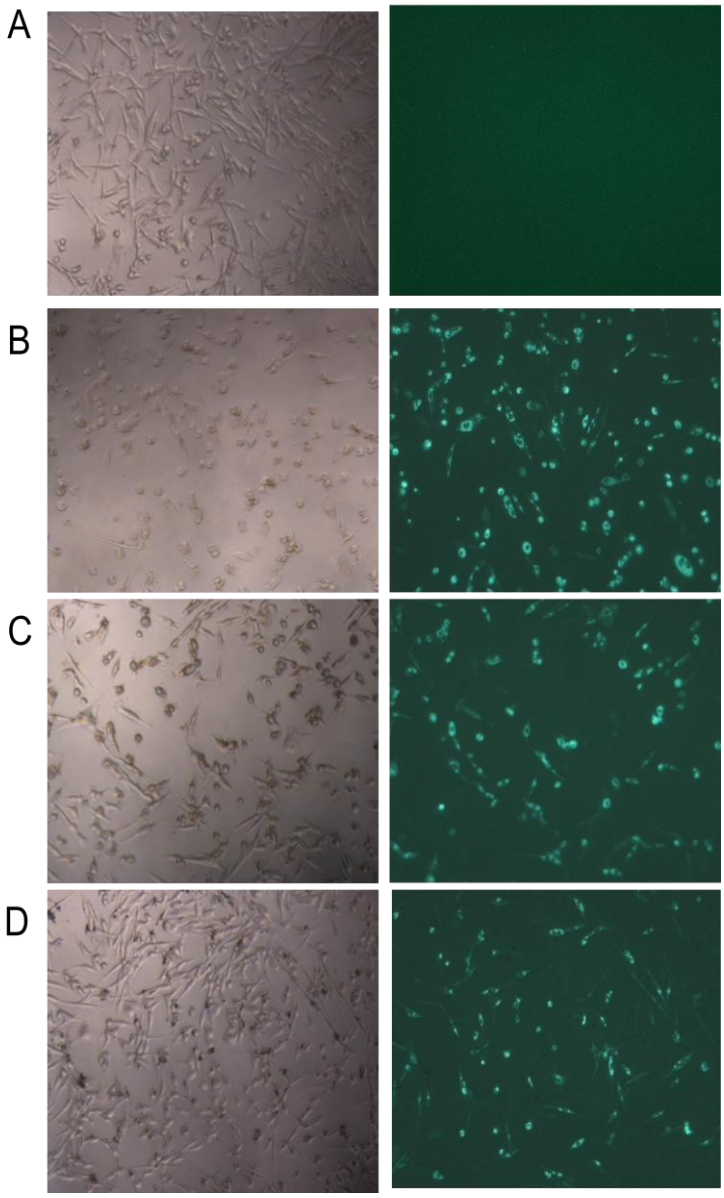

Figure III-III- 19: Images of B92 cells infected with A) the virus alone, B) complexes formed with PEI-Mag NPs, C) complexes formed with SO-Mag NPS and D) complexes formed with G1 NPs. Images were obtained 24h post-infection. Infection was performed at a MOI of 200 and the particle-to-virus ratio for the complexes formation was 2.5 fgFe/VP.

For N2A cells it can be seen that one day after the infection, cells infected with complexes formed with PEI-Mag and SO-Mag particles expressed higher amount of

GFP compared with the cells infected with just the virus and complexes formed with G1 nanoparticles. At MOI of 200, two days after the infection, the expression of GFP was very similar for all the infection procedures. However one day post-infection images reveal that the kinetic of transduction for complexes formed with PEI-Mag and SO-Mag particles in N2A cells was quicker than the kinetic with the virus alone and G1 based complex.

In B92 cells there were no differences in the expression of GFP one day after the infection between the complexes formed with the three kind of MNPs. Furthermore, it was observed no transduction at all in B92 cells infected with just the virus, which is in concordance with the almost null transduction efficiency for the virus alone detected by FACS 48h post-infection, shown above. If it is compared the results obtained by FACS (48h post-infection) and the images taken 24 post-infection, we observe that complexes formed with SO-Mag particles the day after the infection worked as well as the other MNPs based complexes, but two-days after the infection it is observed a big difference in the global efficiency when compared with the other complexes.

Taking all these results into account we can select the best complexes for each cell line. Both, final efficiency and kinetics are very important in order to optimize the transduction process. So, for N2A cells the best complexes were the ones formed with PEI-Mag and SO-Mag particles and for B92 cells the best complexes were the ones formed with PEI-Mag and G1 particles.

Concerning the transduction efficiency similar results were obtained in the literature when PEI-Mag particles were bound to an oncolytic adenovirus and the oncolytic potency was measured obtaining a clear oncolytic potency enhancement [114]. Besides, enhancement of the transduction efficiency in several cell lines, including non-permissive and hard-to-infect cells, was observed using adenovirus

combined to MNPs at very low MOI, 0.5 and 1. The enhancement was detected in terms of percentage of cells positively transduced and also in terms of the amount of protein expressed per cell [197].

Not only magnetofection experiments are performed with viral vectors but also with small units of nucleic acids or plasmids. In the literature there exist very detailed protocols to built complexes combining nucleic acids and cationic lipids or polymers which are associated with MNPs and about how to perform the magnetofection process [109]. In this paper authors showed the feasibility of the magnetic non-viral vectors to enhance the efficiency of the transfection of hard-to-transfect cell lines when using a magnetic field-assisted transfection. Other studies show how non viral methods in combination with the magnetofection are able to enhance the gene transfer in cultures of multipotent rat neural precursor cells and rat oligodendrocyte precursors [198, 199].

Taking all these results, including ours, into account it is possible to anticipate that gene therapy will take advantage of magnetofection. Improvement of the transfection/transduction efficiency and magnetically localized gene delivery in target sites are the most important advances that can be achieved.

III.III.IX. Coculture infections

Once the improvement in transduction efficiency had been demonstrated when using cells in monoculture, transfection experiments were performed in coculture of both cell lines treating to display a most realistic situation, as these cells are present in the human brain in a ratio 9:1, glial:neuronal cells.

Coculture of Red-B92 and N2A cells was prepared at a ratio of 7:3 in order to have enough N2A cells to analyze and to be able to differentiate them from Red-B92 cells.

For all the experiments made with the coculture, Red-B92 obtained by a previous transduction with a lentivirus encoding a red protein. Infections of coculture and monoculture of both cell lines were performed in parallel and cells were analyzed 2 days post-infection. For these experiments one type of magnetic adenoviral complex was chosen, PEI-Mag based complexes.

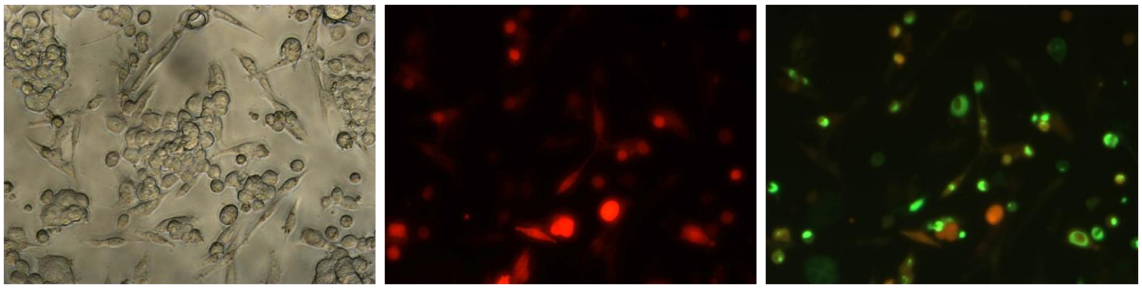

Figure III-III- 20: Images taken 24 h post-infection with a fluorescence microscope of the coculture infection experiment. Red cells are the B92-RED and green cells are both B92-RED and N2A that express GFP after the infection.

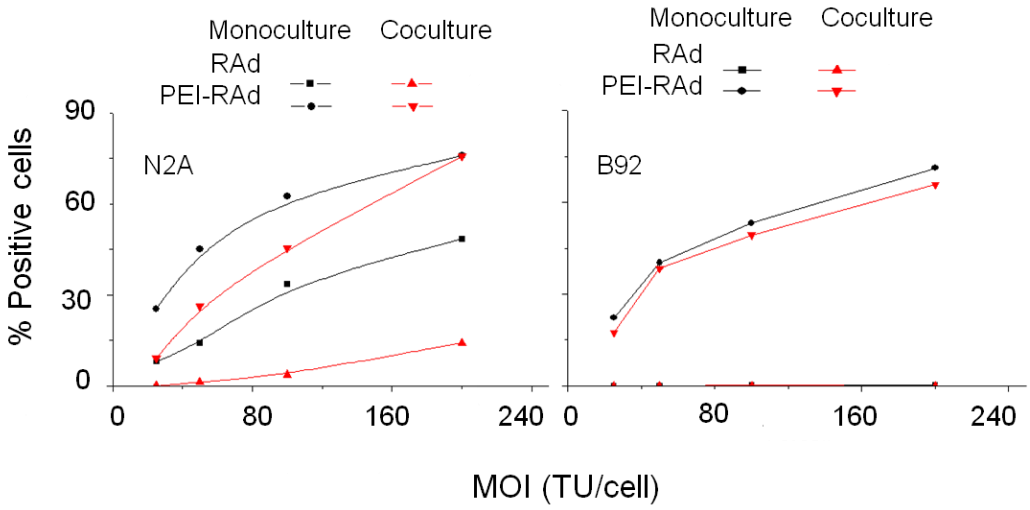

Figure III-III- 21: Transduction efficiency results in N2A and B92 cells in monoculture versus coculture. Transduction efficiency with virus alone and with complex formed with PEI-Mag particles was compared. Black lines represent cells in monoculture and red lines represent cells in coculture.

Figure III-III- 21 represents the percentage of cells that expressed GFP protein when cells were infected with the virus alone and with the PEI-Mag based complexes in cells in monoculture (black lines) and in coculture (red lines) in N2A and B92 cells, respectively. Analyzing in detail Figure III-III- 21 it can be seen that transduction with the virus alone and with the magnetic complexes was impaired when cells were in coculture in presence of B92 cells. The transduction efficiency decreased more in the case of the infection made with the virus alone, like 60 % compared with the 30% of decrease in the case of transfection with the magnetic complexes. However, Figure III-III- 21 shows that the transduction efficiency in B92 cells did not suffer any change no matter that the cells were cultured in coculture or in coculture in presence of N2A cells. Again it can be observed that the efficiency of the magnetic complexes was much higher than the efficiency when infection was performed with the virus alone, in agreement with the results showed in the previous section. In Figure III-III- 20 it can be seen images of the coculture where red cells were B92-RED and green cells were both B92-RED and N2A cells that were positively transduced and subsequently expressed GFP protein.

These results indicate that transduction efficiency of neuronal cells is affected by the presence of glial cells. It should be taken into account when in-vivo experiments need to be carried out. It is known that results of *in vitro* and *in vivo* experiments usually do not match up perfectly because in *in vivo* experiments there are many factors that influence the process that it is being studied. In this coculture experiment we can see how the interaction of two cells change the transduction efficiency of the virus and the magnetic complexes used to enhance the expression of GFP protein when infection is performed in both cell lines separately or in coculture.

III.III.X. In vivo preliminary results

In vivo experiments were performed in order to study the transduction efficiency of the magnetic complexes in a rat brain. The results that are going to be presented were made at the "Instituto de investigaciones biomédicas de la Plata (INIBIOLP)".

In order to performed magnetofection in the rat hippocampus, the adenovector RAd-GFP was complexed with PEI-Mag2 particles (2.5 µg Fe/ml) and the magnetic complex was bilaterally injected in the CA1 region of the hippocampus (in 10 µl magnetic complex suspension containing $2x10^8$ transforming units (TU) vector per side). The dose of RAd-GFP used was suboptimal in order to make more evident the enhancing effect of magnetofection on GFP gene delivery.

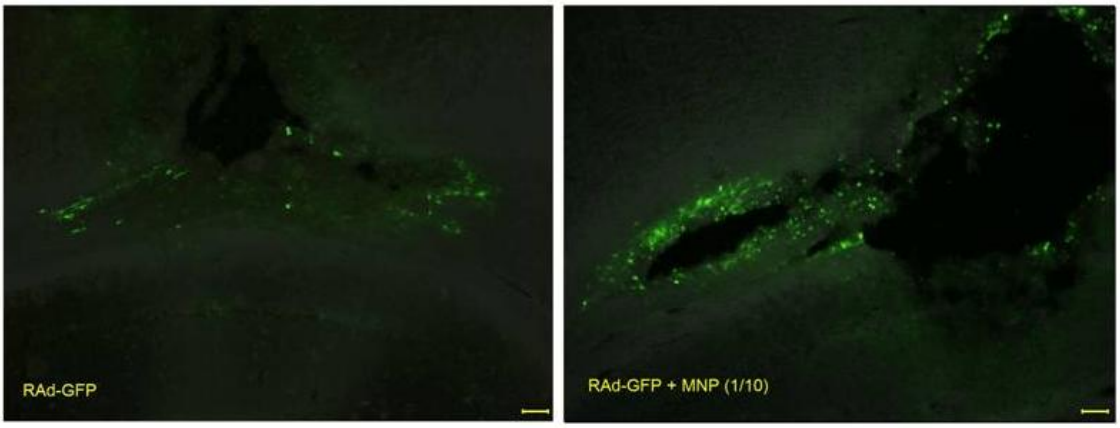

Figure III-III- 22: Injections of the Rad-GFP and MNP-RAd-GFP complex in the hippocampus of rat brains. All animals received the same dose of adenovector (2 X 10^8 TU) either alone (left) or complexed with either a 1/10 dilution of MNPs (right). Scale bars, 100 µm.

Immediately upon withdrawal of the needle a cylindrical magnet was placed on the head of the animals above the injection point. The distance between the proximal

surface of the cylinder and the vector delivery site was 2.4 mm and the estimated magnetic field gradient generated at the injection site was 24 mT/ mm. The magnet was applied for 25 min. Two days after the infection animals were sacrified and perfused with fixative solution and brain sections were cut and observed under a fluorescence microscope. The hippocampal sections were assessed by fluorescence microscopy. Figure III-III- 22 shows that the expression of GFP protein was enchance whent the adenovirus was complexed with the MNPs.

These preliminary results indicate that the strategy of using MNPs bound to virus allows a high expression of the protein encoded by the virus. Other *in vivo* magnetofection experiments are also promising showing that magnetically labeled non-viral and viral vectors can work as powerful tools in research and therapy being able to improve the efficiency of the gene delivery by concentrating and retaining the vector at the target site. One previous study demonstrated the efficacy of the local gene delivery by magnetofection when injecting non-viral vectors bound to MNPs directly in the tumour site and an external magnet was fixed on the tumour site for one hour after the injection [200]. Other recent study showed that directional *in vivo* gene transfer in mouse embryonic brain is feasible using adenovirus linked to MNPs when a magnetic force from the outside of the brain is used, because the magnetic field can attract the magnetic complexes to the target site [201].

All these results point to the idea that magnetofection is a highly promising tool for efficiently targeting gene delivery to specific brain areas, an approach that has been termed Magnetic Gene Targeting (MGT).

III.III.XI. Conclusions

From all the resuts presented in this section we can conclude that the adenovirus bind trough electrostatic forces to MNPs positively charged forming complexes that could be used as gene delivery carriers. The stability of these camplexes in biological media as Cerebrospinal Fluid or Fetal Calf Serum is reduced but almost 60% of the complex remain intact.

The magnetophoretic mobility of all the complexes tested in this work is good, what make them suitable to control by an external magnetic field. However, the complexes formed with SO-Mag and G1 particles have higher magnetophoretic mobility than the ones formed with PEI-Mag particles.

It has been proved that when the cells are infected with the magnetic-adenoviral complexes and placed onto an external magnet the amount of the virus internalized per cell increases with a factor of 5-7. This increase in the amount of virus per cell lead in increases the transduction efficiency when compared to the efficiency of the virus alone. The increase in the efficiency of the transduction is detectable in N2A cells and very impressive in the case of B92 cells. When these cells are co-cultured the transduction efficiency for each cell line changes when compared to the efficiency chieved when the cells are cultured separately. Specifically, the transduction efficicieny for N2A cells decreases when they are cultured in the presence of the B92 cells. However, the efficiency of the process in B92 cells do not change at all when they are cultured with the N2A cells.

Finally, the preliminary *in vivo* results presented in this work show that after injecting the virus complexes with MNPs the GFP expression at the target site was higer when compared with the expression obtained after the injection of the naked virus.

IV. Conclusions

In this chapter it is presented the main conclusions that can be drawn from the results of all the experiments that have been presented in this thesis. As there are two major topis that can be treated as completely independent and solid blocks we are going to separate the conclusions in this two topics.

AMF in DCs

Concerning DCs experimental part, one of the first conclusions is that DCs are capable of incorporating MNPs without presenting any cytotoxic effect in the range of concentration studied up to 5 days of incubation. MNPs are located in the cytosolic area inside phagocytic/endosomal vesicles and several techniques are suitable to study the internalization of NPs inside the cells, as confocal microscopy, transmission and scanning electron microscopy and dual beam. The internalization seems to be higher for negatively charged particles, but the difference is slight.

It is possible to quantify the average amount of MNPs incorporated per cell by SQUID measurements resulting in about 1.5pgFe_3O_4/cell (1 pgFe/cell, 250 MNPs/cell) for the negatively charged particles.

When immature DCs incorporate the MNPs a concentration-dependent maturation effect is observed after 48h of incubation. Maturation is study in terms of membrane molecule expression profile and release of cytokines.

Furthermore, alternating magnetic field originates specific cell death in the MNPs uploaded DCs, without presenting any increase in the temperature of the culture medium. This absence of temperature rise is supported by the fact that 1.5pg Fe_3O_4/cell

in not enough amount of MNPs to provoke the heating of 500 µl of culture medium. It is known that endocytic and phagocytic vesicles fuse with lysosomes ended up in secondary lysosomes. Thus, the cell death mechanisms may be based on the idea that the MNPs confined in the lysosomes provoke the lysosomal membrane disruption when the cells are submitted to AMF. Then, the lysosomal material is released to the cytoplasmatic space triggering the cell death. FACS analysis study indicates that the cell death mechanism is a necrotic-like death mechanism. It could consist of a pure necrotic cell death or a quick apoptosis way in which we observe the secondary necrosis typical of this cell death pathway. After AFM application SEM micrographs show cell membrane disruption with big pores in it, in agreement with the FACS results that show propidium iodide internalization due to membrane damage.

It have been demonstrated that is possible to control the magnitude of the induced cell death of MNPs loaded dendritic cells, by adequate tuning of the physical AMF parameters, the final amount of captured MNPs and/or the exposure time.

Adenoviral magnetic complexes and their use in magnetofection

Regarding the magnetofection experimental part, it can be said that adenoviral magnetic complexes can be formed between MNPs and adenovirus with an optimal ratio of about 2.5 fgFe/VP, having a stability of about 50% in biological mediums as CSF and FCS. The joint between MNPs and adenovirus is governed by electrostatic forces. So, as the adonovirus has negative charges at their surface, posively charged particles are needed for the formation of these complexes.

Internalization studies of these magnetic complexes in neuronal (N2A) and glial (B92) cells revealed that magnetic field assisted transduction lead to an increase in the amount of virus internalized per cell up to 5-7 times. Magnetic complexes

internalization can be observed in dual beam reveling that the MNPs enter into the cells. Besides, viability tests reveal that, comparing the viability of the cells when infected with the virus alone and with magnetic complexes, there is a slight decrease in the viability value. From MOI value of 100 the cytotoxicity reaches their highest value of about 50% compared with the value from the infection with the virus alone of about 80%. However, MOI required for in vivo application are much lower than the MOI values tested, so cytotoxicity should not be a downside.

FACS results show a great enhance of the transduction efficiency when using the magnetic complexes in B92 glial cells. The percentage of positively transducted cells is up to 80-fold at the highest MOI when comparing with the transduction efficiency reached with virus alone. However for N2A neuronal cells the transduction efficiency with the virus without MNPs is already high. Even though, at MOI values up to 100, a slight increase in the cells successfully transfected is observed. It is noteworthy that when infection is performed in coculture conditions the transduction efficiency for N2A cells is impaired for both virus alone and magnetic complexes, whereas for B92 cells remains very similar compared with the efficiency when the infection is made in monoculture.

The first preliminary in vivo results show that, after an ICV injection of the adenoviral magnetic complexes, a high expression of the reporter gene is observed in the ependymal layer of a rat brain. This suggests that this approach could be a useful tool in research and gene therapy.

Bibliography

1. Overgaard, J., et al., *Hyperthermia as an adjuvant to radiation therapy of recurrent or metastatic malignant melanoma. A multicentre randomized trial by the European Society for Hyperthermic Oncology.* Int J Hyperthermia, 1996. **12**(1): p. 3-20.
2. Maier-Hauff, K., et al., *Intracranial thermotherapy using magnetic nanoparticles combined with external beam radiotherapy: results of a feasibility study on patients with glioblastoma multiforme.* J Neurooncol, 2007. **81**(1): p. 53-60.
3. Fernandez Pujol, B., et al., *Dendritic cells derived from peripheral monocytes express endothelial markers and in the presence of angiogenic growth factors differentiate into endothelial-like cells.* Eur J Cell Biol, 2001. **80**(1): p. 99-110.
4. Sozzani, S., et al., *Dendritic cell-endothelial cell cross-talk in angiogenesis.* Trends Immunol, 2007. **28**(9): p. 385-92.
5. Whitesides, G.M., *The 'right' size in nanobiotechnology.* Nat Biotechnol, 2003. **21**(10): p. 1161-5.
6. Cho, K.J., et al., *Therapeutic nanoparticles for drug delivery in cancer.* Clinical Cancer Research, 2008. **14**(5): p. 1310-1316.
7. Park, S.J., T.A. Taton, and C.A. Mirkin, *Array-based electrical detection of DNA with nanoparticle probes.* Science, 2002. **295**(5559): p. 1503-6.
8. Zhang, Z.G., et al., *Advances in bone repair with nanobiomaterials: mini-review.* Cytotechnology, 2011. **63**(5): p. 437-443.
9. Martin CR, M.D., *Nanomaterials in analytical chemistry* Anal Chem, 1998. **70**(9): p. 322A-327A.
10. Harisinghani, M.G., et al., *Noninvasive detection of clinically occult lymph-node metastases in prostate cancer.* N Engl J Med, 2003. **348**(25): p. 2491-9.
11. Pankhurst QA, C.J., Jones SK, et al., *Applications of magnetic nanoparticles in biomedicine* J. Phys. D: Appl. Phys., 2003. **36**: p. R167-R181.
12. Hogemann, D., et al., *High throughput magnetic resonance imaging for evaluating targeted nanoparticle probes.* Bioconjug Chem, 2002. **13**(1): p. 116-21.
13. Wilhelm C, G.F., Roger J, et a, *Interaction of anionic superparamagnetic nanoparticles with cells: Kinetic analyses of membrane adsorption and subsequent internalization* Langmuir, 2002. **18**: p. 8148-8155.
14. Thiel, A., A. Scheffold, and A. Radbruch, *Immunomagnetic cell sorting--pushing the limits.* Immunotechnology, 1998. **4**(2): p. 89-96.

15. Alexiou, C., et al., *Targeting cancer cells: magnetic nanoparticles as drug carriers.* Eur Biophys J, 2006. **35**(5): p. 446-50.
16. Fortin-Ripoche, J.P., et al., *Magnetic targeting of magnetoliposomes to solid tumors with MR imaging monitoring in mice: feasibility.* Radiology, 2006. **239**(2): p. 415-24.
17. Billotey, C., et al., *Cell internalization of anionic maghemite nanoparticles: quantitative effect on magnetic resonance imaging.* Magn Reson Med, 2003. **49**(4): p. 646-54.
18. Bulte, J.W., et al., *Neurotransplantation of magnetically labeled oligodendrocyte progenitors: magnetic resonance tracking of cell migration and myelination.* Proc Natl Acad Sci U S A, 1999. **96**(26): p. 15256-61.
19. Goya, G.F., V. Grazu, and M.R. Ibarra, *Magnetic nanoparticles for cancer therapy.* Current Nanoscience, 2008. **4**(1): p. 1-16.
20. Jordan A, S.R., Wust P, et al., *Endocytosis of dextran and silan-coated magnetite nanoparticles and the effect of intracellular hyperthermia on human mammary carcinoma cells in vitro* J. Mag. Mag. Mat., 1999. **194** (1-3): p. 185-196.
21. Moroz, P., S.K. Jones, and B.N. Gray, *The effect of tumour size on ferromagnetic embolization hyperthermia in a rabbit liver tumour model.* Int J Hyperthermia, 2002. **18**(2): p. 129-40.
22. Plank, C., et al., *Magnetofection: enhancing and targeting gene delivery with superparamagnetic nanoparticles and magnetic fields.* J Liposome Res, 2003. **13**(1): p. 29-32.
23. Graham, B.D.C.a.C.D., *Introduction to Magnetic Materials.* The Institute of Electrical and Electronics Engineers, Inc. , 2009.
24. Storm, F.K., et al., *Magnetic-induction hyperthermia. Results of a 5-year multi-institutional national cooperative trial in advanced cancer patients.* Cancer, 1985. **55**(11): p. 2677-87.
25. Bicher, H.I., T.S. Sandhu, and F.W. Hetzel, *Hyperthermia and radiation in combination: a clinical fractionation regime.* Int J Radiat Oncol Biol Phys, 1980. **6**(7): p. 867-70.
26. Arcangeli, G., et al., *Enhanced effectiveness of adriamycin and bleomycin combined with local hyperthermia in neck node metastases from head and neck cancers.* Tumori, 1979. **65**(4): p. 481-6.
27. Pettigrew, R.T., C.M. Ludgate, and A.N. Smith, *Proceedings: The effect of whole body hyperthermia in advanced cancer.* Br J Cancer, 1974. **30**(2): p. 179.

28. Wust, P., et al., *Radiochemotherapy and hyperthermia in the treatment of rectal cancer.* Recent Results Cancer Res, 1998. **146**: p. 175-91.
29. Atmaca, A., et al., *Whole-body hyperthermia (WBH) in combination with carboplatin in patients with recurrent ovarian cancer - a phase II study.* Gynecol Oncol, 2009. **112**(2): p. 384-8.
30. Bakshandeh, A., Brun, I., Eberhardt, K. et al., *Ifosfamide, carboplatin and etoposide combined with aquatherm-induced 41.8 ºC whole-bogy hyperthermia for adults patients with malignant pleural mesothelioma.* Ann Oncol, 2000. **11**.
31. van der Zee, J., et al., *Comparison of radiotherapy alone with radiotherapy plus hyperthermia in locally advanced pelvic tumours: a prospective, randomised, multicentre trial. Dutch Deep Hyperthermia Group.* Lancet, 2000. **355**(9210): p. 1119-25.
32. Maluta, S., et al., *Regional hyperthermia combined with chemoradiotherapy in primary or recurrent locally advanced pancreatic cancer : An Open-Label Comparative Cohort Trial.* Strahlenther Onkol, 2011. **187**(10): p. 619-625.
33. Datta, N.R., et al., *Head and neck cancers: results of thermoradiotherapy versus radiotherapy.* Int J Hyperthermia, 1990. **6**(3): p. 479-86.
34. Issels, R.D., et al., *Ifosfamide plus etoposide combined with regional hyperthermia in patients with locally advanced sarcomas: a phase II study.* J Clin Oncol, 1990. **8**(11): p. 1818-29.
35. Hildebrandt, B., et al., *Regional hyperthermia for rectal cancer.* Lancet, 2000. **356**(9231): p. 771-2.
36. Gruber, Y., Hegewisch-Becker, S., Bakshandeh-Bath A., Sommer, H., Hoffmann, R., Hossfels, DK., *Whole-body hyperthermia at 41.8ºC combined with ifofasmide and carboplatin in relapsed ovarian carcinome pretreated with a platin-containing regimen.* Ann Oncol, 2000. **11 (Suppl. 4)**.
37. Dewey, W.C., D.E. Thrall, and E.L. Gillette, *Hyperthermia and radiation--a selective thermal effect on chronically hypoxic tumor cells in vivo.* Int J Radiat Oncol Biol Phys, 1977. **2**(1-2): p. 99-103.
38. Hildebrandt, B., et al., *The cellular and molecular basis of hyperthermia.* Crit Rev Oncol Hematol, 2002. **43**(1): p. 33-56.
39. Song, C.W., et al., *Increase in thermosensitivity of tumor cells by lowering intracellular pH.* Cancer Res, 1993. **53**(7): p. 1599-601.
40. Vidair, C.A. and W.C. Dewey, *Evaluation of a role for intracellular Na+, K+, Ca2+, and Mg2+ in hyperthermic cell killing.* Radiat Res, 1986. **105**(2): p. 187-200.

41. Coss, R.A., W.C. Dewey, and J.R. Bamburg, *Effects of hyperthermia on dividing Chinese hamster ovary cells and on microtubules in vitro.* Cancer Res, 1982. **42**(3): p. 1059-71.
42. Overgaard, J., *Ultrastructure of a murine mammary carcinoma exposed to hyperthermia in vivo.* Cancer Res, 1976. **36**(3): p. 983-95.
43. Streffer, C., *Aspects of metabolic change after hyperthermia.* Recent Results Cancer Res, 1988. **107**: p. 7-16.
44. Hahn, G.M., *Hyperthermia and Cancer.* New York: Plenum Press, 1982.
45. Morimoto, R.I., *Cells in stress: transcriptional activation of heat shock genes.* Science, 1993. **259**(5100): p. 1409-10.
46. Lindquist, S., *The heat-shock response.* Annu Rev Biochem, 1986. **55**: p. 1151-91.
47. Agashe, V.R. and F.U. Hartl, *Roles of molecular chaperones in cytoplasmic protein folding.* Semin Cell Dev Biol, 2000. **11**(1): p. 15-25.
48. Jolly, C. and R.I. Morimoto, *Role of the heat shock response and molecular chaperones in oncogenesis and cell death.* J Natl Cancer Inst, 2000. **92**(19): p. 1564-72.
49. White, E., *Life, death, and the pursuit of apoptosis.* Genes Dev, 1996. **10**(1): p. 1-15.
50. Harmon, B.V., et al., *Cell death induced in a murine mastocytoma by 42-47 degrees C heating in vitro: evidence that the form of death changes from apoptosis to necrosis above a critical heat load.* Int J Radiat Biol, 1990. **58**(5): p. 845-58.
51. Gordon, R.T., J.R. Hines, and D. Gordon, *Intracellular hyperthermia. A biophysical approach to cancer treatment via intracellular temperature and biophysical alterations.* Med Hypotheses, 1979. **5**(1): p. 83-102.
52. Hilger, I., et al., *Evaluation of temperature increase with different amounts of magnetite in liver tissue samples.* Invest Radiol, 1997. **32**(11): p. 705-12.
53. Jordan, A., et al., *Inductive heating of ferrimagnetic particles and magnetic fluids: physical evaluation of their potential for hyperthermia.* Int J Hyperthermia, 1993. **9**(1): p. 51-68.
54. Jordan, A., et al., *Cellular uptake of magnetic fluid particles and their effects on human adenocarcinoma cells exposed to AC magnetic fields in vitro.* Int J Hyperthermia, 1996. **12**(6): p. 705-22.
55. Ito, A., Kuga, Y., Honda, H., Hikkawa, H., Horiuchi, A., Watanabe, Y., Kobayashi, T., *Magnetite nanoparticle-loaded anti-HER2 immunoliposomes for*

combination of antibody therapy with hyperthermia. Cancer Letters, 2004. **212**: p. 164-175.
56. Natarajan, A., et al., *NanoFerrite particle based radioimmunonanoparticles: binding affinity and in vivo pharmacokinetics.* Bioconjug Chem, 2008. **19**(6): p. 1211-8.
57. Fortin, J.P., F. Gazeau, and C. Wilhelm, *Intracellular heating of living cells through Neel relaxation of magnetic nanoparticles.* Eur Biophys J, 2008. **37**(2): p. 223-8.
58. Balivada, S., et al., *A/C magnetic hyperthermia of melanoma mediated by iron(0)/iron oxide core/shell magnetic nanoparticles: a mouse study.* BMC Cancer, 2010. **10**: p. 119.
59. van Landeghem, F.K., et al., *Post-mortem studies in glioblastoma patients treated with thermotherapy using magnetic nanoparticles.* Biomaterials, 2009. **30**(1): p. 52-7.
60. Steinman, R.M. and Z.A. Cohn, *Identification of a novel cell type in peripheral lymphoid organs of mice. I. Morphology, quantitation, tissue distribution.* J Exp Med, 1973. **137**(5): p. 1142-62.
61. Inaba, K., et al., *Generation of large numbers of dendritic cells from mouse bone marrow cultures supplemented with granulocyte/macrophage colony-stimulating factor.* J Exp Med, 1992. **176**(6): p. 1693-702.
62. Inaba, K., et al., *Identification of proliferating dendritic cell precursors in mouse blood.* J Exp Med, 1992. **175**(5): p. 1157-67.
63. Caux, C., et al., *GM-CSF and TNF-alpha cooperate in the generation of dendritic Langerhans cells.* Nature, 1992. **360**(6401): p. 258-61.
64. Caux, C., et al., *CD34+ hematopoietic progenitors from human cord blood differentiate along two independent dendritic cell pathways in response to GM-CSF+TNF alpha.* J Exp Med, 1996. **184**(2): p. 695-706.
65. Szabolcs, P., et al., *Dendritic cells and macrophages can mature independently from a human bone marrow-derived, post-colony-forming unit intermediate.* Blood, 1996. **87**(11): p. 4520-30.
66. Sallusto, F. and A. Lanzavecchia, *Efficient presentation of soluble antigen by cultured human dendritic cells is maintained by granulocyte/macrophage colony-stimulating factor plus interleukin 4 and downregulated by tumor necrosis factor alpha.* J Exp Med, 1994. **179**(4): p. 1109-18.
67. Bender, A., et al., *Improved methods for the generation of dendritic cells from nonproliferating progenitors in human blood.* J Immunol Methods, 1996. **196**(2): p. 121-35.

68. Romani, N., et al., *Generation of mature dendritic cells from human blood. An improved method with special regard to clinical applicability.* J Immunol Methods, 1996. **196**(2): p. 137-51.
69. Ardavin, C., et al., *Thymic dendritic cells and T cells develop simultaneously in the thymus from a common precursor population.* Nature, 1993. **362**(6422): p. 761-3.
70. Marquez, C., et al., *The development of T and non-T cell lineages from CD34+ human thymic precursors can be traced by the differential expression of CD44.* J Exp Med, 1995. **181**(2): p. 475-83.
71. Galy, A., et al., *Human T, B, natural killer, and dendritic cells arise from a common bone marrow progenitor cell subset.* Immunity, 1995. **3**(4): p. 459-73.
72. Saunders, D., et al., *Dendritic cell development in culture from thymic precursor cells in the absence of granulocyte/macrophage colony-stimulating factor.* J Exp Med, 1996. **184**(6): p. 2185-96.
73. Banchereau, J., et al., *Immunobiology of dendritic cells.* Annu Rev Immunol, 2000. **18**: p. 767-811.
74. Janeway, C.A., Jr. and R. Medzhitov, *Innate immune recognition.* Annu Rev Immunol, 2002. **20**: p. 197-216.
75. Steinman, R.M., *Some interfaces of dendritic cell biology.* APMIS, 2003. **111**(7-8): p. 675-97.
76. Rescigno, M. and P. Borrow, *The host-pathogen interaction: new themes from dendritic cell biology.* Cell, 2001. **106**(3): p. 267-70.
77. Iwasaki, A. and R. Medzhitov, *Toll-like receptor control of the adaptive immune responses.* Nat Immunol, 2004. **5**(10): p. 987-95.
78. Guermonprez, P., et al., *Antigen presentation and T cell stimulation by dendritic cells.* Annu Rev Immunol, 2002. **20**: p. 621-67.
79. Trombetta, E.S. and I. Mellman, *Cell biology of antigen processing in vitro and in vivo.* Annu Rev Immunol, 2005. **23**: p. 975-1028.
80. Macatonia, S.E., et al., *Dendritic cells produce IL-12 and direct the development of Th1 cells from naive CD4+ T cells.* J Immunol, 1995. **154**(10): p. 5071-9.
81. Mazzoni, A., et al., *Histamine regulates cytokine production in maturing dendritic cells, resulting in altered T cell polarization.* J Clin Invest, 2001. **108**(12): p. 1865-73.
82. Seliger, B., M.J. Maeurer, and S. Ferrone, *Antigen-processing machinery breakdown and tumor growth.* Immunol Today, 2000. **21**(9): p. 455-64.

83. Chaux, P., et al., *Inflammatory cells infiltrating human colorectal carcinomas express HLA class II but not B7-1 and B7-2 costimulatory molecules of the T-cell activation.* Lab Invest, 1996. **74**(5): p. 975-83.
84. Kortylewski, M., et al., *Inhibiting Stat3 signaling in the hematopoietic system elicits multicomponent antitumor immunity.* Nat Med, 2005. **11**(12): p. 1314-21.
85. Hoffmann, T.K., et al., *Alterations in the frequency of dendritic cell subsets in the peripheral circulation of patients with squamous cell carcinomas of the head and neck.* Clin Cancer Res, 2002. **8**(6): p. 1787-93.
86. Troy, A.J., et al., *Minimal recruitment and activation of dendritic cells within renal cell carcinoma.* Clin Cancer Res, 1998. **4**(3): p. 585-93.
87. Fricke, I. and D.I. Gabrilovich, *Dendritic cells and tumor microenvironment: a dangerous liaison.* Immunol Invest, 2006. **35**(3-4): p. 459-83.
88. Whiteside, T.L. and C. Odoux, *Dendritic cell biology and cancer therapy.* Cancer Immunol Immunother, 2004. **53**(3): p. 240-8.
89. Banchereau, J. and A.K. Palucka, *Dendritic cells as therapeutic vaccines against cancer.* Nat Rev Immunol, 2005. **5**(4): p. 296-306.
90. Ito, A., et al., *Heat shock protein 70 expression induces antitumor immunity during intracellular hyperthermia using magnetite nanoparticles.* Cancer Immunol Immunother, 2003. **52**(2): p. 80-8.
91. Todryk, S., et al., *Heat shock protein 70 induced during tumor cell killing induces Th1 cytokines and targets immature dendritic cell precursors to enhance antigen uptake.* J Immunol, 1999. **163**(3): p. 1398-408.
92. Noessner, E., et al., *Tumor-derived heat shock protein 70 peptide complexes are cross-presented by human dendritic cells.* J Immunol, 2002. **169**(10): p. 5424-32.
93. Basu, S., et al., *Necrotic but not apoptotic cell death releases heat shock proteins, which deliver a partial maturation signal to dendritic cells and activate the NF-kappa B pathway.* Int Immunol, 2000. **12**(11): p. 1539-46.
94. Nishioka, Y., et al., *Induction of systemic and therapeutic antitumor immunity using intratumoral injection of dendritic cells genetically modified to express interleukin 12.* Cancer Res, 1999. **59**(16): p. 4035-41.
95. Kikuchi, T., et al., *Tumor regression induced by intratumor administration of adenovirus vector expressing CD40 ligand and naive dendritic cells.* Cancer Res, 2000. **60**(22): p. 6391-5.
96. Tanaka, K., et al., *Intratumoral injection of immature dendritic cells enhances antitumor effect of hyperthermia using magnetic nanoparticles.* Int J Cancer, 2005. **116**(4): p. 624-33.

97. David Dong, Z.M., A.C. Aplin, and R.F. Nicosia, *Regulation of angiogenesis by macrophages, dendritic cells, and circulating myelomonocytic cells.* Curr Pharm Des, 2009. **15**(4): p. 365-79.
98. Conejo-Garcia, J.R., et al., *Vascular leukocytes contribute to tumor vascularization.* Blood, 2005. **105**(2): p. 679-81.
99. Conejo-Garcia, J.R., et al., *Tumor-infiltrating dendritic cell precursors recruited by a beta-defensin contribute to vasculogenesis under the influence of Vegf-A.* Nat Med, 2004. **10**(9): p. 950-8.
100. Gottfried, E., et al., *Differentiation of human tumour-associated dendritic cells into endothelial-like cells: an alternative pathway of tumour angiogenesis.* Scand J Immunol, 2007. **65**(4): p. 329-35.
101. Fernandez Pujol, B., et al., *Endothelial-like cells derived from human CD14 positive monocytes.* Differentiation, 2000. **65**(5): p. 287-300.
102. Inaba, K., et al., *Dendritic cell progenitors phagocytose particulates, including bacillus Calmette-Guerin organisms, and sensitize mice to mycobacterial antigens in vivo.* J Exp Med, 1993. **178**(2): p. 479-88.
103. Thiele, L., et al., *Evaluation of particle uptake in human blood monocyte-derived cells in vitro. Does phagocytosis activity of dendritic cells measure up with macrophages?* J Control Release, 2001. **76**(1-2): p. 59-71.
104. Migdal, C., et al., *Internalisation of hybrid titanium dioxide/para-amino benzoic acid nanoparticles in human dendritic cells did not induce toxicity and changes in their functions.* Toxicol Lett, 2010. **199**(1): p. 34-42.
105. Templeton, N.S., *Gene and Cell Therapy: Therapeutic Mechanisms and Strategies, Third Edition.* CRC Press, 2008.
106. Plank, C., et al., *Enhancing and targeting nucleic acid delivery by magnetic force.* Expert Opin Biol Ther, 2003. **3**(5): p. 745-58.
107. Lubbe, A.S., C. Alexiou, and C. Bergemann, *Clinical applications of magnetic drug targeting.* J Surg Res, 2001. **95**(2): p. 200-6.
108. Lubbe, A.S., et al., *Clinical experiences with magnetic drug targeting: a phase I study with 4'-epidoxorubicin in 14 patients with advanced solid tumors.* Cancer Res, 1996. **56**(20): p. 4686-93.
109. Mykhaylyk, O., et al., *Generation of magnetic nonviral gene transfer agents and magnetofection in vitro.* Nat Protoc, 2007. **2**(10): p. 2391-411.
110. Mah C, Z.I., Fraites TJ, et al., *Microsphere-mediated delivery of recombinant AAV vectors in vitro and in vivo.* Molec Therapy., 2000.
111. Huth, S., et al., *Insights into the mechanism of magnetofection using PEI-based magnetofectins for gene transfer.* J Gene Med, 2004. **6**(8): p. 923-36.

112. Mykhaylyk, O., et al., *Recent advances in magnetofection and its potential to deliver siRNAs in vitro.* Methods Mol Biol, 2009. **487**: p. 111-46.
113. Torres, T.E., et al., *Magnetic properties and energy absorption of CoFe(2)O(4) nanoparticles for magnetic hyperthermia*, in *International Conference on Magnetism*. 2010, Iop Publishing Ltd: Bristol.
114. Tresilwised, N., et al., *Boosting oncolytic adenovirus potency with magnetic nanoparticles and magnetic force.* Mol Pharm, 2010. **7**(4): p. 1069-89.
115. Maizel, J.V., Jr., D.O. White, and M.D. Scharff, *The polypeptides of adenovirus. I. Evidence for multiple protein components in the virion and a comparison of types 2, 7A, and 12.* Virology, 1968. **36**(1): p. 115-25.
116. Lawrence, W.C. and H.S. Ginsberg, *Intracellular uncoating of type 5 adenovirus deoxyribonucleic acid.* J Virol, 1967. **1**(5): p. 851-67.
117. Hanson, C.V., J.L. Riggs, and E.H. Lennette, *Photochemical inactivation of DNA and RNA viruses by psoralen derivatives.* J Gen Virol, 1978. **40**(2): p. 345-58.
118. Mykhaylyk, O., et al., *siRNA delivery by magnetofection.* Curr Opin Mol Ther, 2008. **10**(5): p. 493-505.
119. Stilwell, J.L., et al., *Development and characterization of novel empty adenovirus capsids and their impact on cellular gene expression.* J Virol, 2003. **77**(23): p. 12881-5.
120. MacPherson, G., et al., *Uptake of antigens from the intestine by dendritic cells.* Ann N Y Acad Sci, 2004. **1029**: p. 75-82.
121. Sabado, R.L., et al., *Pathways utilized by dendritic cells for binding, uptake, processing and presentation of antigens derived from HIV-1.* Eur J Immunol, 2007. **37**(7): p. 1752-63.
122. Lutsiak, M.E., et al., *Analysis of poly(D,L-lactic-co-glycolic acid) nanosphere uptake by human dendritic cells and macrophages in vitro.* Pharm Res, 2002. **19**(10): p. 1480-7.
123. Coester, C., P. Nayyar, and J. Samuel, *In vitro uptake of gelatin nanoparticles by murine dendritic cells and their intracellular localisation.* Eur J Pharm Biopharm, 2006. **62**(3): p. 306-14.
124. Uto, T., et al., *Modulation of innate and adaptive immunity by biodegradable nanoparticles.* Immunol Lett, 2009. **125**(1): p. 46-52.
125. Ghoneum, M., A. Ghoneum, and J. Gimzewski, *Nanodiamond and nanoplatinum liquid, DPV576, activates human monocyte-derived dendritic cells in vitro.* Anticancer Res, 2010. **30**(10): p. 4075-9.

126. Wang, J., et al., *Multi-walled carbon nanotubes do not impair immune functions of dendritic cells.* Carbon, 2009. **47**(7): p. 1752-1760.
127. Goya GF, L.E., Arelaro AD, et al., *Magnetic Hyperthermia With Fe3O4 Nanoparticles: The Influence of Particle Size on Energy Absorption* IEEE TRANSACTIONS ON MAGNETICS 2008. **44**(11): p. 4444-4447.
128. Rosensweig, R.E., *Heating magnetic fluid with alternating magnetic field.* Journal of Magnetism and Magnetic Materials, 2002. **252**: p. 370-374.
129. Goya, G.F., et al., *Static and dynamic magnetic properties of spherical magnetite nanoparticles.* Journal of Applied Physics, 2003. **94**(5): p. 3520-3528.
130. Posfai, M., et al., *Properties of intracellular magnetite crystals produced by Desulfovibrio magneticus strain RS-1.* Earth and Planetary Science Letters, 2006. **249**(3-4): p. 444-455.
131. Verges, M.A., et al., *Uniform and water stable magnetite nanoparticles with diameters around the monodomain-multidomain limit.* Journal of Physics D-Applied Physics, 2008. **41**(13).
132. Young, J.W. and R.M. Steinman, *The hematopoietic development of dendritic cells: a distinct pathway for myeloid differentiation.* Stem Cells, 1996. **14**(4): p. 376-87.
133. Coukos, G., et al., *The role of dendritic cell precursors in tumour vasculogenesis.* Br J Cancer, 2005. **92**(7): p. 1182-7.
134. Chapuis, F., et al., *Differentiation of human dendritic cells from monocytes in vitro.* Eur J Immunol, 1997. **27**(2): p. 431-41.
135. Rakhimova, M., et al., *In vitro differentiation of human monocytes into dendritic cells by peptic-tryptic digest of gliadin is independent of genetic predisposition and the presence of celiac disease.* J Clin Immunol, 2009. **29**(1): p. 29-37.
136. Hamoir, J., et al., *Effect of polystyrene particles on lung microvascular permeability in isolated perfused rabbit lungs: role of size and surface properties.* Toxicol Appl Pharmacol, 2003. **190**(3): p. 278-85.
137. Panyam, J., et al., *Rapid endo-lysosomal escape of poly(DL-lactide-co-glycolide) nanoparticles: implications for drug and gene delivery.* FASEB J, 2002. **16**(10): p. 1217-26.
138. Kunzmann, A., et al., *Efficient internalization of silica-coated iron oxide nanoparticles of different sizes by primary human macrophages and dendritic cells.* Toxicol Appl Pharmacol, 2011. **253**(2): p. 81-93.
139. O'Brien, N.M., et al., *Cytotoxicity, genotoxicity and oxidative reactions in cell-culture models: modulatory effects of phytochemicals.* Biochem Soc Trans, 2000. **28**(2): p. 22-6.

140. Altman, S.A., L. Randers, and G. Rao, *Comparison of trypan blue dye exclusion and fluorometric assays for mammalian cell viability determinations.* Biotechnol Prog, 1993. **9**(6): p. 671-4.
141. Borenfreund, E. and J.A. Puerner, *Toxicity determined in vitro by morphological alterations and neutral red absorption.* Toxicol Lett, 1985. **24**(2-3): p. 119-24.
142. Mosmann, T., *Rapid colorimetric assay for cellular growth and survival: application to proliferation and cytotoxicity assays.* J Immunol Methods, 1983. **65**(1-2): p. 55-63.
143. Soenen, S.J. and M. De Cuyper, *Assessing cytotoxicity of (iron oxide-based) nanoparticles: an overview of different methods exemplified with cationic magnetoliposomes.* Contrast Media Mol Imaging, 2009. **4**(5): p. 207-19.
144. Pernodet, N., et al., *Adverse effects of citrate/gold nanoparticles on human dermal fibroblasts.* Small, 2006. **2**(6): p. 766-73.
145. Lipski, A.M., et al., *The effect of silica nanoparticle-modified surfaces on cell morphology, cytoskeletal organization and function.* Biomaterials, 2008. **29**(28): p. 3836-46.
146. de la Fuente, J.M. and C.C. Berry, *Tat peptide as an efficient molecule to translocate gold nanoparticles into the cell nucleus.* Bioconjugate Chemistry, 2005. **16**(5): p. 1176-1180.
147. Kalambur, V.S., E.K. Longmire, and J.C. Bischof, *Cellular level loading and heating of superparamagnetic iron oxide nanoparticles.* Langmuir, 2007. **23**(24): p. 12329-36.
148. Babensee, J.E., *Interaction of dendritic cells with biomaterials.* Semin Immunol, 2008. **20**(2): p. 101-8.
149. Van Vre, E.A., et al., *Human C-reactive protein activates monocyte-derived dendritic cells and induces dendritic cell-mediated T-cell activation.* Arterioscler Thromb Vasc Biol, 2008. **28**(3): p. 511-8.
150. Ma, Y.J. and H.C. Gu, *Study on the endocytosis and the internalization mechanism of aminosilane-coated Fe3O4 nanoparticles in vitro.* Journal of Materials Science-Materials in Medicine, 2007. **18**(11): p. 2145-2149.
151. Sen, D., et al., *Quantum dots for tracking dendritic cells and priming an immune response in vitro and in vivo.* PLoS One, 2008. **3**(9): p. e3290.
152. Geppert, M., et al., *Uptake of dimercaptosuccinate-coated magnetic iron oxide nanoparticles by cultured brain astrocytes.* Nanotechnology, 2011. **22**(14): p. 145101.
153. Owen, C.S. and N.L. Sykes, *Magnetic labeling and cell sorting.* J Immunol Methods, 1984. **73**(1): p. 41-8.

154. Strom, V., et al., *A novel and rapid method for quantification of magnetic nanoparticle-cell interactions using a desktop susceptometer.* Nanotechnology, 2004. **15**(5): p. 457-466.
155. Zupke, O., et al., *Preservation of dendritic cell function upon labeling with amino functionalized polymeric nanoparticles.* Biomaterials, 2010. **31**(27): p. 7086-95.
156. Lacroix, L.M., et al., *Magnetic hyperthermia in single-domain monodisperse FeCo nanoparticles: Evidences for Stoner-Wohlfarth behavior and large losses.* Journal of Applied Physics, 2009. **105**(2).
157. Geijtenbeek, T.B., et al., *Identification of DC-SIGN, a novel dendritic cell-specific ICAM-3 receptor that supports primary immune responses.* Cell, 2000. **100**(5): p. 575-85.
158. Lin, Y.L., et al., *Polysaccharide purified from Ganoderma lucidum induces gene expression changes in human dendritic cells and promotes T helper 1 immune response in BALB/c mice.* Mol Pharmacol, 2006. **70**(2): p. 637-44.
159. Reis ES, B.J., Köhl J, Isaac L., *Impaired dendritic cell differentiation and maturation in the absence of C3.* Molecular Immunology, 2008. **45**: p. 1952-1962.
160. Takei, M. and H. Nakagawa, *A sea urchin lectin, SUL-1, from the Toxopneustid sea urchin induces DC maturation from human monocyte and drives Th1 polarization in vitro.* Toxicol Appl Pharmacol, 2006. **213**(1): p. 27-36.
161. Chang, C.C., A. Wright, and J. Punnonen, *Monocyte-derived CD1a+ and CD1a- dendritic cell subsets differ in their cytokine production profiles, susceptibilities to transfection, and capacities to direct Th cell differentiation.* J Immunol, 2000. **165**(7): p. 3584-91.
162. Koike, E., et al., *Carbon black nanoparticles promote the maturation and function of mouse bone marrow-derived dendritic cells.* Chemosphere, 2008. **73**(3): p. 371-6.
163. Banchereau, J. and R.M. Steinman, *Dendritic cells and the control of immunity.* Nature, 1998. **392**(6673): p. 245-52.
164. De Vries, I.J., et al., *Effective migration of antigen-pulsed dendritic cells to lymph nodes in melanoma patients is determined by their maturation state.* Cancer Res, 2003. **63**(1): p. 12-7.
165. Kiertscher, S.M. and M.D. Roth, *Human CD14+ leukocytes acquire the phenotype and function of antigen-presenting dendritic cells when cultured in GM-CSF and IL-4.* J Leukoc Biol, 1996. **59**(2): p. 208-18.

166. Sallusto, F., et al., *Dendritic cells use macropinocytosis and the mannose receptor to concentrate macromolecules in the major histocompatibility complex class II compartment: downregulation by cytokines and bacterial products.* J Exp Med, 1995. **182**(2): p. 389-400.
167. Jankowska, O., et al., *Phenotype of dendritic cells generated in the presence of non-small cell lung cancer antigens - preliminary report.* Folia Histochem Cytobiol, 2008. **46**(4): p. 465-70.
168. Jahns, J., et al., *Influence of low dose irradiation on differentiation, maturation and T-cell activation of human dendritic cells.* Mutat Res, 2011. **709-710**: p. 32-9.
169. Reis e Sousa, C., *Dendritic cells in a mature age.* Nat Rev Immunol, 2006. **6**(6): p. 476-83.
170. Moser, M. and K.M. Murphy, *Dendritic cell regulation of TH1-TH2 development.* Nat Immunol, 2000. **1**(3): p. 199-205.
171. Pasare, C. and R. Medzhitov, *Toll pathway-dependent blockade of CD4+CD25+ T cell-mediated suppression by dendritic cells.* Science, 2003. **299**(5609): p. 1033-6.
172. Johannsen, M., et al., *Thermotherapy using magnetic nanoparticles combined with external radiation in an orthotopic rat model of prostate cancer.* Prostate, 2006. **66**(1): p. 97-104.
173. Murdoch, C., et al., *The role of myeloid cells in the promotion of tumour angiogenesis.* Nat Rev Cancer, 2008. **8**(8): p. 618-31.
174. Magforce, *Magforce nanotechnologies AG receives European regulatory approval for its Nanocancer therapy.* 2010.
175. Bartczak, D., et al., *Laser-induced damage and recovery of plasmonically targeted human endothelial cells.* Nano Lett, 2011. **11**(3): p. 1358-63.
176. Fung, A.O., et al., *Induction of cell death by magnetic actuation of nickel nanowires internalized by fibroblasts.* Journal of Physical Chemistry C, 2008. **112**(39): p. 15085-15088.
177. Kim, D.H., et al., *Biofunctionalized magnetic-vortex microdiscs for targeted cancer-cell destruction.* Nature Materials, 2010. **9**(2): p. 165-171.
178. Martin-Saavedra, F.M., et al., *Magnetic mesoporous silica spheres for hyperthermia therapy.* Acta Biomaterialia. **6**(12): p. 4522-4531.
179. Fortin, J.P., F. Gazeau, and C. Wilhelm, *Intracellular heating of living cells through Neel relaxation of magnetic nanoparticles.* European Biophysics Journal with Biophysics Letters, 2008. **37**(2): p. 223-228.

180. Rodriguez-Luccioni, H.L., et al., *Enhanced reduction in cell viability by hyperthermia induced by magnetic nanoparticles.* International Journal of Nanomedicine. **6**: p. 373-380.
181. Duguet, E., L. Hardel, and S. Vasseur, *Cell Targeting and Magnetically Induced Hyperthermia*, in *Thermal Nanosystems and Nanomaterials*. 2009, Springer-Verlag Berlin: Berlin. p. 343-365.
182. Prasad, N.K., et al., *Mechanism of cell death induced by magnetic hyperthermia with nanoparticles of gamma-MnxFe2-xO3 synthesized by a single step process.* Journal of Materials Chemistry, 2007. **17**(48): p. 5042-5051.
183. Lunov, O., et al., *Thermal Destruction on the Nanoscale: Cell Membrane Hyperthermia with Functionalized Magnetic Nanoparticles*, in *8th Internatioanl Conference on the Scientific and Clinical Applications of Magnetic Carriers*, U. Hafeli, W. Schutt, and M. Zborowski, Editors, Amer Inst Physics: Melville. p. 288-292.
184. Marcos-Campos, I., et al., *Cell death induced by the application of alternating magnetic fields to nanoparticle-loaded dendritic cells.* Nanotechnology, 2011. **22**(20): p. 13.
185. Creixell, M., et al., *EGFR-targeted magnetic nanoparticle heaters kill cancer cells without a perceptible temperature rise.* ACS Nano, 2011. **5**(9): p. 7124-9.
186. Beaune, G., et al., *Different localizations of hydrophobic magnetic nanoparticles within vesicles trigger their efficiency as magnetic nano-heaters.* Soft Matter. **7**(13): p. 6248-6254.
187. Wilhelm, C., J.P. Fortin, and F. Gazeau, *Tumour cell toxicity of intracellular hyperthermia mediated by magnetic nanoparticles.* J Nanosci Nanotechnol, 2007. **7**(8): p. 2933-7.
188. Scherer, F., et al., *Magnetofection: enhancing and targeting gene delivery by magnetic force in vitro and in vivo.* Gene Therapy, 2002. **9**(2): p. 102-109.
189. Tresilwised, N., et al., *Effects of nanoparticle coatings on the activity of oncolytic adenovirus-magnetic nanoparticle complexes.* Biomaterials, 2012. **33**(1): p. 256-69.
190. J, P.L.T., *The lowered drop method for the preparation of spacimens of partially purified virus lysates for quantitative electron micrographic analysis.* Virology, 1962. **18**: p. 359-371.
191. Murakami, P. and M.T. McCaman, *Quantitation of adenovirus DNA and virus particles with the PicoGreen fluorescent Dye.* Anal Biochem, 1999. **274**(2): p. 283-8.

192. Shabram, P.W., et al., *Analytical anion-exchange HPLC of recombinant type-5 adenoviral particles.* Hum Gene Ther, 1997. **8**(4): p. 453-65.
193. Mittereder, N., K.L. March, and B.C. Trapnell, *Evaluation of the concentration and bioactivity of adenovirus vectors for gene therapy.* J Virol, 1996. **70**(11): p. 7498-509.
194. Summers, M.D. and G.E. Smith, *A MANUAL OF METHODS FOR BACULOVIRUS VECTORS AND INSECT CELL-CULTURE PROCEDURES.* Texas Agricultural Experiment Station Bulletin, 1987(1555): p. 1-56.
195. Gueret, V., et al., *Rapid titration of adenoviral infectivity by flow cytometry in batch culture of infected HEK293 cells.* Cytotechnology, 2002. **38**(1-3): p. 87-97.
196. Nadeau, I., et al., *293SF metabolic flux analysis during cell growth and infection with an adenoviral vector.* Biotechnol Prog, 2000. **16**(5): p. 872-84.
197. Sapet, C., et al., *Magnetic Nanoparticles Enhance Adenovirus Transduction In Vitro and In Vivo.* Pharm Res, 2011.
198. Pickard, M.R., P. Barraud, and D.M. Chari, *The transfection of multipotent neural precursor/stem cell transplant populations with magnetic nanoparticles.* Biomaterials, 2011. **32**(9): p. 2274-84.
199. Jenkins, S.I., et al., *Magnetic nanoparticle-mediated gene transfer to oligodendrocyte precursor cell transplant populations is enhanced by magnetofection strategies.* ACS Nano, 2011. **5**(8): p. 6527-38.
200. Schillinger, U., et al., *Advances in magnetofection - magnetically guided nucleic acid delivery.* Journal of Magnetism and Magnetic Materials, 2005. **293**(1): p. 501-508.
201. Hashimoto, M. and Y. Hisano, *Directional gene-transfer into the brain by an adenoviral vector tagged with magnetic nanoparticles.* J Neurosci Methods, 2011. **194**(2): p. 316-20.

Annexe : Theoretical basis of techniques

VI.I. Specific Power Absorption

When a hyperthermia experiment is performed in the lab, released heat by the sample is measured through the increase in temperature of the colloid. The usual method for heat (Q) measurements is to use thermally-insulated system, and apply the thermodynamic relation:

$$Q = C_S \, m_{ff} \, \Delta T \qquad (1)$$

Where Cs is the specific heat of the fluid in (J/K g), m_{ff} is the mass of the fluid (g) and ΔT is the temperature increase (K). As this amount of heat is an extensive property, which means that it depends on the amount of sample we want to measure, it is more accurate to use the specific power absorption (SPA), defined as the amount of energy converted into heat per time unit and per material mass unit. From the expression (1), Power (P) absorbed and converted into heat can be expressed as:

$$P = \frac{Q}{\Delta t} = C_S \, m_{ff} \, \frac{\Delta T}{\Delta t} \qquad (2)$$

The Power, P, is given in Watts. Specific power (i.e. the absorbed power per material gram) is called the Specific Power Absorption (SPA), and is experimentally

obtained using expression (2) and measuring temperature increase $\Delta T = T_f - T_i$ of a magnetic fluid in a time range $\Delta t = t_f - t_i$

$$SPA = \frac{P}{m_{NP}} = \frac{m_{LIQ} c_{LIQ} + m_{NP} c_{NP}}{m_{NP}} \left(\frac{\Delta T}{\Delta t} \right) \quad (3)$$

Where m_{NP} is the mass of the NPs which are diluted in a mass m_{LIQ} of liquid (colloid), and c_{LIQ} and c_{NP} are the specific heat from the solvent and the NPs, respectively. If the NPs concentration is small, we can approximate $m_{LIQ}\, c_{LIQ} + m_{NP}\, c_{NP} \approx m_{LIQ}\, c_{LIQ}$ and the equation will be:

$$SPA = \frac{c_{LIQ}\, \delta_{LIQ}}{\phi} \left(\frac{\Delta T}{\Delta t} \right) = \frac{m_{LIQ} c_{LIQ}}{m_{NP}} \left(\frac{\Delta T}{\Delta t} \right) \quad (4)$$

Where δ_{LIQ} and $\phi = m_{LIQ}/V_{LIQ}$ are the liquid density and the concentration in terms of weight of the NPs in the colloid, respectively.

The SPA value is an indicator of how good is magnetic colloid to produce an increase of temperature, and this is an important property of the MNPs to be selected for MFH.

VI.II. Dynamic Light Scattering

Dynamic Light Scattering (DLS) also referred to as Photon Correlation Spectroscopy (PCS) or Quasi-Elastic Light Scattering (QELS) is a well-established technique for measuring the size of molecules and particles under the micron region size. It is typically used for measuring the size distribution of particles like proteins, nanoparticles and micelles. These particles in solution undergo Brownian motion due to the fact that solvent molecules are moving themselves because of thermal energy. When these molecules are illuminated with a laser there is light scattering, and light scattering fluctuate due to the molecules movement in the solvent. This variation in the light scattering in a time period is measured in the DLS equipment, and it depends on the particle size as smaller molecules move faster in the solvent than bigger particles.

The diameter that is measured in DLS is called hydrodynamic diameter and refers as how a particles diffuses into a liquid and corresponds with the diameter of a sphere that has the same diffusion coefficient as the particle we are measuring. The diffusion coefficient depends not only in the core dimension but on any molecule which is in the surface. That is why diameters obtained with this technique are frequently bigger that the values obtained by TEM.

We can choose to obtain three different distributions based on the intensity, volume or number. A very simple way of describing the differences between volume, intensity and number distribution is to consider two populations of spherical particles of diameters of 5 and 50 nm presented in equal numbers (Figure 1).

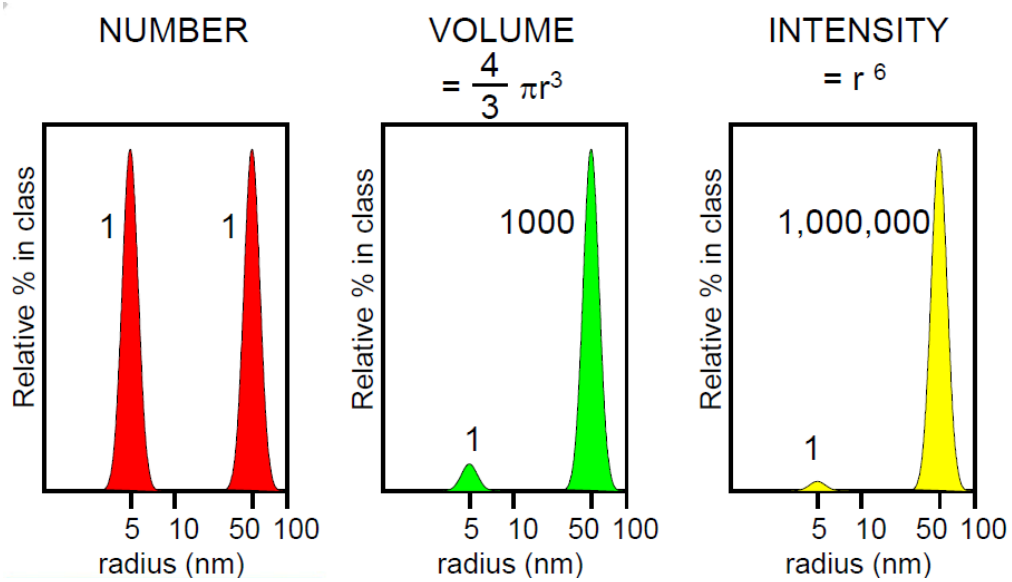

Figure 1: Number, volume and intensity distribution of a mixture of particles with diameter of 5 and 50 nm present in equal numbers.

If a number distribution is represented from this mixture a plot consisting of 2 peaks (positioned at 5 and 50 nm) of a 1:1 ratio would be obtained. When this number distribution is converted into volume, then the two peaks would change to 1:1000 ratio, duo to the fact that volume is proportional to $r^{3.}$ If this was further converted into intensity distribution the ratio would be 1:1,000,000 because intensity is proportional to r^6 (from Rayleighs approximation).

VI.III. SEM

The Scanning Electron Microscope (SEM) uses a focus beam of high-energy electrons rather than light to obtain a variety of signals from the surface of a solid material. The signals obtained from sample-electrons interaction reveal information of the sample, such as morphology, chemical composition and crystalline structure.

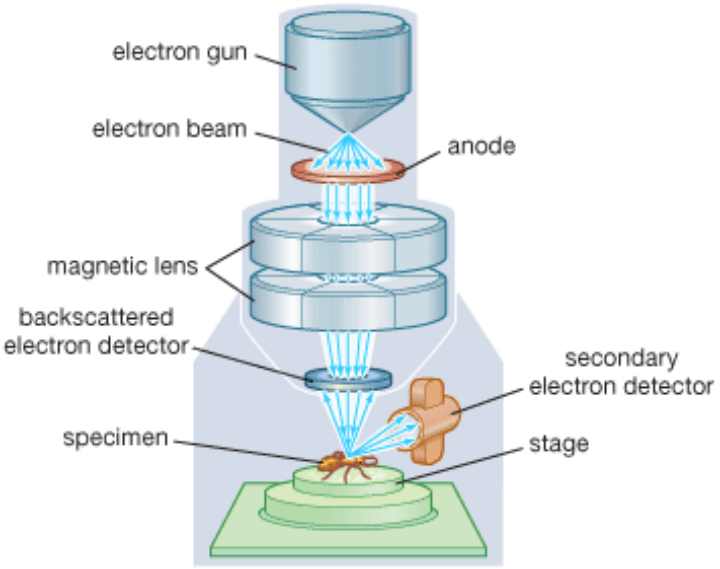

Figure 2: Scanning Electron Microscope scheme. Image taken from the Online Encyclopaedia Britannica.

An electron source at the top of the microscope, which may be a tungsten filament or a Lanthanum hexaboride source, emits the electrons that travel though vacuum in the column, and instead of glass lenses for focusing the light in light microscope SEM uses electromagnetic lenses to focus the electrons into a very thin beam. Accelerated electron in a SEM carry significant amount of kinetic energy, which dissipate when the

interaction with the sample takes place. The signals that are produced include secondary electrons (SE), backscattered electrons (BSE), diffracted backscattered electrons (DBSE), photons (X-Ray), visible light and heat (Figure 3). Secondary electrons and backscattered electrons are commonly used for imaging samples, the former are more used to obtain data about the morphology and came from the incident electrons, and the latter are more valuable to reveal contrast in composition between light and heavy metals as they came from the sample. X-Ray generation is produced by inelastic interaction between the incident electrons and electrons of the sample, and when the excited electron return to the lowest energy state they yield X-Ray that are of a fixed wavelength (corresponding to the difference between the energy in the two states). Thus, characteristics X-Ray are produced in different elements when their electrons are excited by the electron beam in the SEM. They are a useful tool to analyze the materials by SEM.

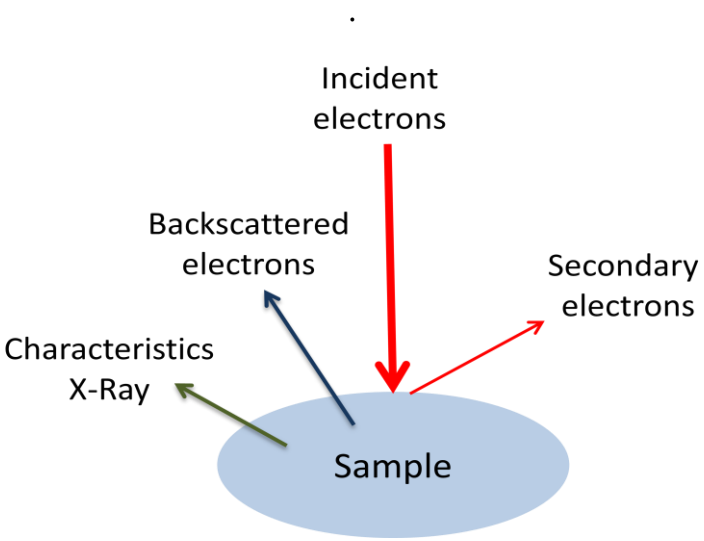

Figure 3: Electron-sample interaction signals

VI.IV. TEM

As in SEM microscope, TEM uses electrons as “light” source and their much lower wavelength makes it possible to get a resolution a thousand times better than with a light microscope. The electron source and the electromagnetic lenses are similar as the ones in SEM microscope. Typically a TEM consists of three stages of lensing, which are the condenser lenses, the objective lenses and the projector lenses. The condenser lenses are responsible for primary electron beam formation, the objective lenses focus the beam that comes though the sample and the projector lenses are used to expand the beam onto the fluorescent screen.

The electron beam travel in vacuum conditions through the sample we want to study and depending on the density and the composition of the material some of the electrons are scattered and disappear from the incident beam. At the bottom of the microscope the unscattered electrons hit a fluorescent screen forming the image of the sample. Image can be recorded using a CCD camera. A schematin illustration of a typical TEM is represented in the Figure 4.

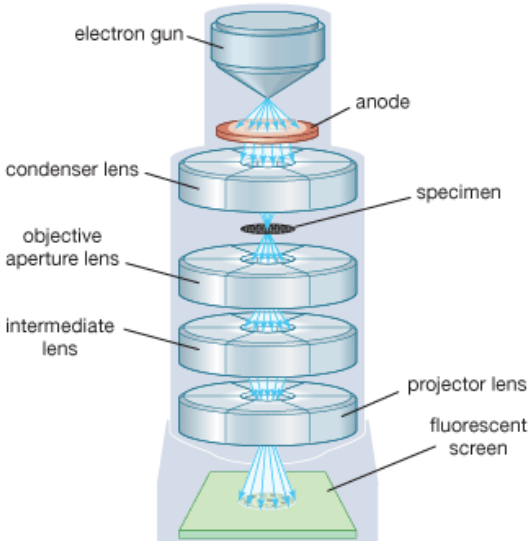

Figure 4: Transmission Electron Microscope scheme. Image taken from the Online Encyclopaedia Britannica.

VI.V. Dual Beam

A dual beam device incorporates a Scanning Electron Microscope (SEM) and a Focus Ion Beam (FIB) column. This configuration makes this technique very useful when morphology and internal composition studies are required in biology samples though it is typically used in nanolithography research studies. Typical dual beam configuration is a vertical electron column with a tilted ion column, as can be seen in Figure 5. In this case the angle between the electron and ion column is 52º, so the sample will be at 0º or 52º respectively for SEM and FIB, depending on the process that is being performed.

The interactions electron-material is the same as it has been explained in the SEM technique, schematized in Figure 3. However, ion beam-material interactions depend on

the kinetic energy that receives the material. If the energy that receives is enough to overcome the surface energy binding the milling of the sample takes place (Figure 6).

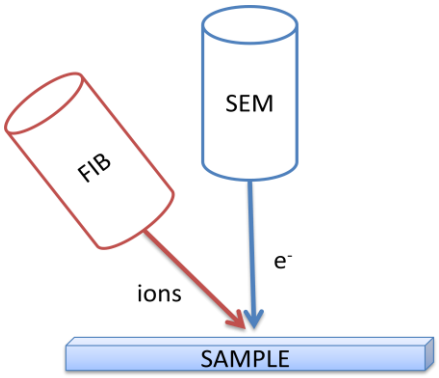

Figure 5: Scheme of the dual beam configuration. Both columns form an angle of 52º and are focused in the same point. The stage where the sample is located rotates depending on the process.

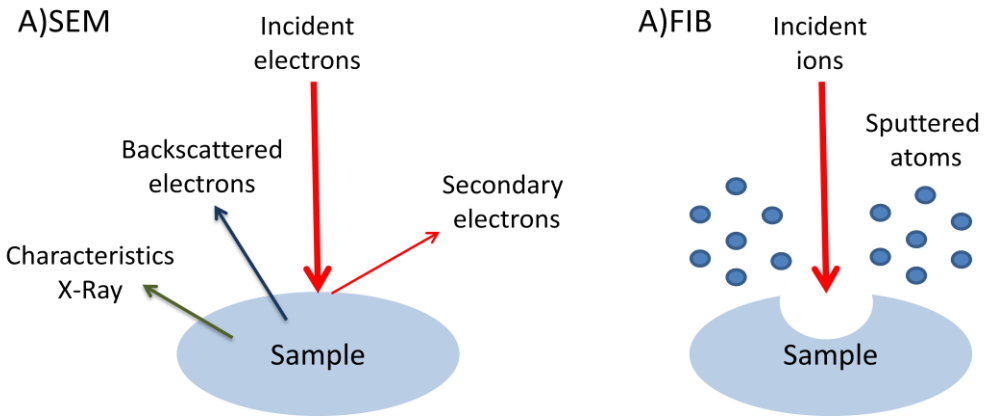

Figure 6: Interaction between a focus electron beam (SEM) (a) and a focus ion beam (FIB) (b) and a substrate.

VI.VI. Confocal

Confocal microscopy is a technique for obtaining images with depth selectivity. Its ability to acquire in-focus images from selected depths makes this technique very useful to study any protein, molecule or particles with intracellular localization. Confocal microscopy has overcome some limitations of the conventional fluorescence microscopy, where the sample is excited and the resulting fluorescence comes from the entire sample. In contrast, a confocal microscope uses pointed illumination and it only collects fluorescence from the on-focus plane, eliminating out-of-focus signal. In the sample depth direction the optical resolution is much better; however, it costs a decrease in the signal intensity.

A schematic illustration of a confocal microscopy is shown in the Figure 7. The source that is used in confocal microscopes in order to provide excitation light is laser. Laser reflects of a dichroic mirror and from there laser is directed to the sample thought some lenses inside the microscope. Dye in the sample fluoresces and the emitted light is passes back thought the same lenses and the dichroic mirror and is focus in the pinhole. The light that passes through the pinhole is measured by the detector. Only the light that comes from the on-focus plane is detected.

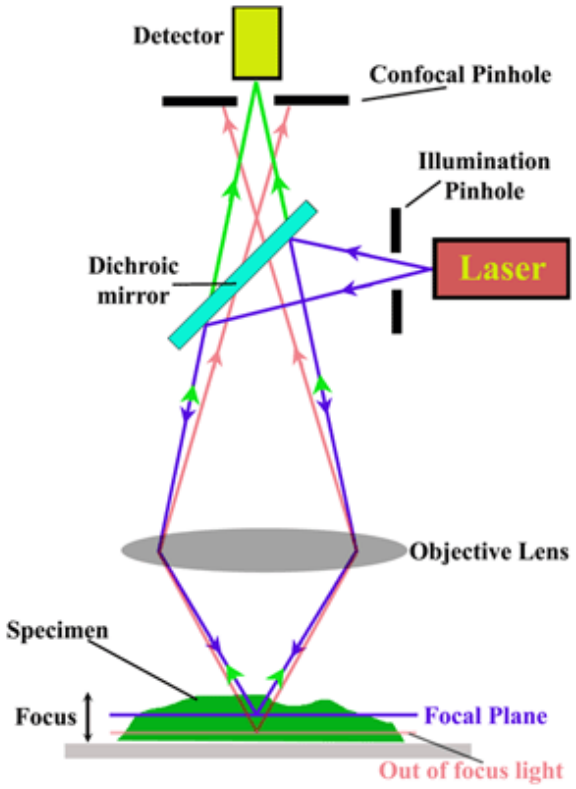

Figure 7: Scheme of a confocal microscopy.

When experiments with various dyes are performed, each fluorescent emitted light is detected in different channels, collecting each of them a wavelength window signal. So it is very important to select dyes that do not overlap their excitation/emission spectres.